The role of cytosolic sensors in host defense to intracellular pathogens

Edited by
Sergio C. Oliveira, Guillermo Hernán Giambartolomei,
Jose Carlos Alves-Filho, Glen N. Barber and Karina Bortoluci

About Frontiers

Frontiers is more than just an open access publisher of scholarly articles: it is a pioneering approach to the world of academia, radically improving the way scholarly research is managed. The grand vision of Frontiers is a world where all people have an equal opportunity to seek, share and generate knowledge. Frontiers provides immediate and permanent online open access to all its publications, but this alone is not enough to realize our grand goals.

Frontiers journal series

The Frontiers journal series is a multi-tier and interdisciplinary set of open-access, online journals, promising a paradigm shift from the current review, selection and dissemination processes in academic publishing. All Frontiers journals are driven by researchers for researchers; therefore, they constitute a service to the scholarly community. At the same time, the *Frontiers journal series* operates on a revolutionary invention, the tiered publishing system, initially addressing specific communities of scholars, and gradually climbing up to broader public understanding, thus serving the interests of the lay society, too.

Dedication to quality

Each Frontiers article is a landmark of the highest quality, thanks to genuinely collaborative interactions between authors and review editors, who include some of the world's best academicians. Research must be certified by peers before entering a stream of knowledge that may eventually reach the public - and shape society; therefore, Frontiers only applies the most rigorous and unbiased reviews. Frontiers revolutionizes research publishing by freely delivering the most outstanding research, evaluated with no bias from both the academic and social point of view. By applying the most advanced information technologies, Frontiers is catapulting scholarly publishing into a new generation.

What are Frontiers Research Topics?

Frontiers Research Topics are very popular trademarks of the *Frontiers journals series*: they are collections of at least ten articles, all centered on a particular subject. With their unique mix of varied contributions from Original Research to Review Articles, Frontiers Research Topics unify the most influential researchers, the latest key findings and historical advances in a hot research area.

Find out more on how to host your own Frontiers Research Topic or contribute to one as an author by contacting the Frontiers editorial office: frontiersin.org/about/contact

The role of cytosolic sensors in host defense to intracellular pathogens

Topic editors

Sergio C. Oliveira — University of São Paulo, Brazil

Guillermo Hernán Giambartolomei — National Scientific and Technical Research Council (CONICET), Argentina

Jose Carlos Alves-Filho — University of São Paulo, Brazil

Glen N. Barber — University of Miami, United States

Karina Bortoluci — Federal University of São Paulo, Brazil

Table of
contents

frontiers | Frontiers in Immunology

DNA-PKcs restricts *Zika virus* spreading and is required for effective antiviral response

Daniel de Oliveira Patricio[1], Greicy Brisa Malaquias Dias[1],
Lucilene Wildner Granella[1], Ben Trigg[2],
Helena Claire Teague[2], Dina Bittencourt[1], André Báfica[1],
Alfeu Zanotto-Filho[3], Brian Ferguson[2]
and Daniel Santos Mansur[1]*

[1]Laboratório de Imunobiologia, Departamento de Microbiologia, Imunologia e Parasitologia,
Universidade Federal de Santa Catarina, Florianópolis, Brazil, [2]Department of Pathology, University
of Cambridge, Cambridge, United Kingdom, [3]Laboratório de Farmacologia e Bioquímica do Câncer,
Departamento de Farmacologia, Universidade Federal de Santa Catarina, Florianópolis, Brazil

Zika virus (ZIKV) is a single-strand RNA mosquito-borne flavivirus with significant public health impact. ZIKV infection induces double-strand DNA breaks (DSBs) in human neural progenitor cells that may contribute to severe neuronal manifestations in newborns. The DNA-PK complex plays a critical role in repairing DSBs and in the innate immune response to infection. It is unknown, however, whether DNA-PK regulates ZIKV infection. Here we investigated the role of DNA-PKcs, the catalytic subunit of DNA-PK, during ZIKV infection. We demonstrate that DNA-PKcs restricts the spread of ZIKV infection in human epithelial cells. Increased ZIKV replication and spread in DNA-PKcs deficient cells is related to a notable decrease in transcription of type I and III interferons as well as *IFIT1, IFIT2,* and *IL6*. This was shown to be independent of IRF1, IRF3, or p65, canonical transcription factors necessary for activation of both type I and III interferon promoters. The mechanism of DNA-PKcs to restrict ZIKV infection is independent of DSB. Thus, these data suggest a non-canonical role for DNA-PK during *Zika virus* infection, acting downstream of IFNs transcription factors for an efficient antiviral immune response.

KEYWORDS

Zika virus, interferon, DNA-PKcs, double-strand DNA breaks, infection

Introduction

Zika virus (ZIKV) is a single-strand RNA mosquito-borne flavivirus (1). First isolated in 1947 in Africa, ZIKV caught public health attention in 2007 with the first viral outbreak in Pacific Islands, from where it spread to South America in 2015 (2–5). In 2016, Zika disease was declared to be a worldwide public health emergency due to severe neurological manifestations in newborns (6, 7). The neurological complications are associated with the tropism of ZIKV for human neural progenitor cells which results in growth arrest, DNA double-strand breaks (DSBs), and cell death (8, 9). DSBs are the most cytotoxic type of DNA lesions that rapidly activate DNA-damage repair response, orchestrated in part by the DNA-dependent protein kinase (DNA-PK) complex (10, 11). However, the relevance of DNA-PK in restricting ZIKV infection is unknown.

DNA-PK is a multifunctional protein complex consisting of Ku70, Ku80, and the catalytic subunit (DNA-PKcs) which are involved, among other functions, in DNA damage repair, V(D)J recombination of lymphocytes receptors, transcriptional regulation, DNA replication, and RNA metabolism (11–13). Present in the cytoplasm and nuclei, DNA-PK also functions as an intracellular DNA receptor critical for primary immune response against DNA virus infections by inducing interferon (IFN)-I and IFN-III expression (14–19). IFNs induce the transcription of interferon-stimulated genes (ISGs) that are critical for inhibition of viral replication cycle (20–22).

During RNA virus infections, IFN-I and IFN-III are mainly induced by intracellular RNA sensing receptors such as retinoic acid-inducible gene I (RIG-I) and melanoma differentiation-associated protein 5 (MDA5) (23). For instance, ZIKV RNA genome detection is mediated by RIG-I, leading to activation and nuclear translocation of the transcription factors belonging to the interferon regulatory factor (IRF) and nuclear factor-kappa B (NF-κB) families (24–35). IRFs and NF-κB bind to interferon-stimulated response element (ISRE) and NF-κB motifs, respectively, both present in the promoter region responsible for IFN-I and IFN-III genes (32, 36).

Several studies associate DNA-PK complex with ZIKV or other flaviviruses, such as *Dengue virus* (DENV). Vetter *et al.* (37) described DNA-PK localization and activation as a very early marker of DENV infection (37). DENV infection causes DNA-PK subunits relocation to the nucleoli, which may regulate RNA splicing (37–39). In addition, human cells with Ku80 protein partially depleted, reduce the interferon response induced by DENV (37). The DNA-PK complex is also associated with both ZIKV and DENV genomic RNA in human cells, with unknown effects (40). In this context and considering ZIKV can induce DSB (8, 9), we investigated whether DNA-PKcs affects ZIKV infection and triggers antiviral immune response pathways.

We found that DNA-PKcs restricts ZIKV spread in human epithelial cells. In the course of infection, DNA-PKcs is required for IFN-related gene transcription, independent of transcription factors IRF1, IRF3, or p65 (NF-κB subunit). In addition, DNA-PKcs role during ZIKV infection was DSB independent. This study provides information about the DNA-PKcs dynamics on the antiviral immune response during ZIKV infection and may contribute to new therapeutic strategies.

Materials and methods

Cell culture and reagents

A549 (ATCC®, CCL-185™), RPE (ATCC, CRL-2302), Vero (ATCC®, CCL-81™), and derived cell lines were maintained in DMEM-F12 (GIBCO, 12400-024) containing 5% fetal bovine serum (FBS – GIBCO, 12657-029) supplemented with 1 U/mL penicillin/streptomycin (Sigma, P4333). C6/36 (ATCC®, CRL-1660™) cells were maintained at 28 °C, in L-15 (Sigma, L4386) containing 5% FBS supplemented with 0.26% tryptose phosphate broth (GIBCO, 18050-39), and 1 U/mL penicillin/streptomycin. Both cell lines were routinely tested for mycoplasma contamination. Cells were treated with 0.5 or 1 μM of NU7441 (BioGems, 5039598), 100 ng/mL human TNF (Peprotech, 300-01A), and 3 μM etoposide (Sigma, E1383).

Virus infection

ZIKV strain BR2015/15261 (41) was kindly provided by Dra. Claudia N. Duarte dos Santos (Fiocruz-PR, Brazil). Viral stocks were purified from infected C6/36 cells supernatants and titrated by plaque assay on Vero cells. This virus was used for infection for indicated times and multiplicity of infection (m.o.i.).

Flow cytometry

Cells were detached from the plate with trypsin-EDTA (GIBCO, 25300-062), centrifuged at 460 x *g* for 5 min, washed in saline solution, and stained with Zombie NIR™ fixable viability kit (Biolegend, 423105) at the dilution 1:2000 for 20 min at room temperature. Cells were then fixed with 3% paraformaldehyde (PFA – Sigma, P6148) for 20 min followed by staining with FITC-conjugated flavivirus E protein antibody (anti-4G2) (provided from Fiocruz-PR, Brazil) in permeabilization buffer (0.25% saponin - Vetec, 1364) for

40 min. All cells were washed with saline solution and acquired on BD FACSVerse with FACSuite software. Analysis was performed using FlowJo software v. 10.1 (TreeStar). The gating strategy used for flow cytometry is available in Supplementary Figure 2.

MTT assay

Cells were incubated with 0.5 mg/mL MTT reagent (Amresco, 793) for 3 hours at 37 °C and 5% CO_2, followed by incubation of DMSO for formazan crystals extraction. Measures were performed at 570 nm abs on a Biotek spectrophotometer using Gen5 1.10 software.

Immunofluorescence

Cells were seeded onto a plate containing a 15 mm glass coverslip, followed by ZIKV infection at determining time and concentration. Cells were then fixed with 3% PFA for 20 min followed by permeabilization with PBS containing 0.1% Triton X-100 (Amresco, 694) and 2% bovine serum albumin (BSA – Inlab, 1870) for 5 min. Primary antibodies (Supplementary Table I) were diluted in PBS with 2% BSA, and incubated for 1 hour at room temperature, followed by detection by secondary antibodies (Supplementary Table II), diluted in PBS with 2% BSA, and incubated for 1 hour at room temperature. Then, cell nuclei were stained with DAPI (Molecular probes, D3571) for 15 minutes and mounted with Mowiol (Sigma, 81381). Pictures were obtained on an Olympus BX41 microscope and processed on Q-capture Pro 5.1 software (Q-imaging). For transcription factors translocation into the nucleus, cells were counted on at least 20 infection plaque from each sample, in biological triplicates using ImageJ software.

Real-time quantitative PCR

Total RNA was extracted from cells using TRIzol reagent (Ambion, 15596026) according to manufacturer's instructions. RT-PCR was performed with M-MLV Reverse Transcriptase (Promega, M170A) using 500 ng of RNA. For qPCR reaction, 2 µL of 1:20 diluted cDNA was used in a final volume of 10 µL, and 0.1 µM forward and reverse primers (Supplementary Table III), performed with GoTaq qPCR Master Mix (Promega, A600A). *GAPDH* was used as the housekeeping gene. Data were obtained on the StepOne Plus Real-Time PCR system (Applied BioSystems) and analyzed with StepOne Software v2.1. Relative mRNA expression was calculated by $2^{-\Delta\Delta CT}$ method.

Immunoblotting

Immunoblotting was used for characterization of A549[PRKDC-/-] cells. Cells were lysed using a lysis buffer containing protease inhibitor (Mini Protease Inhibitor Tablets – Roche, 5056489001). The samples were incubated for 30 min at 4 °C, being briefly vortexed each 10 min followed by centrifugation at 13.000 x *g* for 10 min at 4 °C. The supernatant was transferred to a new tube and the total proteins were quantified using Pierce BCA protein assay kit (Thermo, 23225). From total proteins, 20 µg were transferred to polyacrylamide gel electrophoresis for protein separation and then transferred to nitrocellulose 0.22 µm blotting membranes. The membranes were blocked in 5% non-fat milk in TBS containing 0.1% Tween 20 (TBST) for 1 hour at room temperature. Membranes were then probed with primary antibodies (Supplementary Table IV) diluted in TBST containing 5% BSA, at 4 °C shaking overnight. Membranes were washed with TBST and incubated in secondary antibodies (Supplementary Table V) for 1 hour at room temperature. Then, membranes were washed and chemiluminescence developed using ECL substrate (Pierce, 34577). Tubulin was normalized as the reference control.

CRISPR/Cas9

A549[PRKDC-/-] and RPE[PRKDC-/-] cells were generated with a pair of sgRNA guides (Guide1: GATCACGCCGCCAGTCTCCA; Guide2: CAGACATCTGAACAACTTTA). The guides were inserted in pX458 plasmids containing Cas9 encoded genes plus GFP sequence for clone isolation. The cells were transfected with pX458/Guide using lipofectamine 3000 reagent (Invitrogen, L3000-008) following manufacturer's instructions. For clone selection and expansion, the fluorescent cells were isolated into a 96-well plate using BDMelody cell sorter (BD). Knockout cell line clones were confirmed by immunofluorescence and immunoblotting assays.

Data processing and statistical analyses

Data derived from the experiments were processed using GraphPad Prism nine software. The data were analyzed according to experimental settings using unpaired two-tailed Student's *t*-test or two-way ANOVA, with Sidak's correction where necessary.

Results

DNA-PKcs is required for control of ZIKV infection

DNA-PK complex plays a critical role in DNA damage repair such as DSB as well as in antiviral immune response (10, 11, 14, 16–19). It was demonstrated that ZIKV can induce DSB in neural progenitor cells (8, 9). However, the role of the

catalytic subunit of DNA-PK in controlling ZIKV infection is currently unknown. To determine the role of DNA-PKcs during ZIKV infection, we used CRISPR/Cas9 editing of the *PRKDC* gene to generate DNA-PKcs-deficient A549 and RPE epithelial cells, referred to as A549$^{PRKDC-/-}$ (Figures S1A, B) and RPE$^{PRKDC-/-}$ (Figure S1C). We observed an increase of infectious ZIKV particles released from A549$^{PRKDC-/-}$ (Figure 1A) and RPE$^{PRKDC-/-}$ (Figure 1B) compared with wild-type (WT) cells as well as a significant increase in intracellular ZIKV RNA (Figures 1C, D). In the absence of DNA-PKcs, ZIKV spread to adjacent cells, as measured by plaque area size (Figures 1E, F), as well as the percentage of infected cells (Figure 1G, Figure S2) and dead cells (Figure 1H) are also increased. Altogether, these results indicate DNA-PKcs is required for full control of ZIKV infection in both A549 and RPE cells.

To evaluate whether the DNA-PKcs kinase function is required for ZIKV control, we treated A549 cells with NU7441, a DNA-PKcs inhibitor (42, 43), 24 hours before infecting with ZIKV (Figure 1I). Similar to what we observed in *PRKDC-/-* cells, NU7441 pre-treatment increased ZIKV infection in WT, but not in A549$^{PRKDC-/-}$ cells. These results suggest DNA-PKcs kinase function is necessary for control of ZIKV infection.

ZIKV infection does not induce double-strand DNA breaks in A549 cells

IFN-I is induced by DNA-PKcs through its DNA sensing function following DSB (44). Furthermore, ZIKV infection induces DSB in neural progenitor cells as observed by γH2A.X histone phosphorylation (8, 9). Thus, we evaluated whether ZIKV infection induces DSB in A549 cells, leading to a source of immunostimulatory DNA to activate DNA-PKcs. To assess this, the A549^{WT} and A549$^{PRKDC-/-}$ cells as well as A549 cells pre-treated with 1 μM NU7441 were infected with ZIKV (m.o.i. 1) at 24 hours. As a positive control, cells were treated with 3 μM etoposide, a topoisomerase II inhibitor, for 12 hours (Figures 2A, B). As expected, etoposide treatment increased the number of γH2A.X foci (green) per cell, being enhanced in A549$^{PRKDC-/-}$ or in NU7441-treated cells. However, the γH2A.X foci levels were similar in A549 cells infected with ZIKV (red) compared with uninfected cells. These results suggest that DNA-PKcs controls the ZIKV infection independent of any DSB-induced response.

DNA-PKcs is required for IFN-I and IFN-III genes transcription during ZIKV infection

RIG-I is the major ZIKV RNA sensor, leading to induction of IFN-I and IFN-III transcription, crucial for an efficient

antiviral immune response (33, 34). To evaluate whether RIG-I orchestrates ZIKV sensing in A549 cells, we infected A549^{WT} and A549$^{RIGI-/-}$ with m.o.i. 1 for 24 hours to measure the induction of IFN-related genes transcription (Figure 3A). We observed A549 lacking RIG-I failed to induce IFN-I, IFN-III, ISGs, and *IL6* transcriptions during ZIKV infection, confirming that RIG-I is necessary for activation of antiviral immune response. Next, we investigated whether DNA-PKcs is required for activating the IFNs pathways downstream RIG-I during ZIKV infection. We performed a gene expression analysis of IFN-I, IFN-III, and ISGs in A549^{WT} and A549$^{PRKDC-/-}$ cells infected with ZIKV at an m.o.i. 0.1 (Figure 3B) and m.o.i. 1 (Figure 3C). During ZIKV infection we observed a reduction of *IFNL1*, *IFIT1*, and *IFIT2*, but not *IFNB*, *IFIT3*, and *ISG15* transcription in the absence of DNA-PKcs. Similarly, in RPE cells, where ZIKV infection does not induce *IFNL1* transcription, the absence of DNA-PKcs decreased *IFNB* and *IFIT2*, but not *ISG15* transcription (Figure S3A). In addition, proinflammatory gene transcription induced after RIG-I activation such as *IL6* and *NFKBIA* is independent of DNA-PKcs in A549 cells upon ZIKV infection (Figure 3D), but dependent in RPE cells lacking DNA-PKcs (Figure S3B). Altogether, these results suggest crosstalk between RIG-I and DNA-PKcs during ZIKV infection, which results in an efficient antiviral immune response in A549 and RPE cells.

IRF1, IRF3, and p65 nuclear accumulation during ZIKV infection is DNA-PKcs independent

We evaluated the crosstalk between RIG-I and DNA-PKcs during ZIKV infection analyzing the IFN-I/III-inducing transcription factors including IRF1, IRF3, IRF5, IRF7, and p65 (NF-κB subunit) (24, 25, 27, 29–31, 35). We infected A549 cells with ZIKV and measured the accumulation of the transcription factors in the nucleus. We observed that ZIKV infection induces IRF1 and IRF3, but not IRF5 and IRF7 nuclear accumulation (Figures 4A–D and Figures S4A, B). As expected, A549$^{RIGI-/-}$ cells failed to induce IRF3 and IRF1 nuclear accumulation, confirming that RIG-I is the major ZIKV intracellular sensor (Figures 4A, B). However, the activation of the transcription factors was independent of DNA-PKcs, showing a similar nuclear location percentage of IRF3 and IRF1 (Figure 4C, D). Similarly, the induction of p65 nuclei accumulation was independent of DNA-PKcs (Figure 4E). Interestingly, while IRF3 nuclei translocation occurred exclusively in infected cells, we observed that IRF1 accumulation in the nuclei occurred mostly in bystander cells, confirmed by ZIKV dsRNA staining, which shows the early stage of virus infection (Figure S4C). Altogether, these results suggest that upon ZIKV infection, DNA-PKcs is necessary for
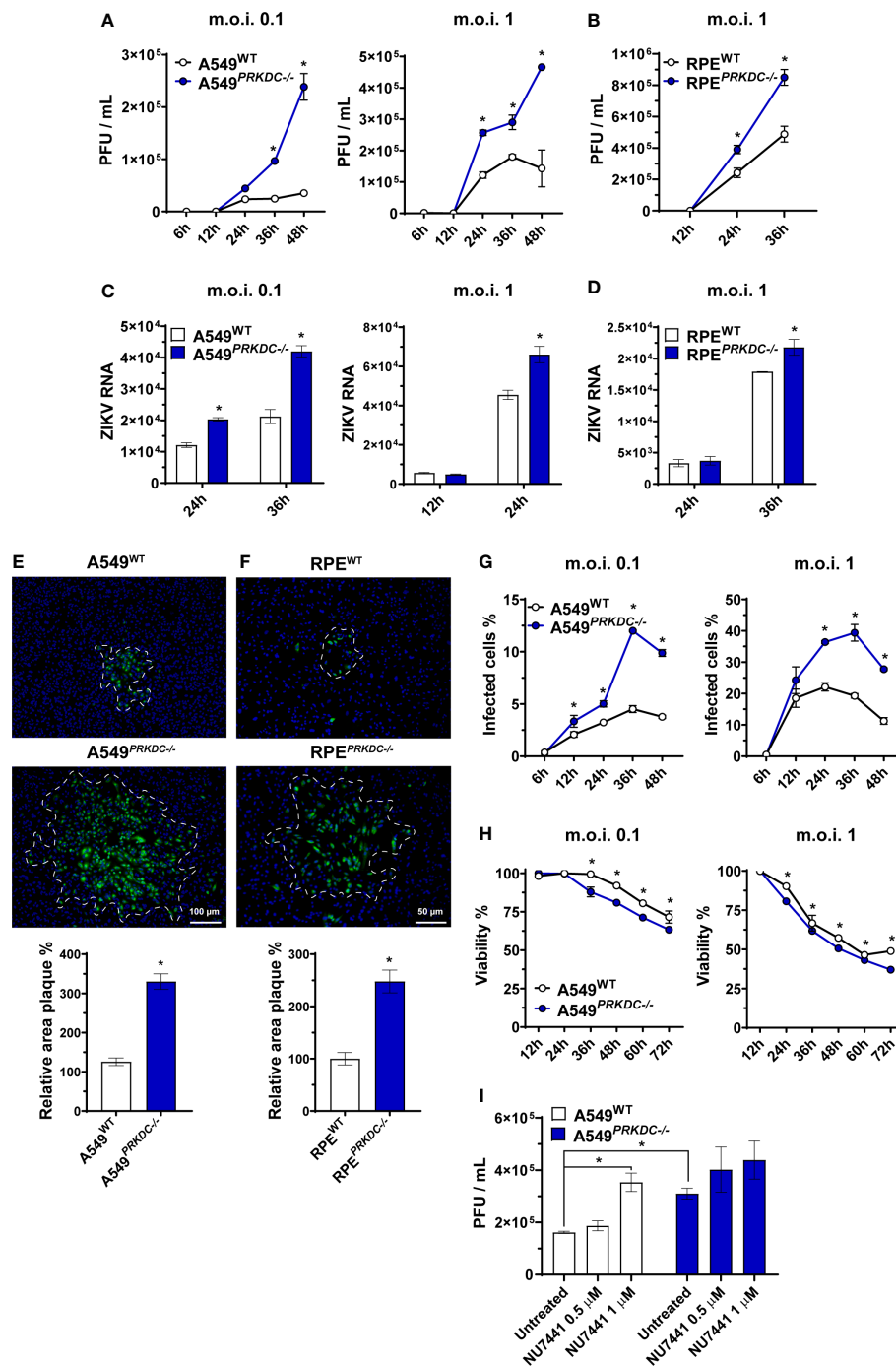
FIGURE 1

DNA-PKcs is critical for control of ZIKV infection. Virus replication measured by plaque assay, expressed as plaque-forming units per mL (PFU/mL), on **(A)** A549^{WT} and A549$^{PRKDC-/-}$ or **(B)** RPE^{WT} and RPE$^{PRKDC-/-}$ cells infected with ZIKV at indicated m.o.i. and time. RT-qPCR analysis to measure ZIKV RNA in **(C)** A549^{WT} and A549$^{PRKDC-/-}$ or **(D)** RPE^{WT} and RPE$^{PRKDC-/-}$ cells infected at indicated m.o.i. and time. **(E)** A549^{WT} and A549$^{PRKDC-/-}$ or **(F)** RPE^{WT} and RPE$^{PRKDC-/-}$ cells infected with 50 PFU of ZIKV at 48 hours in semi-solid medium, then ZIKV-E protein (green) was stained for immunofluorescence analysis, and the relative area of infection percentage was measured using the ImageJ software. The cell nuclei were stained with DAPI (blue). **(G)** Percentage of ZIKV-infected A549^{WT} and A549$^{PRKDC-/-}$ cells at indicated m.o.i. and time, analyzed by flow cytometry. **(H)** Viability analysis by MTT assay of ZIKV-infected A549^{WT} and A549$^{PRKDC-/-}$ cells relative to uninfected cells (mock) at indicated m.o.i. and time. **(I)** A549^{WT} and A549$^{PRKDC-/-}$ were pretreated with NU7441 (0.5 and 1 μM) at 24 hours followed by ZIKV infection (m.o.i. 1) at 24 hours. We used two-way ANOVA with Sidak's correction in **(A–D, G, H)**, and unpaired two-tailed Student's t-test was used in **(E, F)**. * $p < 0.05$, n = 3, error bars $\pm$ SEM.
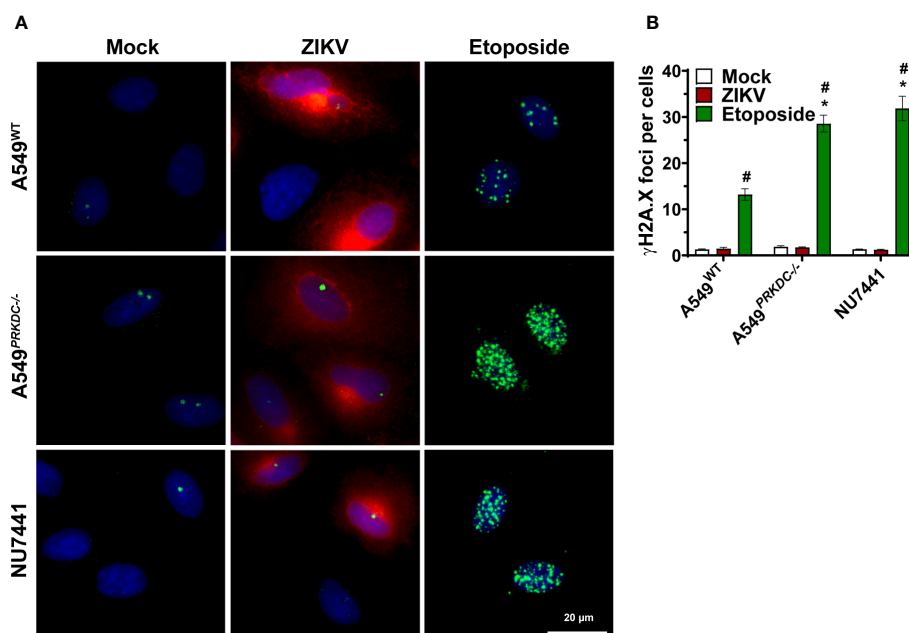
FIGURE 2

ZIKV infection does not induce DSB in A549 cells. A549^{WT}, A549$^{PRKDC-/-}$ and 1 µM NU7441 pre-treated A549^{WT} infected with ZIKV (m.o.i. 1) at 24 hours. Stimulation with 3 µM etoposide for 12 hours was used as a DSB positive control. **(A)** Immunofluorescence to analyze γH2AX (green) in the ZIKV-infected cells (red, ZIKV-E protein). The cell nuclei were stained with DAPI (blue). **(B)** Percentage of γH2AX foci per cell showed in **(A)**. *Compared with WT cells; #Compared with mock. We used two-way ANOVA with Sidak's correction. * or # $p < 0.05$, n = 3, error bars $\pm$ SEM.

enhancement of IFNs and ISGs transcription, acting downstream activation of transcription factors.

Discussion

The DNA-PK complex senses viral DNA with an unknown impact on ZIKV infection. Here we demonstrate that DNA-PKcs, the catalytic subunit of the DNA-PK complex, is critical for control of ZIKV infection by a non-canonical mechanism.

We analyzed different infection profiles such as quantifying viable ZIKV, intracellular ZIKV-RNA, ZIKV spreading to adjacent cells, and ZIKV-infected cells. We showed that absence of DNA-PKcs increases susceptibility to ZIKV infection in two different human epithelial cell lineages, allowing a faster virus spreading. Moreover, we showed that the DNA-PKcs mechanism for controlling ZIKV infection depends on its kinase function. Previous studies have associated DNA-PK complex with infection of flaviviruses. For instance, Vetter et al. (37) demonstrated that Ku70 and Ku80 knockdown in Huh7 cells are insufficient to impact DENV infection, differing from our findings with ZIKV (37). The difference could be explained due to a partial knockdown of the Ku components or the use of different cell lines and flavivirus. In addition, depletion of each DNA-PK subunit

separately varies on number of differentially expressed genes (45). Hence, instead of Ku proteins, only the catalytic subunit may be critical for control of infection.

ZIKV infection induces DSB in human neural stem cells (8, 9), which may implicate DNA-PK activation (46). However, our findings showed that ZIKV does not increase H2A.X phosphorylated foci, a DSB marker, in human epithelial (A549) cells. Hence, ZIKV does not induce DSB in A549 cells, and the role of DNA-PKcs in controlling viral infection is independent of DSB repair response. In addition, we showed that either inhibition of DNA-PKcs kinase function or loss of whole protein has increased DSB sensitivity to etoposide, a genotoxic stressor, as suggested in previous studies (43, 47).

We showed that DNA-PKcs is necessary for an effective antiviral response against ZIKV infection which may explain its role in restricting the infection. The effect of DNA-PKcs on IFN-I and IFN-III transcriptions differs between cell types. Similar to our findings, Vetter et al. (37) demonstrated that inhibition of Ku80 protein expression decreases *IFNB* transcription in DENV-infected cells (37). It is important to notice that DNA-PKcs antiviral response might differ between humans and mice and virus species (19). These could explain why the antiviral response against other RNA viruses is DNA-PKcs independent (14). ZIKV infection might induce mitochondrial DNA release, activating DNA sensors such as DNA-PK or cGAS, which results
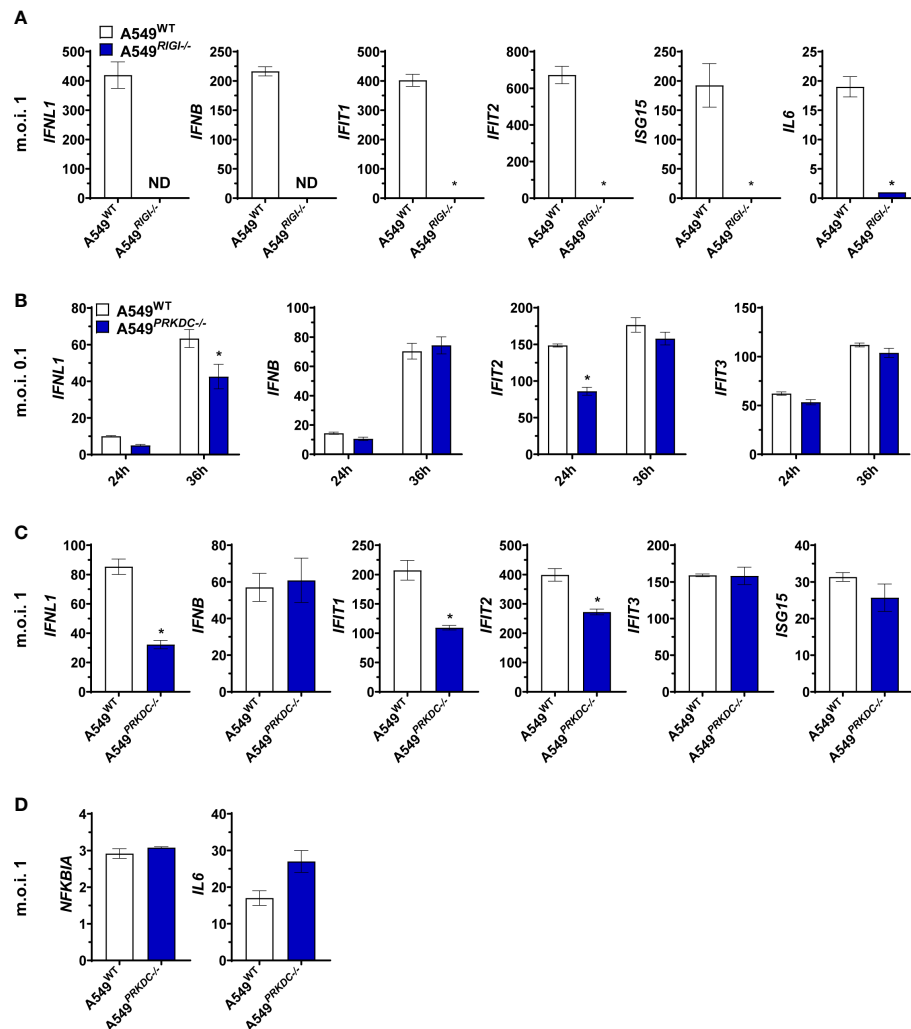
FIGURE 3

DNA-PKcs regulates interferon-related genes during ZIKV infection. **(A)** RT-qPCR to measure the expression of mRNA for indicated genes on A549^{WT} and A549$^{RIGI-/-}$ cells infected with ZIKV m.o.i. 1 for 24 hours. **(B)** RT-qPCR to measure the expression of mRNA for indicated genes on A549^{WT} and A549$^{PRKDC-/-}$ cells infected with ZIKV m.o.i. 0.1 at the indicated time or **(C)** m.o.i. 1 at 24 hours. **(D)** Expression of mRNA for *NFKBIA* and *IL6*, determined by RT-qPCR on A549^{WT} and A549$^{PRKDC-/-}$ cells infected with ZIKV m.o.i. 1 at 24 hours. We used unpaired two-tailed Student's t-test in **(A, C, D)**, and two-way ANOVA with Sidak's correction in **(B)**. ND: Non-detected. * $p<0.05$, n = 3, error bars ± SEM.

in IFN-I and IFN-III transcription (14, 48–50). However, we observed abrogation of the IFNs transcription in A549$^{RIGI-/-}$ cells infected with ZIKV, suggesting only RNA sensing pathway is activated during the infection.

Our data show that ZIKV infection induces nuclear accumulation of the main transcription factors involved in IFN-I and IFN-III transcription independently of DNA-PKcs. These findings implicate that DNA or RNA sensing pathways upstream of the transcription factors are not affected by DNA-PKcs during ZIKV infection. A prior study suggested DNA-PK complex is not required for IRF3 nor p65 nuclear translocation under RNA virus infection or Poly(I:C) stimulation (14).

Furthermore, we showed ZIKV infection fails to induce IRF1 and IRF3 accumulation to the nucleus in absence of the RNA sensor RIG-I, suggesting DNA-PKcs is not a ZIKV sensor receptor. Our findings confirmed that RIG-I is the major nucleic acid sensor activated by ZIKV, as previously demonstrated (33, 34), and suggests novel crosstalk between DNA-PKcs and RIG-I pathway downstream to transcription factors. One possibility is during ZIKV infection, DNA-PKcs acts in the nucleus regulating IFN transcription. The DNA-PK is known to be a regulator of the transcriptome and RNA metabolism (13, 38, 51–55). DNA-PKcs is described to phosphorylate RNA polymerase II, which might enhance the
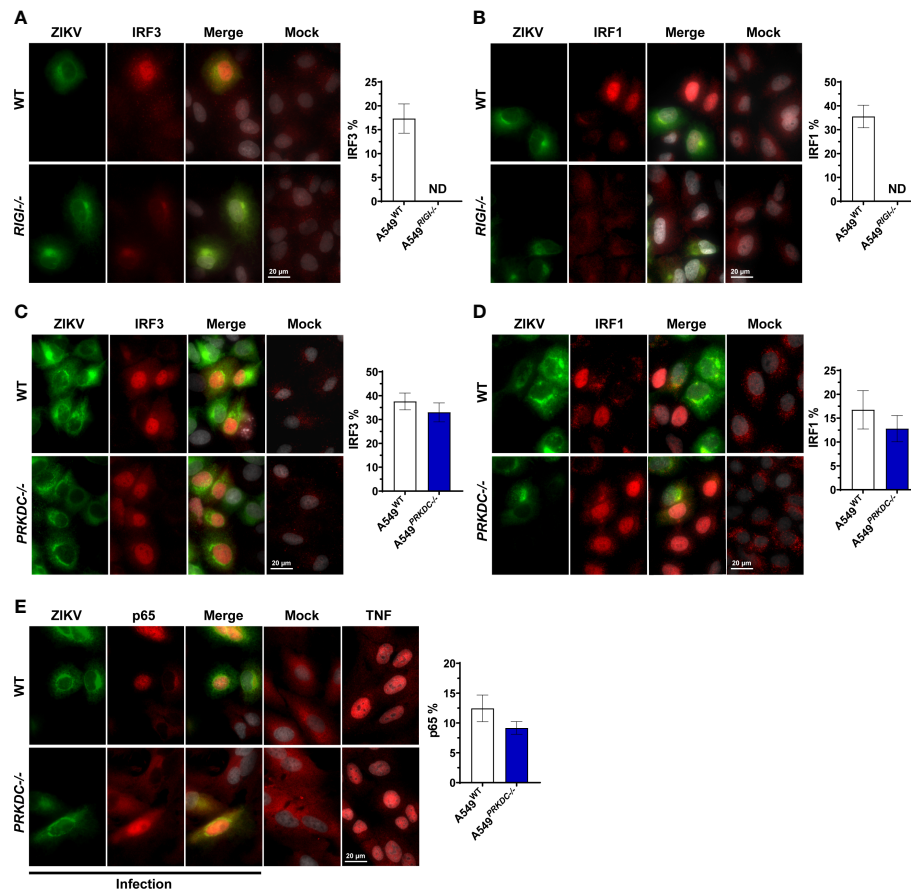
FIGURE 4

ZIKV induces IRF1, IRF3, and p65 nuclei accumulation independent of DNA-PKcs. Immunofluorescence analysis for localization of endogenous **(A)** IRF3 (red) and **(B)** IRF1 (red) on A549^{WT} and A549$^{RIGI-/-}$ cells infected with ZIKV m.o.i. 1 (green, ZIKV-E protein) at 36 hours (left panel), and quantified by scoring cells with nuclear staining (right panel, n = 3, counts of at least 30 nuclei per slide). **(C−E)** Immunofluorescence analysis for localization of endogenous **(C)** IRF3 (red), **(D)** IRF1 (red), and **(E)** p65 (red) on A549^{WT} and A549$^{PRKDC-/-}$ cells infected with ZIKV m.o.i. 1 (green, ZIKV-E protein) at 24 hours (left panel), and quantified by scoring cells with nuclear staining (right panel, n = 3, counts of at least 30 nuclei per slide). TNF was used as a positive control in **(E)**. Cell nuclei were stained with DAPI (grey). We used unpaired two-tailed Student's t-test. N = 3, error bars ± SEM. ND: non-detected.

transcription of some viral genomes such as *Hepatitis B virus* and *Human immunodeficiency virus* (52, 55–57). Genotoxic stress or viral infections such as DENV induce DNA-PKcs localization to the nucleolus, where it acts as a regulator of pre-mRNA splicing (13, 37, 38). The regulation of RNA metabolism by DNA-PKcs should be explored in the future in the context of ZIKV infections.

Overall, these findings provide a role of DNA-PKcs in control of ZIKV virus infection beyond its DNA sensing function or DSB repair response. Future work should consider whether this conclusion can be generalized to different RNA viruses. This study will advance our understanding of the antiviral immune response and may contribute to new therapeutic approaches.

Data availability statement

The original contributions presented in the study are included in the article/Supplementary Materials. Further inquiries can be directed to the corresponding author.

Author contributions

Funding

Acknowledgments

Conflict of interest

The authors declare that the research was conducted in the absence of any commercial or financial relationships that could be construed as a potential conflict of interest.

Publisher's note

All claims expressed in this article are solely those of the authors and do not necessarily represent those of their affiliated organizations, or those of the publisher, the editors and the reviewers. Any product that may be evaluated in this article, or claim that may be made by its manufacturer, is not guaranteed or endorsed by the publisher.

Supplementary material

The Supplementary Material for this article can be found online at: https://www.frontiersin.org/articles/10.3389/fimmu.2022.1042463/full#supplementary-material

References

1. Masmejan S, Musso D, Vouga M, Pomar L, Dashraath P, Stojanov M, et al. Zika virus. *Pathogens* (2020) 9:898. doi: 10.3390/pathogens9110898

2. Cardoso CW, Paploski IAD, Kikuti M, Rodrigues MS, Silva MMO, Campos GS, et al. Outbreak of exanthematous illness associated with zika, chikungunya, and dengue viruses, Salvador, Brazil. *Emerg Infect Dis* (2015) 21:2274–6. doi: 10.3201/eid2112.151167

3. Musso D, Nilles EJ, Cao-Lormeau V-M. Rapid spread of emerging zika virus in the pacific area. *Clin Microbiol Infection* (2014) 20:O595–6. doi: 10.1111/1469-0691.12707

4. Duffy MR, Chen T-H, Hancock WT, Powers AM, Kool JL, Lanciotti RS, et al. Zika virus outbreak on yap island, federated states of Micronesia. *New Engl J Med* (2009) 360:2536–43. doi: 10.1056/NEJMoa0805715

5. Dick GWA, Kitchen SF, Haddow AJ. Zika virus (I). isolations and serological specificity. *Trans R Soc Trop Med Hyg* (1952) 46:509–20. doi: 10.1016/0035-9203(52)90042-4

6. Gulland A. Zika virus is a global public health emergency, declares WHO. *BMJ* (2016) 352:i657. doi: 10.1136/bmj.i657

7. Lazear HM, Diamond MS. Zika virus: New clinical syndromes and its emergence in the Western hemisphere. *J Virol* (2016) 90:4864–75. doi: 10.1128/JVI.00252-16

8. Hammack C, Ogden SC, Madden JC, Medina A, Xu C, Phillips E, et al. Zika virus infection induces DNA damage response in human neural progenitors that enhances viral replication. *J Virol* (2019) 93(20):e00638–19. doi: 10.1128/JVI.00638-19

9. Devhare P, Meyer K, Steele R, Ray RB, Ray R. Zika virus infection dysregulates human neural stem cell growth and inhibits differentiation into neuroprogenitor cells. *Cell Death Dis* (2017) 8:e3106–6. doi: 10.1038/cddis.2017.517

10. Callén E, Jankovic M, Wong N, Zha S, Chen H-T, Difilippantonio S, et al. Essential role for DNA-PKcs in DNA double-strand break repair and apoptosis in ATM-deficient lymphocytes. *Mol Cell* (2009) 34:285–97. doi: 10.1016/j.molcel.2009.04.025

11. Anderson CW. DNA Damage and the DNA-activated protein kinase. *Trends Biochem Sci* (1993) 18:433–7. doi: 10.1016/0968-0004(93)90144-C

12. Nussenzweig A, Chen C, da Costa Soares V, Sanchez M, Sokol K, Nussenzweig MC, et al. Requirement for Ku80 in growth and immunoglobulin V(D)J recombination. *Nature* (1996) 382:551–5. doi: 10.1038/382551a0

13. Abbasi S, Schild-Poulter C. Mapping the Ku interactome using proximity-dependent biotin identification in human cells. *J Proteome Res* (2019) 18:1064–77. doi: 10.1021/acs.jproteome.8b00771

14. Ferguson BJ, Mansur DS, Peters NE, Ren H, Smith GL. DNA-PK is a DNA sensor for IRF-3-dependent innate immunity. *Elife* (2012) 14:1–e00047. doi: 10.7554/eLife.00047

15. Kotula E, Faigle W, Berthault N, Dingli F, Loew D, Sun J-S, et al. DNA-PK target identification reveals novel links between DNA repair signaling and cytoskeletal regulation. *PLoS One* (2013) 8:e80313. doi: 10.1371/journal.pone.0080313

16. Karpova AY, Trost M, Murray JM, Cantley LC, Howley PM. Interferon regulatory factor-3 is an *in vivo* target of DNA-PK. *Proc Natl Acad Sci* (2002) 99:2818–23. doi: 10.1073/pnas.052713899

17. Zhang X, Brann TW, Zhou M, Yang J, Oguariri RM, Lidie KB, et al. Cutting edge: Ku70 is a novel cytosolic DNA sensor that induces type III rather than type I IFN. *J Immunol* (2011) 186:4541–5. doi: 10.4049/jimmunol.1003389

18. Sui H, Zhou M, Imamichi H, Jiao X, Sherman BT, Lane HC, et al. STING is an essential mediator of the Ku70-mediated production of IFN-λ1 in response to exogenous DNA. *Sci Signal* (2017) 10(488):eaah5054. doi: 10.1126/scisignal.aah5054

19. Burleigh K, Maltbaek JH, Cambier S, Green R, Gale M, James RC, et al. Human DNA-PK activates a STING-independent DNA sensing pathway. *Sci Immunol* (2020) 19(430):eaba4219. doi: 10.1126/sciimmunol.aba4219

20. Lanford RE, Guerra B, Lee H, Chavez D, Brasky KM, Bigger CB. Genomic response to interferon-α in chimpanzees: Implications of rapid downregulation for hepatitis c kinetics. *Hepatology* (2006) 43:961–72. doi: 10.1002/hep.21167

21. Schoggins JW, Wilson SJ, Panis M, Murphy MY, Jones CT, Bieniasz P, et al. A diverse range of gene products are effectors of the type I interferon antiviral response. *Nature* (2011) 472:481–5. doi: 10.1038/nature09907

22. Mostafavi S, Yoshida H, Moodley D, LeBoité H, Rothamel K, Raj T, et al. Parsing the interferon transcriptional network and its disease associations. *Cell* (2016) 164:564–78. doi: 10.1016/j.cell.2015.12.032

23. Yoneyama M, Kikuchi M, Matsumoto K, Imaizumi T, Miyagishi M, Taira K, et al. Shared and unique functions of the DExD/H-box helicases RIG-I, MDA5, and LGP2 in antiviral innate immunity. *J Immunol* (2005) 175:2851–8. doi: 10.4049/jimmunol.175.5.2851

24. Dou L, Liang H-F, Geller DA, Chen Y-F, Chen X-P. The regulation role of interferon regulatory factor-1 gene and clinical relevance. *Hum Immunol* (2014) 75:1110–4. doi: 10.1016/j.humimm.2014.09.015

25. Panda D, Gjinaj E, Bachu M, Squire E, Novatt H, Ozato K, et al. IRF1 maintains optimal constitutive expression of antiviral genes and regulates the early antiviral response. *Front Immunol* (2019) 10:1019. doi: 10.3389/fimmu.2019.01019

26. Au WC, Moore PA, Lowther W, Juang YT, Pitha PM. Identification of a member of the interferon regulatory factor family that binds to the interferon-stimulated response element and activates expression of interferon-induced genes. *Proc Natl Acad Sci* (1995) 92:11657–61. doi: 10.1073/pnas.92.25.11657

27. Juang Y-T, Lowther W, Kellum M, Au W-C, Lin R, Hiscott J, et al. Primary activation of interferon a and interferon b gene transcription by interferon regulatory factor 3. *Proc Natl Acad Sci* (1998) 95:9837–42. doi: 10.1073/pnas.95.17.9837

28. Lin R, Heylbroeck C, Pitha PM, Hiscott J. Virus-dependent phosphorylation of the IRF-3 transcription factor regulates nuclear translocation, transactivation potential, and proteasome-mediated degradation. *Mol Cell Biol* (1998) 18:2986–96. doi: 10.1128/MCB.18.5.2986

29. Marie I, Durbin J, Levy D. Differential viral induction of distinct interferon-alpha genes by positive feedback through interferon regulatory factor-7. *EMBO J* (1998) 17:6660–9. doi: 10.1093/emboj/17.22.6660

30. Andrilenas KK, Ramlall V, Kurland J, Leung B, Harbaugh AG, Siggers T. DNA-Binding landscape of IRF3, IRF5 and IRF7 dimers: implications for dimer-specific gene regulation. *Nucleic Acids Res* (2018) 46:2509–20. doi: 10.1093/nar/gky002

31. Barnes BJ, Moore PA, Pitha PM. Virus-specific activation of a novel interferon regulatory factor, IRF-5, results in the induction of distinct interferon α genes. *J Biol Chem* (2001) 276:23382–90. doi: 10.1074/jbc.M101216200

32. Visvanathan K v, Goodbourn S. Double-stranded RNA activates binding of NF-kappa b to an inducible element in the human beta-interferon promoter. *EMBO J* (1989) 8:1129–38. doi: 10.1002/j.1460-2075.1989.tb03483.x

33. Chazal M, Beauclair G, Gracias S, Najburg V, Simon-Lorière E, Tangy F, et al. RIG-I recognizes the 5′ region of dengue and zika virus genomes. *Cell Rep* (2018) 24:320–8. doi: 10.1016/j.celrep.2018.06.047

34. Schilling M, Bridgeman A, Gray N, Hertzog J, Hublitz P, Kohl A, et al. RIG-I plays a dominant role in the induction of transcriptional changes in zika virus-infected cells, which protect from virus-induced cell death. *Cells* (2020) 9:1476. doi: 10.3390/cells9061476

35. Lenardo MJ, Fan C-M, Maniatis T, Baltimore D. The involvement of NF-κB in β-interferon gene regulation reveals its role as widely inducible mediator of signal transduction. *Cell* (1989) 57:287–94. doi: 10.1016/0092-8674(89)90966-5

36. Levy DE, Kessler DS, Pine R, Reich N, Darnell JE. Interferon-induced nuclear factors that bind a shared promoter element correlate with positive and negative transcriptional control. *Genes Dev* (1988) 2:383–93. doi: 10.1101/gad.2.4.383

37. Vetter ML, Rodgers MA, Patricelli MP, Yang PL. Chemoproteomic profiling identifies changes in DNA-PK as markers of early dengue virus infection. *ACS Chem Biol* (2012) 7:2019–26. doi: 10.1021/cb300420z

38. Liu S, Shao Y, Wang Q, Zhai Y, Li X. Genotoxic stress causes the accumulation of DNA-dependent protein kinase catalytic subunit phosphorylated at serine 2056 at nuclear speckles and alters pre- mRNA alternative splicing. *FEBS Open Bio* (2019) 9:304–14. doi: 10.1002/2211-5463.12569

39. Miao M, Yu F, Wang D, Tong Y, Yang L, Xu J, et al. Proteomics profiling of host cell response *via* protein expression and phosphorylation upon dengue virus infection. *Virol Sin* (2019) 34:549–62. doi: 10.1007/s12250-019-00131-2

40. Ooi YS, Majzoub K, Flynn RA, Mata MA, Diep J, Li JK, et al. An RNA-centric dissection of host complexes controlling flavivirus infection. *Nat Microbiol* (2019) 4:2369–82. doi: 10.1038/s41564-019-0518-2

41. Strottmann DM, Zanluca C, Mosimann ALP, Koishi AC, Auwerter NC, Faoro H, et al. Genetic and biological characterisation of zika virus isolates from different Brazilian regions. *Mem Inst Oswaldo Cruz* (2019) 114:e190150. doi: 10.1590/0074-02760190150

42. Leahy JJJ, Golding BT, Griffin RJ, Hardcastle IR, Richardson C, Rigoreau L, et al. Identification of a highly potent and selective DNA-dependent protein kinase

(DNA-PK) inhibitor (NU7441) by screening of chromenone libraries. *Bioorg Med Chem Lett* (2004) 14:6083–7. doi: 10.1016/j.bmcl.2004.09.060

43. Zhao Y, Thomas HD, Batey MA, Cowell IG, Richardson CJ, Griffin RJ, et al. Preclinical evaluation of a potent novel DNA-dependent protein kinase inhibitor NU7441. *Cancer Res* (2006) 66:5354–62. doi: 10.1158/0008-5472.CAN-05-4275

44. Morales AJ, Carrero JA, Hung PJ, Tubbs AT, Andrews JM, Edelson BT, et al. A type I IFN-dependent DNA damage response regulates the genetic program and inflammasome activation in macrophages. *Elife* (2017) 6:e24655. doi: 10.7554/eLife.24655

45. Shadrina O, Garanina I, Anisenko A, Kireev I, Gottikh M. Transcriptome analysis of HEK 293T cells revealed different significance of the depletion of DNA-dependent protein kinase subunits, Ku70, Ku80, and DNA-PKcs. *Biochimie* (2022) 199:139–49. doi: 10.1016/j.biochi.2022.04.004

46. Gu Y, Jin S, Gao Y, Weaver DT, Alt FW. Ku70-deficient embryonic stem cells have increased ionizing radiosensitivity, defective DNA end-binding activity, and inability to support V(D)J recombination. *Proc Natl Acad Sci* (1997) 94:8076–81. doi: 10.1073/pnas.94.15.8076

47. Yang L, Yang X, Tang Y, Zhang D, Zhu L, Wang S, et al. Inhibition of DNA-PK activity sensitizes A549 cells to X-ray irradiation by inducing the ATM-dependent DNA damage response. *Mol Med Rep* (2018) 17(6):7545–7552. doi: 10.3892/mmr.2018.8828

48. Sun L, Wu J, Du F, Chen X, Chen ZJ. Cyclic GMP-AMP synthase is a cytosolic DNA sensor that activates the type I interferon pathway. *Sci (1979)* (2013) 339:786–91. doi: 10.1126/science.1232458

49. White MJ, McArthur K, Metcalf D, Lane RM, Cambier JC, Herold MJ, et al. Apoptotic caspases suppress mtDNA-induced STING-mediated type I IFN production. *Cell* (2014) 159:1549–62. doi: 10.1016/j.cell.2014.11.036

50. West AP, Khoury-Hanold W, Staron M, Tal MC, Pineda CM, Lang SM, et al. Mitochondrial DNA stress primes the antiviral innate immune response. *Nature* (2015) 520:553–7. doi: 10.1038/nature14156

51. Zhang S, Schlott B, Görlach M, Grosse F. DNA-Dependent protein kinase (DNA-PK) phosphorylates nuclear DNA helicase II/RNA helicase a and hnRNP proteins in an RNA-dependent manner. *Nucleic Acids Res* (2004) 32:1–10. doi: 10.1093/nar/gkg933

52. Dvir A, Peterson SR, Knuth MW, Lu H, Dynan WS. Ku Autoantigen is the regulatory component of a template-associated protein kinase that phosphorylates RNA polymerase II. *Proc Natl Acad Sci* (1992) 89:11920–4. doi: 10.1073/pnas.89.24.11920

53. Song Z, Xie Y, Guo Z, Han Y, Guan H, Liu X, et al. Genome-wide identification of DNA-PKcs-associated RNAs by RIP-seq. *Signal Transduct Target Ther* (2019) 4:22. doi: 10.1038/s41392-019-0057-6

54. Song L, Yu M, Jin R, Gu M, Wang Z, Hou D, et al. Long-read sequencing annotation of the transcriptome in DNA-PK inactivated cells. *Front Oncol* (2022) 12:941638. doi: 10.3389/fonc.2022.941638

55. Peterson SR, Jesch SA, Chamberlin TN, Dvir A, Rabindran SK, Wu C, et al. Stimulation of the DNA-dependent protein kinase by RNA polymerase II transcriptional activator proteins. *J Biol Chem* (1995) 270:1449–54. doi: 10.1074/jbc.270.3.1449

56. Zicari S, Sharma AL, Sahu G, Dubrovsky L, Sun L, Yue H, et al. DNA Dependent protein kinase (DNA-PK) enhances HIV transcription by promoting RNA polymerase II activity and recruitment of transcription machinery at HIV LTR. *Oncotarget* (2020) 11:699–726. doi: 10.18632/oncotarget.27487

57. Fan Y, Liang Y, Liu Y, Fan H. PRKDC promotes hepatitis b virus transcription through enhancing the binding of RNA pol II to cccDNA. *Cell Death Dis* (2022) 13:404. doi: 10.1038/s41419-022-04852-3

The endoplasmic reticulum stress sensor IRE1α modulates macrophage metabolic function during *Brucella abortus* infection

Erika S. Guimarães[1,2], Marco Túlio R. Gomes[2],
Rodrigo C. O. Sanches[2], Kely Catarine Matteucci[3,4],
Fábio V. Marinho[2] and Sergio C. Oliveira[2,5]*

[1]Departamento de Genética, Ecologia e Evolução, Programa de Pós-Graduação em Genética, Instituto de Ciências Biológicas, Universidade Federal de Minas Gerais, Belo Horizonte, Minas Gerais, Brazil, [2]Departamento de Bioquímica e Imunologia, Instituto de Ciências Biológicas, Universidade Federal de Minas Gerais, Belo Horizonte, Minas Gerais, Brazil, [3]Departamento de Bioquímica e Imunologia, Faculdade de Medicina de Ribeirão Preto, Universidade de São Paulo, Ribeirão Preto, Brazil, [4]Plataforma de Medicina Translacional Fundação Oswaldo Cruz/Faculdade de Medicina de Ribeirão Preto, Universidade de São Paulo, Ribeirão Preto, Brazil, [5]Departamento de Imunologia, Instituto de Ciências Biomédicas, Universidade de São Paulo, São Paulo, Brazil

Endoplasmic reticulum (ER) stress plays a major role in several inflammatory disorders. ER stress induces the unfolded protein response (UPR), a conserved response broadly associated with innate immunity and cell metabolic function in various scenarios. *Brucella abortus*, an intracellular pathogen, triggers the UPR *via* Stimulator of interferon genes (STING), an important regulator of macrophage metabolism during *B. abortus* infection. However, whether ER stress pathways underlie macrophage metabolic function during *B. abortus* infection remains to be elucidated. Here, we showed that the UPR sensor inositol-requiring enzyme 1α (IRE1α) is as an important component regulating macrophage immunometabolic function. In *B. abortus* infection, IRE1α supports the macrophage inflammatory profile, favoring M1-like macrophages. IRE1α drives the macrophage metabolic reprogramming in infected macrophages, contributing to the reduced oxidative phosphorylation and increased glycolysis. This metabolic reprogramming is probably associated with the IRE1α-dependent expression and stabilization of hypoxia-inducible factor-1 alpha (HIF-1α), an important molecule involved in cell metabolism that sustains the inflammatory profile in *B. abortus*-infected macrophages. Accordingly, we demonstrated that IRE1α favors the generation of mitochondrial reactive oxygen species (mROS) which has been described as an HIF-1α stabilizing factor. Furthermore, in infected macrophages, IRE1α

drives the production of nitric oxide and the release of IL-1β. Collectively, these data unravel a key mechanism linking the UPR and the immunometabolic regulation of macrophages in *Brucella* infection and highlight IRE1α as a central pathway regulating macrophage metabolic function during infectious diseases.

Introduction

The Endoplasmic reticulum (ER) is a central organelle responsible for synthesis, processing, and folding of secreted and transmembrane proteins. Physiologic stresses, such as increased secretory load, or pathological stresses, such as inflammatory challenges, cause an imbalance between protein load and the ER folding capacity, resulting in accumulation of misfolded proteins [1].Thenceforward, ER stress can induce the unfolded protein response (UPR), a physiological response aimed to restore ER homeostasis and preserve cellular functions [2, 3]. The UPR consists of three major signaling pathways, activated by protein sensors: PKR-like ER kinase (PERK), activating transcription factor 6α (ATF6) and inositol-requiring enzyme 1α (IRE1α) [4]. IRE1α, the most conserved UPR stress sensor, has been involved in a variety of cellular processes [5, 6], being considered a metabolic stress sensor and broadly associated with several metabolic disorders [6, 7].

Brucella, the etiologic agent of brucellosis, the most prevalent bacterial zoonosis worldwide [8], induces the UPR upon trafficking to the ER [9–11]. Moreover, we and others have shown that *Brucella* infection activates the IRE1α axis of the UPR [9, 11, 12]. Remarkably, full UPR induction during *B. abortus* infection in macrophages requires Stimulator of interferon genes (STING) [9]. STING is an ER-transmembrane protein that was recently implicated in the metabolic reprogramming of *Brucella*-infected macrophages [13]. Nevertheless, the possible interaction between the UPR and macrophage metabolic function in *Brucella* infection is poorly understood.

Macrophage metabolic reprogramming refers to the process whereby macrophages phenotypically mount a specific functional response to distinct microenvironment stimuli and signals. In this regard, macrophage polarization is not fixed [14], and two distinct populations, inflammatory M1 and anti-inflammatory M2 macrophages, represent the opposing ends of the full spectrum of macrophage polarization. Macrophages that display the M1 phenotype express various pro-inflammatory components such as nitric oxide (NO) and reactive oxygen species (ROS). By contrast, M2 phenotype macrophages are associated with generation of interleukin (IL)-10 and relate with tissue remodeling and wound healing [15]. Regarding cellular metabolism, M1 macrophages energy production shifts from mitochondrial oxidative phosphorylation (OXPHOS) to glycolysis to support macrophage function [16]. Our group recently demonstrated that the macrophage metabolic reprogramming during *B. abortus* infection is regulated by STING *via* HIF-1α [13], a global regulator of cellular metabolism that sustains the inflammatory phenotype in macrophages [17]. Therefore, we aimed to determine the role of the UPR in mediating macrophage metabolic function in *B. abortus* infection. Here, we defined that IRE1α supports the inflammatory profile in macrophages and modulates its metabolic function. Notably, IRE1α is important for the metabolic shift from OXPHOS to an enhanced glycolytic metabolism that occurs upon *B. abortus* infection. Furthermore, IRE1α induces the generation of mitochondrial ROS (mROS) and HIF-1α stabilization. Additionally, IRE1α enhances canonical and non-canonical inflammasome activation, IL-1β release, NO production and cytokine secretion in infected macrophages, supporting the inflammatory profile in macrophages.

Material and methods

Mice

C57BL/6 animals were obtained from the Federal University of Minas Gerais (UFMG). HIF-1α conditional knockout mice in their myeloid cell lineage, termed here as HIF-1α KO (LysM-Cre$^{+/-}$/HIF-1α$^{fl/fl}$); HIF-1α-non-deletable littermate controls negative for Cre recombinase, termed here as HIF-1α WT (LysM-Cre$^{-/-}$/HIF-1α$^{fl/fl}$), were donated by Dr. Jose Carlos Alves-Filho (Ribeirão Preto Medical School, University of Sao Paulo, Brazil). Animals were maintained at UFMG and used at 6-8 weeks of age. All animal experiments were conducted in agreement with the Brazilian Federal Law number 11,794 and were preapproved by the Institutional Animal Care and Use Committee of the Federal University of Minas Gerais (CEUA no. 87/2017).

Bacterial strain

Brucella abortus virulent strain S2308 was acquired from our laboratory collection. Prior to infection, *Brucella* was grown in *Brucella* broth medium (BD Pharmingen, San Diego, CA) under constant agitation for 3 days at 37°C.

Bone marrow-derived macrophages

Bone marrow-derived macrophages (BMDMs) were generated as previously described, with some adaptations (18). Briefly, bone marrow cells from tibias and femurs were isolated and differentiated in DMEM (Gibco/Thermo Fisher Scientific, Waltham, MA) supplemented with 20% LCCM, 10% fetal bovine serum (FBS) (Life Technologies, Carlsbad, CA), 100 U/ml penicillin-streptomycin (Life Technologies), 1% HEPES (Life Technologies) at 37°C in 5% CO_2 for 7 days until use. Then, unless otherwise specified, 5 x 10^5 macrophages were seeded in 24 wells culture plates and cultivated in DMEM supplemented with 10% FBS, 100 U/ml penicillin-streptomycin and 1% HEPES at 37°C in 5% CO_2.

UPR treatment and macrophage infection with *Brucella*

Macrophages were treated with 1 µg/mL of the ER stress inducer Tunicamycin (Sigma-Aldrich, St. Louis, MO) for 6 hrs (9). Where indicated, macrophages were pretreated with 50 µM 4µ8c (Sigma-Aldrich) for 30 min (9), with 1mM of 2-DG (Sigma-Aldrich) for 4 hrs (13) or with 0.5 mM Mito-TEMPO (Sigma-Aldrich), an mitochondrial superoxide scavenger, for 1 hr (19). Then, macrophages were infected *in vitro* with *B. abortus* in DMEM (5.5 mM glucose, 2 mM L-glutamine and no pyruvate) supplemented with 1% FBS for 24 h at 37°C in 5% CO_2 at the multiplicity of infection (MOI) of 100:1, as previously described (13). Cellular lysates and culture supernatants were collected and stored at -80°C.

Knockdown *via* small interfering RNA

BMDMs were transfected with small interfering RNA (siRNA) from siGENOME SMARTpools (Dharmacon, Lafayette, CO), according to the manufacturer's instructions, using the GenMute siRNA transfection reagent (SignaGen Laboratories, Rockville, MD). Since IRE1α is ubiquitously expressed, the X-box binding protein 1 (XBP1) is a specific downstream target of the activation of the IRE1α axis of the UPR (20) used to asses IRE1α activation. Therefore, siGENOME SMARTpool siRNAs specific for mouse XBP1 (M-040825-00-0005) (siXBP1) and a control siRNA pool (D-001206-14-05) (siCNT) were used in this study. Forty-six hours after siRNA transfection, cells were infected with *B. abortus* as described above. Cellular lysates and culture supernatants were collected and stored at -80°C.

qPCR analysis

Samples were resuspended in TRIzol (Invitrogen, Carlsbad, CA) to isolate total RNA in conformity with the manufacturer's instructions. Genomic DNA was removed from total RNA by treatment with DNase I (Invitrogen). According to the manufacturer's guidelines, reverse transcription of 1 µg of total RNA was performed using the Illustra Ready-To-Go RT-PCR Beads (GE Healthcare, Chicago, IL). Real-time RT-PCR was performed using SYBR Green PCR master mix (Applied Biosystems, Foster City, CA) on a QuantStudio3 real-time PCR instrument (Applied Biosystems), using the following parameters: 60°C for 10 min, 95°C for 10 min, 40 cycles of 95°C for 15 sec, and 60°C for 1 min, and a dissociation stage of 95°C for 15 sec, 60°C for 1 min, 95°C for 15 sec, and 60°C for 15 sec. The proper primers were used to amplify a specific fragment corresponding to specific gene targets as described: NOS2 forward: 5'- AGCACTTTGGGTGACCACCAGGA-3', NOS2 reverse: 5'-AGCTAAGTATTAGAGCGGCGGCA-3'; IL-6 forward: 5'-CAGAATTGCCATCGTACAACTCTTTTC-3', IL-6 reverse: 5'-AAGTGCATCATCGTTGTTCATACA-3'; TGF-β forward: 5'-CGCCATCTATGAGAAAACC-3', TGF-β reverse: 5'-GTAACGCCAGGAATTGT-3'; YM1 forward: 5'-GGG CATACCTTTATCCTGAG-3', YM1 reverse: 5'-CCA CTGAAGTCATCCATGTC-3'; GLUT1 forward: 5'-GCT GTGCTTATGGGCTTCTC-3', GLUT1 reverse: 5'-CACATACATGGGCACAAAGC-3'; HIF-1α forward: 5'-GG GTACAAGAAACCACCCAT-3', HIF-1α reverse: 5'-GAGG CTGTGTCGACTGAGAA-3', and β-actin forward: 5'-GGCTGTATTCCCCTCCATCG-3', β-actin reverse: 5'-CCAGTTGGTAACAATGCCATGT-3'. The threshold cycle method was used to analyze all data. Data were analyzed as relative expression after normalization to the *β-actin* gene and fold changes are normalized to the non-infected. All measurements were conducted in triplicate.

Cytokine measurements and nitric oxide assay

IL-6, IL-12, IL-1β, and TNF-α production in macrophages supernatants was assessed using ELISA (R&D systems, Minneapolis, MN), according to the manufacturer's specifications. The NO assay was performed as previously described (21).

Seahorse glycolytic rate analysis

The glycolytic profile of cells was assessed using the Extracellular Flux Analyzer XF96 (Agilent, Santa Clara, CA), as previously described (13). Briefly, 1×10^5 macrophages were seeded per well on a Seahorse XF96 cell culture microplate and allowed to attach overnight. The next day, cells were treated or not with 50μM 4μ8c and infected or not with *B. abortus* for 24 hrs in culture medium. Proton efflux rate (PER), extracellular acidification rate (ECAR) and oxygen consumption rate (OCR) were determined using the Glycolytic Rate Assay Kit (Agilent) in accordance with the manufacturer's instructions and as previously described (13). The Seahorse XF DMEM medium pH 7.4 (Agilent), supplemented with 4 mM L-glutamine, 2 mM pyruvate and 25 mM glucose was used during the assay. Experiments were executed in 5 replicates for each condition. MitoPER and glycoPER were calculated as previously described (13, 22).

Measurement of mitochondrial reactive oxygen species

mROS were detected using MitoSOX Red (Invitrogen), a fluorescent dye specific for the detection of O_2^- in the mitochondria. For confocal microscopy, MitoSOX Red staining evaluation was performed similarly as previously described (19). Briefly, 1×10^5 macrophages were added on glass coverslips and non-infected or infected with *B. abortus* for 3 hrs or pre-treated with 50μM 4μ8c for 30 min and then infected with *B. abortus* for 3 hrs. Subsequently, cells were incubated with MitoSOX Red at a final concentration of 2.5 mM for 5 min, washed with Phosphate Buffered Saline (PBS) (Gibco), fixed with 4% formaldehyde, and washed once more with Phosphate Buffered Saline (PBS) (Gibco). Then, glass coverslips were mounted with Prolong Gold Antifade with DAPI (Invitrogen) and visualized by fluorescence microscopy, using equal settings. Three coverslips were analyzed per condition and representative images were taken using an ×40 objective using a Nikon A1 confocal microscope. The mean fluorescence intensity (MFI) for MitoSOX Red staining reflects mean fluorescence intensity x cell area and was quantified per whole cell. MFI was measured using ImageJ Software.

Generation of mROS was additionally evaluated by flow cytometry in macrophages as previously described (13). Briefly, macrophages were added to microcentrifuge tubes at a cell density of 5×10^5. Then, cells were treated were indicated with 50μM 4μ8c for 30 min or with 0.5mM Mito-TEMPO for 1 hr and then infected or not with *B. abortus* for 1 hr. Then, cells were washed and resuspended in 200 μL PBS per microtube and transferred to a 96-well plate. mROS generation was assessed by flow cytometry using Attune Acoustic Focusing equipment (Life

Technologies) and results were evaluated using FlowJo software. The data is expressed as MitoSOX Red median fluorescence intensity (MFI) fold change; particularly, mROS production by infected cells was relativized to mROS production by non-infected cell for each group, as previously described (13).

Western blot analysis

Macrophages were lysed using the M-PER Mammalian Protein Extraction Reagent (Thermo Fisher Scientific) with 1:100 protease inhibitors (Sigma-Aldrich). Protein concentrations from macrophage lysates were determined by BCA assay and identical amounts of supernatants or lysates were loaded onto 12% or 15% SDS-polyacrylamide gel and transferred to nitrocellulose membranes (Amersham Biosciences) according to standard protocols. Membranes were treated for 1 hr in Tris-buffered saline (TBS) containing 0.1% Tween-20 containing 5% nonfat dry milk and incubated overnight with primary antibodies at 4°C, as previously described (13). Primary antibodies used are the following: a monoclonal antibody against IL-1β (clone 3A6, Cell Signaling Technology), a monoclonal antibody against HIF-1α (clone D1S7W, Cell Signaling Technology, Danvers, MA), a monoclonal antibody against caspase-11 (clone Flamy-1, Adipogen, San Diego, CA), a monoclonal antibody against gasdermin D (clone EPR19828, Abcam, Cambridge, U.K.), and a monoclonal antibody against the p20 subunit of caspase-1 (clone Casper-1, Adipogen), all at a 1:1000 dilution. A mouse monoclonal anti–β-actin (clone 13E5, Cell Signaling Technology) at a 1:5000 dilution was used as loading control. The blots were washed in TBS with 0.1% Tween 20 and incubated for 1 hr at 25°C with the suitable HRP-conjugated secondary antibody at a 1:1000 dilution. The bands were visualized in an Amersham Imager 600 (GE Healthcare) using Luminol chemiluminescent HRP substrate (Millipore).

Lactate dehydrogenase release assay

The lactate dehydrogenase (LDH) enzyme activity was detected according to the manufacturer's recommendations using a CytoTox96 LDH release kit (Promega, Madison, WI).

Statistical analysis

Data analyses were performed using Student's *t*- test, one-way ANOVA, or two-way ANOVA, as indicated, using GraphPad Prism 9 (GraphPad Software, San Diego, CA). A p value <0.05 (p<0.05) was considered statistically significant.

Results

The unfolded protein response supports the inflammatory profile in macrophages

UPR signaling has been extensively associated with inflammatory responses in various settings (23, 24). Therefore, we investigated whether UPR regulates macrophage polarization i.e., the macrophage profile typically associated with an inflammatory (M1) or anti-inflammatory (M2) profile. Quantitative real-time RT-PCR analysis demonstrated that treatment of macrophages with Tunicamycin, a potent ER stress inducer, enhanced the expression of the inflammatory macrophage-related markers, NOS2 (inducible nitric oxide synthase) and IL-6 (Figure 1A). Remarkably, treatment with Tunicamycin did not alter the expression of anti-inflammatory markers such as, YM1 (chitinase-like 3) and TGF-β (transforming growth factor beta) compared to non-treated macrophages (Figure 1B). These results indicate that Tunicamycin-induced UPR favors macrophage polarization towards an inflammatory profile.

Considering that the UPR has been extensively described as crucial for inducing an appropriate inflammatory response during *Brucella* infection (9, 10, 25), we investigated whether the IRE1α axis of the UPR contributes to macrophage polarization. Inhibition of IRE1α by pre-treatment with 4μ8c (4-methyl umbelliferone 8-carbaldehyde), a potent and selective IRE1α inhibitor (26), reduced the expression of the inflammatory macrophage-related markers, NOS2 and IL-6 in *B. abortus*-infected macrophages (Figure 1C). Meanwhile, IRE1α inhibition did not alter the expression of the anti-inflammatory macrophage-related markers, YM1 and TGF-β in infected macrophages (Figure 1D).

Corroborating these results, knockdown of XBP1 [a specific downstream target of the activation of the IRE1α axis of the UPR (20)], *via* small interfering RNA, also reduced the expression of the inflammatory macrophage-related markers, NOS2 and IL-6, in *B. abortus*-infected macrophages compared to the control infected with *B. abortus* (Figure 1E), and did not alter the expression of the anti-inflammatory macrophage-related markers, YM1 and TGF-β, in infected macrophages (Figure 1F). Altogether, these results demonstrate that IRE1α modulates macrophage polarization, favoring the induction of inflammatory macrophages during *B. abortus* infection.

The unfolded protein response modulates the inflammatory response in macrophages

ER stress is strongly associated with the immune signaling response to invading microorganisms (20). Given that the UPR regulates macrophage polarization during *B. abortus* infection, we evaluated cytokine secretion in *Brucella*-infected macrophages pre-treated with 4μ8c or transfected with small interfering RNA. Inhibition of IRE1α impaired IL-6 (Figure 2A) and IL-12 (Figure 2B) secretion and NO production (Figure 2C), inflammatory mediators typically associated with inflammatory macrophages (14), whereas TNF-α secretion was unaltered (Figure 2D). Furthermore, XBP1 silencing likewise reduced IL-6 (Figure 2E) and IL-12 (Figure 2F) secretion and NO production (Figure 2G), whereas TNF-α secretion was unaltered (Figure 2H). These results indicate that IRE1α has an important role in inducing pro-inflammatory responses during *B. abortus* infection.

The metabolic reprogramming in infected macrophages is IRE1α-dependent

Macrophage polarization is closely associated with the metabolic rewiring required to sustain macrophage biological functions (16). Moreover, IRE1α senses cellular metabolic stressful conditions acting to sustain metabolic homeostasis (7). Therefore, we evaluated the role of the IRE1α in the metabolic function of macrophages in *Brucella* infection using a glycolytic rate assay. In that context, the glycolytic acidification was determined by calculating the glycolytic proton efflux rate (glycoPER) as previously described (13). The time-course measurements of glycoPER showed that macrophages infected with *B. abortus* displayed a higher proton flux rate due to the glycolytic acidification compared to non-infected macrophages (Figure 3A). The reduction of proton flux rate achieved after addition of the inhibitor 2-deoxy-D-glucose (2-DG) confirms that this acidification is provided by the glycolytic pathway (Figure 3A). In addition, we calculated the basal glycolysis levels, which were determined before OXPHOS blockage by rotenone and antimycin A, and the compensatory glycolysis levels, that were observed after OXPHOS inhibition. We demonstrated that *B. abortus* infection increased basal and compensatory glycolysis. Markedly, our results revealed that inhibition of IRE1α reduced the basal and compensatory glycolysis when compared to non-treated infected macrophages (Figure 3B). Moreover, we evaluated the acidification rate derived from the CO_2 produced entirely by the mitochondria (mitoPER) as previously described (13) to evaluate OXPHOS. Remarkably, our results indicate that the decrease in OXPHOS induced by *B. abortus* occurs in an IRE1α-dependent manner as IRE1α inhibition restored OXPHOS to levels similar to non-infected cells (Figure 3C). Together these results indicate that IRE1α participates in the metabolic reprogramming of macrophages and is crucial for the increase in glycolysis and the reduction in OXPHOS observed during *Brucella* infection, distinctive metabolic features of inflammatory macrophages (16).
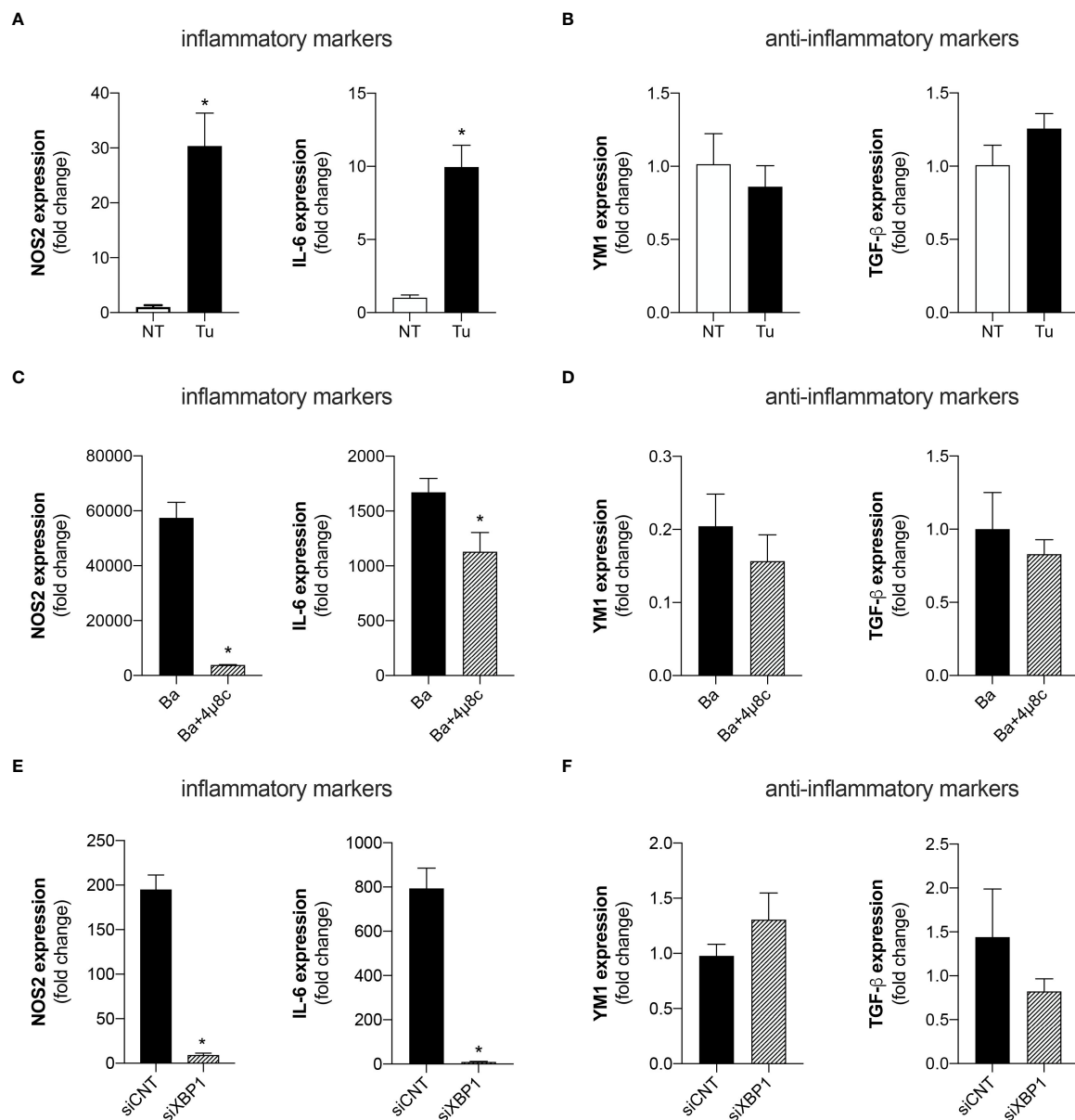
FIGURE 1

The UPR favors the polarization of inflammatory macrophages. **(A)** NOS2 and IL-6 expression levels determined by real-time PCR in macrophages from C57BL/6 mice non-treated (NT) or treated with Tunicamycin (Tu) (1 μg/mL). **(B)** YM1 and TGF-β expression levels determined by real-time PCR in macrophages from C57BL/6 mice non-treated (NT) or treated with Tunicamycin (Tu) (1 μg/mL). **(C)** NOS2 and IL-6 expression levels determined by real-time PCR in macrophages from C57BL/6 mice infected with *B abortus* (Ba) or pre-treated with 4μ8c (50 μM) and infected with *B abortus* (Ba+4μ8c). **(D)** YM1 and TGF-β expression levels determined by real-time PCR in macrophages from C57BL/6 mice infected with *B abortus* (Ba) or pre-treated with 4μ8c (50 μM) and infected with *B abortus* (Ba+4μ8c). **(E)** NOS2 and IL-6 expression levels determined by real-time PCR in macrophages from C57BL/6 mice subjected to specific XBP1 gene knockdown and then infected with *B abortus*. **(F)** YM1 and TGF-β expression levels determined by real-time PCR in macrophages from C57BL/6 mice subjected to specific XBP1 gene knockdown and then infected with *B abortus*. The data are representative of three independent experiments. The data are presented as mean $\pm$ SD, * p < 0.05, Student's t test.
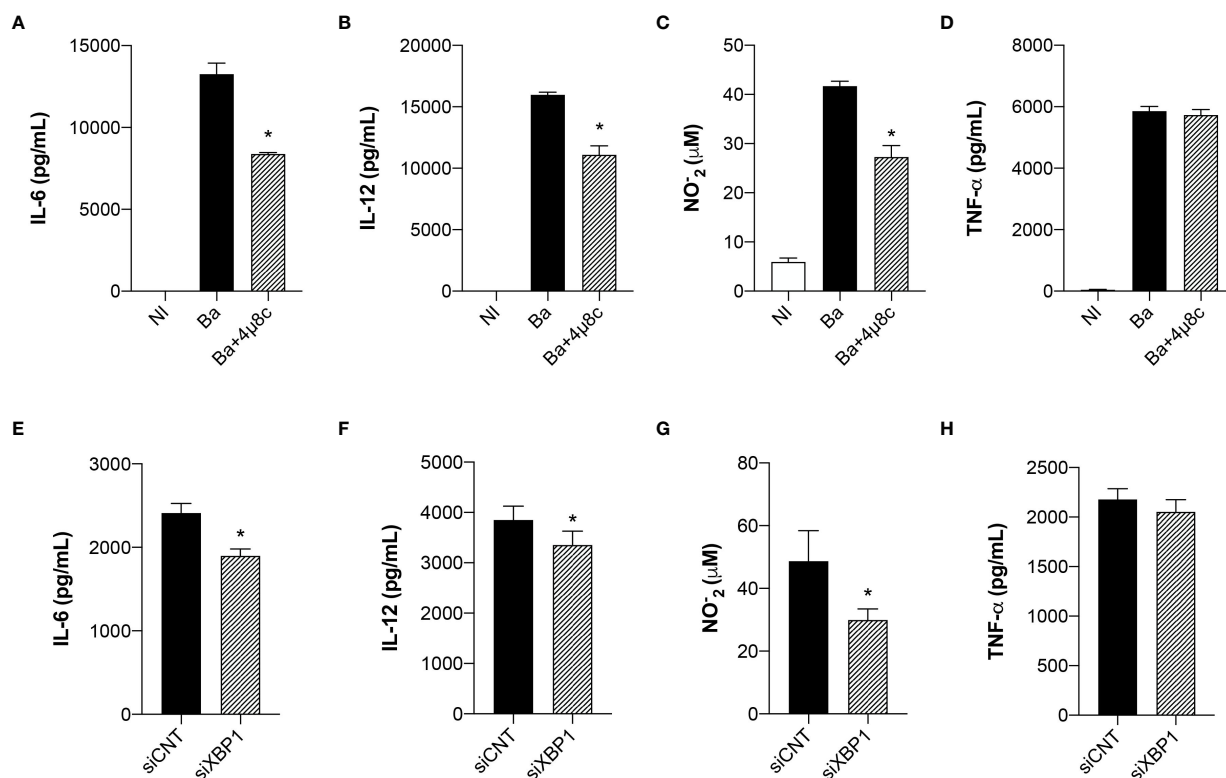
FIGURE 2

The UPR modulates the inflammatory response in infected macrophages. **(A)** IL-6, **(B)** IL-12 and **(D)** TNF-α produced by macrophages from C57BL/6 mice non-infected (NI), infected with *B abortus* (Ba) or pre-treated with 4µ8c (50 µM) and infected with *B abortus* (Ba+4µ8c), detected in cell supernatants using ELISA. **(C)** NO$_2^-$ (nitrite) accumulation in the media of macrophages from C57BL/6 mice non-infected (NI), infected with *B abortus* (Ba) or pre-treated with 4µ8c (50 µM) and infected with *B abortus* (Ba+4µ8c), measured by Griess reaction. **(E)** IL-6, **(F)** IL-12 and **(H)** TNF-α produced by macrophages from C57BL/6 mice subjected to specific XBP1 gene knockdown and then infected with *B abortus*. **(G)** NO$_2^-$ (nitrite) accumulation in the media of macrophages from C57BL/6 mice subjected to specific XBP1 gene knockdown and then infected with *B abortus*. The data are representative of three independent experiments. The data **(A–D)** are presented as mean $\pm$ SD, * $p < 0.05$, one-way ANOVA. The data **(E–H)** are presented as mean $\pm$ SD, * $p < 0.05$, Student's t test.

IRE1α drives mROS generation in infected macrophages

The inflammatory profile in macrophages is characterized by the efficient generation of ROS (16). Furthermore, the cellular metabolic shift (from producing ATP mainly by OXPHOS to the increased production of ATP by glycolysis) repurposes mitochondria from ATP production to ROS generation, which promotes the inflammatory profile in macrophages (27). Therefore, we evaluated mROS production, to unravel how the UPR regulates the macrophage metabolic function during *B. abortus* infection.

Confocal microscopy analysis of MitoSOX Red, a mitochondrial superoxide indicator, demonstrated that infection with *B. abortus* enhanced mROS generation when compared to non-infected macrophages (Figures 4A, B). Moreover, inhibition of IRE1α reduced mROS production in infected macrophages to levels similar to those of non-infected (Figures 4A, B).

Corroborating these results, MitoSOX Red flow cytometry analysis confirmed that infection with *B. abortus* enhanced mROS generation compared to non-infected macrophages, while IRE1α inhibition reduced mROS production compared to infected non-treated cells (Figure 4C). As expected, in infected macrophages, pretreatment with a scavenger specific for mROS, Mito-TEMPO, abrogated mROS production (Figure 4C). Altogether, these results strongly indicate that IRE1α contributes to mROS generation in *Brucella*-infected macrophages.

IRE1α modulates HIF-1α stabilization in *Brucella*-infected macrophages

Recent reports have shown that mROS modulates HIF-1α activity (27). Moreover, it was recently demonstrated that mROS stabilizes HIF-1α expression in macrophages infected with *B. abortus* (13). Considering that HIF-1α drives the
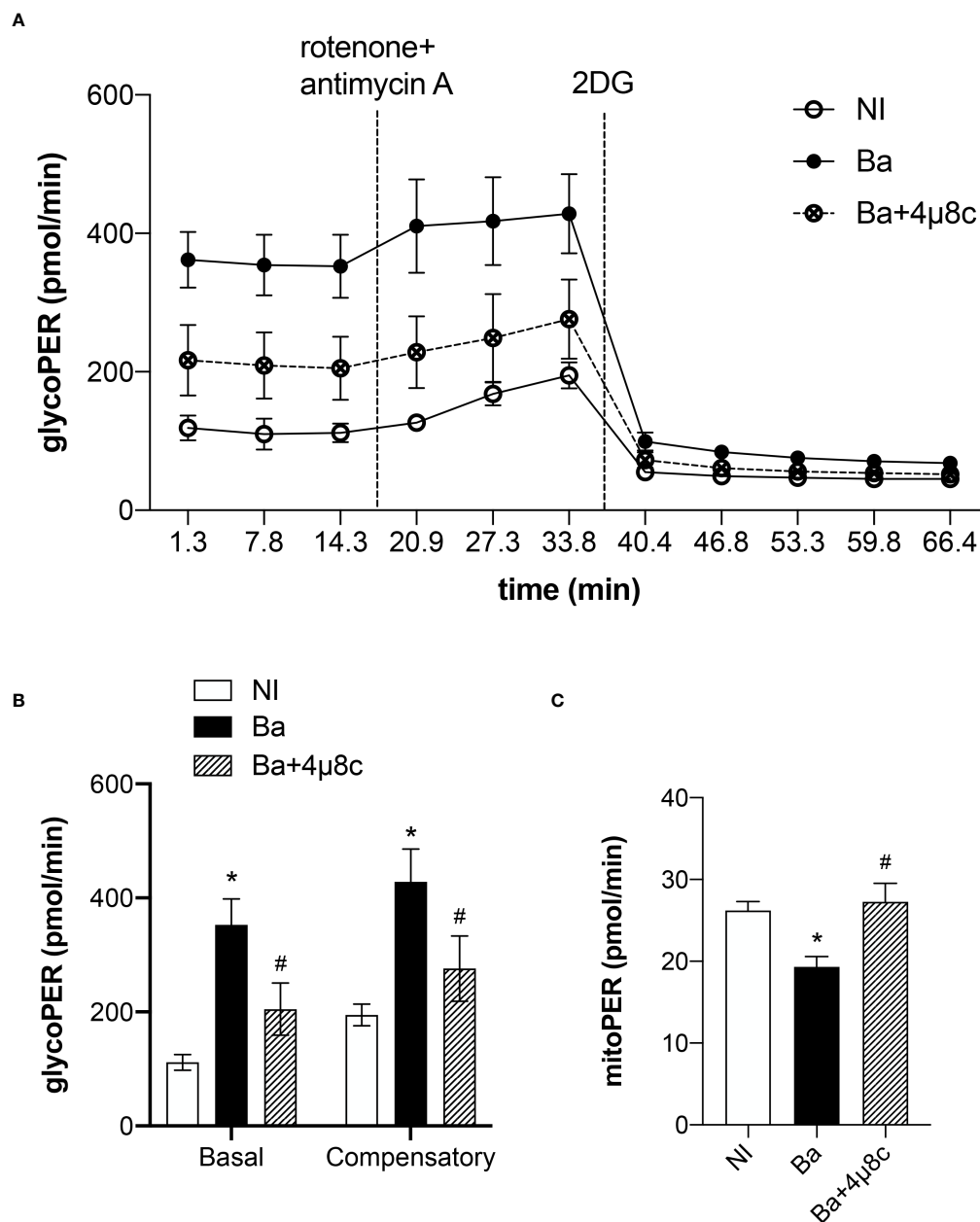
FIGURE 3

IRE1α regulates the metabolic function of infected macrophages. **(A)** Time-course quantification of glycolytic proton efflux rate (glycoPER) in macrophages from C57BL/6 mice non-infected (NI), infected with *B abortus* (Ba) or pre-treated with 4µ8c (50 µM) and infected with (*B abortus*) (Ba+4µ8c). **(B)** Quantification of basal and compensatory glycoPER. **(C)** Quantification of mitoPER. The data are representative of three independent experiments. The data **(B, C)** are presented as mean $\pm$ SD, * $p < 0.05$, one-way ANOVA. * $p < 0.05$, compared to NI and # $p < 0.05$, compared to Ba, one-way ANOVA.

metabolic reprogramming in macrophages in *Brucella* infection (13), we addressed whether IRE1α could modulate HIF-1α expression and stabilization. Quantitative real-time RT-PCR analysis revealed that inhibition of IRE1α reduced HIF-1α (Figure 5A) and GLUT1 (glucose transporter 1, a marker for the HIF-1α-induced glycolysis) (Figure 5B) (28) expression

compared to non-treated infected macrophages. Accordingly, XBP1 silencing also reduced HIF-1α (Figure 5C) and GLUT1 (Figure 5D) expression in infected macrophages compared to the infected control. Furthermore, inhibition of IRE1α reduced HIF-1α protein level in infected macrophages compared to non-treated infected macrophages (Figure 5E). Altogether, these
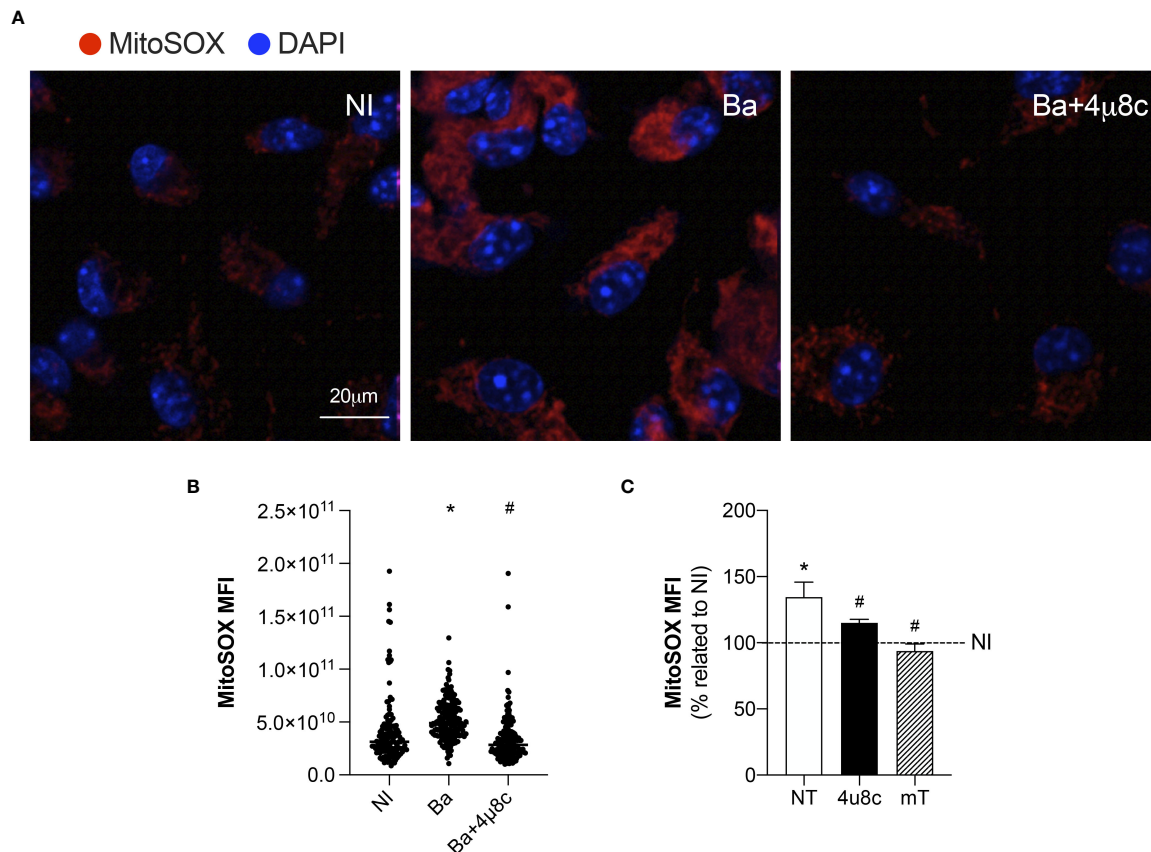
FIGURE 4
IRE1α drives mROS generation. **(A)** Representative confocal microscopy of MitoSOX Red staining in macrophages from C57BL/6 mice non-infected (NI), infected with *B abortus* (Ba) or pre-treated with 4μ8c (50 μM) and infected with *B abortus* (Ba+4μ8c). MitoSOX Red is in red, and nuclei (DAPI) is in blue. Scale bar, 20 μm. **(B)** MitoSOX Red mean fluorescent intensity, determined as described in Materials and Methods. **(C)** MitoSOX Red flow cytometry analysis of mROS production fold change induced by *B abortus* relativized to non-infected (NI) cells for each experimental group: non-treated (NT), pre-treated with 50 μM 4μ8c (Ba+4μ8c) or pre-treated with 0.5 mM Mito-TEMPO (mT). The data are representative of three independent experiments. The data **(B)** is presented as mean ± SD, * p < 0.05 (compared to NI) and # p < 0,05 (compared to Ba), one-way ANOVA. The data **(C)** is presented as mean ± SD, * p < 0.05 [compared to non-infected (NI, set to 100%)] and # p < 0.05 (compared to NT), one-way ANOVA.

results indicate that IRE1α contributes to HIF-1α expression and stabilization in *Brucella*-infected cells. Recent studies showed that HIF-1α and HIF-1α-induced glycolysis are important modulators of innate immunity (29, 30). Considering that the UPR is crucial for triggering immune responses against infections (20), we evaluated the role of glycolysis in the immune responses in *B. abortus*-infected macrophages. Inhibition of glucose flux using 2-DG in infected macrophages reduced IL-6 (Figure 5F), IL-12 (Figure 5G), and NO secretion (Figures 5H) compared to non-treated infected macrophages whereas TNF-α secretion was unaltered (Figure 5I). Overall, these results demonstrate that IRE1α modulates HIF-1α function and confirms that the HIF-1α-glycolysis axis contributes for triggering inflammatory responses in *B. abortus* infection.

IRE1α-dependent stabilization of HIF-1α is required for induction of inflammatory responses in Brucella-infected macrophages

It is widely known that HIF-1α is involved in inflammation (31). Therefore, to further investigate the contribution of the IRE1α-HIF-1α axis in inducing inflammatory responses during *B. abortus* infection, we inhibited IRE1α in HIF-1α WT and HIF-1α WT KO in non-infected and infected macrophages and assessed the production of inflammatory cytokines. Lack of HIF-1α reduced IL-6 (Figure 6A) and IL-12 secretion (Figures 6B) in infected macrophages. Furthermore, absence of HIF-1α also impaired IL-1β release (Figure 6C) whereas TNF-α secretion was unaltered (Figure 6D).
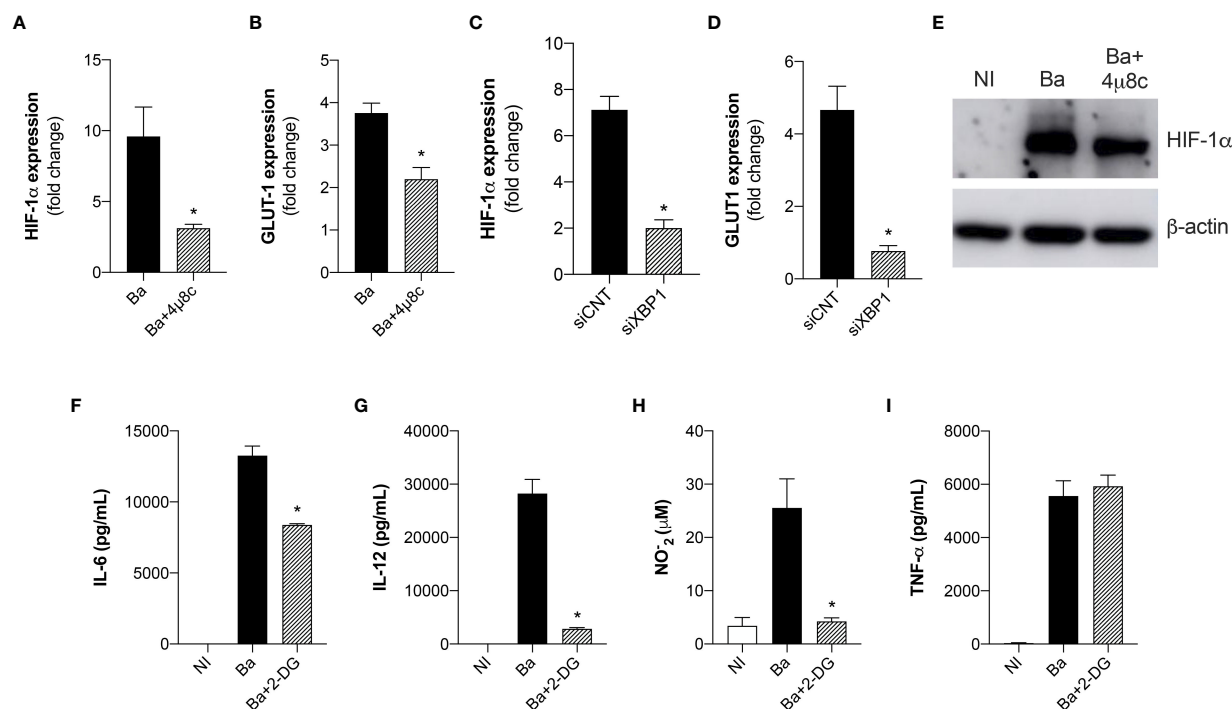
FIGURE 5

The expression and stabilization of HIF-1α in *Brucella*-infected macrophages requires IRE1α. **(A)** HIF-1α and **(B)** GLUT-1 expression levels determined by real-time RT-PCR in macrophages from C57BL/6 mice infected with *B abortus* (Ba) or pre-treated with 4μ8c (50 μM) and infected with *B abortus* (Ba+4μ8c). **(C)** HIF-1α and **(D)** GLUT-1 expression levels determined by real-time RT-PCR in macrophages from C57BL/6 mice subjected to specific XBP1 gene knockdown and then infected with *B abortus*. **(E)** Western blot analysis of HIF-1α in cell lysates from macrophages from C57BL/6 mice non-infected (NI), infected with *B abortus* (Ba) or pre-treated with 4μ8c (50 μM) and infected with *B abortus* (Ba+4μ8c). Equal loading was controlled by measuring β- actin in the corresponding cell lysates. **(F)** IL-6, **(G)** IL-12, **(I)** TNF-α produced by macrophages from C57BL/6 mice non-infected (NI), infected with *B abortus* (Ba) or pre-treated with 2-DG (1mM) and infected with *B abortus* (Ba+2-DG), detected in cell supernatants using ELISA. **(H)** NO_2^- (nitrite) accumulation in the media of macrophages from C57BL/6 mice non-infected (NI), infected with *B abortus* (Ba) or pre-treated with 2-DG (1mM) and infected with *B abortus* (Ba+2-DG), measured by Griess reaction. The data are representative of three independent experiments. The data **(A–D)** are presented as mean ± SD, * $p < 0.05$, student's t test. The data **(F–I)** are presented as mean ± SD, * $p < 0.05$, one-way ANOVA.

In addition, inhibition of IRE1α using 4μ8c in HIF-1α WT infected macrophages reduced IL-6 (Figure 6A), IL-12 (Figure 6B) and IL-1β (Figure 6C) release compared to non-treated HIF-1α WT infected macrophages, whereas TNF-α secretion was unaffected (Figure 6D). Remarkably, inhibition of IRE1α in HIF-1α KO infected macrophages did not alter IL-6 (Figure 6A) and IL-12 (Figure 6B) secretion compared to non-treated HIF-1α KO infected macrophages. These data indicate that IRE1α induces the production of these cytokines, at least partially, in a HIF-1α-dependent fashion. Interestingly, inhibition of IRE1α further reduced IL-1β secretion (Figure 6C) in HIF-1α KO infected macrophages in comparison with non-treated HIF-1α KO infected macrophages. Collectively, these results suggest that the IRE1α-dependent stabilization of HIF-1α is indispensable for inducing the inflammatory responses against *B. abortus* infection.

IRE1α induces inflammasome activation in *Brucella*-infected macrophages

Here, we demonstrated that IRE1α is crucial for inducing IL-1β release both in HIF-1α WT and HIF-1α KO infected macrophages, suggesting an important role of IRE1α in regulating IL-1β release in *Brucella* infection. Therefore, to better address this, we evaluated inflammasome activation. Corroborating our data showing that inhibition of IRE1α reduced IL-1β secretion in HIF-1α WT and HIF-1α KO infected macrophages, inhibition of IRE1α also reduced IL-1β release in C57BL/6 wild type infected macrophages compared to non-treated infected cells (Figure 7A). Corroborating these data, XBP1 silencing also reduced IL-1β secretion in infected macrophages compared to the infected siRNA control (Figure 7B).

Furthermore, IRE1α inhibition reduced pro-IL-1β protein level in infected macrophages and also processing of caspase-1
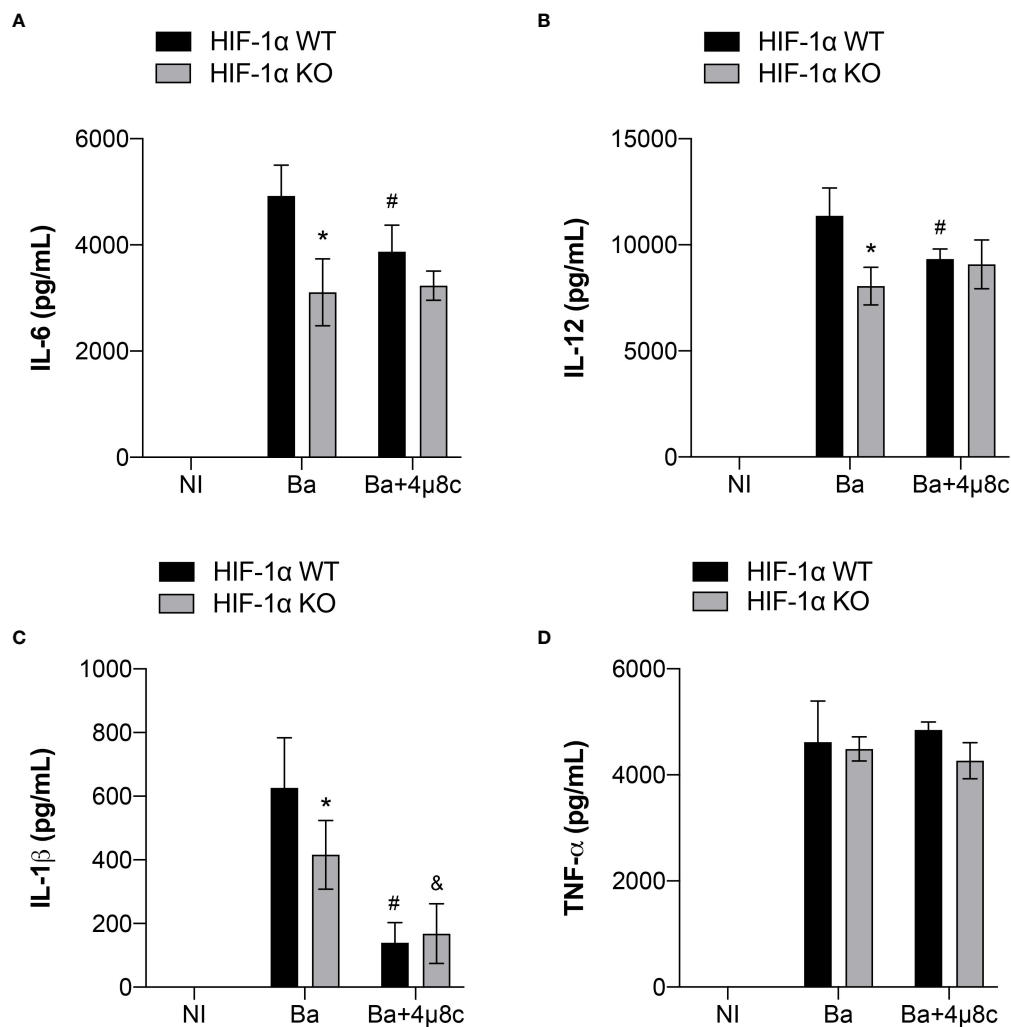
FIGURE 6
IRE1α is necessary for full induction of HIF-1α-dependent inflammatory responses during infection. **(A)** IL-6, **(B)** IL-12, **(C)** IL-1β and **(D)** TNF-α produced by macrophages derived from HIF-1α WT and HIF-1α KO mice non-infected (NI), infected with *B abortus* (Ba) or pre-treated with 4μ8c (50 μM) and infected with *B abortus* (Ba+4μ8c), detected in cell supernatants using ELISA. The data are representative of three independent experiments. The data are presented as mean $\pm$ SD, * $p < 0.05$ (compared between WT and KO), # $p < 0.05$ (compared to Ba from WT), & $p < 0.05$ (compared to Ba from KO), two-way ANOVA.

(p20 subunit in supernatant) was reduced in 4μ8c-treated infected macrophages compared to non-treated infected cells (Figure 7C). Altogether these results indicate decreased canonical-inflammasome assembly upon IRE1α inhibition in infected macrophages.

In addition to canonical-inflammasome activation, *B. abortus* also activates the non-canonical inflammasome and IL-1β release in this case is partially dependent on caspase-11 and gasdermin-D (GSDMD) (32). Furthermore, activation of non-canonical inflammasome triggers pyroptosis and consequent membrane disruption, releasing lactate dehydrogenase (LDH) as well as other cytosolic contents (32).

Hence, we further evaluated the role of IRE1α in non-canonical inflammasome activation. Inhibition of IRE1α reduced the intracellular protein level of caspase-11 and GSDMD cleavage (p30 fragment) in 4μ8c-treated infected macrophages compared to non-treated infected macrophages (Figure 7C). Regarding LDH, inhibition of IRE1α diminished LDH release in infected macrophages to levels similar to non-infected macrophages (Figure 7D), suggesting that IRE1α participates in non-canonical inflammasome activation and pyroptosis. Altogether, these results indicate that IRE1α is indispensable for canonical and non-canonical inflammasome activation and IL-1β release in *B. abortus*-infected macrophages.
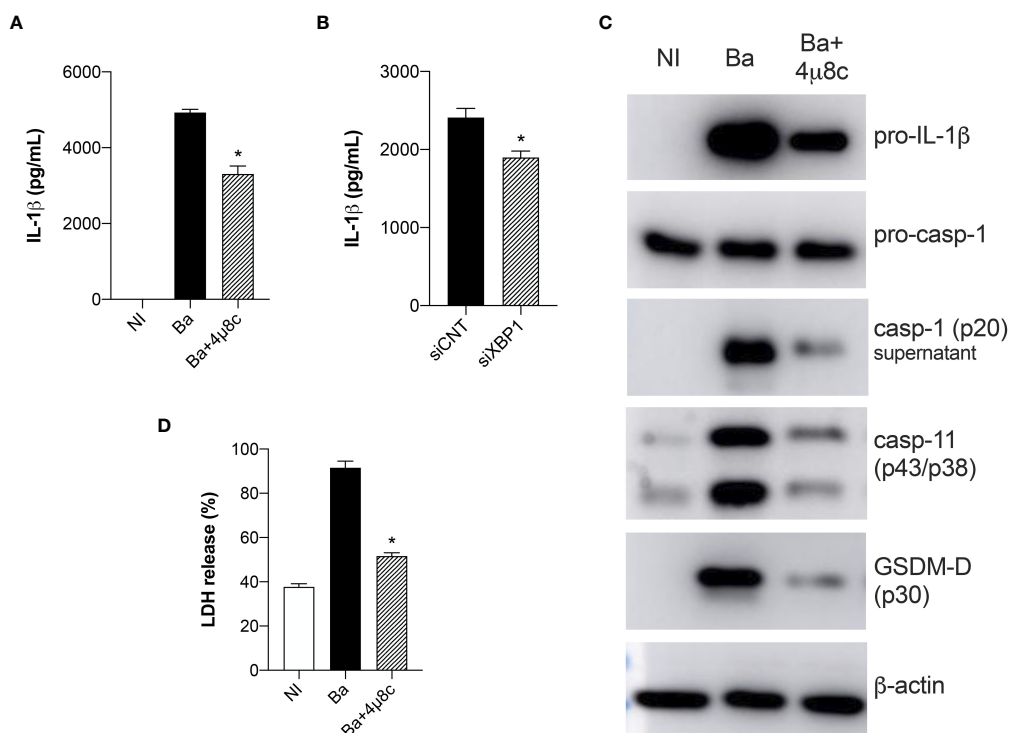
FIGURE 7

IRE1α induces inflammasome activation and IL-1β release in infected macrophages. **(A)** IL-1β released by macrophages derived from C57BL/6 mice non-infected (NI), infected with *B abortus* (Ba) or pre-treated with 4μ8c (50 μM) and infected with *B abortus* (Ba+4μ8c), detected in cell supernatants using ELISA. **(B)** IL-1β released by macrophages derived from C57BL/6 mice subjected to specific XBP1 gene knockdown and then infected with *B abortus*. **(C)** Western blot analysis of pro-IL-1β, pro-caspase-1, caspase-11 and p30 fragment of GSDMD in cell lysates and caspase-1 (p20 subunit) in supernatants from macrophages derived from C57BL/6 mice, non-infected (NI), infected with *B abortus* (Ba) or pre-treated with 4μ8c (50 μM) and infected with *B abortus* (Ba+4μ8c). Equal loading was controlled by measuring β-actin in the corresponding cell lysates. **(D)** LDH release in macrophages derived from C57BL/6 mice non-infected (NI), infected with *B abortus* (Ba) or pre-treated with 4μ8c (50 μM) and infected with *B abortus* (Ba+4μ8c). Values represent the percentage of LDH release compared with lysed cells. The data are representative of three independent experiments. The data **(A, D)** are presented as mean ± SD, * $p < 0.05$, one-way ANOVA. The data **(B)** are presented as mean ± SD, * $p < 0.05$, Student's t test.

Discussion

The UPR has been linked to macrophage polarization in various settings and especially in metabolic disorders. For example, IRE1α specific deletion in adipose tissue promotes M2 and decreases M1 polarization of macrophages. This M1-M2 imbalance limits energy expenditure capacity and promotes insulin resistance in mice (33). Furthermore, IRE1α knockdown reduces M1 proinflammatory macrophages and promotes the M2-pheynotypic shift in macrophages in a mouse model of steatosis, aggravating the ischemia reperfusion injury of fatty liver (34). Accordingly, we demonstrated here that IRE1α inhibition reduces M1 macrophage polarization in *Brucella*-infected macrophages without affecting M2 macrophages, corroborating the UPR role as an important inflammatory signal during bacterial infections.

Regarding *B. abortus* infection, infected human-like and mouse macrophages undergo reprogramming that resembles the inflammatory macrophage profile also known as the Warburg effect (13, 35). We demonstrated that IRE1α modulates the macrophage metabolic function, supporting the metabolic shift towards glycolysis, unraveling the UPR as a regulator of macrophage metabolism during *Brucella* infection. A recent report from our group demonstrated that HIF-1α drives the metabolic reprogramming in infected macrophages (13). Accordingly, we demonstrated that IRE1α favors HIF-1α expression and stabilization, indicating that the IRE1α-dependent HIF-1α pathway may play a role in regulating the macrophage metabolic function during *B. abortus* infection. Previous reports suggest an intimate relationship between hypoxia responses and ER stress leading to macrophage polarization (36). For instance, the UPR enhances HIF-1α phosphorylation and interacts with hypoxia response pathways to augment HIF-1α mRNA expression (37). Moreover, the ubiquitin ligase Siah2 is another example of the interaction of HIF-1α and the UPR during hypoxia as it limits prolyl
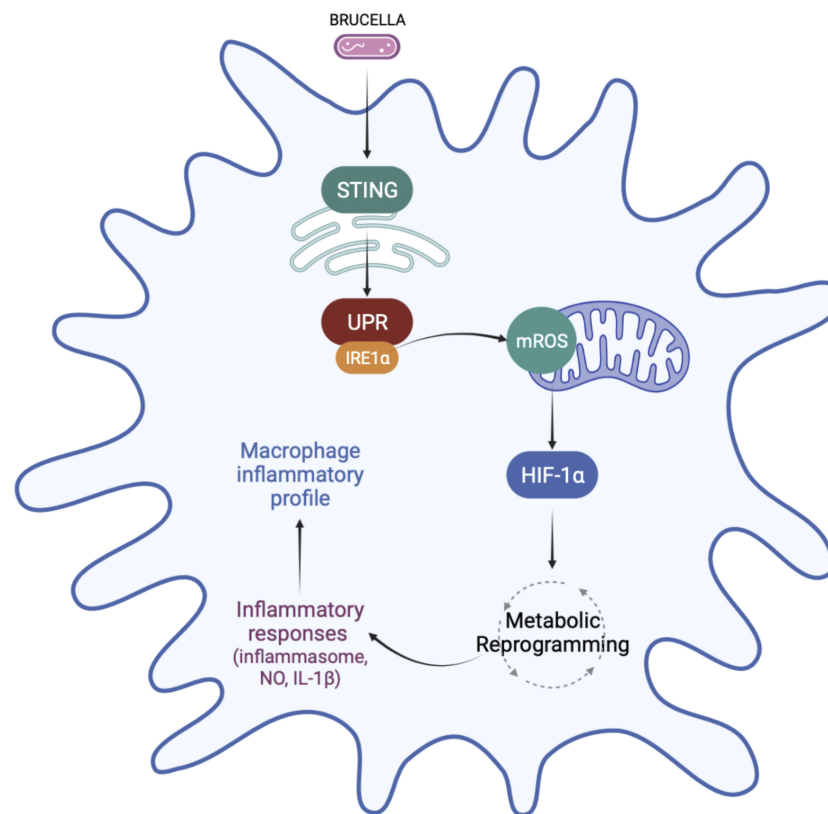
FIGURE 8

Regulation of macrophage metabolic function by IRE1α in *Brucella abortus* infection. IRE1α activation by *Brucella abortus* triggers mROS generation that induces HIF-1α stabilization in infected macrophages. IRE1α drives the metabolic reprogramming in macrophages, contributing to the enhanced glycolysis and reduced OXPHOS observed in *Brucella*-infected macrophages possibly *via* HIF-1α. This IRE1α-dependent HIF-1α stabilization is crucial for inducing inflammatory responses during infection. IRE1α induces inflammasome assembly, IL-1β release and NO production, supporting the inflammatory profile in macrophages infected with *B abortus*. Figure created using BioRender (https://biorender.com).

hydroxylase domains (PHD) protein availability during hypoxia, stabilizing HIF-1α (38). Notably, our results show a connection between HIF-1α and UPR that occurs outside of a hypoxic setting.

Regarding inflammasome activation, we demonstrated that IRE1α participates in IL-1β secretion and directly interferes with pro-IL-β synthesis. Additionally, IRE1α stimulates caspase-1 and caspase-11 activation and GSDMD cleavage, indicating its crucial function in inducing canonical and non-canonical inflammasome activation in *B. abortus* infection. Previous studies corroborate the involvement of the IRE1α in the activation of the NLRP3 canonical inflammasome. For example, IRE1α mediates saturated fatty-acid-induced activation of the NLRP3 inflammasome (39). Moreover, during irremediable ER stress, IRE1α promotes inflammasome activation by inducing Thioredoxin-Interacting Protein (TXNIP), which is crucial for pro-caspase-1 cleavage and IL-β secretion (40). Furthermore, it was previously demonstrated in macrophages that *Brucella*-induced mROS is crucial for NLRP3-

caspase-1 inflammasome activation (19) and a previous report indicated that infection with an attenuated *Brucella* strain induces IRE1α and activates the inflammasome *via* NLRP3-driven mitochondrial damage (41). Accordingly, we demonstrated here that IRE1α drives the production of mROS in *Brucella*-infected macrophages.

Moreover, mROS stabilizes HIF-1α that induces canonical inflammasome activation in *B. abortus*-infected macrophages (13). Therefore, our results imply that IRE1α-dependent mROS might contribute to caspase-1 activation and inflammasome assembly *via* modulation of HIF-1α stabilization. Remarkably, HIF-1α is not required for non-canonical inflammasome activation in *B. abortus* infection (13), raising the hypothesis that the UPR may affect non-canonical inflammasome assembly in a HIF-1α-independent manner. This hypothesis is supported by our data concerning IL-1β release in HIF-1α KO macrophages. Whereas secretion of other inflammatory cytokines such as IL-6 and IL-12 relies on IRE1α-dependent induction of HIF-1α, IL-1β release in

HIF-1α KO macrophages is further reduced upon treatment with 4u8c.

Intracellular bacteria uses host cell metabolites to survive and replicate (42). In that context, the macrophage metabolic profile is particularly relevant in *Brucella* infection. Previous data showed that the increase in glycolysis and lactate production favors *B. abortus* intracellular survival, suggesting that *Brucella* might take advantage of the metabolic change in macrophages to support bacterial growth (35). Accordingly, we demonstrated here that IRE1α participates in the metabolic shift during *B. abortus* infection, while previous reports indicated that the UPR favors *Brucella* replication in macrophages (9, 11). Thus, our results indicate that the IRE1α-induced metabolic shift may be involved in *B. abortus* survival. On the contrary, another report showed that during chronic infection, *Brucella* replicates preferentially in anti-inflammatory M2 macrophages which display a contrasting metabolic profile with decreased aerobic glycolysis. In this case, peroxisome proliferator-activated receptor γ (PPARγ)-mediated increase in glucose availability favors *Brucella* growth (43). Interestingly, M2 macrophages are more abundant during chronic brucellosis (13, 43). Hence, determining the influence of the UPR on macrophage metabolism during the course of *Brucella* infection may reveal exciting information about the role of UPR-induced metabolic changes in bacterial replication.

In summary, the data presented here reveals that IRE1α favors M1 inflammatory polarization and regulates macrophage metabolism. We demonstrated that IRE1α activation increases mROS production, which may contribute to the stabilization of HIF-1α, an important regulator of macrophage metabolic function during *B. abortus* infection. Accordingly, IRE1α contributes to the metabolic reprogramming of macrophages, favoring the glycolytic phenotype during infection. In addition, IRE1α favors inflammatory cytokine secretion, NO production and inflammasome activation (Figure 8). The results presented here revealed an important link between UPR and HIF-1α, which ultimately regulates macrophage metabolic profile and the immune response against *B. abortus* infection. Finally, our findings improve the understanding of how these UPR-induced immunometabolic changes impact bacterial pathogenesis.

Data availability statement

The raw data supporting the conclusions of this article will be made available by the authors, without undue reservation.

Ethics statement

All experiments involving animals were conducted in accordance with the Brazilian Federal Law number 11,794, which regulates the scientific use of animals in Brazil, the Institutional Animal Care and Use Committees (IACUC) guidelines, and the Animal Welfare Act and Regulations guidelines established by the American Veterinary Medical Association Panel on Euthanasia. Animals were fed, housed, and handled in strict agreement with these recommendations. All protocols were approved by the Committee for Ethics in Animal Experimentation (CEUA) at UFMG under permit #87/2017.

Author contributions

EG, MG and SO devised the project and the main conceptual ideas. EG, MG, RS, KM, FM, designed and carried out the experiments. EG analyzed the data and prepared the figures. EG and SO wrote the manuscript with the input of all authors. SO provided the funding acquisition, supervised the project, reviewed, and submitted the manuscript. All authors contributed to the article and approved the submitted version.

Funding

Conflict of interest

The authors declare that the research was conducted in the absence of any commercial or financial relationships that could be construed as a potential conflict of interest.

Publisher's note

References

1. Hebert DN, Molinari M. In and out of the ER: Protein folding, quality control, degradation, and related human diseases. *Physiol Rev* (2007) 87(4):1377–408. doi: 10.1152/physrev.00050.2006

2. Walter P, Ron D. The unfolded protein response: From stress pathway to homeostatic regulation. *Science* (2011) 334(6059):1081–6. doi: 10.1126/science.1209038

3. Wang S, Kaufman RJ. The impact of the unfolded protein response on human disease. *J Cell Biol* (2012) 197(7):857–67. doi: 10.1083/jcb.201110131

4. Schroder M, Kaufman RJ. ER stress and the unfolded protein response. *Mutat Res* (2005) 569(1-2):29–63. doi: 10.1016/j.mrfmmm.2004.06.056

5. Hetz C, Martinon F, Rodriguez D, Glimcher LH. The unfolded protein response: integrating stress signals through the stress sensor IRE1alpha. *Physiol Rev* (2011) 91(4):1219–43. doi: 10.1152/physrev.00001.2011

6. Hotamisligil GS. Endoplasmic reticulum stress and the inflammatory basis of metabolic disease. *Cell* (2010) 140(6):900–17. doi: 10.1016/j.cell.2010.02.034

7. Huang S, Xing Y, Liu Y. Emerging roles for the ER stress sensor IRE1alpha in metabolic regulation and disease. *J Biol Chem* (2019) 294(49):18726–41. doi: 10.1074/jbc.REV119.007036

8. Pappas G, Akritidis N, Bosilkovski M, Tsianos E. Brucellosis. *N Engl J Med* (2005) 352(22):2325–36. doi: 10.1056/NEJMra050570

9. Guimaraes ES, Gomes MTR, Campos PC, Mansur DS, Dos Santos AA, Harms J, et al. Brucella abortus cyclic dinucleotides trigger STING-dependent unfolded protein response that favors bacterial replication. *J Immunol* (2019) 202 (9):2671–81. doi: 10.4049/jimmunol.1801233

10. Keestra-Gounder AM, Byndloss MX, Seyffert N, Young BM, Chavez-Arroyo A, Tsai AY, et al. NOD1 and NOD2 signalling links ER stress with inflammation. *Nature* (2016) 532(7599):394–7. doi: 10.1038/nature17631

11. Smith JA, Khan M, Magnani DD, Harms JS, Durward M, Radhakrishnan GK, et al. Brucella induces an unfolded protein response *via* TcpB that supports intracellular replication in macrophages. *PLoS Pathog* (2013) 9(12):e1003785. doi: 10.1371/journal.ppat.1003785

12. Taguchi Y, Imaoka K, Kataoka M, Uda A, Nakatsu D, Horii-Okazaki S, et al. Yip1A, a novel host factor for the activation of the IRE1 pathway of the unfolded protein response during brucella infection. *PLoS Pathog* (2015) 11(3):e1004747. doi: 10.1371/journal.ppat.1004747

13. Gomes MTR, Guimaraes ES, Marinho FV, Macedo I, Aguiar E, Barber GN, et al. STING regulates metabolic reprogramming in macrophages *via* HIF-1alpha during brucella infection. *PLoS Pathog* (2021) 17(5):e1009597. doi: 10.1371/journal.ppat.1009597

14. Murray PJ. Macrophage polarization. *Annu Rev Physiol* (2017) 79:541–66. doi: 10.1146/annurev-physiol-022516-034339

15. Russell DG, Huang L, VanderVen BC. Immunometabolism at the interface between macrophages and pathogens. *Nat Rev Immunol* (2019) 19(5):291–304. doi: 10.1038/s41577-019-0124-9

16. O'Neill LA, Kishton RJ, Rathmell J. A guide to immunometabolism for immunologists. *Nat Rev Immunol* (2016) 16(9):553–65. doi: 10.1038/nri.2016.70

17. Tannahill GM, Curtis AM, Adamik J, Palsson-McDermott EM, McGettrick AF, Goel G, et al. Succinate is an inflammatory signal that induces IL-1beta through HIF-1alpha. *Nature* (2013) 496(7444):238–42. doi: 10.1038/nature11986

18. Marim FM, Silveira TN, Lima DSJr., Zamboni DS. A method for generation of bone marrow-derived macrophages from cryopreserved mouse bone marrow cells. *PLoS One* (2010) 5(12):e15263. doi: 10.1371/journal.pone.0015263

19. Gomes MT, Campos PC, Oliveira FS, Corsetti PP, Bortoluci KR, Cunha LD, et al. Critical role of ASC inflammasomes and bacterial type IV secretion system in caspase-1 activation and host innate resistance to brucella abortus infection. *J Immunol* (2013) 190(7):3629–38. doi: 10.4049/jimmunol.1202817

20. Celli J, Tsolis RM. Bacteria, the endoplasmic reticulum and the unfolded protein response: friends or foes? *Nat Rev Microbiol* (2015) 13(2):71–82. doi: 10.1038/nrmicro3393

21. Campos PC, Gomes MTR, Marinho FAV, Guimaraes ES, de Moura Lodi Cruz MGF, Oliveira SC. Brucella abortus nitric oxide metabolite regulates inflammasome activation and IL-1beta secretion in murine macrophages. *Eur J Immunol* (2019) 49(7):1023–37. doi: 10.1002/eji.201848016

22. Cumming BM, Addicott KW, Adamson JH, Steyn AJ. Mycobacterium tuberculosis induces decelerated bioenergetic metabolism in human macrophages. *Elife* (2018) 7. doi: 10.7554/eLife.39169

23. Grootjans J, Kaser A, Kaufman RJ, Blumberg RS. The unfolded protein response in immunity and inflammation. *Nat Rev Immunol* (2016) 16(8):469–84. doi: 10.1038/nri.2016.62

24. Smith JA. Regulation of cytokine production by the unfolded protein response; implications for infection and autoimmunity. *Front Immunol* (2018) 9:422. doi: 10.3389/fimmu.2018.00422

25. de Jong MF, Starr T, Winter MG, den Hartigh AB, Child R, Knodler LA, et al. Sensing of bacterial type IV secretion *via* the unfolded protein response. *mBio* (2013) 4(1):e00418–12. doi: 10.1128/mBio.00418-12

26. Cross BC, Bond PJ, Sadowski PG, Jha BK, Zak J, Goodman JM, et al. The molecular basis for selective inhibition of unconventional mRNA splicing by an IRE1-binding small molecule. *Proc Natl Acad Sci U S A* (2012) 109(15):E869–78. doi: 10.1073/pnas.1115623109

27. Mills EL, Kelly B, Logan A, Costa ASH, Varma M, Bryant CE, et al. Succinate dehydrogenase supports metabolic repurposing of mitochondria to drive inflammatory macrophages. *Cell* (2016) 167(2):457–70.e13. doi: 10.1016/j.cell.2016.08.064

28. Behrooz A, Ismail-Beigi F. Dual control of glut1 glucose transporter gene expression by hypoxia and by inhibition of oxidative phosphorylation. *J Biol Chem* (1997) 272(9):5555–62. doi: 10.1074/jbc.272.9.5555

29. Eltzschig HK, Carmeliet P. Hypoxia and inflammation. *N Engl J Med* (2011) 364(7):656–65. doi: 10.1056/NEJMra0910283

30. Zinkernagel AS, Johnson RS, Nizet V. Hypoxia inducible factor (HIF) function in innate immunity and infection. *J Mol Med (Berl)* (2007) 85 (12):1339–46. doi: 10.1007/s00109-007-0282-2

31. Corcoran SE, O'Neill LA. HIF1alpha and metabolic reprogramming in inflammation. *J Clin Invest* (2016) 126(10):3699–707. doi: 10.1172/JCI84431

32. Cerqueira DM, Gomes MTR, Silva ALN, Rungue M, Assis NRG, Guimaraes ES, et al. Guanylate-binding protein 5 licenses caspase-11 for gasdermin-d mediated host resistance to brucella abortus infection. *PLoS Pathog* (2018) 14 (12):e1007519. doi: 10.1371/journal.ppat.1007519

33. Shan B, Wang X, Wu Y, Xu C, Xia Z, Dai J, et al. The metabolic ER stress sensor IRE1alpha suppresses alternative activation of macrophages and impairs energy expenditure in obesity. *Nat Immunol* (2017) 18(5):519–29. doi: 10.1038/ni.3709

34. Wang JM, Qiu Y, Yang Z, Kim H, Qian Q, Sun Q, et al. IRE1alpha prevents hepatic steatosis by processing and promoting the degradation of select microRNAs. *Sci Signal* (2018) 11(530). doi: 10.1126/scisignal.aao4617

35. Czyz DM, Willett JW, Crosson S. Brucella abortus induces a warburg shift in host metabolism that is linked to enhanced intracellular survival of the pathogen. *J Bacteriol* (2017) 199(15). doi: 10.1128/JB.00227-17

36. Diaz-Bulnes P, Saiz ML, Lopez-Larrea C, Rodriguez RM. Crosstalk between hypoxia and ER stress response: A key regulator of macrophage polarization. *Front Immunol* (2019) 10:2951. doi: 10.3389/fimmu.2019.02951

37. Pereira ER, Frudd K, Awad W, Hendershot LM. Endoplasmic reticulum (ER) stress and hypoxia response pathways interact to potentiate hypoxia-inducible factor 1 (HIF-1) transcriptional activity on targets like vascular endothelial growth factor (VEGF). *J Biol Chem* (2014) 289(6):3352–64. doi: 10.1074/jbc.M113.507194

38. Nakayama K, Frew IJ, Hagensen M, Skals M, Habelhah H, Bhoumik A, et al. Siah2 regulates stability of prolyl-hydroxylases, controls HIF1alpha abundance, and modulates physiological responses to hypoxia. *Cell* (2004) 117(7):941–52. doi: 10.1016/j.cell.2004.06.001

39. Robblee MM, Kim CC, Porter Abate J, Valdearcos M, Sandlund KL, Shenoy MK, et al. Saturated fatty acids engage an IRE1alpha-dependent pathway to activate the NLRP3 inflammasome in myeloid cells. *Cell Rep* (2016) 14(11):2611–23. doi: 10.1016/j.celrep.2016.02.053

40. Lerner AG, Upton JP, Praveen PV, Ghosh R, Nakagawa Y, Igbaria A, et al. IRE1alpha induces thioredoxin-interacting protein to activate the NLRP3 inflammasome and promote programmed cell death under irremediable ER stress. *Cell Metab* (2012) 16(2):250–64. doi: 10.1016/j.cmet.2012.07.007

41. Bronner DN, Abuaita BH, Chen X, Fitzgerald KA, Nunez G, He Y, et al. Endoplasmic reticulum stress activates the inflammasome *via* NLRP3- and caspase-2-Driven mitochondrial damage. *Immunity* (2015) 43(3):451–62. doi: 10.1016/j.immuni.2015.08.008

42. Abu Kwaik Y, Bumann D. Host delivery of favorite meals for intracellular pathogens. *PLoS Pathog* (2015) 11(6):e1004866. doi: 10.1371/journal.ppat.1004866

43. Xavier MN, Winter MG, Spees AM, den Hartigh AB, Nguyen K, Roux CM, et al. PPARgamma-mediated increase in glucose availability sustains chronic brucella abortus infection in alternatively activated macrophages. *Cell Host Microbe* (2013) 14(2):159–70. doi: 10.1016/j.chom.2013.07.009

Pathogen recognition by sensory neurons: hypotheses on the specificity of sensory neuron signaling

Antoine Millet[1] and Nicholas Jendzjowsky[1,2]*

[1]Respiratory & Exercise Physiology, The Lundquist Institute for Biomedical Innovation at Harbor University of California Los Angeles (UCLA) Medical Center, Torrance, CA, United States, [2]Division of Respiratory and Critical Care Medicine and Physiology, David Geffen School of Medicine, University of California Los Angeles (UCLA), Los Angeles, CA, United States

Sensory neurons cooperate with barrier tissues and resident immune cells to form a significant aspect of defensive strategies in concert with the immune system. This assembly of neuroimmune cellular units is exemplified across evolution from early metazoans to mammalian life. As such, sensory neurons possess the capability to detect pathogenic infiltrates at barrier surfaces. This capacity relies on mechanisms that unleash specific cell signaling, trafficking and defensive reflexes. These pathways exploit mechanisms to amplify and enhance the alerting response should pathogenic infiltration seep into other tissue compartments and/or systemic circulation. Here we explore two hypotheses: 1) that sensory neurons' potential cellular signaling pathways require the interaction of pathogen recognition receptors and ion channels specific to sensory neurons and; 2) mechanisms which amplify these sensing pathways require activation of multiple sensory neuron sites. Where possible, we provide references to other apt reviews which provide the reader more detail on specific aspects of the perspectives provided here.

Introduction

Without the ability to detect, combat and evade harmful pathogens, the survival of early metazoan and, evolution to mammalian life would not have been possible (1). The importance of pathogenic detection and mitigation is evidenced by innate systems, mostly confined to the earliest sensory units, which originated in early multicellular organisms such as *Caenorhabditis elegans* (2, 3) and Hydra (4, 5). The mammalian development of pathogenic control was enabled by the divergence from one to two systems which evolved in parallel but in a mutually interrelated manner (1, 3). Mammalian immune and nervous

systems are organized in such a way that sentinel cells, with pathogenic detecting capabilities emanate alerting signals. When amplified chemical messengers are released to recruit combative cells that attack and/or eliminate invading threats (1).

Layers of defenses are involved in the intricacy of the immune system. Structural barrier cells within epithelial barrier layers coordinate a signalling cascade to recruit additional patrolling and cytotoxic cells, granulocytes, monocytes and lymphocytes to act and counter the invading threat. Following the cellular signalling posed by the epithelium, the immune system is then organized into lymphoid and secondary lymphoid organs, which harbor lymphoid-lineage cells that enable bi-directional communication with myeloid lineage cells, which have multiple methods to neutralize pathogens. Lymphoid lineage cells are triggered by numerous signals, simultaneously deployed at any one time, which was thought initially to be a failsafe system to back-up disruptions to poorly performing pathways (6, 7). However, the diversity and coordination of multiple cytokine and chemokine release appear to mediate the specificity of immune cell activation in response to pathogenic detection. This is due to the unique receptor gene expression profile on any single immune cell, providing a unique signature and the potential for differing modes of activation (8–10). Thus, deployment of a specific cytokine and chemokine pattern would then, presumably, activate a particular set of cells, in an exact way, to target a specific pathogen.

Like the immune system, the nervous system is partitioned to enable the sensing of the environment (sensory neurons within the peripheral nervous system), integrate and process information (medullary autonomic nervous system – and central hypothalamic centers) and finally, carry out signalling pathways (efferent nerves of the autonomic nervous system) to implement reflexes to receive information regarding deviations from homeostasis (1, 3). In the case of immediate pathogenic invasion, sensory neurons innervate all barrier (11–13) and mucosal surfaces (11–13) and patrol the bloodstream (14–16); interfaces which are vulnerable to infection and can come into contact with the outside environment. These important neural sensory clusters lie within the dorsal root ganglion (13), trigeminal ganglion (17), nodose/jugular ganglion (11, 18) and petrosal ganglion (14, 18), respectively. These neurons communicate with immune (19) and neuroendocrine cells (20, 21), either by the direct release of neurotransmitters into the immediate vicinity (19) or by relaying more extensive neural networks to innervate secondary lymphoid organs (22) and recruit other cells via secondary neurotransmitter release.

As such, it is clear that the anatomical association of sensory neurons with epithelial layers and indwelling immune cells form "neuroimmune cell units" (23) where their bidirectional communication between distinct neuronal and hematopoietic lineage cell types has afforded the ability to direct specific responses to a multitude of homeostatic disturbances. Prominent examples of the effects of these neuroimmune cell units are the cholinergic anti-inflammatory pathway (24, 25) or sympathetic influence on lymphopoiesis (26, 27). These modes of neural stimulation of immune function provide a sensory system which can quickly act should it identify pathogenic infiltration. Notably, the stimulation of this fast-acting sensory neuron pathogenic

detection has been demonstrated to either assist with 'immune' cell recruitment (19) or provide antimicrobial protection in and of itself through antimicrobial neuropeptides (28). If the specific recruitment of immune cell subsets occurs due to the unique chemokine receptor expression signature on any immune cell (5, 6), what is the mode of specific sensory neuron activation in the face of pathogenic detection?

Early sensory systems are a blueprint for neuroimmune cell units

Pathogen recognition in early metazoan life likely developed in sensory neurons first (3). These sensory units acquired innate defenses to detect and counter initial pathogenic infiltration. The concurrent development of early PRRs and ion channels shows a sharing of potential physiologic outcomes in response to pathogen detection. Both pathogenic opsonization and sensory neuron depolarization induce avoidance behaviors brought on upon specific neurotransmitter release. This subsequent release of neuropeptides also demonstrates microbial neutralization properties akin to bacteriocins (29, 30); which appears to be conserved in mammalian life (28). Neuronal cell death to implement calcium release for both additional cell recruitment and adjacent neuron stimulation (31, 32) was an additional strategy of early alerting responses and, in select cases, is a last resort for mammalian defences (33). Intriguingly, it would appear that apoptotic signalling and not apoptosis per se, are necessary for neuroimmune interactions as blockade of cell death does not diminish immune cell trafficking (34). Nevertheless, these early alerting responses occur rapidly, and it has been suggested that the speed of the neural response may influence the speed of the subsequent immune response (3, 34); a relationship which appears to hold in mammalian life (19, 33). However, early strategies evolved and gained more specificity with the increased dispersion of duties amongst cell types. The conservation of intracellular signalling pathways throughout the evolution of defensive strategies is exemplified in neuroimmune cell units (11–13, 35–39). How these signalling systems interact, and their functional outcome are now the focus of intense investigation.

Hypotheses on the specificity of sensory neuron PRR sensing of microbes

In the case of sensory neuron depolarization, ion channels often form the terminal portion of the cell signalling cascade as these channels are phosphorylated by upstream kinases set in motion when receptors are activated (40). The phosphorylation of ion channels on sensory neurons then increases the probability of depolarization, leading to neuronal excitation and neurotransmitter release (41, 42). Neuronal ion channel expression has allowed the sorting/clustering of neuronal subsets (11–13, 35–39). It is likely that the complexity of neural depolarization mediated by the activation of multiple but

sensory-specific ion channels in various ganglia would also enable a failsafe method to carry important information to the central nervous system (35, 43). It is equally likely that the specificity of neuronal activation also involves the activation of multiple receptors on any one neuron to offer specific neuron excitation. A notion carried from specific lymphoid cell activation afforded by chemokine receptor expression (8–10).

Furthermore, how and at which site of phosphorylation of each channel could offer another layer of complexity to add to the specific coding of neuronal activation by upstream receptors. Finally, subclusters of specific sensory neurons exist in multiple ganglia; can stimulation of neurons in multiple ganglia may augment neuroimmune reflexes? Therefore, the perspectives explored here are: whether the stimulation of multiple neurons within or between sensory ganglia, are phosphorylated differentially, and on differential phosphorylation sites, to provide a mechanism to code specific information to engage the appropriate neuroimmune reflex. In addition, the activation of ion channel phosphorylation on more than one set of nerves (ganglia) could augment these alerting reflexes.

Evidence for specificity of neuronal sub-clusters and ion channel phosphorylation as a means for specific neural responses

Detection of pathogenic invasion by sensory neurons, epithelial/barrier and innate antigen sensing/presenting immune cells is afforded by direct and indirect means (44). The direct recognition of pathogen-associated molecular patterns (PAMPs) and, therefore, neural activation involves four families of PRRs, including Toll-like receptors (TLRs), NOD-like receptors (NLRs), retinoic acid-inducible gene I (RIG-I)-like receptors (RLRs), formyl peptide receptors (FPRs) and C-lectin receptors (CLRs), each of which show notable differences regarding pathogen recognition, signal transduction, and intracellular downstream pathways (45–51) (Figure 1). The indirect activation of sensory neurons by pathogenic stimuli involves cytokines, chemokine, prostaglandin and, phospholipid stimulation of sensory neurons as a result of their release from either myeloid and lymphoid cells or, on neurons themselves (44, 80).

The differential expression of PRRs, cytokine, chemokine, prostaglandin and phospholipid receptors in sensory neurons has been shown in DRGs and trigeminal ganglia, nodose/jugular ganglia and carotid chemoreceptors using a multitude of transcriptomic technologies including single-cell/differential RNA sequencing (sc/dRNA-seq), *in situ* hybridization, immunohistochemistry, and electrophysiology (11–13, 35–39). This potential for neuronal activation by multiple ligands is clearly a distinct possibility, both by direct (sensing of microbes by PRRs) and indirect (sensing of cytokines released by immune cell sensing of microbes and recognition of alarmins which are produced or released by damaged and dying cells) means. Is it possible that the composition of these molecules released upon

initial immune cell sensing and the direct pathogenic stimulation of neurons can code specific neuronal signalling? To test this hypothesis would require a multitude of conditions with differing amounts and compositions of ligands in response to different pathogenic conditions; a difficult task which may be made easier with new-generation bioinformatic approaches involving RNA-protein interactions or the functional processing of neural activity. However, this same stimulation would also activate many other cell types with a similar receptor signature. Therefore, an additional layer of neuronal specificity is required to allow sensory neuron signaling specificity.

The composition of downstream ion channels is the defining characteristic of sensory neurons (11–13, 41). Protein phosphorylation is the most important post-translational protein modification which regulates enzymatic and ion channel activity, cell signalling and cellular localization (40, 81–83). Given the prominent role of protein kinases, which are readily activated as part of multiple signaling pathways (84–86), it is likely that their deployment can elicit downstream post-translational modification of ion channels to increase the probability of depolarization and/or neurotransmitter release which, in turn, could code specific nociceptor signals (Figure 1).

There are multiple examples of PRR receptors eliciting the engagement of kinases, including protein kinases, tyrosine, and Syk-family kinases as part of both PRR signalling (84–87) and indirect signaling from phospholipid, prostaglandin and cytokine receptors (87, 88). Further, the role phosphorylation plays in the modification of ion channel function in regards to neuronal depolarization has been documented in response, mainly, to GPCR mediated kinase activation such as prostaglandins and phospholipids (89, 90), and in response to some, but not all, neuroimmune conditions, examples include itch (91) and pain (92, 93). Subsequent activation of kinases in association with PRRs such as TLRs or CLRs and cytokines are certainly evidenced (87); whether their kinase activation results in ion channel depolarization or sensitization in these cases is not clear (Figure 1).

An additional possibility, in terms of the specificity of neuronal activation, appears to involve multiple phosphorylation sites per ion channel. The most prominent examples of these, within sensory neurons, lie with TRPV1, TRPC3 and Nav channels. Indeed, TRPV1 has three prominent phosphorylation sites, S502, S800 and T704 (94, 95), TRPC3 is phosphorylated on T11, S263, T646 and (96–98), and sensory neuron specific Nav channels, subtypes 1.8 and 1.9 are phosphorylated on D1-DII linker sites (99, 100). Each of these sites accepts kinases that appear to be directed in response to specific ligands such as prostaglandins and cytokines (40). This array of cellular signaling may be a manner in which multiple ion channels may be simultaneously phosphorylated and afford specificity similar to the multiple chemokine and cytokine stimulation of immune cells (44). The wide-ranging consequences of the multiplicity of signals contributing to ion channel phosphorylation could result in either pro- or anti-inflammatory responses. But an essential factor, which remains unanswered, is how the activation of kinases by specific receptors are directed/trafficked to particular phosphorylation sites on specific ion channels. There are examples of apparent coupling between PRRs

FIGURE 1

Neuronal pathogenic detection and cellular signaling pathways. Do ion channels incur specificity? The pathogenic sensing capability of sensory neurons is exemplified by the multitude of pathogenic detection receptors (51–79). These receptors appear to be linked spatially and by protein kinase stimulation/phosphorylation of downstream ion channels. *However, as indicated by the diamond, what forces direct the specific trafficking of protein kinases to specific phosphorylation sites on downstream ion channels? And, to which specific ion channel/set of ion channels?

and TRPs, such as TLR4 to TRPV1 and TLR7 to TRPA1 (44). What is a more probable cellular signalling scenario is that the dispersion of kinases, in response to stimulation, by a multitude of receptors, phosphorylates/post-translationally modifies the composition of channels present within each specific neuron subset. This would speak to the mode of specificity mentioned above. However, this hypothesis remains to be tested.

Evidence for multiple ganglion stimulation and alteration of defensive reflexes

In early eukaryotic life, the capability of neural signals to recruit cells from seemingly 'distant' sites (3, 101) demonstrated the capability for early neuroimmune cell unit coordination and broader protective capabilities. However, as eukaryotic life gained the complexity and partitioning of organ systems, both the immune and nervous systems organized themselves by sub-dividing specific hubs for either the storage of cells (e.g. secondary lymphoid organs, resident tissue cells) or to serve as a relay station for information (e.g. neural ganglia).

In the case of the sensory nervous system, necessary to form a part of the neuroimmune landscape, neurons are sorted and partitioned into different peripheral ganglia which innervate different organ systems or components of organ systems (19, 102). For example, the dorsal root ganglia innervate the skin (13, 102). In contrast, the vagus senses internal organs, and each neuron/neuron subset is responsible for a single organ system (11, 35, 102) and, possibly, tissue layer (11, 103, 104).

Signals from sensory neurons travel to the nucleus tractus solitarius and synapse onto the dorsal motor nucleus of the vagus (to elicit immediate efferent nerve activity) and the paraventricular nucleus within the hippocampus, amygdala and periaqueductal grey (to carry out grander neuroendocrine signalling involving the hypothalamic pituitary adrenal axis; HPA). Effective neural signalling of immunity is critically dependent on adrenal cortex release of glucocorticoids in response to a number of perturbations (105, 106) The integration of the neuroendocrine involvement in neuroimmune signalling is highlighted by stress responses (involved in a wide variety of threats to homeostasis) which signals the adrenal cortex to induce corticosteroid release which has a wide array of immune influence (105–107). Additionally, new and important reflexes of HPA involvement are highlighted with

the cholinergic anti-inflammatory pathway (108) and humoral immunity (109) in response to infection.

Intriguingly, disease and its severity can often be magnified when it is 'leaked' beyond the initial site of infection into other tissue layers, organ systems and/or the blood; examples of these lie with infections that can quickly precipitate sepsis (16). Therefore, a situation may arise where multiple neurons that may signal differing ganglia could signal an alerting response should the disease spread beyond the initial site/tissue of infection.

One such case where infection could travel beyond the initial site of infection but remain within a single organ system, yet stimulate multiple sensory neurons which are housed in differing ganglia, is exemplified in the gut (103). Indeed, the colon is partitioned into intrinsic and extrinsic sensory neurons, with cell bodies in the intrinsic and nodose ganglia, respectively (103) (Figure 2). It is likely that stimulation of both ganglia by the detection of pathogenic harm by both sets of sensory neurons may provide an increased alerting response.

Indeed, the above discussion readily acknowledges that the first line of neuroimmune defence occurs with the release of these sensory neurotransmitters which act to recruit the appropriate cell to clear the pathogenic invasion. However, should disease progress to such a state where barrier surfaces become leaky/ decoupled and allow the passage of microbial pathogens and/or cytokines into the bloodstream, additional defenses would be stimulated. In this regard, an additional line of defense would be recruited if pathogenic infiltration should enter the blood stream;

the carotid chemoreceptors (16) the main sensory organ which patrols hemolytic homeostasis (15) would also be stimulated. Evidence demonstrates the carotid chemoreceptors' ability to detect pathogenic patterns (16) as well as substances released in response to disease states/allergy (110, 111) as their composition of pathogenic detection is notable (38). We have demonstrated the possibility for this biologic scenario to occur in our dual vagus and carotid chemoreceptor preparation (43). Specifically, we showed that when the sensory neurons within the lungs are stimulated with either proteases or adenosine triphosphate and the carotid chemoreceptors with their known stimulus, low oxygen tension of their perfusate (blood), signals emanating to the efferent vagus are augmented, likely to regulate defensive reflexes such as mucus secretion and airway constriction (35) and/or to signal the cholinergic anti-inflammatory pathway (24, 25). This scenario shows that not only are subtypes of neurons within ganglia able to regulate and code specific neural signals in response to pathogenic stimulation but, also that augmentation of reflexes is possible when anatomically specific and important ganglia are stimulated at the same time. Therefore, the cascading stimulation of sensory neurons would provide the potential to augment and/or strengthen the neural coordination of immune cells, should pathogenic stimuli be sensed by multiple immune capable ganglia. In the context of specific coding of neural depolarization by the expression of differential receptors, ion channels and their respective phosphorylation, how would stimulation of two neuron sets with similar receptor/ion channel composition augment
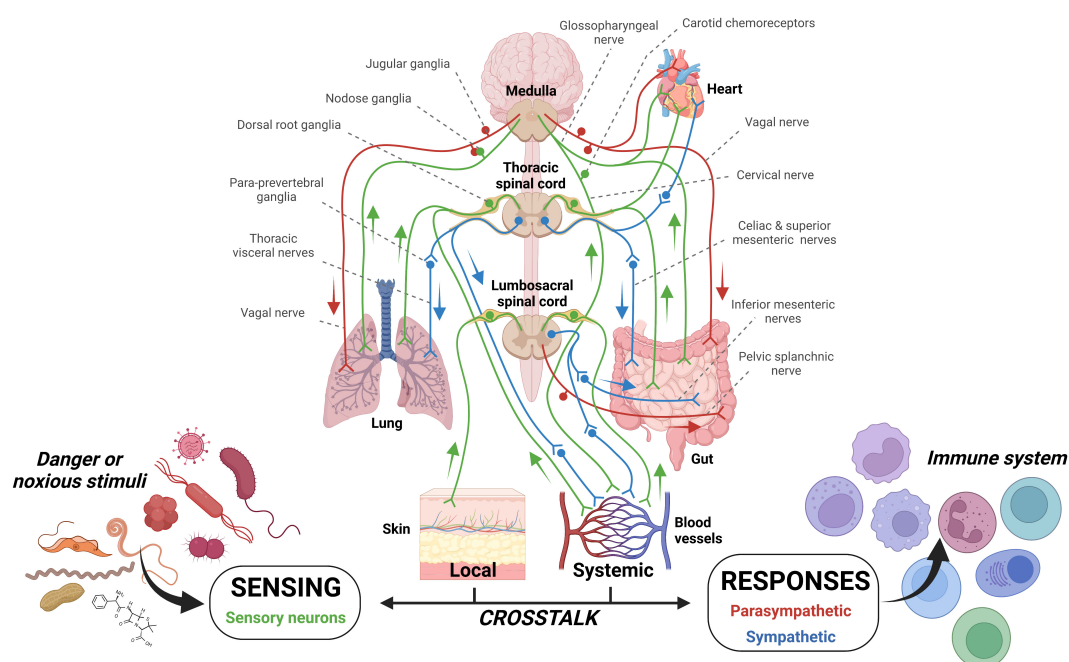
FIGURE 2
Sensory innervation of barrier tissues. The innervation of tissues by sensory neurons and the parasympathetic and sympathetic arms of the autonomic nervous system affords constant patrol of mammalian systems. In addition, the enteric nervous system has a layered system of innervation within the gut. These systems allow constant detection and also the possibility of dual stimulation should multiple neurons in different locations/tissues be stimulation. Can parallel and concurrent sensory neuron pathogenic stimulation increase signaling magnitude? The potential for this case has been examined previously (43, 103).

neuroimmune signalling? One possibility would simply be an increased rate of neuronal firing to elicit immunogenic neurotransmitter release. How would dual stimulation of two neuron sets with differing receptor/ion channel composition augment neuroimmune signalling? Would such an instance change the composition of neurotransmitter release and ultimately affect the chemotaxis of immune cells?

Perspectives/conclusions

Protection and evasion of disease has required an ever-evolving system with additive layers throughout the evolution of eukaryotic life. With the increasing complexity of mammalian body plans, host defence involves coordinating two defensive systems and organising cell clusters within and between systems. This perspectives essay has attempted to highlight how sensory neurons, an important part of the defensive response to microbial invasion, code specific information to either influence neuronal and immune cell stimulation at the site of infection. Additionally, should invasion extend beyond this site, larger reflexes which may be required to clear the pathogenic infiltration would become activated. However, much remains to be uncovered and, as recently posed by others (44), information regarding what this excitation means in a (patho) physiologic context and how it coordinates the release of neurotransmitter to act directly on immune cells or signal the central nervous system to coordinate grander neuro-immune regulation requires further intense investigation.

Data availability statement

The original contributions presented in the study are included in the article/supplementary material. Further inquiries can be directed to the corresponding author.

Author contributions

All authors contributed to the conception and composition of the manuscript. AM completed the figures. All authors approve the manuscript in the submitted form.

Funding

Acknowledgments

Conflict of interest

The authors declare that the research was conducted in the absence of any commercial or financial relationships that could be construed as a potential conflict of interest.

Publisher's note

All claims expressed in this article are solely those of the authors and do not necessarily represent those of their affiliated organizations, or those of the publisher, the editors and the reviewers. Any product that may be evaluated in this article, or claim that may be made by its manufacturer, is not guaranteed or endorsed by the publisher.

References

1. Veiga-Fernandes H, Freitas AA. The s(c)ensory immune system theory. *Trends Immunol* (2017) 38(10):777–88. doi: 10.1016/j.it.2017.02.007

2. Wani KA, Goswamy D, Irazoqui JE. Nervous system control of intestinal host defense in c. elegans. *Curr Opin Neurobiol* (2020) 62:1–9. doi: 10.1016/j.conb.2019.11.007

3. Kraus A, Buckley KM, Salinas I. Sensing the world and its dangers: an evolutionary perspective in neuroimmunology. *eLife* (2021) 10:e66706. doi: 10.7554/eLife.66706

4. Klimovich AV, Bosch TCG. Rethinking the role of the nervous system: lessons from the hydra holobiont. *Bioessays* (2018) 40(9):e1800060. doi: 10.1002/bies.201800060

5. Franzenburg S, Fraune S, Künzel S, Baines JF, Domazet-Loso T, Bosch TCG. MyD88-deficient hydra reveal an ancient function of TLR signaling in sensing bacterial colonizers. *Proc Natl Acad Sci U.S.A.* (2012) 109(47):19374–9. doi: 10.1073/pnas.1213110109

6. O'Boyle G. The yin and yang of chemokine receptor activation. *Br J Pharmacol* (2012) 166(3):895–7. doi: 10.1111/j.1476-5381.2011.01759.x

7. Proudfoot AEI, Bonvin P, Power CA. Targeting chemokines: pathogens can, why can't we? *Cytokine* (2015) 74(2):259–67. doi: 10.1016/j.cyto.2015.02.011

8. Dyer DP. Understanding the mechanisms that facilitate specificity, not redundancy, of chemokine-mediated leukocyte recruitment. *Immunology* (2020) 160 (4):336–44. doi: 10.1111/imm.13200

9. Ridley AJ, Ou Y, Karlsson R, Pun N, Birchenough HL, Jowitt TA, et al. Chemokines form complex signals during inflammation and disease that can be decoded by extracellular matrix proteoglycans. *bioRxiv* (2022), 508420. doi: 10.1101/2022.09.20.508420

10. Dyer DP, Medina-Ruiz L, Bartolini R, Schuette F, Hughes CE, Pallas K, et al. Chemokine receptor redundancy and specificity are context dependent. *Immunity* (2019) 50(2):378–389.e5. doi: 10.1016/j.immuni.2019.01.009

11. Kupari J, Häring M, Agirre E, Castelo-Branco G, Ernfors P. An atlas of vagal sensory neurons and their molecular specialization. *Cell Rep* (2019) 27(8):2508–2523.e4. doi: 10.1016/j.celrep.2019.04.096

12. Häring M, Zeisel A, Hochgerner H, Rinwa P, Jakobsson JET, Lönnerberg P, et al. Neuronal atlas of the dorsal horn defines its architecture and links sensory input to transcriptional cell types. *Nat Neurosci* (2018) 21(6):869–80. doi: 10.1038/s41593-018-0141-1

13. Usoskin D, Furlan A, Islam S, Abdo H, Lönnerberg P, Lou D, et al. Unbiased classification of sensory neuron types by large-scale single-cell RNA sequencing. *Nat Neurosci* (2015) 18(1):145–53. doi: 10.1038/nn.3881

14. Ackland GL, Kazymov V, Marina N, Singer M, Gourine AV. Peripheral neural detection of danger-associated and pathogen-associated molecular patterns. *Crit Care Med* (2013) 41(6):e85–92. doi: 10.1097/CCM.0b013e31827c0b05

15. Prabhakar NR, Joyner MJ. Tasting arterial blood: what do the carotid chemoreceptors sense? *Front Physiol* (2015) 5:524. doi: 10.3389/fphys.2014.00524

16. Katayama PL, Leirão IP, Kanashiro A, Luiz JPM, Cunha FQ, Navegantes LCC, et al. The carotid body detects circulating tumor necrosis factor-alpha to activate a sympathetic anti-inflammatory reflex. *Brain Behav Immun* (2022) 102:370–86. doi: 10.1016/j.bbi.2022.03.014

17. de Moraes ER, Kushmerick C, Naves LA. Morphological and functional diversity of first-order somatosensory neurons. *Biophys Rev* (2017) 9(5):847–56. doi: 10.1007/s12551-017-0321-3

18. Prescott SL, Liberles SD. Internal senses of the vagus nerve. *Neuron* (2022) 110: P579–599. doi: 10.1016/j.neuron.2021.12.020

19. Udit S, Blake K, Chiu IM. Somatosensory and autonomic neuronal regulation of the immune response. *Nat Rev Neurosci.* (2022) 23:57–171. doi: 10.1038/s41583-021-00555-4

20. Huang Y, Zhao C, Su X. Neuroimmune regulation of lung infection and inflammation. *QJM* (2019) 112(7):483–7. doi: 10.1093/qjmed/hcy154

21. Quatrini L, Vivier E, Ugolini S. Neuroendocrine regulation of innate lymphoid cells. *Immunol Rev* (2018) 286(1):120–36. doi: 10.1111/imr.12707

22. De Virgiliis F, Oliva VM, Kizil B, Scheiermann C. Control of lymph node activity by direct local innervation. *Trends Neurosci* (2022) 45(9):704–12. doi: 10.1016/j.tins.2022.06.006

23. Godinho-Silva C, Cardoso F, Veiga-Fernandes H. Neuro-immune cell units: a new paradigm in physiology. *Annu Rev Immunol* (2019) 37:19–46. doi: 10.1146/annurev-immunol-042718-041812

24. Tracey KJ. Approaching the next revolution? evolutionary integration of neural and immune pathogen sensing and response [Internet]. *Cold Spring Harb Perspect Biol* (2015) 7(2). doi: 10.1101/cshperspect.a016360

25. Tracey KJ. Reflex control of immunity. *Nat Rev Immunol* (2009) 9(6):418–28. doi: 10.1038/nri2566

26. Hanoun M, Maryanovich M, Arnal-Estapé A, Frenette PS. Neural regulation of hematopoiesis, inflammation, and cancer. *Neuron* (2015) 86(2):360–73. doi: 10.1016/j.neuron.2015.01.026

27. Katayama Y, Battista M, Kao W-M, Hidalgo A, Peired AJ, Thomas SA, et al. Signals from the sympathetic nervous system regulate hematopoietic stem cell egress from bone marrow. *Cell* (2006) 124(2):407–21. doi: 10.1016/j.cell.2005.10.041

28. Lee EY, Chan LC, Wang H, Lieng J, Hung M, Srinivasan Y, et al. PACAP is a pathogen-inducible resident antimicrobial neuropeptide affording rapid and contextual molecular host defense of the brain. *Proc Natl Acad Sci U.S.A.* (2021) 118(1): e1917623117. doi: 10.1073/pnas.1917623117

29. Hanson MA, Lemaitre B, Unckless RL. Dynamic evolution of antimicrobial peptides underscores trade-offs between immunity and ecological fitness. *Front Immunol* (2019) 10:2620. doi: 10.3389/fimmu.2019.02620

30. Lezi E, Zhou T, Koh S, Chuang M, Sharma R, Pujol N, et al. An antimicrobial peptide and its neuronal receptor regulate dendrite degeneration in aging and infection. *Neuron* (2018) 97(1):125–138.e5. doi: 10.1016/j.neuron.2017.12.001

31. Ma Y, Li J, Chiu I, Wang Y, Sloane JA, Lü J, et al. Toll-like receptor 8 functions as a negative regulator of neurite outgrowth and inducer of neuronal apoptosis. *J Cell Biol* (2006) 175(2):209–15. doi: 10.1083/jcb.200606016

32. Kamm K, Schierwater B, DeSalle R. Innate immunity in the simplest animals - placozoans. *BMC Genomics* (2019) 20(1):5. doi: 10.1186/s12864-018-5377-3

33. Neel DV, Basu H, Gunner G, Chiu IM. Catching a killer: mechanisms of programmed cell death and immune activation in amyotrophic lateral sclerosis. *Immunol Rev* (2022) 311(1):130–50. doi: 10.1111/imr.13083

34. Sepahi A, Kraus A, Casadei E, Johnston CA, Galindo-Villegas J, Kelly C, et al. Olfactory sensory neurons mediate ultrarapid antiviral immune responses in a TrkA-dependent manner. *PNAS* (2019) 116(25):12428–36. doi: 10.1073/pnas.1900083116

35. Prescott SL, Umans BD, Williams EK, Brust RD, Liberles SD. An airway protection program revealed by sweeping genetic control of vagal afferents. *Cell* (2020) 181(3):574–589.e14. doi: 10.1016/j.cell.2020.03.004

36. Zeisel A, Hochgerner H, Lönnerberg P, Johnsson A, Memic F, van der Zwan J, et al. Molecular architecture of the mouse nervous system. *Cell* (2018) 174(4):999–1014.e22. doi: 10.1016/j.cell.2018.06.021

37. Zheng Y, Liu P, Bai L, Trimmer JS, Bean BP, Ginty DD. Deep sequencing of somatosensory neurons reveals molecular determinants of intrinsic physiological properties. *Neuron* (2019) 103(4):598–616.e7. doi: 10.1016/j.neuron.2019.05.039

38. Zhou T, Chien M, Kaleem S, Matsunami H. Single cell transcriptome analysis of mouse carotid body glomus cells. *J Physiol* (2016) 594(15):4225–51. doi: 10.1113/JP271936

39. Chang AJ. Acute oxygen sensing by the carotid body: from mitochondria to plasma membrane. *J Appl Physiol* (2017) 123(5):1335–43. doi: 10.1152/japplphysiol.00398.2017

40. Voolstra O, Huber A. Post-translational modifications of TRP channels. *Cells* (2014) 3(2):258–87. doi: 10.3390/cells3020258

41. Nilius B, Owsianik G. The transient receptor potential family of ion channels. *Genome Biol* (2011) 12(3):218. doi: 10.1186/gb-2011-12-3-218

42. Chahine M, O'Leary ME. Regulation/modulation of sensory neuron sodium channels. *Handb Exp Pharmacol* (2014) 221:111–35. doi: 10.1007/978-3-642-41588-3_6

43. Zyuzin J, Jendzjowsky N. Neuroanatomical and neurophysiological evidence of pulmonary nociceptor and carotid chemoreceptor convergence in the nucleus tractus solitarius and nucleus ambiguus. *J Neurophysiol* (2022) 127(6):1511–8. doi: 10.1152/jn.00125.2022

44. Donnelly CR, Chen O, Ji R-R. How do sensory neurons sense danger signals? *Trends Neurosci* (2020) 43(10):822–38. doi: 10.1016/j.tins.2020.07.008

45. Takeuchi O, Akira S. Pattern recognition receptors and inflammation. *Cell* (2010) 140(6):805–20. doi: 10.1016/j.cell.2010.01.022

46. Kumar H, Kawai T, Akira S. Pathogen recognition in the innate immune response. *Biochem J* (2009) 420(1):1–16. doi: 10.1042/BJ20090272

47. Carneiro L a. M, Magalhaes JG, Tattoli I, Philpott DJ, Travassos LH. Nod-like proteins in inflammation and disease. *J Pathol* (2008) 214(2):136–48. doi: 10.1002/path.2271

48. Kufer TA, Banks DJ, Philpott DJ. Innate immune sensing of microbes by nod proteins. *Ann N Y Acad Sci* (2006) 1072:19–27. doi: 10.1196/annals.1326.020

49. Goubau D, Deddouche S, Reis e Sousa C. Cytosolic sensing of viruses. *Immunity* (2013) 38(5):855–69. doi: 10.1016/j.immuni.2013.05.007

50. Abe T, Marutani Y, Shoji I. Cytosolic DNA-sensing immune response and viral infection. *Microbiol Immunol* (2019) 63(2):51–64. doi: 10.1111/1348-0421.12669

51. Chiu IM, Heesters BA, Ghasemlou N, Von Hehn CA, Zhao F, Tran J, et al. Bacteria activate sensory neurons that modulate pain and inflammation. *Nature* (2013) 501(7465):52–7. doi: 10.1038/nature12479

52. Akira S, Uematsu S, Takeuchi O. Pathogen recognition and innate immunity. *Cell* (2006) 124(4):783–801. doi: 10.1016/j.cell.2006.02.015

53. Meseguer V, Alpizar YA, Luis E, Tajada S, Denlinger B, Fajardo O, et al. TRPA1 channels mediate acute neurogenic inflammation and pain produced by bacterial endotoxins. *Nat Commun* (2014) 5:3125. doi: 10.1038/ncomms4125

54. Chiu IM, Pinho-Ribeiro FA, Woolf CJ. Pain and infection: pathogen detection by nociceptors. *Pain* (2016) 157(6):1192–3. doi: 10.1097/j.pain.0000000000000559

55. Han Q, Liu D, Convertino M, Wang Z, Jiang C, Kim YH, et al. miRNA-711 binds and activates TRPA1 extracellularly to evoke acute and chronic pruritus. *Neuron* (2018) 99(3):449–463.e6. doi: 10.1016/j.neuron.2018.06.039

56. Samad TA, Moore KA, Sapirstein A, Billet S, Allchorne A, Poole S, et al. Interleukin-1beta-mediated induction of cox-2 in the CNS contributes to inflammatory pain hypersensitivity. *Nature* (2001) 410(6827):471–5. doi: 10.1038/35068566

57. Mathivanan S, Devesa I, Changeux J-P, Ferrer-Montiel A. Bradykinin induces TRPV1 exocytotic recruitment in peptidergic nociceptors. *Front Pharmacol* (2016) 7:178. doi: 10.3389/fphar.2016.00178

58. Binshtok AM, Wang H, Zimmermann K, Amaya F, Vardeh D, Shi L, et al. Nociceptors are interleukin-1beta sensors. *J Neurosci* (2008) 28(52):14062–73. doi: 10.1523/JNEUROSCI.3795-08.2008

59. Kashem SW, Riedl MS, Yao C, Honda CN, Vulchanova L, Kaplan DH. Nociceptive sensory fibers drive interleukin-23 production from CD301b+ dermal dendritic cells and drive protective cutaneous immunity. *Immunity* (2015) 43(3):515–26. doi: 10.1016/j.immuni.2015.08.016

60. Wagner R, Myers RR. Endoneurial injection of TNF-alpha produces neuropathic pain behaviors. *Neuroreport* (1996) 7(18):2897–901. doi: 10.1097/00001756-199611250-00018

61. Hepburn L, Prajsnar TK, Klapholz C, Moreno P, Loynes CA, Ogryzko NV, et al. Innate immunity. a spaetzle-like role for nerve growth factor β in vertebrate immunity to staphylococcus aureus. *Science* (2014) 346(6209):641–6. doi: 10.1126/science.1258705

62. Qi J, Buzas K, Fan H, Cohen JI, Wang K, Mont E, et al. Painful pathways induced by TLR stimulation of dorsal root ganglion neurons. *J Immunol* (2011) 186(11):6417–26. doi: 10.4049/jimmunol.1001241

63. Miller JJ, Aoki K, Moehring F, Murphy CA, O'Hara CL, Tiemeyer M, et al. Neuropathic pain in a fabry disease rat model. *JCI Insight* (2018) 3(6):e99171, 99171. doi: 10.1172/jci.insight.99171

64. Xu Z-Z, Kim YH, Bang S, Zhang Y, Berta T, Wang F, et al. Inhibition of mechanical allodynia in neuropathic pain by TLR5-mediated a-fiber blockade. *Nat Med* (2015) 21(11):1326–31. doi: 10.1038/nm.3978

65. Maruyama K, Takayama Y, Sugisawa E, Yamanoi Y, Yokawa T, Kondo T, et al. The ATP transporter VNUT mediates induction of dectin-1-Triggered candida nociception. *iScience* (2018) 6:306–18. doi: 10.1016/j.isci.2018.08.007

66. Diogenes A, Ferraz CCR, Akopian AN, Henry MA, Hargreaves KM. LPS sensitizes TRPV1 via activation of TLR4 in trigeminal sensory neurons. *J Dent Res* (2011) 90(6):759–64. doi: 10.1177/0022034511400225

67. Bautista DM, Jordt S-E, Nikai T, Tsuruda PR, Read AJ, Poblete J, et al. TRPA1 mediates the inflammatory actions of environmental irritants and proalgesic agents. *Cell* (2006) 124(6):1269–82. doi: 10.1016/j.cell.2006.02.023

68. Lim JY, Choi S-I, Choi G, Hwang SW. Atypical sensors for direct and rapid neuronal detection of bacterial pathogens. *Mol Brain* (2016) 9:26. doi: 10.1186/s13041-016-0202-x

69. Caterina MJ, Leffler A, Malmberg AB, Martin WJ, Trafton J, Petersen-Zeitz KR, et al. Impaired nociception and pain sensation in mice lacking the capsaicin receptor. *Science* (2000) 288(5464):306–13. doi: 10.1126/science.288.5464.306

70. Davis JB, Gray J, Gunthorpe MJ, Hatcher JP, Davey PT, Overend P, et al. Vanilloid receptor-1 is essential for inflammatory thermal hyperalgesia. *Nature* (2000) 405(6783):183–7. doi: 10.1038/35012076

71. Szabo-Pardi TA, Barron LR, Lenert ME, Burton MD. Sensory neuron TLR4 mediates the development of nerve-injury induced mechanical hypersensitivity in female mice. *Brain Behav Immun* (2021) 97:42–60. doi: 10.1016/j.bbi.2021.06.011

72. Amaya F, Wang H, Costigan M, Allchorne AJ, Hatcher JP, Egerton J, et al. The voltage-gated sodium channel Na(v)1.9 is an effector of peripheral inflammatory pain hypersensitivity. *J Neurosci* (2006) 26(50):12852–60. doi: 10.1523/JNEUROSCI.4015-06.2006

73. Stirling LC, Forlani G, Baker MD, Wood JN, Matthews EA, Dickenson AH, et al. Nociceptor-specific gene deletion using heterozygous NaV1.8-cre recombinase mice. *Pain* (2005) 113(1–2):27–36. doi: 10.1016/j.pain.2004.08.015

74. Nassar MA, Stirling LC, Forlani G, Baker MD, Matthews EA, Dickenson AH, et al. Nociceptor-specific gene deletion reveals a major role for Nav1.7 (PN1) in acute and inflammatory pain. *Proc Natl Acad Sci U.S.A.* (2004) 101(34):12706–11. doi: 10.1073/pnas.0404915101

75. Kerr BJ, Souslova V, McMahon SB, Wood JN. A role for the TTX-resistant sodium channel nav 1.8 in NGF-induced hyperalgesia, but not neuropathic pain. *Neuroreport* (2001) 12(14):3077–80. doi: 10.1097/00001756-200110080-00019

76. Romagnani A, Vettore V, Rezzonico-Jost T, Hampe S, Rottoli E, Nadolni W, et al. TRPM7 kinase activity is essential for T cell colonization and alloreactivity in the gut. *Nat Commun* (2017) 8:1917. doi: 10.1038/s41467-017-01960-z

77. Beesetty P, Wieczerzak KB, Gibson JN, Kaitsuka T, Luu CT, Matsushita M, et al. Inactivation of TRPM7 kinase in mice results in enlarged spleens, reduced T-cell proliferation and diminished store-operated calcium entry. *Sci Rep* (2018) 8(1):1–22. doi: 10.1038/s41598-018-21004-w

78. Khalil M, Babes A, Lakra R, Försch S, Reeh PW, Wirtz S, et al. Transient receptor potential melastatin 8 ion channel in macrophages modulates colitis through a balance-shift in TNF-alpha and interleukin-10 production. *Mucosal Immunol* (2016) 9 (6):1500–13. doi: 10.1038/mi.2016.16

79. Schappe MS, Szteyn K, Stremska ME, Mendu SK, Downs TK, Seegren PV, et al. Chanzyme TRPM7 mediates the Ca2+ influx essential for lipopolysaccharide-induced toll-like receptor 4 endocytosis and macrophage activation. *Immunity* (2018) 48(1):59–74.e5. doi: 10.1016/j.immuni.2017.11.026

80. Santoni G, Cardinali C, Morelli MB, Santoni M, Nabissi M, Amantini C. Danger- and pathogen-associated molecular patterns recognition by pattern-recognition receptors and ion channels of the transient receptor potential family triggers the inflammasome activation in immune cells and sensory neurons. *J Neuroinflamm* (2015) 12:21. doi: 10.1186/s12974-015-0239-2

81. Morrison RS, Kinoshita Y, Johnson MD, Uo T, Ho JT, McBee JK, et al. Proteomic analysis in the neurosciences. *Mol Cell Proteomics* (2002) 1(8):553–60. doi: 10.1074/mcp.R200004-MCP200

82. Pei Z, Pan Y, Cummins TR. Posttranslational modification of sodium channels. *Handb Exp Pharmacol* (2018) 246:101–24. doi: 10.1007/164_2017_69

83. Karve TM, Cheema AK. Small changes huge impact: the role of protein posttranslational modifications in cellular homeostasis and disease. *J Amino Acids* (2011) 2011:207691. doi: 10.4061/2011/207691

84. Dj L, Mr L. Protein kinase c and toll-like receptor signaling [Internet]. *Enzyme Res* (2011) 2011. doi: 10.4061/2011/537821

85. Tang J, Lin G, Langdon WY, Tao L, Zhang J. Regulation of c-type lectin receptor-mediated antifungal immunity. *Front Immunol* (2018) 9:123. doi: 10.3389/fimmu.2018.00123

86. Lim PS, Sutton CR, Rao S. Protein kinase c in the immune system: from signalling to chromatin regulation. *Immunology* (2015) 146(4):508–22. doi: 10.1111/imm.12510

87. Neagu M, Constantin C. Signal transduction in immune cells and protein kinases. *Adv Exp Med Biol* (2021) 1275:133–49. doi: 10.1007/978-3-030-49844-3_5

88. Jiang H, Galtes D, Wang J. Rockman HA. G protein-coupled receptor signaling: transducers and effectors. *Am J Physiology-Cell Physiol* (2022) 323(3):C731–48. doi: 10.1152/ajpcell.00210.2022

89. Kollarik M, Undem BJ. Activation of bronchopulmonary vagal afferent nerves with bradykinin, acid and vanilloid receptor agonists in wild-type and TRPV1-/- mice. *J Physiol (Lond)* (2004) 555(Pt 1):115–23. doi: 10.1113/jphysiol.2003.054890

90. Patil MJ, Meeker S, Bautista D, Dong X, Undem BJ. Sphingosine-1-phosphate activates mouse vagal airway afferent c-fibres via S1PR3 receptors. *J Physiol* (2019) 597 (7):2007–19. doi: 10.1113/JP277521

91. Liu Q, Tang Z, Surdenikova L, Kim S, Patel KN, Kim A, et al. Sensory neuron-specific GPCR mrgprs are itch receptors mediating chloroquine-induced pruritus. *Cell* (2009) 139(7):1353–65. doi: 10.1016/j.cell.2009.11.034

92. Costello RW, Maloney M, Atiyeh M, Gleich G, Walsh MT. Mechanism of sphingosine 1-phosphate- and lysophosphatidic acid-induced up-regulation of adhesion molecules and eosinophil chemoattractant in nerve cells. *Int J Mol Sci* (2011) 12(5):3237–49. doi: 10.3390/ijms12053237

93. Juárez-Contreras R, Rosenbaum T, Morales-Lázaro SL. Lysophosphatidic acid and ion channels as molecular mediators of pain. *Front Mol Neurosci* (2018) 11:462. doi: 10.3389/fnmol.2018.00462

94. Numazaki M, Tominaga T, Toyooka H, Tominaga M. Direct phosphorylation of capsaicin receptor VR1 by protein kinase cε and identification of two target serine residues. *J Biol Chem* (2002) 277(16):13375–8. doi: 10.1074/jbc.C200104200

95. Jung J, Shin JS, Lee S-Y, Hwang SW, Koo J, Cho H, et al. Phosphorylation of vanilloid receptor 1 by Ca2+/calmodulin-dependent kinase II regulates its vanilloid binding. *J Biol Chem* (2004) 279(8):7048–54. doi: 10.1074/jbc.M311448200

96. Trebak M, Hempel N, Wedel BJ, Smyth JT, Bird GSJ, Putney JW. Negative regulation of TRPC3 channels by protein kinase c-mediated phosphorylation of serine 712. *Mol Pharmacol* (2005) 67(2):558–63. doi: 10.1124/mol.104.007252

97. Kwan H-Y, Huang Y, Yao X. Regulation of canonical transient receptor potential isoform 3 (TRPC3) channel by protein kinase G. *Proc Natl Acad Sci U.S.A.* (2004) 101(8):2625–30. doi: 10.1073/pnas.0304471101

98. Vazquez G, Wedel BJ, Kawasaki BT, Bird GSJ, Putney JW. Obligatory role of src kinase in the signaling mechanism for TRPC3 cation channels. *J Biol Chem* (2004) 279 (39):40521–8. doi: 10.1074/jbc.M405280200

99. Scheuer T. Regulation of sodium channel activity by phosphorylation. *Semin Cell Dev Biol* (2011) 22(2):160–5. doi: 10.1016/j.semcdb.2010.10.002

100. Kerth CM, Hautvast P, Körner J, Lampert A, Meents JE. Phosphorylation of a chronic pain mutation in the voltage-gated sodium channel Nav1.7 increases voltage sensitivity. *J Biol Chem* (2020) 296:100227. doi: 10.1074/jbc.RA120.014288

101. Labed SA, Wani KA, Jagadeesan S, Hakkim A, Najibi M, Irazoqui JE. Intestinal epithelial wnt signaling mediates acetylcholine-triggered host defense against infection. *Immunity* (2018) 48(5):963–978.e3. doi: 10.1016/j.immuni.2018.04.017

102. Crawford LK, Caterina MJ. Functional anatomy of the sensory nervous system: updates from the neuroscience bench. *Toxicol Pathol* (2020) 48(1):174–89. doi: 10.1177/0192623319869011

103. Meerschaert KA, Adelman PC, Friedman RL, Albers KM, Koerber HR, Davis BM. Unique molecular characteristics of visceral afferents arising from different levels of the neuraxis: location of afferent somata predicts function and stimulus detection modalities. *J Neurosci* (2020) 40(38):7216–28. doi: 10.1523/JNEUROSCI.1426-20.2020

104. Su Y, Barr J, Jaquish A, Xu J, Verheyden JM, Sun X. Identification of lung innervating sensory neurons and their target specificity. *Am J Physiol Lung Cell Mol Physiol* (2022) 322(1):L50–63. doi: 10.1152/ajplung.00376.2021

105. Webster JI, Tonelli L, Sternberg EM. Neuroendocrine regulation of immunity. *Annu Rev Immunol* (2002) 20:125–63. doi: 10.1146/annurev.immunol.20.082401.104914

106. Mueller B, Figueroa A, Robinson-Papp J. Structural and functional connections between the autonomic nervous system, hypothalamic–pituitary–adrenal axis, and the immune system: a context and time dependent stress response network. *Neurol Sci* (2022) 43(2):951–60. doi: 10.1007/s10072-021-05810-1

107. Wohleb ES, McKim DB, Sheridan JF, Godbout JP. Monocyte trafficking to the brain with stress and inflammation: a novel axis of immune-to-brain communication that influences mood and behavior. *Front Neurosci* (2015) 8:447. doi: 10.3389/fnins.2014.00447

108. Souza ACP, Souza CM, Amaral CL, Lemes SF, Santucci LF, Milanski M, et al. Short-term high-fat diet consumption reduces hypothalamic expression of the nicotinic acetylcholine receptor α7 subunit (α7nAChR) and affects the anti-inflammatory response in a mouse model of sepsis. *Front Immunol* (2019) 10:565. doi: 10.3389/fimmu.2019.00565

109. Zhang X, Lei B, Yuan Y, Zhang L, Hu L, Jin S, et al. Brain control of humoral immune responses amenable to behavioural modulation. *Nature* (2020) 581 (7807):204–8. doi: 10.1038/s41586-020-2235-7

110. Jendzjowsky NG, Roy A, Wilson RJA. Asthmatic allergen inhalation sensitises carotid bodies to lysophosphatidic acid. *J Neuroinflamm* (2021) 18:191. doi: 10.1186/s12974-021-02241-9

111. Jendzjowsky NG, Roy A, Barioni NO, Kelly MM, Green FHY, Wyatt CN, et al. Preventing acute asthmatic symptoms by targeting a neuronal mechanism involving carotid body lysophosphatidic acid receptors. *Nat Commun* (2018) 9(1):4030. doi: 10.1038/s41467-018-06189-y

Uncovering new insights into the role of the ubiquitin ligase Smurf1 on the regulation of innate immune signaling and resistance to infection

Luiz Pedro Souza-Costa[1†], Josiane Teixeira Andrade-Chaves[1†], Juvana Moreira Andrade[1], Vivian Vasconcelos Costa[2] and Luis Henrique Franco[1*]

[1]Departamento de Bioquímica e Imunologia, Instituto de Ciências Biológicas, Universidade Federal de Minas Gerais, Belo Horizonte, Brazil, [2]Departamento de Morfologia, Instituto de Ciências Biológicas, Universidade Federal de Minas Gerais, Belo Horizonte, Brazil

Innate immunity is the body's first line of defense against infections. Innate immune cells express pattern recognition receptors in distinct cellular compartments that are responsible to detect either pathogens-associated molecules or cellular components derived from damaged cells, to trigger intracellular signaling pathways that lead to the activation of inflammatory responses. Inflammation is essential to coordinate immune cell recruitment, pathogen elimination and to keep normal tissue homeostasis. However, uncontrolled, misplaced or aberrant inflammatory responses could lead to tissue damage and drive chronic inflammatory diseases and autoimmunity. In this context, molecular mechanisms that tightly regulate the expression of molecules required for the signaling of innate immune receptors are crucial to prevent pathological immune responses. In this review, we discuss the ubiquitination process and its importance in the regulation of innate immune signaling and inflammation. Then, we summarize the roles of Smurf1, a protein that works on ubiquitination, on the regulation of innate immune signaling and antimicrobial mechanisms, emphasizing its substrates and highlighting its potential as a therapeutic target for infectious and inflammatory conditions.

KEYWORDS

ubiquitin ligase, ubiquitination, Smurf1, innate immunity, infection

1 Introduction

The innate immune system is the first line of defense against microbial infections. In addition to chemical and physical components, innate immunity is composed of cells such as macrophages, dendritic cells, and neutrophils, which sense the presence of infectious pathogens and activate inflammatory responses required for their elimination. The

recognition of molecular components from pathogens by pattern recognition receptors (PRR) triggers a variety of intracellular signaling cascades in innate immune cells with subsequent activation of transcription factors that migrate to the nucleus and command the transcription of genes related to inflammatory and antimicrobial responses (1). Intracellular signaling triggered by innate immune receptors is a dynamic process composed of a complex combination of regulatory mechanisms that tightly regulate protein-protein interaction, protein subcellular localization, and protein abundance. One such regulatory mechanism is ubiquitination (2), a reversible post-translational modification that consists of the conjugation of ubiquitin to lysine residues in substrates (3). Substrates bound to ubiquitin are targeted to the proteasome for degradation or may interact with other proteins to play key physiological processes (4). In innate immune signaling, ubiquitination regulates the fate of substrates that actively work on signal transduction of PRR, and fine-tunes inflammatory immune responses to avoid tissue damage (5). In this review, we summarize the role of Smurf1, a protein required for the process of ubiquitination, on the regulation of innate immune signaling and antimicrobial mechanisms, emphasizing its substrates and highlighting its potential as a therapeutic target for infectious and inflammatory diseases.

2 Ubiquitination and ubiquitin ligases

Ubiquitination is a reversible enzymatic modification consisting of the covalent attachment of ubiquitin to target substrates, including proteins (3) and lipids (6). The ubiquitination process is crucial to regulate a number of cellular functions such as protein homeostasis, gene transcription, DNA repair and replication, intracellular traffic, and autophagy (7, 8). In the immune system, ubiquitination precisely regulates immune functions and signaling

of a diverse set of cells including B and T lymphocytes, and innate immune cells (9). Ubiquitination is catalyzed by the sequential and orchestrated action of three classes of enzymes known as E1, E2, and E3 enzymes. The first step of ubiquitination consists of the activation of cytoplasmic ubiquitin by the E1 ubiquitin-activating enzyme, followed by the transfer of activated ubiquitin to the E2 ubiquitin-conjugating enzyme. Lastly, E2 conjugating enzyme may form a complex with the E3 ubiquitin ligase to promote the direct or indirect transfer of ubiquitin to a specific lysine residue in a protein substrate (Figure 1). During the last step of ubiquitination, E3 ubiquitin ligases interact directly with substrates and play a critical role in determining the specificity of ubiquitin attachment to them (10). Therefore, the enzymatic activity of E3 ubiquitin ligases is a key factor commanding the specificity of substrate ubiquitination. As the human genome codes around 600 E3 ubiquitin ligases (11), and considering the vast repertoire of intracellular substrates that are targeted for ubiquitination, it is reasonable to assume that each E3 ubiquitin ligase is capable to interact with and ubiquitinate more than one substrate, implicating them as key mediators of cellular homeostasis. For this reason, host E3 ubiquitin ligases have become attractive targets for pharmaceutical development of drugs against infectious, inflammatory, and tumor diseases (12–14).

E3 ubiquitin ligases are grouped into three families, according to their structure and mechanisms of action: Really interesting new gene (RING), homologous to the E6AP carboxy terminus (HECT), and ring-in-between-ring (RBR) (Figure 2). While E3 ubiquitin ligases of the RING family catalyze the direct transfer of ubiquitin from the E2 conjugating enzyme to the substrate (15), E3 ligases of either HECT and RBR families feature an intermediate step in which ubiquitin is first transferred from E2 to E3 ligase before being attached to the substrate (16, 17). E3 ligases from the HECT family are further classified into three subfamilies: Neuronal precursor cell-expressed developmentally downregulated 4 (NEDD4); HECT and RLD domain containing E3 ubiquitin protein ligase 2 (HERC);
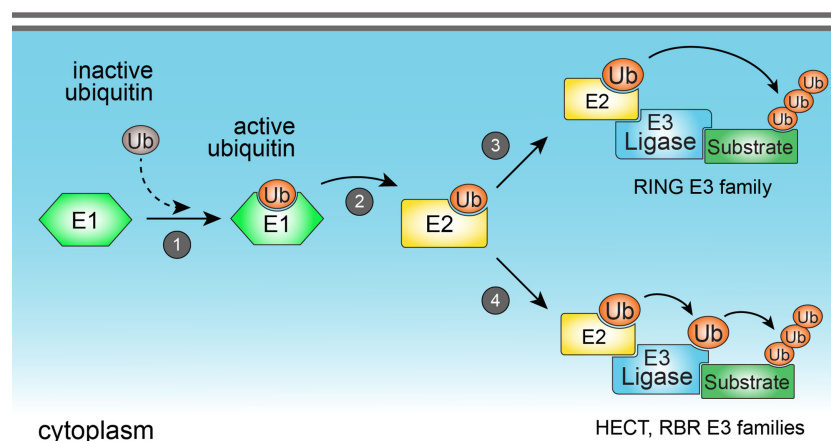
FIGURE 1
The ubiquitination process. Ubiquitination is catalyzed by the sequential action of three classes of enzymes (E1, E2, and E3 enzymes). Ubiquitination starts with the activation of cytoplasmic ubiquitin by the E1 ubiquitin-activating enzyme (1), followed by the transfer of activated ubiquitin to the E2 ubiquitin-conjugating enzyme (2). E2 enzyme may form a complex with the E3 ubiquitin ligase to promote the direct (3) (in the case of members from RING E3 ligase family), or indirect (4) (in the case of HECT and RBR E3 ligase families) transfer of ubiquitin to a specific lysine residue in a protein substrate.
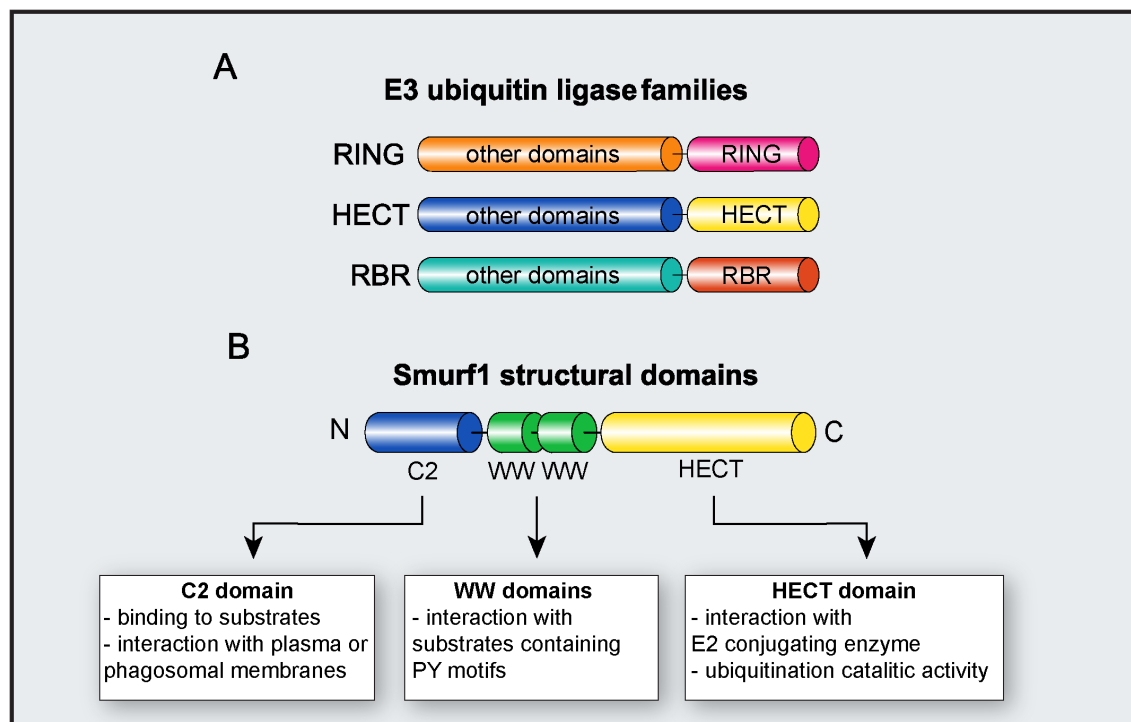
FIGURE 2
E3 ubiquitin ligase Smurf1. **(A)** Major families of E3 ubiquitin ligases. The diagram depicts RING, HECT, and RBR families and their respective functional domains. "Other domains" indicate variable domains, specific to each family of E3 ligase. **(B)** Molecular structure of Smurf1 and its identified domains.

and other members of the HECT family (18). From these three subfamilies, members from NEDD4 are the most well-studied and characterized, and all of them share an N-terminal C2 domain (required for their binding to either phospholipids or substrates), two to four central WW domains (for binding to substrates), and a C-terminal HECT domain, responsible for their enzymatic activity (19). HERC and other members of the HECT family share the same HECT domain, with distinct substrate binding domains (18).

Following the ligation of the first ubiquitin residue on the substrate mediated by the E3 ubiquitin ligase, additional ubiquitin chains may be sequentially added into the lysine residues of the initial ubiquitin, resulting in the formation of polyubiquitin chains. Ubiquitin protein is composed of seven lysine residues (K6, K11, K27, K29, K33, K48, and K63) that are responsible for forming distinct topologies of polyubiquitin chains. The nature of each polyubiquitin chain regulates several homeostatic processes, and it dictates the substrate fate in the cell (20). K48-linked polyubiquitinated substrates are generally directed for proteasomal degradation and it represents the most abundant polyubiquitin topology found in the cells. The second most abundant and characterized polyubiquitin topology is the K63-linked polyubiquitin (4). The coupling of K63-linked polyubiquitin to substrates leads to the formation of a docking site that allows for the recruitment of downstream interactors that work in subsequent intracellular signaling pathways (21). The functions of the other polyubiquitin linkages and their roles in the regulation of cellular processes are currently under investigation (22).

3 E3 ubiquitin ligase Smurf1

SMAD ubiquitin regulatory factor 1 (Smurf1) is an E3 ubiquitin ligase belonging to the NEDD4 subfamily of E3 ligases (18). Smurf1 was first identified in 1999 as a factor capable to target for ubiquitination and proteasomal degradation of SMAD family member 1 (Smad1) and Smad5 during cellular responses to *bone morphogenetic protein* (BMP) (23). In subsequent years, several groups have identified Smurf1 substrates required for the regulation of a plethora of physiological functions including bone formation, osteoblast differentiation, cell growth and migration, cell adhesion and polarity, embryonic development (24), and selective autophagy (25, 26). Smurf1 has also been implicated in tumor development by ubiquitination of cancer-suppressing proteins (27, 28), in cancer metastasis by suppression of epithelial-mesenchymal cell transition (EMT) pathway (29–31), in pancreatic cancer invasiveness (32, 33), cardiovascular diseases (34), and in liver steatosis (35).

As a member of the NEDD4 subfamily, Smurf1 is composed of an N-terminal C2 domain, two central WW domains, and a C-terminal HECT domain (18) (Figure 2). The Smurf1 C2 domain contains a phospholipid-binding sequence that mediates Smurf1 interaction with plasma or phagosomal membranes (26, 36). Smurf1 C2 domain may also facilitate its interaction with substrates such as Ras homolog family member A (RhoA) and Axin (36, 37). WW domains are required for Smurf1 interaction with substrates containing PY motifs, and phosphorylation of substrates may increase their affinity of ligation with Smurf1 (38).

Smurf1 HECT domain interacts with both E2 conjugating enzyme and ubiquitin during ubiquitination, and it is required for Smurf1 catalytic activity. The importance of the HECT domain in Smurf1 ubiquitin ligase activity is evidenced by findings that the C699A point mutation in the HECT domain completely abrogates its enzymatic activity (39, 40).

Besides being involved in physiological and pathological processes, Smurf1 has been implicated in the regulation of innate immune signaling and control of microbial replication. In the next sections, we will summarize major substrates and processes related to immune responses and host resistance to infection that are directly regulated by Smurf1. Figure 3 shows all Smurf1 substrates and interactors discussed in this review, highlighting the experimental conditions in which they were described, as well as the effect of their interaction with Smurf1 on the regulation of innate immune response and resistance to infections.

4 Regulation of innate immune signaling and inflammation by Smurf1

Innate immunity is characterized by a rapid response to infection and contributes to the induction of adaptive immune responses. PRRs are key components of innate immunity that have a main function to detect and initiate immune responses against microbial invasion. Innate immune cells including macrophages, neutrophils, and dendritic cells, express PRRs in distinct cellular compartments that detect not only molecular patterns associated with pathogens (PAMPs) but also molecules secreted by damaged or dead cells (DAMPs) (41). The engagement of PRR by PAMP or DAMP triggers signaling intracellular cascades that result in the activation of transcription factors that migrate to the nucleus and promote the transcription of genes related to inflammatory and antimicrobial responses (42). Toll-like receptors (TLR) are the most well-studied and characterized family of PRRs (41). TLR family is composed of 10 members in humans (TLR1-TLR10) and 12 members in mice (TLR1-TLR12). This family recognizes lipids, proteins, lipoproteins, and nucleic acids derived from a broad range of microbes such as bacteria, viruses, parasites, and fungi (43). The engagement of TLRs by microbial-derived components triggers the recruitment of adapter molecules to initiate downstream signaling pathways. Myeloid differentiation primary response 88 (MyD88) and TIR-domain-containing adapter-inducing interferon-β (TRIF) are two of the most well-studied adapter molecules that work in the TLR signaling pathway. In the MyD88-dependent pathway, the Interleukin-1 receptor-associated kinase (IRAK) proteins are phosphorylated, and they recruit and activate TNF receptor-associated factor-6 (TRAF6). TRAF6 coordinates the activation of mitogen-activated protein kinase (MAPK) and *nuclear factor kappa B* (NF-κB) pathways, which promote the production of proinflammatory cytokines and chemokines, and the activation of microbicidal mechanisms important for microbial elimination (43). The TRIF-dependent signaling leads to the activation of interferon regulatory factor (IRF) transcription factors responsible for the transcription of type I interferons and genes related to antiviral resistance, synthesis of proinflammatory cytokines, and regulation

of immune responses (44). Given the importance of TLR signaling in host resistance against infections and inflammatory responses, it is crucial to understand the molecular mechanisms underlying the regulation of their intracellular signaling. Uncontrolled or excessive inflammation triggered by TLR may lead to tissue damage and increased susceptibility to infections, inflammatory disorders, and autoimmune diseases (45, 46).

TLR9 is a PRR that recognizes unmethylated cytidine-phosphate-guanosine (CpG) oligodeoxynucleotides derived from pathogens and responds to cellular components including proteins, nucleotides, and DNA, conferring protection against infections and maintaining homeostasis by removing cellular debris during physiological conditions. Uncontrolled or aberrant TLR9 signaling favors the development of inflammatory and autoimmune diseases during pathological cellular damage and stress signals (47). It was shown that Smurf1 is required for the negative regulation of TLR9-mediated inflammatory responses (Figure 3). During CpG-dependent TLR9 signaling, Smurf1 interacts with serine/threonine kinase 38 (Stk38), also known as NDR2, a kinase highly conserved from yeast to humans (48), and it facilitates Smurf1-mediated ubiquitination and degradation of mitogen-activated protein kinase kinase 2 (MEKK2). MEKK2 is a member of the MAP3K family of proteins that play important roles in TLR signal transduction (49). Smurf1 interaction with Stk38 was demonstrated to occur both in primary mouse peritoneal macrophages and in human embryonic kidney (HEK293) lineage cells. Smurf1-dependent ubiquitination and degradation of MEKK2 leads to reduced CpG-induced (but not LPS (*lipopolysaccharide*)-induced) activation of the extracellular signal–regulated protein kinase 1/2 (ERK1/2) MAPK and decreased production of tumoral necrosis factor (TNF) and IL-6 in macrophages. Mice deficient for Stk38 produce increased TNF and IL-6 levels and are more susceptible to *Escherichia coli* infection or sepsis induced by cecal ligation and puncture (CLP), compared to control littermates, due to uncontrolled systemic inflammation (50). In addition, it was shown that Smurf1 attenuates IL-17-induced IL-6, CXCL2, and CCL20 expression in both HeLa and HT-29 human lineage cells in a similar mechanism dependent on Smurf1 interaction with Stk38 and MEKK2 degradation (51). Taken together, these data suggest that Smurf1-dependent degradation of MEKK2 may be an important physiological mechanism to regulate inflammatory immune responses to avoid tissue damage.

In vivo ubiquitination assays demonstrated that Smurf1 also interacts with TRAF4 and TRAF6 to induce their ubiquitination and degradation in a ubiquitination-dependent manner (52, 53) (Figure 3). TRAF4 is described as a negative regulator of NF-κB signaling (54), and co-expression of Smurf1 with TRAF4 in HEK293 human cell line attenuates TRAF4's negative effect on NF-κB activation (52). Similarly, HEK293 cells treated with IL-1β presented an attenuation in TRAF6 ubiquitination after Smurf1 knockdown, and an increased NF-κB activation (52). It suggests that Smurf1 may regulate innate immune signaling by targeting TRAF proteins for proteasome degradation.

Soluble mediators, including cytokines and eicosanoids, play a key role in regulating TLR signaling and inflammatory responses. Transforming growth factor beta (TGF-β) is a cytokine produced by
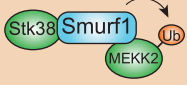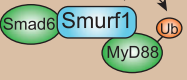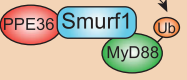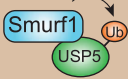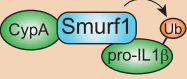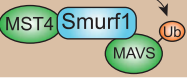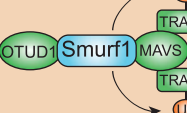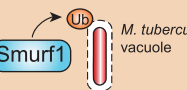
Smurf1 substrates/interactors	Experimental conditions	Effect of Smurf1-substrate interaction on immune response
Stk38 Smurf1 Ub MEKK2	mouse peritoneal macrophages and HEK293 lineage cells treated with CpG; HeLa and HT-29 cell lines treated with IL-17	reduced ERK1/2 activation, TNF, and IL-6 secretion by primary macrophages deficient for Stk38 treated with CpG; reduced expression of IL-6, CXCL-2, CCL20, and reduced ERK1/2 activation in lineage cells treated with siRNA for Stk38 (NDR2); increased inflammation and lethality in response to *E. coli* infection *in vivo* and high susceptibility to CLP sepsis model in Stk38-deficient mice
Smurf1 Ub TRAF4	yeast two-hybrid screening; HEK293 cells coexpressing Smurf1 and TRAF4	increased activity of NF-κB in HEK293 lineage cells coexpressing Smurf1 and TRAF4
Smurf1 Ub TRAF6	yeast two-hybrid screening; HEK293 cells coexpressing Smurf1 and TRAF6	reduced activity of NF-κB under treatment with IL-1β or TNF in HEK293 lineage cells coexpressing Smurf1 and TRAF6
Smad6 Smurf1 Ub MyD88	CMT-93 mouse cell line coexpressing Smurf1, MyD88, and Smad6 mouse peritoneal macrophage	reduced activity of NF-κB under treatment with LPS in mouse peritoneal macrophages
PPE36 Smurf1 Ub MyD88	HEK293 cell line and RAW264.7 mouse cell line overexpressing *M. tuberculosis* PPE36	increased production of cytokines by primary mouse macrophages in response to infection with BCG deficient for PPE36; increased *in vivo* resistance to infection by a *M. tuberculosis* strain deficient for PPE36
Smurf1 Ub USP5	HEK293 cell line coexpressing Smurf1 and USP5	reduced transcription of TNF in HeLa human cell line treated with shRNA for USP5; increased transcription of TNF in HeLa human cell line treated with shRNA for Smurf1
CypA Smurf1 Ub pro-IL1β	HEK293 cells coexpressing Smurf1, CypA and pro-IL-1β; primary mouse macrophages treated with LPS	increased K63-dependent pro-IL-1β processing (with higher IL-1β secretion); increased K48-dependent pro-IL-1β degradation (with lower IL-1β secretion) in primary mouse macrophages; reduced lung injury at early stages, followed by increased IL-1β-dependent lung injury at late stages of inflammation in CypA-deficient mice treated with LPS
Smurf1 Ub STAT1	RAW264.7 mouse cell line treated with IFN-γ; HEK293 lineage cells coexpressing Smurf1 and STAT1	increased transcription of *Cxcl9*, *Cxcl10*, *Irf1*, and *Nox2* in Smurf1-knocked down peritoneal macrophages treated with IFN-γ; impaired viral replication in Smurf1-knocked down peritoneal macrophages infected with VSV
Smurf1 Ub Ndfip1 MAVS	HEK293 lineage cells coexpressing Smurf1, MAVS, and Ndfip1	inhibition of MAVS-mediated activation of IFN-β, NF-κB, and ISRE in response to Poli (I:C), flu RNA and Sendai virus infection in mouse primary macrophages and HEK293 human cell line
MST4 Smurf1 Ub MAVS	HEK293 lineage cells coexpressing Smurf1, MAVS, and MST4	reduced activation of IFN-β, IFIT1, and ISRE in response to Poli (I:C) and Sendai virus infection in HEK293 cells treated with siRNA for MST4
OTUD1 Smurf1 MAVS Ub TRAF3 Ub TRAF6	primary mouse macrophages and 2fTGH human lineage cells infected with Sendai virus	increased transcription of type I IFN, TNF, and IL-6 in response to infection with RNA viruses by OTUD1-deficient mouse embryonic fibroblasts (MEF); high production of antiviral cytokines and increased resistance to infection with RNA virus in OTUD1-deficient mice
Smurf1 Ub UPS25	HEK293 lineage cells coexpressing Smurf1 and USP25	increased VSV replication in HEK293 cells overexpressing Smurf1
Smurf1 Sindbis virus capsid	MEF and HeLa human lineage cell line infected with Sindbis virus	increased levels of intracellular Sindbis virus capsid in Smurf1-deficient MEFs and in Smurf1-knocked down HeLa cells
Smurf1 SARS-CoV-2 spike protein	HEK293 cells coexpressing Smurf1 and SARS-CoV-2 spike protein	not evaluated
Smurf1 Ub M. tuberculosis vacuole	primary mouse macrophages infected with *M. tuberculosis*	ubiquitin-dependent autophagic elimination of *M. tuberculosis* in both primary mouse and human macrophages; high expression of Smurf1 in human lung biopsies from patients with tuberculosis; increased resistance to tuberculosis in a mice experimental model

FIGURE 3

Smurf1 substrates that work on innate immune signaling pathways and resistance to infection. The first row depicts major Smurf1 substrates and interactors identified thus far; the second row details the specific experimental conditions in which Smurf1 interaction with substrates was identified; the third row shows the effect of Smurf1 interaction with a specific substrate on immune responses and susceptibility to infections.

many cell types in the body and it participates in key biological processes including cell growth, apoptosis, and proliferation. TGF-β is a critical anti-inflammatory factor that negatively regulates innate immune responses triggered by TLR agonists (55). It has been shown that Smurf1 is required for the anti-inflammatory effect of TGF-β through a mechanism dependent on the ubiquitination and degradation of the MyD88 adaptor (56) (Figure 3). Treatment of primary mouse peritoneal macrophages with TGF-β results in the degradation of endogenous MyD88, while the knockdown of Smurf1 abrogates TGF-β-dependent MyD88 degradation (56). Smurf1 interacts with MyD88 in CMT-93 mouse cell line under TGF-β-treatment and promotes MyD88 K48-linked ubiquitination and degradation (56). Interaction between Smurf1 and MyD88 is facilitated by Smad6, a protein that works in TGF-β-signaling (57), as the knockdown of Smad6 abrogated Smurf1-MyD88 interaction in mouse peritoneal macrophages. In addition, TGF-β loses its inhibitory activity when Smurf1 is knockdown in peritoneal macrophages treated with LPS (56). Thus, Smurf1 is required for the TGF-β-dependent negative regulation of inflammatory responses by targeting MyD88 for proteasomal degradation. It was recently shown that the negative regulation of MyD88 by Smurf1 may be exploited by pathogens to facilitate the establishment of infection. PPE36 is a 27-kDa cell-wall-associated protein expressed by *Mycobacterium tuberculosis*, the bacilli that cause human tuberculosis. PPE36 expression is enriched in *M. tuberculosis* virulent strains and is a potent inhibitor of NF-κB and MAPK pathways (58). It was shown that *M. tuberculosis* PPE36 facilitates the interaction between Smurf1 and MyD88 both in HEK293 human cell line and RAW264.7 mouse macrophage cell line overexpressing PPE36, resulting in increased K48-linked MyD88 ubiquitination and degradation in a Smurf1-dependent manner (58) (Figure 3). Accordingly, PPE36 depletion in *M. tuberculosis* leads to increased inflammation and decreased bacterial loads in the lungs of *M. tuberculosis*-infected mice (58), suggesting that PPE36-mediated Smurf1-dependent MyD88 degradation contributes to reduced inflammatory response and increased susceptibility to *M. tuberculosis* infection. Likewise, *M. tuberculosis* also secretes PtpA and Rv0222, two virulence factors capable to subvert the function and enzymatic activity of other host E3 ubiquitin ligases to favor its survival (59–61). These findings raise the possibility that besides *M. tuberculosis*, other pathogens may produce virulence factors that may subvert inflammatory immune responses through modulation of Smurf1 or other E3 ubiquitin ligases.

Innate immune responses triggered by TLR and other PRR lead to the secretion of TNF, a key proinflammatory cytokine with antimicrobial and antitumor activities (62, 63). It has been shown that Smurf1 may also regulate inflammatory responses by suppressing TNF transcription. Ubiquitin specific peptidase 5 (USP5), a deubiquitinase that is involved in multiple cellular processes such as DNA repair, reaction to stress, and cancer (64), is essential for the production of TNF (65). Smurf1 was shown to interact with USP5 and promote its proteasomal degradation in HEK293 human cell line (66) (Figure 3). As a consequence, Smurf1 represses mRNA TNF transcription (66). Overall, Smurf1 works as a negative regulator of inflammatory innate immune responses by

interacting with and stimulating proteasome-dependent degradation of molecules such as MyD88 and USP5.

IL-1β is an atypical proinflammatory cytokine secreted in response to the activation of inflammasomes, initially produced as an inactive cytosolic precursor (pro-IL-1β), which then suffers proteolytic cleavage to generate biologically active IL-1β (67). Pro-IL-1β processing is primarily mediated by the action of caspase-1, although other proteases derived from distinct cell sources have been reported as capable of cleaving pro-IL-1β (68). In absence of proper cell stimulation, the processing and release of IL-1β are inefficient, as intracellular unprocessed IL-1β products are degraded by the proteasome system (69). It was recently shown that Smurf1 participates in a delicate mechanism of regulation of IL-1β-dependent inflammation (70). Smurf1 interacts with intracellular pro-IL-1β in primary mouse macrophages treated with LPS and promotes both K63- and K48-linked ubiquitination of pro-IL-1β. While Smurf1-dependent K63-linked ubiquitination contributes to pro-IL-1β processing, K48-linked ubiquitination leads to pro-IL-1β proteasomal degradation (70), which suggests that Smurf1 may either stimulate or inhibit IL-1β secretion. It was further shown that Smurf1-pro-IL-1β interaction is enhanced by the interaction between Smurf1 and cyclophilin A (CypA), a peptidyl-prolyl isomerase that works on immune regulation (71, 72) (Figure 3). CypA-deficient mice treated with LPS present reduced lung injury at early stages of inflammation, followed by an increased lung injury at late stages of inflammation, in a mechanism dependent on the production of IL-1β (70). These data suggest that at early stages of inflammation, CypA promotes inflammation by increasing Smurf1-dependent pro-IL-1β processing, *via* K63-linked ubiquitination, while at late stages of inflammation, CypA inhibits inflammation by stimulating pro-IL-1β degradation by Smurf1 through K48-linked ubiquitination. Therefore, in addition to negatively regulating innate immune signaling, Smurf may promote inflammatory immune responses by stimulating CypA-dependent K63-linked ubiquitination of pro-IL-1β.

5 IFN-γ signaling

PRR signaling during innate immune responses promotes the release of cytokines required for cell recruitment and activation of adaptive immune responses. Interferon-gamma (IFN-γ) is a cytokine primarily secreted by natural killer (NK) cells and Th1 lymphocytes that has a key role to potentialize antimicrobial mechanisms mediated by innate immune cells. IFN-γ is a potent stimulator of antimicrobial mechanisms in macrophages including the production of reactive oxygen and nitrogen species, and antimicrobial autophagy (73–75). IFN-γ acts through a pathway dependent on the activation of the transcription factor signal transducer and activator of transcription 1 (STAT1) (76, 77). Smurf1 has been shown to interact with STAT1 to promote its K48-linked ubiquitination and proteasomal degradation in RAW264.7 mouse macrophage cell line treated with IFN-γ (40) (Figure 3). Smurf1 knockdown in peritoneal macrophages treated with IFN-γ increases the transcription of CXC chemokine ligand 9 (*Cxcl9*), CXC chemokine ligand 10 (*Cxcl10*), *Irf1*, and inducible

nitric oxide synthase (*Nos2*) (40). Given the importance of IFN-γ in the regulation of innate immune responses and antimicrobial mechanisms, additional studies to better understand the interplay between Smurf1 and regulation of IFN-γ signaling using experimental models of infectious diseases might accelerate the development of host-directed therapies.

6 Antiviral immune responses

During viral infections, PRRs such as retinoic acid-inducible gene I (RIG-I), RIG-I-like receptors (RLR), and NOD-like receptors (NLR), recognize viral nucleic acid to trigger signaling cascades dependent on proteins including the adaptor protein mitochondrial antiviral signaling protein (MAVS) and the kinase TRAF-associated factor binding kinase 1 (TBK1). Activation of these proteins leads to the production of type I interferons and other cytokines, essential to drive/trigger antiviral responses (78). It has been shown that Smurf1 is required for the regulation of antiviral immune responses through the ubiquitination of members involved in the signaling cascades. Smurf1 interacts with MAVS, and overexpression of Smurf1 increased MAVS degradation in HEK293 human cell line in a mechanism dependent on the proteasome (79). The interaction between MAVS and Smurf1 is enhanced by NEDD4 family interacting protein 1 (Ndfip1), described as a recruiter and activator of members from the NEDD4 E3 ubiquitin ligases (80). Overexpression of Ndfip1 leads to increased Smurf1-dependent MAVS degradation and impairs the activation of several antiviral mechanisms both in mouse primary macrophages and HEK293 human cell line (79) (Figure 3). In addition to Ndfip1, it was recently reported that mammalian sterile 20-like kinase 4 (MST4), a ubiquitously expressed and highly conserved serine/threonine kinase of the MST family, enhances Smurf1-MAVS interaction, increases Smurf1-dependent MAVS degradation, and impairs type I IFN production in HEK293 cells transfected with polyino-sinic-polycytidylic acid (Poli (I:C)) or infected with Sendai Virus (81), in a similar mechanism as reported for Ndfip1 (Figure 3). Besides MAVS, Smurf1 interacts with STAT1 (40), a transcription factor required for antiviral immunity (82). Overexpression of Smurf1 in HEK293 cell line increases STAT1 degradation, and Smurf1-mediated STAT1 degradation impairs antiviral response in macrophages infected with vesicular stomatitis virus (VSV) (40) (Figure 3). Therefore, Smurf1 seems to work as a negative regulator of signaling pathways required for antiviral resistance. These findings raise the question of whether viruses could manipulate the inhibitory function of Smurf1 to favor their replication. Indeed, it was shown that infection with RNA viruses stimulates the expression of the enzyme OTU deubiquitinase1 (OTUD1), which interacts with Smurf1 and increases its intracellular expression in HEK293 lineage cells (83). In this condition, Smurf1 interacts not only with MAVS but with TRAF3 and TRAF6 as well, directing them to proteasomal degradation, which results in reduced antiviral response both in primary mouse macrophages and 2fTGH human lineage cells. Knockout mice for OTUD1 produce high levels of antiviral cytokines and are more resistant to infection with RNA viruses (83) (Figure 3). It suggests that an increased Smurf1-

dependent inhibition of antiviral signaling is a mechanism that could be exploited by viruses to establish infection. New studies need to be conducted in order to evaluate whether RNA viruses could actively stimulate Smurf1 expression or manipulate other E3 ligase functions to favor their replication.

Deubiquitination enzymes work by removing ubiquitin chains from target substrates and are essential to fine-tune antiviral immune responses (84). Ubiquitin-specific protease 25 (USP25) is a deubiquitination enzyme expressed in most human tissues (85) that is capable to deubiquitinate TRAF3, TRAF6, and promoting host resistance to infection with DNA and RNA viruses (86). It was demonstrated that Smurf1 interacts with and induces USP25 K48-linked ubiquitination and degradation (Figure 3). In HEK293 cells infected with VSV, overexpression of Smurf1 results in increased viral replication, whereas USP25 overexpression leads to a decrease in viral replication (87). Thus, Smurf1 regulates antiviral immune responses by promoting ubiquitination and degradation of USP25.

Besides working on the regulation of antiviral immune responses, Smurf1 may target viral components to ubiquitin-dependent antiviral pathways. Smurf1 was identified as a factor required to mediate the selective delivery of virus components to the autophagy pathway (25). Smurf1 interacts with the Sindbis virus capsid protein in the cytoplasm of both mouse embryonic fibroblast and HeLa human lineage cells and promotes its delivery to autophagosomes for degradation (25) (Figure 3). In addition to components from the Sindbis virus, it was shown that Smurf1 interacts with the Spike protein from SARS-CoV-2 in HEK293 cells, and mRNA for Smurf1 was found to be overexpressed in swab samples from the nasopharynx and oropharynx of patients positive for COVID-19 (13) (Figure 3), which suggests that Smurf1 might present a relevant role to regulate immune resistance against COVID-19. To complete understand the role of Smurf1 in the regulation of antiviral host resistance, additional studies need to be carried out using experimental models of viral infections, or even drugs that target Smurf1 activity.

7 Antibacterial xenophagy

Autophagy is a cellular process in which components such as protein aggregates, misfolded proteins, and damaged organelles are sequestered in a double-layered vesicle, called autophagosome, for subsequent fusion with lysosomes for their degradation. Autophagy is a key mechanism to maintain cellular homeostasis, and its activation provides energy to cells when nutrients are scarce (88). It has been shown that autophagy may also target intracellular pathogens for lysosomal degradation, in a specialized type of autophagy known as xenophagy (89). One critical intracellular signaling that triggers xenophagy for the elimination of pathogens is the recognition of ubiquitin-bound pathogens by autophagy adaptors in the cytoplasm, followed by recruitment of the autophagy machinery, which commands the formation of the autophagosome membrane surrounding the microorganism. When bound to a ubiquitinated target, autophagy adaptors, including neighbor of BRCA1 gene 1 (NBR1), calcium-binding and coiled-coil domain-containing protein 2 (CALCOCO2, also

known as NDP52), and sequestosome 1 (SQSTM1, also known as p62), couple to microtubule-associated protein light chain 3 II (LC3-II) (a protein present at the forming autophagosome membrane and commonly used as an autophagosomal marker (90)) to facilitate their delivering to autophagosomes for degradation. Therefore, the ubiquitination of intracellular pathogens is a crucial event required for the initiation of antimicrobial xenophagy (91, 92). It has been shown that Smurf1 is a host factor necessary to mediate ubiquitination and autophagic elimination of intracellular bacteria (26) (Figure 3). Mouse macrophages deficient for Smurf1 present defective ubiquitination of *M. tuberculosis*, reduced recruitment of the autophagy adaptor NBR1 to *M. tuberculosis*-containing structures, reduced targeting of *M. tuberculosis* to autophagosomes, and impaired capacity to contain *M. tuberculosis* replication (26). In addition to *M. tuberculosis*, mouse macrophages deficient for Smurf1 has a defective ability to control the replication of intracellular *Listeria monocytogenes* as well. Similarly, knockout mice for Smurf1 are more susceptible to *M. tuberculosis* infection with a high bacterial burden in the lungs and reduced survival in response to chronic mycobacterial infection. Interestingly, in addition to Smurf1 being highly expressed in lung biopsies of human patients infected with *M. tuberculosis* (26), it was shown that three Smurf1 polymorphisms were associated with a higher susceptibility to tuberculous meningitis (while they were not correlated to the severity or prognosis of tuberculous meningitis) in China (93), suggesting that Smurf1 might also participate in resistance against human tuberculosis. Despite the identification of Smurf1 as a factor required for mycobacterial xenophagy, the specific substrate(s) targeted by Smurf1 for ubiquitination remains to be discovered.

8 Concluding remarks and future perspectives

E3 ubiquitin ligases are a key family of proteins that functions in the post-transcriptional regulation of many cellular processes, including immune responses. Fine-tuning the intracellular pathways that work on inflammation, recognition of pathogens by innate immunity, or during physiological adaptation to pathological cell damage and stress is an essential condition to avoid the development of inflammatory diseases and autoimmunity. In this review, we highlighted the major identified functions of Smurf1 in the regulation of innate immune mechanisms related to the recognition of pathogens and elimination of microorganisms. With the exception of TRAF4, all Smurf1 substrates pointed in this review (MyD88, TRAF3, TRAF6, MEKK2, USP5, STAT1, MAVS) work on the positive regulation of innate immune signaling pathways and inflammation. Given that Smurf1 catalyzes the proteasomal degradation of innate immune-related substrates, future research focusing on identification of new Smurf1 substrates during innate immune responses and the search for pharmacological modulators of Smurf1's activity could be a key strategy for the development of novel therapeutics against infectious, sterile inflammation, and autoimmune diseases. On one hand, to fight infectious diseases, strategies that aim at the

positive regulation of innate immunity and inflammation may be successful. In such cases, the pharmacological inhibition of Smurf1 activity (94) might be able to stimulate inflammatory immune responses and drive the elimination of the pathogen. On the other hand, the search for new treatments for inflammatory and autoimmune diseases must be focused on the stimulation of intracellular synthesis of Smurf1 or on the positive regulation of its E3 ligase activity. Thus far, it has been identified a number of proteins capable of either regulating Smurf1 intracellular expression or Smurf1 ligase activity (95, 96). However, the effect of those proteins on the regulation of immune responses needs to be further investigated. In conclusion, additional studies using *in vivo* animal models of infectious and autoimmune diseases, in combination with pharmacological strategies, need to be conducted in order to define whether Smurf1could represent a therapeutic target for future clinical studies. Lastly, to better define the role of Smurf1 in human health and its potential as a therapeutic target, new genetic and functional studies with human samples need to be completed, as for now, most of the generated knowledge are based on human cell lines and mouse experimental models.

Author contributions

All authors contributed to the manuscript preparation. LF developed the concept, general content, and structure of the figures. VC did a critical review of concepts regarding inflammation and antiviral immune responses. JA worked on the literature review and curation of articles used in manuscript preparation. LS-C and JA-C contributed equally to writing the manuscript. All the authors revised and approved the final version of the manuscript.

Funding

Acknowledgments

Conflict of interest

The authors declare that the research was conducted in the absence of any commercial or financial relationships that could be construed as a potential conflict of interest.

Publisher's note

All claims expressed in this article are solely those of the authors and do not necessarily represent those of their affiliated organizations, or those of the publisher, the editors and the reviewers. Any product that may be evaluated in this article, or claim that may be made by its manufacturer, is not guaranteed or endorsed by the publisher.

References

1. Takeda K, Akera S. TLR signaling pathways. *Semin Immunol* (2004) 16:3–9.

2. Zinngrebe J, Montinaro A, Peltzer N, Walczak H. Ubiquitin in the immune system. *EMBO Rep* (2014) 15:28–45. doi: 10.1002/EMBR.201338025

3. Laney JD, Hochstrasser M. Substrate targeting in the ubiquitin system. *Cell* (1999) 97:427–30. doi: 10.1016/S0092-8674(00)80752-7

4. Woelk T, Sigismund S, Penengo L, Polo S. The ubiquitination code: a signalling problem. *Cell Div* (2007) 2:11. doi: 10.1186/1747-1028-2-11

5. Liu X, Wang Q, Chen W, Wang C. Dynamic regulation of innate immunity by ubiquitin and ubiquitin-like proteins. *Cytokine Growth Factor Rev* (2013) 24:559–70. doi: 10.1016/j.cytogfr.2013.07.002

6. Otten EG, Werner E, Crespillo-Casado A, Boyle KB, Dharamdasani V, Pathe C, et al. Ubiquitylation of lipopolysaccharide by RNF213 during bacterial infection. *Nature* (2021) 594:111–6. doi: 10.1038/s41586-021-03566-4

7. Chen R-H, Chen Y-H, Huang T-Y. Ubiquitin-mediated regulation of autophagy. *J Biomed Sci* (2019) 26:1–12. doi: 10.1186/S12929-019-0569-Y

8. Oh E, Akopian D, Rape M. Principles of ubiquitin-dependent signaling. *Annual Review Of Cell And Developmental Biol* (2018) 34:137–62. doi: 10.1146/ANNUREV-CELLBIO-100617-062802

9. Ebner P, Versteeg GA, Ikeda F. Ubiquitin enzymes in the regulation of immune responses. *Crit Rev Biochem Mol Biol* (2017) 52:425. doi: 10.1080/10409238.2017.1325829

10. Pickart CM. Mechanisms underlying ubiquitination. *Annual Review of Biochem* (2003) 70:503–33. doi: 10.1146/ANNUREV.BIOCHEM.70.1.503

11. Zheng N, Shabek N. Ubiquitin ligases: structure, function, and regulation. *Annu Rev Biochem* (2017) 86:129–57. doi: 10.1146/annurev-biochem-060815-014922

12. Bielskiene K, Bagdoniene L, Mozuraitiene J, Kazbariene B, Janulionis E. E3 ubiquitin ligases as drug targets and prognostic biomarkers in melanoma. *Medicina (B Aires)* (2015) 51:1–9. doi: 10.1016/J.MEDICI.2015.01.007

13. Novelli G, Liu J, Biancolella M, Alonzi T, Novelli A, Patten JJ, et al. Inhibition of HECT E3 ligases as potential therapy for COVID-19. *Cell Death Dis* (2021) 12:310. doi: 10.1038/s41419-021-03513-1

14. Bulatov E, Zagidullin A, Valiullina A, Sayarova R, Rizvanov A. Small molecule modulators of RING-type E3 ligases: MDM and cullin families as targets. *Front Pharmacol* (2018) 9:450/BIBTEX. doi: 10.3389/FPHAR.2018.00450/BIBTEX

15. Deshaies RJ, Joazeiro CAP. RING domain E3 ubiquitin ligases. *Annual Review of Biochem* (2009) 78:399–434. doi: 10.1146/ANNUREV.BIOCHEM.78.101807.093809

16. Wang Y, Argiles-Castillo D, Kane EI, Zhou A, Spratt DE. HECT E3 ubiquitin ligases – emerging insights into their biological roles and disease relevance. *J Cell Sci* (2020) 133. doi: 10.1242/JCS.228072

17. Walden H, Rittinger K. RBR ligase-mediated ubiquitin transfer: a tale with many twists and turns. *Nat Struct Mol Biol* (2018) 25:440–5. doi: 10.1038/s41594-018-0063-3

18. Weber J, Polo S, Maspero E. HECT E3 ligases: a tale with multiple facets. *Front Physiol* (2019) 10:370. doi: 10.3389/FPHYS.2019.00370

19. Ingham RJ, Gish G, Pawson T. The Nedd4 family of E3 ubiquitin ligases: functional diversity within a common modular architecture. *Oncogene* (2004) 1:1972–84. doi: 10.1038/sj.onc.1207436

20. Kwon YT, Ciechanover A. The ubiquitin code in the ubiquitin-proteasome system and autophagy. *Trends Biochem Sci* (2017) 42:873–86. doi: 10.1016/j.tibs.2017.09.002

21. Morreale FE, Walden H. Types of ubiquitin ligases. *Cell* (2016) 165:248–248.e1. doi: 10.1016/j.cell.2016.03.003

22. Akutsu M, Dikic I, Bremm A. Ubiquitin chain diversity at a glance. *J Cell Sci* (2016) 129:875–80. doi: 10.1242/JCS.183954

23. Zhu H, Kavsak P, Abdollah S, Wrana JL, Thomsen GH. A SMAD ubiquitin ligase targets the BMP pathway and affects embryonic pattern formation. *Nature* (1999) 400:687–93. doi: 10.1038/23293

24. Cao Y, Zhang L. A Smurf1 tale: function and regulation of an ubiquitin ligase in multiple cellular networks. *Cell Mol life Sci* (2013) 70:2305–17. doi: 10.1007/s00018-012-1170-7

25. Orvedahl A, Sumpter R, Xiao G, Ng A, Zou Z, Tang Y, et al. Image-based genome-wide siRNA screen identifies selective autophagy factors. *Nature* (2011) 480:113–7. doi: 10.1038/nature10546

26. Franco LH, Nair VR, Scharn CR, Xavier RJ, Torrealba JR, Shiloh MU, et al. The ubiquitin ligase Smurf1 functions in selective autophagy of mycobacterium tuberculosis and anti-tuberculous host defense. *Cell Host Microbe* (2017) 21:59–72. doi: 10.1016/j.chom.2016.11.002

27. Xia Q, Li Y, Han D, Dong L. SMURF1, a promoter of tumor cell progression? *Cancer Gene Ther* (2020) 28:551–65. doi: 10.1038/s41417-020-00255-8

28. Kwon A, Lee H-L, Woo KM, Ryoo H-M, Baek J-H. SMURF1 plays a role in EGF-induced breast cancer cell migration and invasion. *Mol Cells* (2013) 36:548–55. doi: 10.1007/s10059-013-0233-4

29. Zheng J, Shi Z, Yang P, Zhao Y, Tang W, Ye S, et al. ERK-Smurf1-RhoA signaling is critical for TGFβ-drived EMT and tumor metastasis. *Life Sci Alliance* (2022) 5. doi: 10.26508/LSA.202101330

30. Chaudhary KR, Kinslow CJ, Cheng H, Silva JM, Yu J, Wang TJ, et al. Smurf2 inhibition enhances chemotherapy and radiation sensitivity in non-small-cell lung cancer. *Sci Rep* (2022) 12. doi: 10.1038/S41598-022-14448-8

31. Singh K, Rustagi Y, Abouhashem AS, Tabasum S, Verma P, Hernandez E, et al. Genome-wide DNA hypermethylation opposes healing in patients with chronic wounds by impairing epithelial-mesenchymal transition. *J Clin Invest* (2022) 132. doi: 10.1172/JCI157279

32. Kwei KA, Shain AH, Bair R, Montgomery K, Karikari CA, van de Rijn M, et al. SMURF1 amplification promotes invasiveness in pancreatic cancer. *PloS One* (2011) 6. doi: 10.1371/journal.pone.0023924

33. Suzuki A, Shibata T, Shimada Y, Murakami Y, Horii A, Shiratori K, et al. Identification of SMURF1 as a possible target for 7q21.3-22.1 amplification detected in a pancreatic cancer cell line by in-house array-based comparative genomic hybridization. *Cancer Sci* (2008) 99:986–94. doi: 10.1111/j.1349-7006.2008.00779.x

34. Roh JD, Hobson R, Chaudhari V, Quintero P, Yeri A, Benson M, et al. Activin type II receptor signaling in cardiac aging and heart failure. *Sci Transl Med* (2019) 11. doi: 10.1126/SCITRANSLMED.AAU8680

35. Lin W, Zhang X, Zhang C, Li L, Zhang J, Xie P, et al. Deletion of Smurf1 attenuates liver steatosis *via* stabilization of p53. *Lab Invest* (2022) 102:1075–87. doi: 10.1038/s41374-022-00802-x

36. Fei C, He X, Xie S, Miao H, Zhou Z, Li L. Smurf1-mediated axin ubiquitination requires Smurf1 C2 domain and is cell-cycle dependent. *J Biol Chem* (2014) 289:14170–7. doi: 10.1074/jbc.M113.536714

37. Tian M, Bai C, Lin Q, Lin H, Liu M, Ding F, et al. Binding of RhoA by the C2 domain of E3 ligase Smurf1 is essential for Smurf1-regulated RhoA ubiquitination and cell protrusive activity. *FEBS Lett* (2011) 585:2199–204. doi: 10.1016/J.FEBSLET.2011.06.016

38. Aragón E, Goerner N, Zaromytidou AI, Xi Q, Escobedo A, Massagué J, et al. A smad action turnover switch operated by WW domain readers of a phosphoserine code. *Genes Dev* (2011) 25:1275–88. doi: 10.1101/GAD.2060811

39. Cheng P, Lu H, Shelly M, Gao H, Poo M. Phosphorylation of E3 ligase Smurf1 switches its substrate preference in support of axon development. *Neuron* (2011) 69:231–43. doi: 10.1016/j.neuron.2010.12.021

40. Yuan C, Qi J, Zhao X, Gao C. Smurf1 protein negatively regulates interferon-γ signaling through promoting STAT1 protein ubiquitination and degradation. *J Biol Chem* (2012) 287:17006–15. doi: 10.1074/jbc.M112.341198

41. Akira S, Takeda K. Toll-like receptor signalling. *Nat Rev Immunol* (2004) 4:499–511. doi: 10.1038/nri1391

42. Li D, Wu M. Pattern recognition receptors in health and diseases. *Signal Transduction Targeted Ther* (2021) 6:1–24. doi: 10.1038/s41392-021-00687-0

43. Kawasaki T, Kawai T. Toll-like receptor signaling pathways. *Front Immunol* (2014) 5:461. doi: 10.3389/FIMMU.2014.00461

44. Lukhele S, Boukhaled GM, Brooks DG. Type I interferon signaling, regulation and gene stimulation in chronic virus infection. *Semin Immunol* (2019) 43:101277. doi: 10.1016/J.SMIM.2019.05.001

45. Hosseini AM, Majidi J, Baradaran B, Yousefi M. Toll-like receptors in the pathogenesis of autoimmune diseases. *Adv Pharm Bull* (2015) 5:605. doi: 10.15171/APB.2015.082

46. Gao W, Xiong Y, Li Q, Yang H. Inhibition of toll-like receptor signaling as a promising therapy for inflammatory diseases: a journey from molecular to nano therapeutics. *Front Physiol* (2017) 8:508/BIBTEX. doi: 10.3389/FPHYS.2017.00508/BIBTEX

47. Saber MM, Monir N, Awad AS, Elsherbiny ME, Zaki HF. TLR9: a friend or a foe. *Life Sci* (2022) 307. doi: 10.1016/J.LFS.2022.120874

48. Millward T, Cron P, Hemmings BA. Molecular cloning and characterization of a conserved nuclear serine(threonine) protein kinase. *Proc Natl Acad Sci U.S.A.* (1995) 92:5022. doi: 10.1073/PNAS.92.11.5022

49. Zhang D, Facchinetti V, Wang X, Huang Q, Qin J, Su B. Identification of MEKK2/3 serine phosphorylation site targeted by the toll-like receptor and stress pathways. *EMBO J* (2006) 25:97–107. doi: 10.1038/SJ.EMBOJ.7600913

50. Wen M, Ma X, Cheng H, Jiang W, Xu X, Zhang Y, et al. Stk38 protein kinase preferentially inhibits TLR9-activated inflammatory responses by promoting MEKK2 ubiquitination in macrophages. *Nat Commun* (2015) 6:7167. doi: 10.1038/ncomms8167

51. Ma X, Wang D, Li N, Gao P, Zhang M, Zhang Y. Hippo kinase NDR2 inhibits IL-17 signaling by promoting Smurf1-mediated MEKK2 ubiquitination and degradation. *Mol Immunol* (2019) 105:131–6. doi: 10.1016/J.MOLIMM.2018.10.005

52. Li S, Lu K, Wang J, An L, Yang G, Chen H, et al. Ubiquitin ligase Smurf1 targets TRAF family proteins for ubiquitination and degradation. *Mol Cell Biochem* (2010) 338:11–7. doi: 10.1007/s11010-009-0315-y

53. Wang X, Jin C, Tang Y, Tang LY, Zhang YE. Ubiquitination of tumor necrosis factor receptor-associated factor 4 (TRAF4) by smad ubiquitination regulatory factor 1 (Smurf1) regulates motility of breast epithelial and cancer cells. *J Biol Chem* (2013) 288:21784–92. doi: 10.1074/jbc.M113.472704

54. Kedinger V, Rio MC. TRAF4, the unique family member. *Adv Exp Med Biol* (2007) 597:60–71. doi: 10.1007/978-0-387-70630-6_5

55. Li MO, Wan YY, Sanjabi S, Robertson AKL, Flavell RA. Transforming growth factor-B regulation of immune responses. *Annual Review of Immunology* (2006) 24:99–146. doi: 10.1146/ANNUREV.IMMUNOL.24.021605.090737

56. Lee YS, Park JS, Kim JH, Jung SM, Lee JY, Kim S-J, et al. Smad6-specific recruitment of smurf E3 ligases mediates TGF-β1-induced degradation of MyD88 in TLR4 signalling. *Nat Commun* (2011) 2:460. doi: 10.1038/ncomms1469

57. Imamura T, Takase M, Nishihara A, Oeda E, Hanai JI, Kawabata M, et al. Smad6 inhibits signalling by the TGF-β superfamily. *Nature* (1997) 389:622–6. doi: 10.1038/39355

58. Peng Z, Yue Y, Xiong S. Mycobacterial PPE36 modulates host inflammation by promoting E3 ligase Smurf1-mediated MyD88 degradation. *Front Immunol* (2022) 13:690667. doi: 10.3389/FIMMU.2022.690667

59. Wang L, Wu J, Li J, Yang H, Tang T, Liang H, et al. Host-mediated ubiquitination of a mycobacterial protein suppresses immunity. *Nature* (2020) 577:682–8. doi: 10.1038/s41586-019-1915-7

60. Fu B, Xue W, Zhang H, Zhang R, Feldman K, Zhao Q, et al. MicroRNA-325-3p facilitates immune escape of mycobacterium tuberculosis through targeting LNX1 *via* NEK6 accumulation to promote anti-apoptotic STAT3 signaling. *MBio* (2020) 11. doi: 10.1128/mBio.00557-20

61. Campos PC, Cunha DT, Souza-Costa LP, Shiloh MU, Franco LH. Bag it, tag it: ubiquitin ligases and host resistance to mycobacterium tuberculosis. *Trends Microbiol* (2022) 30:973–85. doi: 10.1016/J.TIM.2022.03.010

62. Tracey KJ, Cerami A. Tumor necrosis factor and regulation of metabolism in infection: role of systemic versus tissue levels. *Proc Soc Exp Biol Med* (1992) 200:233–9. doi: 10.3181/00379727-200-43426

63. Bemelmans MHA, van Tits LJH, Buurman WA. Tumor necrosis factor: Function, release and clearance. *Crit Rev Immunol* (2017) 37:249–59. doi: 10.1615/CRITREVIMMUNOL.V37.I2-6.50

64. Ning F, Xin H, Liu J, Lv C, Xu X, Wang M, et al. Structure and function of USP5: Insight into physiological and pathophysiological roles. *Pharmacol Res* (2020) 157:104557. doi: 10.1016/J.PHRS.2019.104557

65. Yoshioka Y, Ye YQ, Okada K, Taniguchi K, Yoshida A, Sugaya K, et al. Ubiquitin-specific peptidase 5, a target molecule of vialinin a, is a key molecule of TNF-α production in RBL-2H3 cells. *PloS One* (2013) 8:e80931. doi: 10.1371/JOURNAL.PONE.0080931

66. Qian G, Ren Y, Zuo Y, Yuan Y, Zhao P, Wang X, et al. Smurf1 represses TNF-alpha production through ubiquitination and destabilization of USP5. *Biochem Biophys Res Commun* (2016) 474:491–6. doi: 10.1016/j.bbrc.2016.04.135

67. Martinon F, Burns K, Tschopp J. The inflammasome: a molecular platform triggering activation of inflammatory caspases and processing of proIL-β. *Mol Cell* (2002) 10:417–26. doi: 10.1016/S1097-2765(02)00599-3

68. Afonina IS, Müller C, Martin SJ, Beyaert R. Proteolytic processing of interleukin-1 family cytokines: variations on a common theme. *Immunity* (2015) 42:991–1004. doi: 10.1016/J.IMMUNI.2015.06.003

69. Ainscough JS, Gerberick GF, Zahedi-Nejad M, Lopez-Castejon G, Brough D, Kimber I, et al. Dendritic cell IL-1α and IL-1β are polyubiquitinated and degraded by the proteasome. *J Biol Chem* (2014) 289:35582–92. doi: 10.1074/JBC.M114.595686

70. Yang W, Bai X, Luan X, Min J, Tian X, Li H, et al. Delicate regulation of IL-1β-mediated inflammation by cyclophilin a. *Cell Rep* (2022) 38:110513. doi: 10.1016/J.CELREP.2022.110513

71. Colgan J, Asmal M, Neagu M, Yu B, Schneidkraut J, Lee Y, et al. Cyclophilin a regulates TCR signal strength in CD4+ T cells *via* a proline-directed conformational switch in itk. *Immunity* (2004) 21:189–201. doi: 10.1016/J.IMMUNI.2004.07.005

72. Liu W, Li J, Zheng W, Shang Y, Zhao Z, Wang S, et al. Cyclophilin a-regulated ubiquitination is critical for RIG-i-mediated antiviral immune responses. *Elife* (2017) 6. doi: 10.7554/ELIFE.24425

73. Schroder K, Hertzog PJ, Ravasi T, Hume DA. Interferon-γ: an overview of signals, mechanisms and functions. *J Leukoc Biol* (2004) 75:163–89. doi: 10.1189/JLB.0603252

74. Matsuzawa T, Kim B-H, Shenoy AR, Kamitani S, Miyake M, MacMicking JD. IFN-γ elicits macrophage autophagy *via* the p38 MAPK signaling pathway. *J Immunol* (2012) 189:813–8. doi: 10.4049/JIMMUNOL.1102041

75. Matsuzawa T, Fujiwara E, Washi Y. Autophagy activation by interferon-γ *via* the p38 mitogen-activated protein kinase signalling pathway is involved in macrophage bactericidal activity. *Immunology* (2014) 141:61–9. doi: 10.1111/imm.12168

76. Ramana CV, Gil MP, Schreiber RD, Stark GR. Stat1-dependent and -independent pathways in IFN-γ-dependent signaling. *Trends Immunol* (2002) 23:96–101. doi: 10.1016/S1471-4906(01)02118-4

77. Kisseleva T, Bhattacharya S, Braunstein J, Schindler CW. Signaling through the JAK/STAT pathway, recent advances and future challenges. *Gene* (2002) 285:1–24. doi: 10.1016/S0378-1119(02)00398-0

78. Brennan K, Bowie AG. Activation of host pattern recognition receptors by viruses. *Curr Opin Microbiol* (2010) 13:503–7. doi: 10.1016/J.MIB.2010.05.007

79. Wang Y, Tong X, Ye X. Ndfip1 negatively regulates RIG-I–dependent immune signaling by enhancing E3 ligase Smurf1-mediated MAVS degradation. *J Immunol* (2012) 189:5304–13. doi: 10.4049/jimmunol.1201445

80. Mund T, Pelham HRB. Control of the activity of WW-HECT domain E3 ubiquitin ligases by NDFIP proteins. *EMBO Rep* (2009) 10:501. doi: 10.1038/EMBOR.2009.30

81. Liu W, Ma Z, Wu Y, Yuan C, Zhang Y, Liang Z, et al. MST4 negatively regulates type I interferons production *via* targeting MAVS-mediated pathway. *Cell Commun Signal* (2022) 20. doi: 10.1186/S12964-022-00922-3

82. Horvath CM, Darnell JE. The antiviral state induced by alpha interferon and gamma interferon requires transcriptionally active Stat1 protein. *J Virol* (1996) 70:647–50. doi: 10.1128/JVI.70.1.647-650.1996

83. Zhang L, Liu J, Qian L, Feng Q, Wang X, Yuan Y, et al. Induction of OTUD1 by RNA viruses potently inhibits innate immune responses by promoting degradation of the MAVS/TRAF3/TRAF6 signalosome. *PloS Pathog* (2018) 14. doi: 10.1371/JOURNAL.PPAT.1007067

84. Zong Z, Zhang Z, Wu L, Zhang L, Zhou F. The functional deubiquitinating enzymes in control of innate antiviral immunity. *Advanced Sci* (2021) 8:2002484. doi: 10.1002/ADVS.202002484

85. Valero R, Marfany G, González-Angulo O, González-González G, Puelles L, Gonzàlez-Duarte R. USP25, a novel gene encoding a deubiquitinating enzyme, is located in the gene-poor region 21q11.2. *Genomics* (1999) 62:395–405. doi: 10.1006/GENO.1999.6025

86. Lin D, Zhang M, Zhang MX, Ren Y, Zhao Q, Jin J, et al. Induction of USP25 by viral infection promotes innate antiviral responses by mediating the stabilization of TRAF3 and TRAF6. *Proc Natl Acad Sci U.S.A.* (2015) 112:11324–9. doi: 10.1073/PNAS.1509968112/SUPPL_FILE/PNAS.201509968SI.PDF

87. Qian G, Hu X, Li G, Ding Y, Zhu L, Zheng H, et al. Smurf1 restricts the antiviral function mediated by USP25 through promoting its ubiquitination and degradation. *Biochem Biophys Res Commun* (2018) 498:537–43. doi: 10.1016/J.BBRC.2018.03.015

88. Levine B, Klionsky DJ. Autophagy wins the 2016 Nobel prize in physiology or medicine: Breakthroughs in baker's yeast fuel advances in biomedical research. *Proc Natl Acad Sci* (2017) 114:201–5. doi: 10.1073/PNAS.1619876114

89. Levine B, Kroemer G. Autophagy in the pathogenesis of disease. *Cell* (2008) 132:27–42. doi: 10.1016/j.cell.2007.12.018

90. Kabeya Y, Mizushima N, Ueno T, Yamamoto A, Kirisako T, Noda T, et al. LC3, a mammalian homologue of yeast Apg8p, is localized in autophagosome membranes after processing. *EMBO J* (2000) 19:5720–8. doi: 10.1093/emboj/19.21.5720

91. Grumati P, Dikic I. Ubiquitin signaling and autophagy. *J Biol Chem* (2018) 293:5404–13. doi: 10.1074/JBC.TM117.000117

92. Shaid S, Brandts CH, Serve H, Dikic I. Ubiquitination and selective autophagy. *Cell Death Differentiation* (2012) 20:21–30. doi: 10.1038/cdd.2012.72

93. Zhang M, He JQ. The impact of common Smurf1 gene variants on the risk, clinical characteristics and short-term prognosis of tuberculous meningitis. *Int J Infect Dis* (2021) 106:115–22. doi: 10.1016/J.IJID.2021.03.007

94. Cao Y, Wang C, Zhang X, Xing G, Lu K, Gu Y, et al. Selective small molecule compounds increase BMP-2 responsiveness by inhibiting Smurf1-mediated Smad1/5 degradation. *Sci Rep* (2014) 4:4965. doi: 10.1038/srep04965

95. Fu L, Cui CP, Zhang X, Zhang L. The functions and regulation of smurfs in cancers. *Semin Cancer Biol* (2020) 67:102–16. doi: 10.1016/J.SEMCANCER.2019.12.023

96. Lu K, Yin X, Weng T, Xi S, Li L, Xing G, et al. Targeting WW domains linker of HECT-type ubiquitin ligase Smurf1 for activation by CKIP-1. *Nat Cell Biol* (2008) 10:994–1002. doi: 10.1038/ncb1760

![frontiers] Frontiers in **Immunology**

Role of the cGAS/STING pathway in the control of *Brucella abortus* infection acquired through the respiratory route

Iván M. Alonso Paiva[1,2], Raiany A. Santos[3], Camila B. Brito[3], Mariana C. Ferrero[1,2], Juan Manuel Ortiz Wilczyñski[4], Eugenio A. Carrera Silva[4], Sergio C. Oliveira[3,5]* and Pablo C. Baldi[1,2]*

[1]Cátedra de Inmunología, Facultad de Farmacia y Bioquímica, Universidad de Buenos Aires, Buenos Aires, Argentina, [2]Instituto de Estudios de la Inmunidad Humoral (IDEHU), CONICET-Universidad de Buenos Aires, Buenos Aires, Argentina, [3]Departamento de Bioquímica e Imunologia, Instituto de Ciências Biológicas, Universidade Federal de Minas Gerais, Belo Horizonte, Minas Gerais, Brazil, [4]Laboratorio de Trombosis Experimental, Instituto de Medicina Experimental (IMEX, CONICET-Academia Nacional de Medicina (ANM)), Buenos Aires, Argentina, [5]Departamento de Imunologia, Instituto de Ciências Biomédicas, Universidade de São Paulo, São Paulo, Brazil

Despite the importance of the respiratory route for *Brucella* transmission, the lung immune response to this pathogen is scarcely characterized. We investigated the role of the cGAS/STING pathway of microbial DNA recognition in the control of respiratory *Brucella* infection. After *in vitro B. abortus* infection, CFU numbers were significantly higher in alveolar macrophages (AM) and lung explants from STING KO mice than in samples from wild type (WT) mice, but no difference was observed for cGAS KO samples. CFU were also increased in WT AM and lung epithelial cells preincubated with the STING inhibitor H151. Several proinflammatory cytokines (TNF-α, IL-1β, IL-6, IP-10/CXCL10) were diminished in *Brucella*-infected lung explants and/or AM from STING KO mice and cGAS KO mice. These cytokines were also reduced in infected AM and lung epithelial cells pretreated with H151. After intratracheal infection with *B. abortus*, STING KO mice exhibited increased CFU in lungs, spleen and liver, a reduced expression of IFN-β mRNA in lungs and spleen, and reduced levels of proinflammatory cytokines and chemokines in bronchoalveolar lavage fluid (BALF) and lung homogenates. Increased lung CFU and reduced BALF cytokines were also observed in cGAS KO mice. In summary, the cGAS/STING pathway induces the production of proinflammatory cytokines after respiratory *Brucella* infection, which may contribute to the STING-dependent control of airborne brucellosis.

1 Introduction

Brucellosis, a disease produced by Gram-negative bacteria of the *Brucella* genus, is a worldwide-distributed zoonosis. Among the various species included in the genus, *B. abortus*, *B. melitensis* and *B. suis* are the most pathogenic for humans. Domestic and wild animals can be affected, and humans can acquire the infection from several sources, among which contaminated aerosols and food are predominant (1). Given its high infectivity through the respiratory route, *Brucella* has been classified by the CDC as an agent of potential use in bioterrorism (2). Airborne *Brucella* transmission has been linked with several outbreaks of human brucellosis in slaughterhouses, laboratories, and rural areas (3–6). Despite the importance of the respiratory route for *Brucella* transmission, the lung immune response to this pathogen is only partially characterized. Given the ability of this pathogen to disseminate systemically within a few days after respiratory infection, the study of the lung innate immune response to the bacterium is of special interest.

Inhaled microorganisms first contact lung epithelial cells and alveolar macrophages (AM), which can respond to this threat by several mechanisms, including not only macrophage phagocytosis but also the production of proinflammatory factors, antimicrobial peptides and type I interferons (7–9). Previous studies have shown that lung epithelial cells produce proinflammatory factors upon infection with *Brucella abortus* or upon interaction with *Brucella*-infected macrophages (10). AM also produce proinflammatory cytokines in response to *B. abortus* infection (11). These immune responses depend in a great proportion on the recognition of microbial components by innate immunity receptors. The cytokine response of AM to *B. abortus* depends mainly on TLR2 recognition (11). A role for TLR2 and TLR4 in the control of respiratory *Brucella* infection has been shown by some studies (12) (13). Besides TLR, other innate sensors may contribute to induce immune responses to *Brucella* in the lung. Inflammasomes are multimeric complexes located in the cytosol that activate caspase-1 to mediate the cleavage of pro-IL-1β and pro-IL-18 into their mature active forms. It has been shown that some inflammasomes (NLRP3, AIM2) contribute to the control of pulmonary *Brucella* infection, probably through the induction of IL-1β maturation (14). While NLRP3 responds to diverse stimuli that exert cellular perturbations (pathogens, microbial toxins, etc.), AIM2 is a cytosolic sensor capable of detecting double-stranded DNA of microbial or host origin. Besides AIM2, one of the main cytosolic receptors for microbial nucleic acids is STING, although its activation leads to other biological consequences (15). Whereas STING recognizes directly some cyclic dinucleotides produced by invading pathogens, it does not recognize whole DNA. Instead, the cyclic GMP-AMP synthase (cGAS) binds DNA and catalyzes the production of cyclic dinucleotides that are subsequently recognized by STING (16, 17). Upon this sensing STING suffers a conformational change that triggers its association with TANK-binding kinase 1 (TBK1) and the migration of the STING-TBK1 complex from the ER to endosomal/lysosomal perinuclear regions. The translocation of TBK1 induces the phosphorylation of the transcription factors IRF3 and NF-κB. The latter translocate to the nucleus and trigger the transcription of genes coding for type I IFNs and proinflammatory cytokines, respectively (18, 19).

Whereas the STING pathway was initially believed to be only relevant for the immune response against viruses (due to its role in type I IFN production), later studies revealed a role for STING in the control of infections produced by bacteria and protozoans (18, 20, 21). Although cGAS and STING have been shown to be expressed in alveolar macrophages and lung epithelial cells (22–24), the role played be the cGAS/STING pathway in the lung immune response to inhaled *Brucella* is unknown. While a previous study has shown that STING is important in the defense against systemic (intraperitoneal) *B. abortus* infection (25), the role of the cGAS/STING pathway in *Brucella* infections acquired through a natural (mucosal) route has not been explored. This difference is not trivial, as the anatomical barriers and the cellular components involved in the host-pathogen interaction are quite different for both infection routes. In this study we show that the cGAS/STING pathway is involved in the control of *Brucella* infection acquired through the respiratory route in the mouse model. We also show that this pathway mediates the production of proinflammatory cytokines and IFN-β in the lung in response to *B. abortus* infection.

2 Materials and methods

2.1 Bacterial strains and growth conditions

B. abortus 2308 were grown in tryptic soy broth (TSB) at 37°C with agitation grown until the bacterial suspension reached an $OD_{600} \approx 1.0$. After centrifugation and washing of the bacterial pellet with sterile phosphate buffered saline (PBS), inocula were prepared by resuspending bacteria to the desired OD_{600}. *Brucella* manipulations for both *in vitro* and *in vivo* experiments were conducted under BSL3 conditions.

2.2 Mice

Animals for in vivo studies were C57BL/6 wild-type mice (6–9 wk of age) and knock-out (KO) mice of the same background (cGAS and STING KO mice), all provided by the Federal University of Minas Gerais (UFMG), Brazil. Both strains of KO mice have been described previously (26, 27). Housing conditions were: 5 animals per cage, controlled temperature (22°C±2°C) and a 12 h cycle period of artificial light. Animals received sterile food and water *ad libitum*, and were maintained under specific pathogen-free conditions in positive-pressure cabinets. C57BL/6 mice for in vitro studies (primary cultures) were provided by IMEX, National Academy of Medicine, Buenos Aires, Argentina, and were kept under similar conditions as mentioned above until processing. All animal experiments were conducted according to international ethical standards (Amsterdam Protocol of welfare and animal protection, and National Institutes of Health, USA, guidelines:

Guide for the Care and Use of Laboratory Animals), and are reported in accordance with ARRIVE Guidelines. The animal protocols used in this study were approved by the respective Committees for the Care and Use of Experimentation Animals from the UFMG (CETEA no. 69/2020) and the School of Pharmacy and Biochemistry of the University of Buenos Aires (Res. D1879/2019).

2.3 Intratracheal inoculation

Intratracheal inoculation of animals with *B. abortus* was performed as previously described (28) with minor modifications (29). Briefly, after receiving isoflurane anesthesia mice were intraperitoneally injected with ketamine/xylazine (100mg/kg and 8mg/kg). Animals were placed over an acrylic backboard in supine position and their head movements were restrained with a rubber band passed under their upper incisors. Under translucent illumination of the trachea each mice was injected in between the vocal cords using a blunt-ended probe with 20 µl of *B. abortus* suspension containing 10^5 CFU (as estimated by OD_{600}).

2.4 CFU and cytokine analysis

Colony-forming units (CFU) of *B. abortus* and cytokine levels in homogenates of selected organs from infected mice were determined as described previously (14). Briefly, at different post-infection (p.i.) time-points an intraperitoneal lethal dose of ketamine and xylazine was given to each animal. Their lungs, livers and spleens were homogenized in sterile PBS using a tissue homogenizer (Bio-Gen PRO200™). Some homogenate aliquots were serially diluted and plated on TSA for CFU counting, whereas the remaining homogenate volumes were processed for cytokine measurements. In the later case, samples were centrifuged at 4°C and the supernatants were mixed with protease inhibitors (cOmplete™, Roche) and stored at -70°C. Cytokine and chemokine determinations were performed using commercial ELISA kits (R&D).

2.5 Murine alveolar macrophages and broncho-alveolar lavage fluid

Murine alveolar macrophages were isolated following previously described procedures (11). Mice were euthanized with the ketamine/xylazine lethal dose. Their tracheas were exposed and a small incision was performed to insert a fine-tipped pipette. Sterile cold PBS containing 1 mM EDTA was perfused (3 times, 1 ml each) to obtain broncho-alveolar lavage fluid (BALF). After centrifugation (400 x*g*, 10 min, 4°C) BALF supernatants were stored at -70°C for cytokine measurements, whereas pellet cells were resuspended in complete medium (RPMI 1640 containing 10% heat inactivated fetal bovine serum -FBS, Gibco-, 100 U/mL of penicillin and 50 µg/mL of streptomycin). In trypan blue exclusion assays the viability of BALF cells was routinely greater than 95%. After incubation for 2

hours (37 °C, 5% CO_2 humidified atmosphere) in 48-wells culture plates (2×10^5 cells/well) to allow adhesion of alveolar macrophages, non-adherent cells were removed by repeated washes with fresh culture medium.

2.6 RT-PCR for *IFN-β* expression

The expression of IFN-β in lungs and spleen from mice intratracheally infected with *B. abortus* was evaluated by RT-PCR as previously described (25). Total RNA was extracted from lungs and spleens with TRIzol reagent (Invitrogen) and was quantified with a NanoDrop® spectrophotometer (PeqLab, Erlangen, Germany). The synthesis of cDNA from RNA (1 µg) was carried out in a final reaction volume of 20 µl. The reverse transcription was carried out at 50°C for 30 min and the reaction was stopped by denaturation of the enzyme (85°C, 10 min) using Illustra Ready-To-Go RT-PCR Beads (GE Healthcare) following the manufacturer's instructions. Real-time RT-PCR was performed on a QuantStudio3 real-time PCR instrument (Applied Biosystems) with 2X SYBR Green PCR master mix (Applied Biosystems). The following primers were used to amplify a specific fragment of specific gene targets: 18S, forward, 5′-CGTTCCACCAACTAAGAACG-3′, reverse, 5′-CTCAACACG GGAAACCTCAC-3′; IFN-β, forward, 5'-GCC TTT GCC ATC CAA GAG ATG C-3', reverse, 5'-ACA CTG TCT GCT GGT GGA GTT C-3'. The sequence of the 18S primer was previously published (30). For each gene a negative control (NTC, non-template control) was used and the presence of non-specific amplification product was checked by the melting curve. Data were analyzed using the threshold cycle (*ΔΔCT*) method and are informed as relative expression units after normalization to the *18S* gene. The calibrator used were samples from uninfected mice, compared to infected WT and KO animals.

2.7 Primary lung epithelial cells

Lung epithelial cells (LEC, mostly type II pneumocytes) were isolated from murine lungs as described previously (14). Briefly, remaining blood in the lungs was eliminated by perfusion through the heart with sterile PBS. After washing with an appropriate buffer, the organs were cut into small pieces which were digested with trypsin at 37°C for 10 min. Filtration through a 100 µm mesh was performed, with the filtrate recovered on FBS containing DNAse. After a second filtration through a 40 µm mesh, the final filtrate (containing individual cells) was centrifuged. The LEC-enriched pellet was resuspended in DMEM/F12 containing DNAse. The cellular suspension was incubated for 2 h in 6-well culture plates, after which the supernatant containing non-adherent cells was subjected to a discontinuous Percoll gradient (1.089 g/l and 1.04 g/l; Sigma). The LEC-enriched interface was recovered and washed twice. An aliquot was taken for viability determination (Trypan blue) and counting. For infection experiments, LEC were resuspended in supplemented DMEM/F12 and seeded at 2×10^5 cells/well in 48-well plates coated with type I collagen. Culture medium was changed daily until the cells reached confluence (5-7 days).

2.8 Cell infections

Alveolar macrophages (AM) and LEC were infected *in vitro* with *B. abortus* at multiplicities of infection (MOI) of 100 bacteria/cell (AM) or 200 bacteria/cell (LEC) as described previously (14). Bacteria were dispensed suspended in culture medium without antibiotics, followed by centrifugation of the plates and incubation for 2 hours (37°C, 5% CO_2 atmosphere). Bacteria not adhered or internalized into the cells were removed by three washes with sterile PBS (time 0 p.i.). To kill non-internalized bacteria the cells were incubated in culture medium containing 100 μg/ml of gentamicin (Sigma, USA) and 50 μg/ml of streptomycin (Sigma, USA). Culture supernatants were harvested for cytokine measurement 24 h after antibiotics addition. At the same time, cell lysates prepared using 0.2% Triton X100 were plated on TSA to enumerate CFU of intracellular bacteria. In some experiments, a STING inhibitor (H151, InvivoGen, 15 μM) or its vehicle (DMSO) were added to AM and LEC for 24 h before infection, and were maintained during the whole infection period.

2.9 Statistical analysis

Data were analyzed using Student's *t* test or analysis of variances (ANOVA). Tukey's post-test and Dunnett's post-test were used for multiple comparisons between all pairs of groups and against a control group, respectively. A p<0.05 was considered as statistically significant. All statistical analyses were performed with the GraphPad software (San Diego, CA).

3 Results

3.1 STING is involved in the control of *Brucella* infection by pulmonary cells

Alveolar macrophages ($5x10^5$/well) and lung explants (1 cm³) of wild type C57BL/6 mice and STING KO and cGAS KO mice of the same genetic background were infected with *B. abortus* 2308, and were processed at different time points to determine intracellular CFU. At both 24 and 48 h p.i., CFU levels were significantly higher in alveolar macrophages and explants from STING KO mice than in samples from normal mice (Figure 1A). In contrast, the bacterial load did not differ significantly between cGAS KO and wild type mice for any sample at any time point. Given this last observation, the ensuing experiments were focused on the role of STING. The involvement of STING in the control of *Brucella* infection by lung cells was confirmed when alveolar macrophages and LEC were pretreated with the specific STING inhibitor H151 before infection. As shown in Figure 1B, CFU were significantly increased at 24 and/or 48 h p.i. in cells preincubated with the inhibitor than in untreated cells or those pretreated with vehicle (DMSO).

3.2 STING and cGAS mediate the production of proinflammatory cytokines by *Brucella*-infected pulmonary cells

As mentioned, the cGAS/STING pathway mediates not only the production of type I interferons but also the production of proinflammatory cytokines and chemokines. As shown in Figure 2A, the levels of several proinflammatory cytokines (TNF-α, IL-1β, IL-6) and of the proinflammatory chemokine IP-10/CXCL10 were significantly reduced in lung explants from STING KO mice and cGAS KO mice infected *in vitro* with *B. abortus* as compared to explants from wild type mice. Although several cell types can produce proinflammatory mediators in the lung, alveolar macrophages and epithelial cells are especially important as they are the first to contact inhaled pathogens. Therefore, the role of STING and cGAS in the proinflammatory response of these two cell types was investigated. As shown in Figure 2B, the secretion of TNF-α, IL-1β and IL-6 in response to *B. abortus* infection was significantly reduced in alveolar macrophages from STING KO mice and cGAS KO mice as compared to wild type mice. In line with these findings, the levels of these cytokines were significantly reduced in LEC (Figure 3A) and alveolar macrophages (Figure 3B) pretreated with the STING inhibitor H151 than in untreated cells or those pretreated with vehicle (DMSO).

3.3 STING is involved in the control of *Brucella* infection acquired through the airways

In view of the role of STING in the control of in vitro *B. abortus* infection in lung explants, alveolar macrophages and lung epithelial cells, we decided to test the role of this receptor in the control of the in vivo respiratory infection. To this end, wild type and STING KO mice were infected intratracheally and CFU were measured at 7 and 14 days p.i. in lungs and peripheral target organs (spleen and liver). As shown in Figure 4, at both time points the bacterial load was significantly higher in all the investigated organs in STING KO mice than in wild type mice, revealing that this receptor is involved in the control of respiratory *Brucella* infection.

3.4 *Brucella abortus* induces a STING-dependent expression of *IFN-β* in the lungs

The STING pathway constitutes a central mediator of type I IFN responses, which have recently been shown to have a role not only in protection against viruses but also against other microorganisms, including some respiratory bacterial pathogens. Therefore, we tested the expression of *IFN-β* mRNA by qRT-PCR in lungs and spleens of mice at 7 days after intratracheal *B. abortus* infection. As shown in Figure 5, *IFN-β* expression was significantly reduced in both organs in STING KO mice as compared to wild type mice.
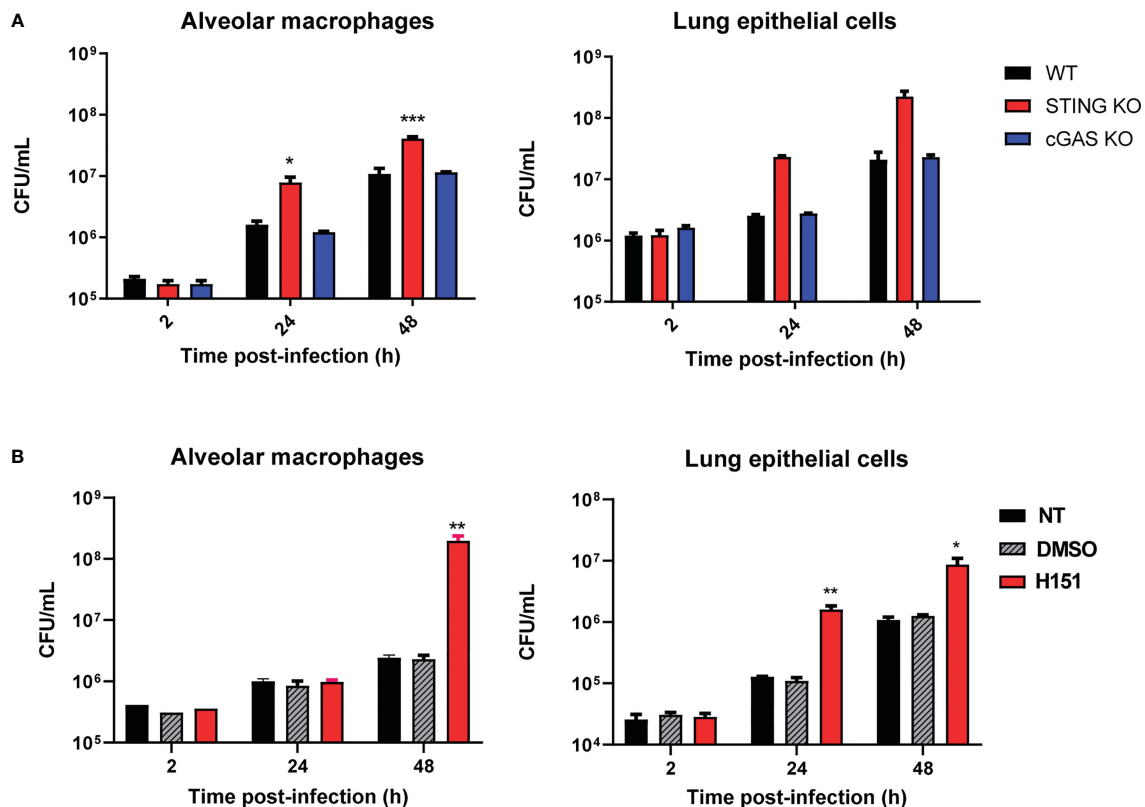
FIGURE 1

Influence of STING and cGAS on the course of *B. abortus* infection in lung explants and cells infected in vitro. **(A)** Alveolar macrophages (5×10^5/well) and lung explants (1 cm³) of wild type (WT) C57BL/6 mice and STING KO and cGAS KO mice were infected with *B. abortus* 2308, and were processed at different time points to determine intracellular colony-forming units (CFU) (n= 3 per time and mouse strain). **(B)** Alveolar macrophages and lung epithelial cells from C57BL/6 mice were pretreated (H151) or not (NT) with the specific STING inhibitor H151 before infection, and CFU were determined at different post-infection times. Cells pretreated with the vehicle (DMSO) served as controls (n= 3 per time and treatment). Values are means ± SD of two independent experiments (*p<0.05, **p<0.01, ***p<0.001 versus WT **(A)** or INF **(B)**, ANOVA followed by Tukey´s test).

3.5 STING mediates the production of proinflammatory cytokines in lungs and peripheral organs after respiratory *Brucella* infection

Proinflammatory cytokines play a central role in the control of infections by mediating the recruitment of phagocytes, increasing the expression of cell adhesion molecules and antimicrobial peptides, and activating the microbicidal and antigen-presenting function of phagocytes, among other functions. Given the role of STING in the control of *Brucella* infection in lungs and peripheral organs, and its known contribution to the induction of proinflammatory cytokines, we decided to evaluate the role of STING in the proinflammatory response of lungs and spleen in mice infected with *B. abortus* through the intratracheal route. As shown in Figure 6A, the levels of proinflammatory cytokines and chemokines were reduced in the broncho-alveolar lavage fluid (BALF) of STING KO mice as compared to wild type mice at both 7 and 14 days p.i. A similar picture was observed when lung homogenates were tested (Figure 6B). Overall, our findings reveal a reduced proinflammatory response to intratracheal *B. abortus* infection in the lungs of STING KO mice as compared to wild type mice. From its respiratory portal of entry *Brucella* can

disseminate systemically and reach peripheral organs, among which the spleen is a preferred target in the mouse model of infection. Also in this organ STING appeared to have an important role as a mediator of proinflammatory responses to *B. abortus*. As shown in Figure 7, the levels of IL-1β, IL-6 and IP-10 were significantly reduced in the spleens of STING KO mice at 7 and 14 days after intratracheal infection.

3.6 cGAS is also involved in the control of respiratory *Brucella* infection

Whereas cGAS did not seem to have a role in the control of *B. abortus* infection in alveolar macrophages or lung explants infected *in vitro*, this receptor was shown to have a role in the production of proinflammatory cytokines by these samples during in vitro infection. Therefore, a potential role of cGAS in the control of respiratory *B. abortus* infection was evaluated. As shown in Figure 8, lung CFU were significantly increased in cGAS KO mice at 14 days after intratracheal infection as compared to WT controls. In addition, the levels of TNF-α and IL-6 were significantly reduced in BALF samples from infected cGAS KO mice as compared to their WT counterparts (Figure 9).
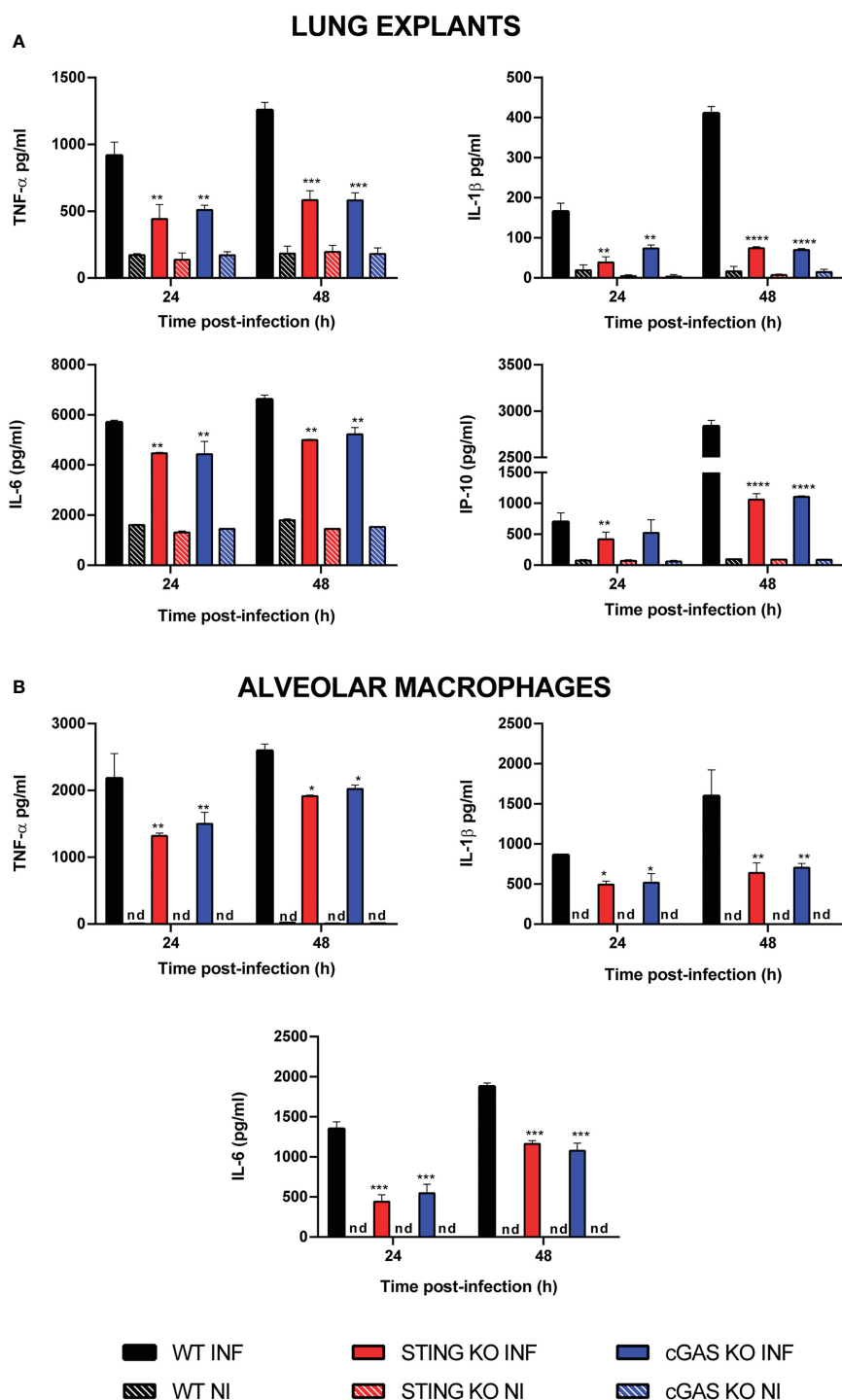
FIGURE 2

Influence of STING on the production of proinflammatory factors by *Brucella*-infected lung explants **(A)** and alveolar macrophages **(B)**. Explants (1 cm³) or alveolar macrophages from wild type (WT) and STING KO C57BL/6 mice were infected in vitro with *B. abortus* 2308, and culture supernatants were collected at 24 and 48 h post-infection to measure cytokine levels by sandwich ELISA (n= 3 per time and mouse strain). Values are means $\pm$ SD of two independent experiments (*p<0.05, **p<0.01, ***p<0.001, ****p<0.0001, STING KO versus WT, Student's *t* test). INF: infected, NI: non-infected, nd: not detected.

4 Discussion

Inhalation of aerosols containing *Brucella* spp. constitutes an important form of contagion with this bacterium. From its pulmonary port of entry, the pathogen passes into the systemic circulation and invades various organs. The pulmonary immune response to *Brucella* is poorly understood, and it is not precisely known why it fails to prevent the passage of the bacteria into the general circulation. Nucleic acids are microbial components that can be recognized by the innate immune system. If microbial DNA

is found in endosomal compartments it can be recognized by TLR9, while if it is found in the cytosol it can be detected by non-TLR receptors such as AIM2 (component of inflammasomes that mediate secretion of IL-1β and IL-18) and components of the cGAS/STING pathway (that mediate production of type I interferons, autophagy and activation of NF-κB).

Although it was initially considered that cytosolic DNA receptors would only have relevance in the immune control of

FIGURE 4

STING is involved in the control of *Brucella* infection acquired through the airways. Wild type (WT) and STING KO mice (n=5 per group) were infected intratracheally with *B. abortus* (10^5 CFU/mice) and CFU were measured at 7 and 14 days p.i. in lungs and peripheral target organs (spleen and liver). Values are data from a representative experiment of two performed with similar results (*p<0.05, **p<0.01, ***p<0.001, Student's *t* test).

viral infections, later studies showed that these receptors are also important for the control of infections by other pathogens, including bacteria acquired through the respiratory route (31). For example, AIM2-has been shown to be involved in the control of intratracheal infection with *M. tuberculosis* or *Brucella abortus*, and in both cases AIM2 deficiency was associated with increased bacterial loads in lungs (14, 32). Gram-negative and Gram-positive bacteria, among other microorganisms, are known to promote STING signaling. Moreover, a role for STING in the control of infections produced by bacteria has been reported (18, 20). Both type I IFNs and proinflammatory cytokines may be involved in the STING-dependent response to bacterial infections (33).

It has been shown that STING is important in defense against systemic (intraperitoneal) *B. abortus* infection, mediating not only the production of IFN-β but also proinflammatory cytokines (25). That study also showed that c-di-GMP produced by this pathogen can activate STING and trigger type I IFN responses and inflammasome activation in murine and human cells, and it has been suggested that this cyclic dinucleotide induces the initial STING signaling during *B. abortus* infections. STING activation was absent in cells infected with a *B. abortus* mutant deficient in c-di-GMP production (c-di-GMP guanylate cyclase mutant Δ1520)

while it was observed in cells infected with the parental wild type strain. Of note, the mutant induced lower expression levels of IFN-β and IL-1β secretion in bone marrow-derived macrophages (BMDM) as compared with the virulent strain. Recently it has been also shown that STING regulates metabolic reprogramming in macrophages and promotes a tendency towards an inflammatory profile in spleen macrophages in the first days after intraperitoneal *B. abortus* infection in mice (34). Although cGAS and STING have been shown to be expressed in lung cells (22–24), the importance of the cGAS/STING axis in the defense against *Brucella* infection by the respiratory route has not been explored. In this study, we show that alveolar macrophages and lung explants from STING KO mice infected in vitro with *B. abortus* had significantly increased CFU counts as compared to those from wild-type mice. The same phenomenon was observed when alveolar macrophages and lung epithelial cells were treated with a STING chemical inhibitor before infection. Thus, the impaired control of *B. abortus* infection in lung explants from STING KO mice may be due to the combined effect of STING deficiency on the infection control capacity of macrophages, epithelial cells and eventually other cell types. While STING deficiency impaired the ability of alveolar macrophages or lung explants to control *B. abortus* infection, no
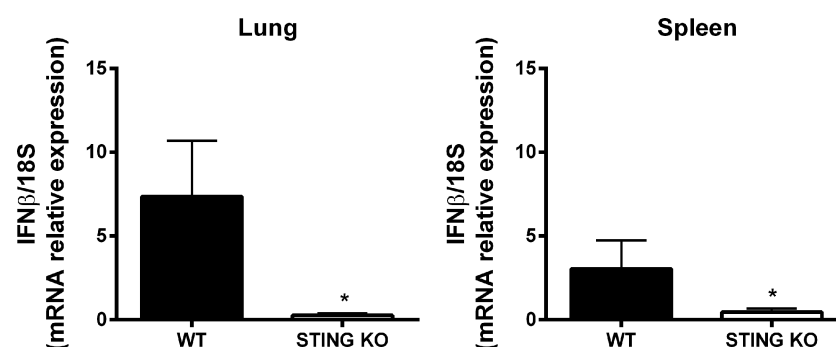
FIGURE 5

STING-dependent expression of *IFN-β* in mouse organs after intratracheal *B. abortus* infection. Wild type (WT) and STING KO mice (n=5 per group) were infected intratracheally with *B. abortus* (10^5 CFU/mice) and the expression of *IFN-β* was measured by RT-PCR at 7 days p.i. in lungs and spleen. Values are means ± SD of two independent experiments (*p<0.05, Student's *t* test).

FIGURE 6

Influence of STING on the pulmonary production of proinflammatory factors after intratracheal *Brucella* infection. Wild type (WT) and STING KO mice (n=6 per group) were infected intratracheally with *B. abortus* (10^5 CFU/mice) and proinflammatory cytokines were measured at 7 and 14 days p.i. in broncho-alveolar lavage fluid (BALF) **(A)** and lung homogenates **(B)**. Values are means $\pm$ SD of two independent experiments (*p<0.05, **p <0.01, ***p<0.001, Student's *t* test).

such effect was observed for cGAS deficiency. These results agree with those previously reported for *B. abortus* infections in BMDM (25).

In the present study, lung cells from STING KO or cGAS KO mice or those treated with H151, a STING inhibitor, secreted less TNF-α, IL-1β, IL-6 and/or IP-10 in response to in vitro *Brucella* infection. A reduced production of proinflammatory cytokines in response to bacterial pathogens in cells deficient in the cGAS/

STING pathway has been reported in some studies. For example, STING KO and cGAS KO BMDM produced less cytokines than their WT counterparts after *B. abortus* infection (25). Macrophages from cGAS- and STING-deficient mice were severely impaired in producing proinflammatory cytokines (and type I IFNs) in response to *Legionella pneumophila*, and the same defect was observed when the infection was performed on cells from patients carrying the HAQ variant of STING (35). In addition, cGAS and STING are

FIGURE 7

Influence of STING on the production of proinflammatory factors in the spleen after intratracheal *Brucella* infection. Wild type (WT) and STING KO mice (n=5 per group) were infected intratracheally with *B. abortus* (10^5 CFU/mice) and proinflammatory cytokines were measured at 7 and 14 days p.i. in their spleens. Values are means $\pm$ SD of two independent experiments (*p<0.05, **p <0.01, ***p<0.001, Student's *t* test).

essential for inducing IFN-β and other ISGs in response to *Mycobacterium tuberculosis* infection in both human and mouse macrophages (36).

The cGAS/STING pathway is involved in the response to several bacterial infections, but its role differs depending on the pathogen and the infection model. The possible contribution of this pathway to defense against bacterial infections raised some doubts, since this pathway mediates the production of type I IFNs (37), which in some cases have been associated with negative effects on antibacterial immunity. However, it has been shown that a negative effect of type I IFNs is not observed in all bacterial infections, with cases in which these IFNs contribute to immune control. Such is the case of *Legionella pneumophila*, *Streptococcus pyogenes*, *Streptococcus pneumoniae* and *Helicobacter pylori*, among others (38). In *Francisella tularensis* infections, STING-dependent type I IFN production is necessary for the activation of the AIM2 inflammasome, possibly due to the ability of type I IFNs to activate guanylate-binding proteins (GBPs) by increasing bacteriolysis and the release of DNA into the cytosol (39). Of

note, the role of the cGAS/STING pathway cannot be predicted solely from the effects that type I IFNs can exert. For example although mice deficient for the type I IFN receptor (IFNAR) have been described as more resistant to *Listeria monocytogenes* infection (40), STING-deficient mice do not show significant differences in splenic load compared to normal ones (41). Apart from this last study, there are few reports on the impact of the absence of STING (and/or cGAS) in the control of bacterial infections. In the case of *Mycobacterium tuberculosis* infection, STING-deficient mice appear to have no modifications in their bacterial load (pulmonary or extrapulmonary), survival, and proinflammatory cytokine levels compared to normal mice (36, 42). In contrast, we found that STING-deficient mice have higher loads of *B. abortus* in lung, spleen and liver after intratracheal infection, demonstrating that STING is beneficial in controlling *Brucella* infection acquired through the respiratory route. These results agree with the previously reported protective role of STING against intraperitoneal *Brucella* infection (25). While it has been reported that in the first hours after in vitro *Brucella* infection of
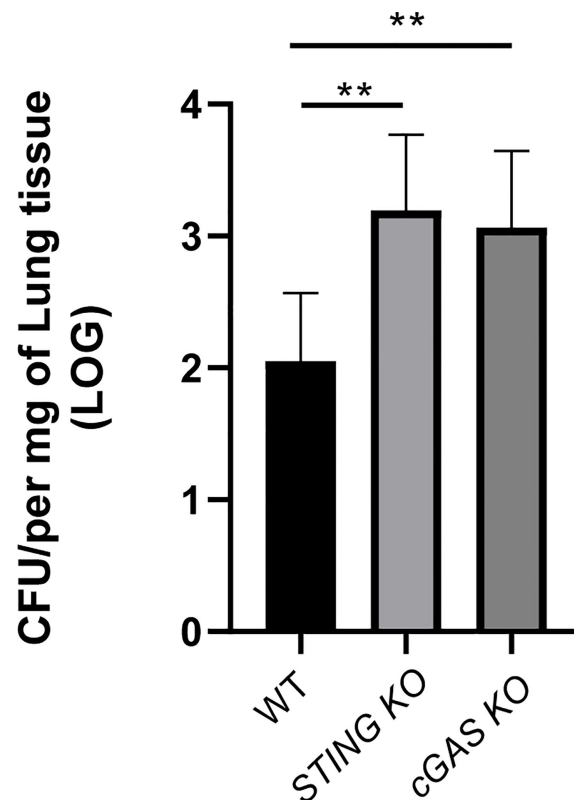
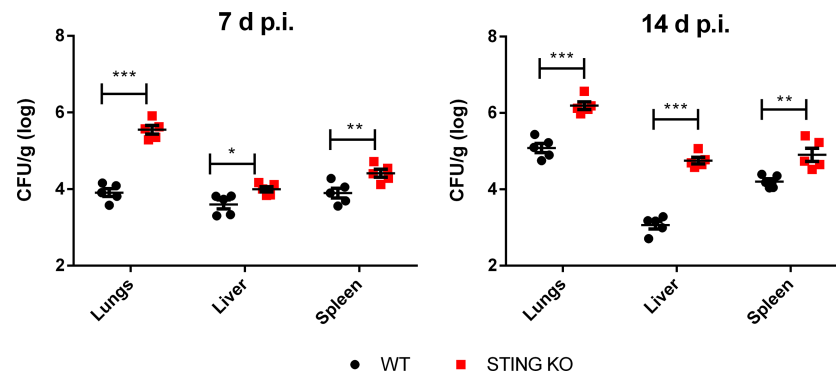**FIGURE 8**
cGAS is involved in the control of *Brucella* infection acquired through the airways. Wild type (WT), cGAS KO and STING KO mice (used for comparison) (n=5 per group) were infected intratracheally with *B. abortus* (10^5 CFU/mice) and CFU were measured at 14 days p.i. in the lungs. Values are data from a representative experiment of two performed with similar results (**p<0.01, Student's *t* test).

macrophages the levels of a microRNA (miR-24) that targets the STING messenger RNA are increased, resulting in a transient reduction of STING levels, this receptor is still required for controlling acute and chronic *B. abortus* infection in mice (43). It has been also reported that STING mediates the induction of the unfolded protein response (UPR) in macrophages infected with *B. abortus* (44). This UPR exerted some control on the production of several proinflammatory mediators (IL-6, IL-1β), and regulated the production of IFN-β and the expression of several factors linked to type I IFN responses. While the UPR was shown to favor *B. abortus* replication in macrophages, the influence of STING on proinflammatory mediators may explain the increased susceptibility of STING KO–derived macrophages to *B. abortus* infection observed in previous studies (25). In agreement with our results showing an increased susceptibility of STING KO mice and cGAS KO mice to respiratory *B. abortus* infection, a recent study in a murine model of intranasal *Legionella pneumophila* infection found that both KO mice have higher bacterial burdens than control mice (35).

As already mentioned, the cGAS/STING pathway mediates the production of both type I IFNs and proinflammatory cytokines. The role of type I IFNs as antiviral cytokines is widely established, and it is well known that they are induced when pattern recognition receptors (PRRs) sense foreign molecules. Nevertheless, recent evidence suggests that type I IFNs can also mediate inflammatory responses to bacterial infections (45). Regarding the role that type I IFNs would play in the control of *Brucella* infection, contradictory results have been obtained. While in 129Sv/Ev mice the absence of IFNAR was beneficial for infection control (15 days p.i.) (46), it did not lead to significant changes in mice from Balb/c background up to 4 weeks p.i (47). In contrast to what was observed in vivo, the absence of IFNAR in macrophages from 129Sv/Ev strain mice resulted in a significant increase in the bacterial load at 24 hours p.i., suggesting a protective role for type I IFNs (25). In our model, a reduced *IFN-β* expression, as well as lower concentrations of IP-10, in lungs and spleen of C57BL/6 mice lacking STING were detected. Further studies will be required to establish the role of IFN-β in the reduced protection of STING KO mice against *B. abortus* respiratory infection.

As mentioned, STING exerts other effects in addition to the induction of type I IFN, including stimulation of the NF-kB pathway with the consequent production of proinflammatory cytokines. Previous studies also suggest that type I IFN contribute to the activation of the AIM2 inflammasome, and therefore to caspase-1 activation and IL-1β secretion, through its ability to induce the expression of GBPs that lyse pathogen-containing vacuoles and allow the release of bacterial products, including DNA, to the cytosol (25, 39). We found lower concentrations of proinflammatory cytokines in the BALF, lungs and spleen of *Brucella*-infected STING KO mice and also in BALF of cGAS KO

FIGURE 9

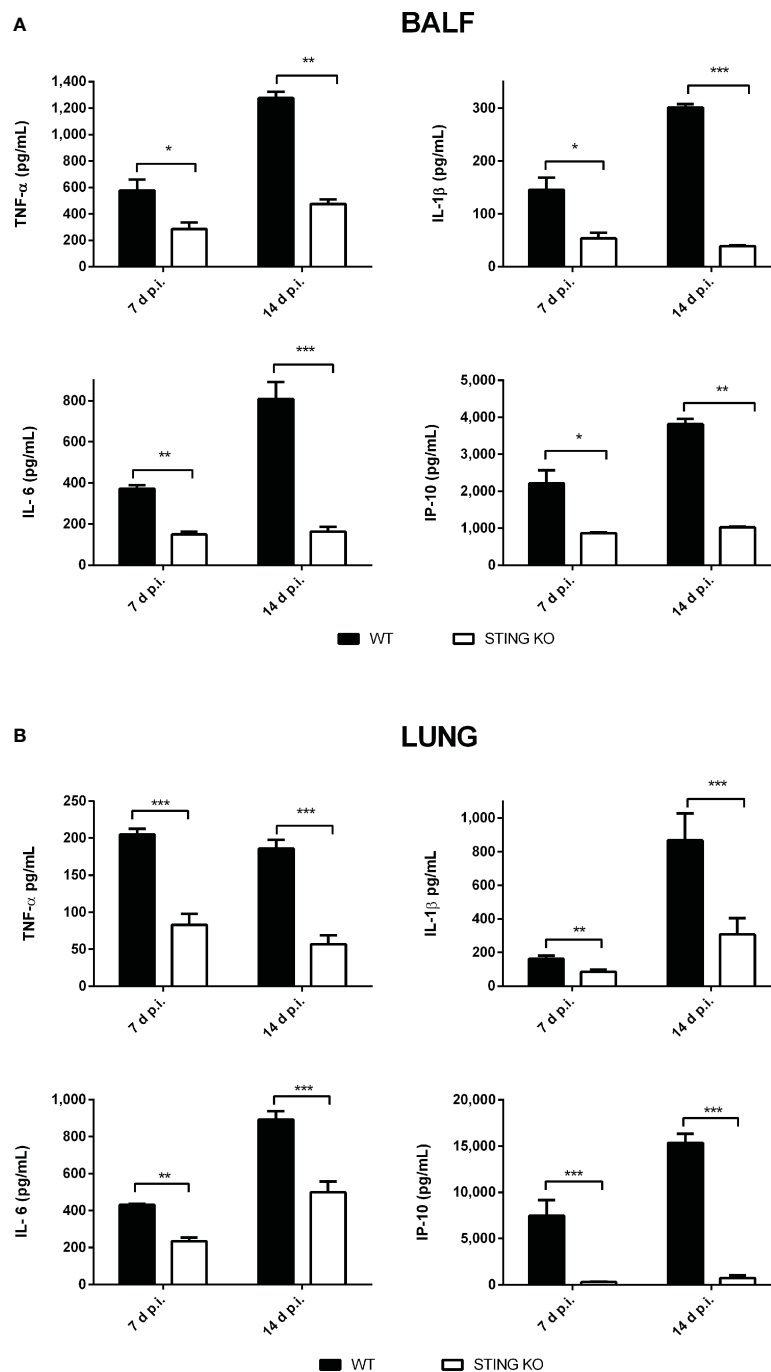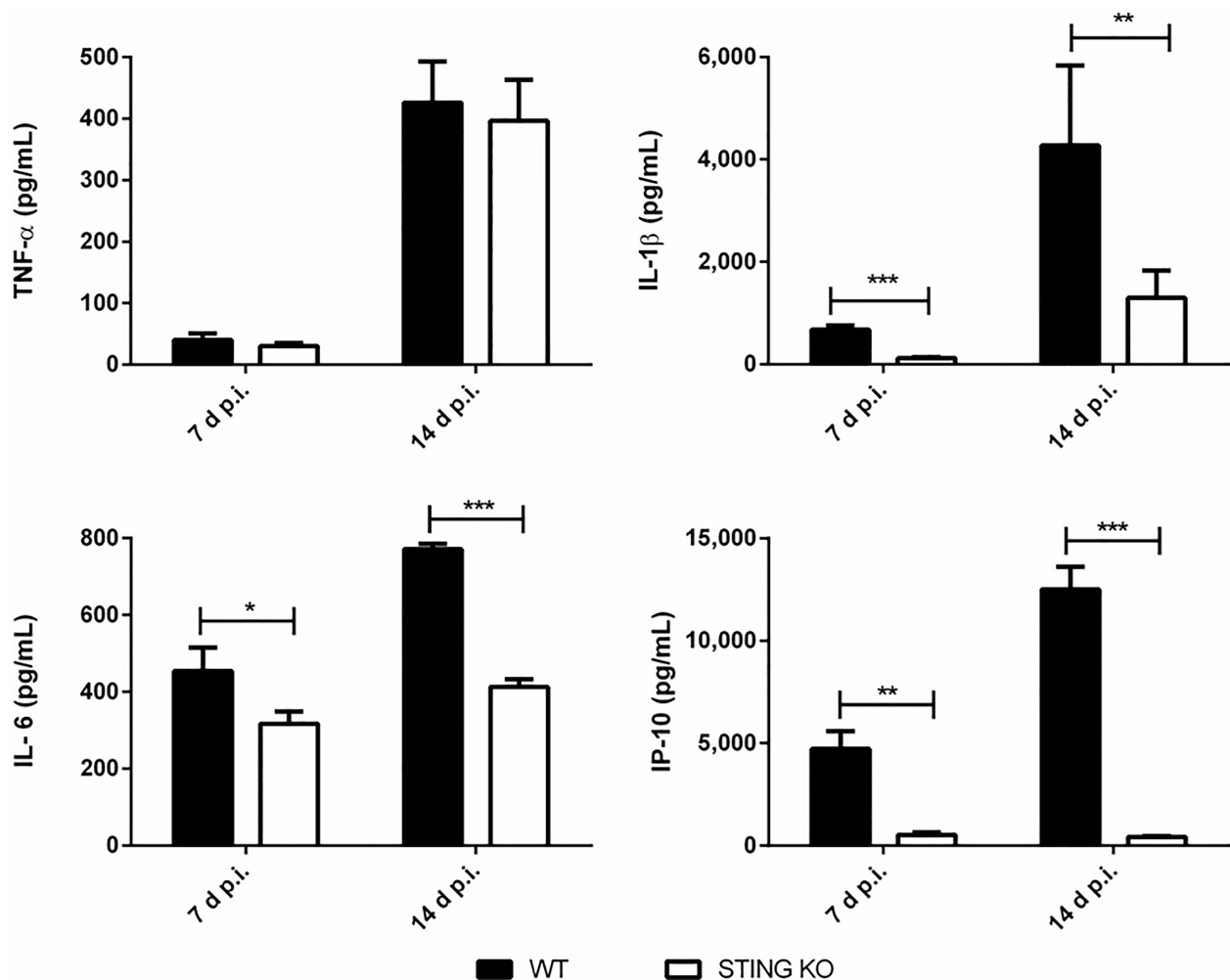Influence of cGAS on the pulmonary production of proinflammatory factors after intratracheal *Brucella* infection. Wild type (WT) and cGAS KO mice (n=5 per group) were infected intratracheally with *B. abortus* (10^5 CFU/mice) and proinflammatory cytokines were measured at 14 days p.i. in broncho-alveolar lavage fluid (BALF). Values are means $\pm$ SD of two independent experiments (**p <0.01, Student's *t* test).

mice, suggesting that these cytokines may be involved in the protective role of STING and cGAS against respiratory *B. abortus* infection.

In conclusion, the present study reveals a protective role of the cGAS/STING pathway during acute respiratory *Brucella abortus* infection. In this context, the cGAS/STING pathway induces the production of proinflammatory cytokines in lungs and peripheral tissues, which may contribute to the cGAS/STING-dependent control of airborne brucellosis. Further research is warranted to establish the precise contribution of this, and eventually other mechanisms, to the cGAS/STING-dependent reduction of bacterial burden.

Data availability statement

The raw data supporting the conclusions of this article will be made available by the authors, without undue reservation.

Ethics statement

The animal study was reviewed and approved by Committees for the Care and Use of Experimentation Animals from the UFMG (CETEA no. 69/2020) and the School of Pharmacy and Biochemistry of the University of Buenos Aires (Res. D1879/2019).

Author contributions

Conceived and designed the experiments: IAP, MF, SCO, PB. Performed the experiments: IAP, MF, RAS, CB, JOW, ECS. Analyzed the data: IAP, RAS, CB, MF, JOW, ECS, SCO, PB. Wrote the draft and/or final version of the paper: IAP, MF, SCO, PB. All authors reviewed the manuscript. All authors contributed to the article and approved the submitted version.

Funding

Acknowledgments

Conflict of interest

The authors declare that the research was conducted in the absence of any commercial or financial relationships that could be construed as a potential conflict of interest.

Publisher's note

All claims expressed in this article are solely those of the authors and do not necessarily represent those of their affiliated organizations, or those of the publisher, the editors and the reviewers. Any product that may be evaluated in this article, or claim that may be made by its manufacturer, is not guaranteed or endorsed by the publisher.

References

1. Pappas G, Akritidis N, Bosilkovski M, Tsianos E. Brucellosis. *N Engl J Med* (2005) 352:2325–36. doi: 10.1056/NEJMra050570

2. Pappas G, Panagopoulou P, Christou L, Akritidis N. Brucella as a biological weapon. *Cell Mol Life Sci* (2006) 63:2229–36. doi: 10.1007/s00018-006-6311-4

3. Kaufmann AF, Fox MD, Boyce JM, Anderson DC, Potter ME, Martone WJ, et al. Airborne spread of brucellosis. *Ann N Y Acad Sci* (1980) 353:105–14. doi: 10.1111/j.1749-6632.1980.tb18912.x

4. Olle-Goig JE, Canela-Soler J. An outbreak of brucella melitensis infection by airborne transmission among laboratory workers. *Am J Public Health* (1987) 77:335–8. doi: 10.2105/AJPH.77.3.335

5. Wallach JC, Samartino LE, Efron A, Baldi PC. Human infection by brucella melitensis: an outbreak attributed to contact with infected goats. *FEMS Immunol Med Microbiol* (1997) 19:315–21. doi: 10.1016/S0928-8244(97)00098-9

6. Yagupsky P, Baron EJ. Laboratory exposures to brucellae and implications for bioterrorism. *Emerg Infect Dis* (2005) 11:1180–5. doi: 10.3201/eid1108.041197

7. Marriott HM, Gascoyne KA, Gowda R, Geary I, Nicklin MJH, Iannelli F, et al. Interleukin-1β regulates CXCL8 release and influences disease outcome in response to streptococcus pneumoniae, defining intercellular cooperation between pulmonary epithelial cells and macrophages. *Infect Immun* (2012) 80:1140–9. doi: 10.1128/IAI.05697-11

8. Whitsett JA, Alenghat T. Respiratory epithelial cells orchestrate pulmonary innate immunity. *Nat Immunol* (2015) 16:27–35. doi: 10.1038/ni.3045

9. Hussell T, Bell TJ. Alveolar macrophages: plasticity in a tissue-specific context. *Nat Rev Immunol* (2014) 14:81–93. doi: 10.1038/nri3600

10. Ferrero MC, Fossati CA, Baldi PC. Direct and monocyte-induced innate immune response of human lung epithelial cells to brucella abortus infection. *Microbes Infect* (2010) 12:736–47. doi: 10.1016/j.micinf.2010.05.002

11. Ferrero MC, Hielpos MS, Carvalho NB, Barrionuevo P, Corsetti PP, Giambartolomei GH, et al. Key role of toll-like receptor 2 in the inflammatory response and major histocompatibility complex class ii downregulation in brucella abortus-infected alveolar macrophages. *Infect Immun* (2014) 82:626–39. doi: 10.1128/IAI.01237-13

12. Pei J, Ding X, Fan Y, Rice-Ficht A, Ficht TA. Toll-like receptors are critical for clearance of brucella and play different roles in development of adaptive immunity following aerosol challenge in mice. *Front Cell Infect Microbiol* (2012) 2:115. doi: 10.3389/fcimb.2012.00115

13. Surendran N, Hiltbold EM, Heid B, Akira S, Standiford TJ, Sriranganathan N, et al. Role of TLRs in brucella mediated murine DC activation in vitro and clearance of pulmonary infection *in vivo*. *Vaccine* (2012) 30:1502–12. doi: 10.1016/j.vaccine.2011.12.036

14. Hielpos MS, Fernández AG, Falivene J, Paiva IMA, González FM, Ferrero MC, et al. IL-1R and inflammasomes mediate early pulmonary protective mechanisms in respiratory brucella abortus infection. *Front Cell Infect Microbiol* (2018) 8:391. doi: 10.3389/fcimb.2018.00391

15. Burdette DL, Vance RE. STING and the innate immune response to nucleic acids in the cytosol. *Nat Immunol* (2013) 14:19–26. doi: 10.1038/ni.2491

16. Sun L, Wu J, Du F, Chen X, Chen ZJ. Cyclic GMP-AMP synthase is a cytosolic DNA sensor that activates the type I interferon pathway. *Sci (80-)* (2013) 339:786–91. doi: 10.1126/science.1232458

17. Wu J, Sun L, Chen X, Du F, Shi H, Chen C, et al. Cyclic GMP-AMP is an endogenous second messenger in innate immune signaling by cytosolic DNA. *Sci (80-)* (2013) 339:826–30. doi: 10.1126/science.1229963

18. Ahn J, Barber GN. STING signaling and host defense against microbial infection. *Exp Mol Med* (2019) 51:1–10. doi: 10.1038/s12276-019-0333-0

19. Ishikawa H, Ma Z, Barber GN. STING regulates intracellular DNA-mediated, type i interferon-dependent innate immunity. *Nature* (2009) 461:788–92. doi: 10.1038/nature08476

20. Louie A, Bhandula V, Portnoy DA. Secretion of c-di-AMP by listeria monocytogenes leads to a STING-dependent antibacterial response during enterocolitis. *Infect Immun* (2020) 88:e00407–20. doi: 10.1128/IAI.00407-20

21. Wang P, Li S, Zhao Y, Zhang B, Li Y, Liu S, et al. The GRA15 protein from toxoplasma gondii enhances host defense responses by activating the interferon stimulator STING. *J Biol Chem* (2019) 294:16494–508. doi: 10.1074/jbc.RA119.009172

22. Koppe U, Högner K, Doehn J-M, Müller HC, Witzenrath M, Gutbier B, et al. Streptococcus pneumoniae stimulates a STING- and IFN regulatory factor 3-dependent type I IFN production in macrophages, which regulates RANTES production in macrophages, cocultured alveolar epithelial cells, and mouse lungs. *J Immunol* (2012) 188:811–7. doi: 10.4049/jimmunol.1004143

23. Lu C, Zhang X, Ma C, Xu W, Gan L, Cui J, et al. Nontypeable haemophilus influenzae DNA stimulates type I interferon expression *via* STING signaling pathway. *Biochim Biophys Acta - Mol Cell Res* (2018) 1865:665–73. doi: 10.1016/j.bbamcr.2018.01.011

24. Yamamoto K, Ferrari JD, Cao Y, Ramirez MI, Jones MR, Quinton LJ, et al. Type I alveolar epithelial cells mount innate immune responses during pneumococcal pneumonia. *J Immunol* (2012) 189:2450–9. doi: 10.4049/jimmunol.1200634

25. Costa Franco MM, Marim F, Guimarães ES, Assis NRG, Cerqueira DM, Alves-Silva J, et al. Brucella abortus triggers a cGAS-independent STING pathway to induce host protection that involves guanylate-binding proteins and inflammasome activation. *J Immunol* (2018) 200:607–22. doi: 10.4049/jimmunol.1700725

26. Ishikawa H, Barber GN. STING is an endoplasmic reticulum adaptor that facilitates innate immune signalling. *Nature* (2008) 455:674–8. doi: 10.1038/nature07317

27. Gao D, Wu J, Wu YT, Du F, Aroh C, Yan N, et al. Cyclic GMP-AMP synthase is an innate immune sensor of HIV and other retroviruses. *Sci (80-)* (2013) 341:903–6. doi: 10.1126/science.1240933

28. Revelli DA, Boylan JA, Gherardini FC. A non-invasive intratracheal inoculation method for the study of pulmonary melioidosis. *Front Cell Infect Microbiol* (2012) 2:164. doi: 10.3389/fcimb.2012.00164

29. Hielpos MS, Ferrero MC, Fernández AG, Falivene J, Vanzulli S, Comerci DJ, et al. Btp proteins from brucella abortus modulate the lung innate immune response to infection by the respiratory route. *Front Immunol* (2017) 8:1011. doi: 10.3389/fimmu.2017.01011

30. Campos PC, Gomes MTR, Marinho FAV, Guimarães ES, de Moura Lodi Cruz MGF, Oliveira SC. Brucella abortus nitric oxide metabolite regulates inflammasome activation and IL-1β secretion in murine macrophages. *Eur J Immunol* (2019) 49:1023–37. doi: 10.1002/EJI.201848016

31. Keesha M. Matz R, Marena Guzman AGG. The role of nucleic acid sensing in controlling microbial and autoimmune disorders. *Int Rev Cell Mol Biol* (2019) 345:35–136. doi: 10.1016/bs.ircmb.2018.08.002

32. Saiga H, Kitada S, Shimada Y, Kamiyama N, Okuyama M, Makino M, et al. Critical role of AIM2 in mycobacterium tuberculosis infection. *Int Immunol* (2012) 24:637–44. doi: 10.1093/intimm/dxs062

33. Barber GN. STING: infection, inflammation and cancer. *Nat Rev Immunol* (2015) 15:760–70. doi: 10.1038/nri3921

34. Gomes MTR, Guimarães ES, Marinho FV, Macedo I, Aguiar ERGR, Barber GN, et al. STING regulates metabolic reprogramming in macrophages *via* HIF-1α during brucella infection. *PloS Pathog* (2021) 17:e1009597. doi: 10.1371/journal.ppat.1009597

35. Ruiz-Moreno JS, Hamann L, Shah JA, Verbon A, Mockenhaupt FP, Puzianowska-Kuznicka M, et al. The common HAQ STING variant impairs cGAS-dependent antibacterial responses and is associated with susceptibility to legionnaires' disease in humans. *PloS Pathog* (2018) 14:1–22. doi: 10.1371/journal.ppat.1006829

36. Collins AC, Cai H, Li T, Franco LH, Li XD, Nair VR, et al. Cyclic GMP-AMP synthase is an innate immune DNA sensor for mycobacterium tuberculosis. *Cell Host Microbe* (2015) 17:820–8. doi: 10.1016/j.chom.2015.05.005

37. Marinho FV, Benmerzoug S, Oliveira SC, Ryffel B, Quesniaux VFJ. The emerging roles of STING in bacterial infections. *Trends Microbiol* (2017) 25:906–18. doi: 10.1016/j.tim.2017.05.008

38. Boxx GM, Cheng G. The roles of type i interferon in bacterial infection. *Cell Host Microbe* (2016) 19:760–9. doi: 10.1016/j.chom.2016.05.016

39. Meunier E, Wallet P, Dreier RF, Costanzo S, Anton L, Rühl S, et al. Guanylate-binding proteins promote activation of the AIM2 inflammasome during infection with francisella novicida. *Nat Immunol* (2015) 16:476–84. doi: 10.1038/ni.3119

40. Auerbuch V, Brockstedt DG, Meyer-Morse N, O'Riordan M, Portnoy DA. Mice lacking the type I interferon receptor are resistant to listeria monocytogenes. *J Exp Med* (2004) 200:527–33. doi: 10.1084/jem.20040976

41. Sauer JD, Sotelo-Troha K, Von Moltke J, Monroe KM, Rae CS, Brubaker SW, et al. The n-ethyl-N-nitrosourea-induced goldenticket mouse mutant reveals an essential function of sting in the *in vivo* interferon response to listeria monocytogenes and cyclic dinucleotides. *Infect Immun* (2011) 79:688–94. doi: 10.1128/IAI.00999-10

42. Marinho FV, Benmerzoug S, Rose S, Campos PC, Marques JT, Báfica A, et al. The cGAS/STING pathway is important for dendritic cell activation but is not essential to induce protective immunity against mycobacterium tuberculosis infection. *J Innate Immun* (2018) 10:239–52. doi: 10.1159/000488952

43. Khan M, Harms JS, Liu Y, Eickhoff J, Tan JW, Hu T, et al. Brucella suppress STING expression *via* miR- 24 to enhance infection. *PloS Pathog* (2020) 16:1–21. doi: 10.1371/journal.ppat.1009020

44. Guimarães ES, Gomes MTR, Campos PC, Mansur DS, dos Santos AA, Harms J, et al. Brucella abortus cyclic dinucleotides trigger STING-dependent unfolded protein response that favors bacterial replication. *J Immunol* (2019) 202:2671–81. doi: 10.4049/JIMMUNOL.1801233

45. Alphonse N, Dickenson RE, Odendall C. Interferons : tug of war between bacteria and their host. *Front Cell Infect Microbiol* (2021) 11:624094. doi: 10.3389/fcimb.2021.624094

46. de Almeida LA, Carvalho NB, Oliveira FS, Lacerda TLS, Vasconcelos AC, Nogueira L, et al. MyD88 and STING signaling pathways are required for IRF3-mediated IFN-β induction in response to brucella abortus infection. *PloS One* (2011) 6: e23135. doi: 10.1371/journal.pone.0023135

47. Roux CM, Rolán HG, Santos RL, Beremand PD, Thomas TL, Adams LG, et al. Brucella requires a functional type IV secretion system to elicit innate immune responses in mice. *Cell Microbiol* (2007) 9:1851–69. doi: 10.1111/j.1462-5822.2007.00922.x

frontiers | Frontiers in Immunology

Check for updates

Leishmania braziliensis exosomes activate human macrophages to produce proinflammatory mediators

Fabio C. Peixoto[1,2]*, Dalila L. Zanette[3], Thiago M. Cardoso[1], Mauricio T. Nascimento[1,2], Rodrigo C. O. Sanches[4], Mateus Aoki[3], Phillip Scott[5], Sérgio C. Oliveira[6,7], Edgar M. Carvalho[1,2,7] and Lucas P. Carvalho[1,2,7]*

[1]Laboratório de Pesquisas Clínicas (LAPEC), Instituto Gonçalo Moniz (IGM), Oswaldo Cruz Foundation (FIOCRUZ), Salvador, Bahia, Brazil, [2]Programa de Pós Graduação em Ciências da Saúde, Universidade Federal da Bahia, UFBA, Salvador, Bahia, Brazil, [3]Laboratory for Applied Science and Technology in Health, Instituto Carlos Chagas – Oswaldo Cruz Foundation (FIOCRUZ) Paraná (ICC), Curitiba, Paraná, Brazil, [4]Departamento de Bioquímica e Imunologia, Universidade Federal de Minas Gerais, Belo Horizonte, Minas Gerais, Brazil, [5]University of Pennsylvania, School of Veterinary Medicine, Philadelphia, PA, United States, [6]Departamento de Imunologia, Instituto de Ciencias Biomédicas, Universidade de São Paulo, São Paulo, Brazil, [7]Instituto Nacional de Ciências e Tecnologia-Doenças Tropicais, Salvador, Brazil

Exosomes, organelles measuring 30-200nm, are secreted by various cell types. *Leishmania* exosomes consist of many proteins, including heat shock proteins, annexins, Glycoprotein 63, proteins exerting signaling activity and those containing mRNA and miRNA. Studies have demonstrated that *Leishmania donovani* exosomes downregulate IFN-γ and inhibit the expression of microbicidal molecules, such as TNF and nitric oxide, thus creating a microenvironment favoring parasite proliferation. Despite lacking immunological memory, data in the literature suggest that, following initial stimulation, mononuclear phagocytes may become "trained" to respond more effectively to subsequent stimuli. Here we characterized the effects of macrophage sensitization using *L. braziliensis* exosomes prior to infection by the same pathogen. Human macrophages were stimulated with *L. braziliensis* exosomes and then infected with *L. braziliensis*. Higher levels of IL-1β and IL-6 were detected in cultures sensitized prior to infection compared to unstimulated infected cells. Moreover, stimulation with *L. braziliensis* exosomes induced macrophage production of IL-1β, IL-6, IL-10 and TNF. Inhibition of exosome secretion by *L. braziliensis* prior to macrophage infection reduced cytokine production and produced lower infection rates than untreated infected cells. Exosome stimulation also induced the consumption/regulation of NLRP3 inflammasome components in macrophages, while the blockade of NLRP3 resulted in lower levels of IL-6 and IL-1β. Our results suggest that *L. braziliensis* exosomes stimulate macrophages, leading to an exacerbated inflammatory state that may be NLRP3-dependent.

Introduction

Cutaneous leishmaniasis (CL), due to *L. braziliensis* infection, is characterized by the presence of few or rare parasites, a predominance of lymphocytes and mononuclear phagocytes in the inflammatory infiltrate (1). Host immunological factors are known to play an important role in the pathogenesis of this disease. Mononuclear cells from CL patients stimulated with soluble *Leishmania* antigen (SLA) produce exacerbated amounts of IFN-γ and TNF, as well as low levels of IL-10 in culture (2). While the production of IFN-γ is important for parasite killing, high levels of TNF have been associated with tissue damage and lesion development (2, 3). Studies on lesion tissue samples have confirmed the contribution of inflammation to ulcer development, as evidenced by the presence of Granzyme B produced by CD8+ and NK cells, in addition to metalloproteinases and inflammatory cytokines (4–11). Moreover, *Leishmania braziliensis*-infected mononuclear phagocytes have been shown to produce high levels of reactive oxygen species (ROS), molecules with leishmanicidal properties that have also been associated with tissue damage (12, 13).

An important role of IL-1β in CL pathogenesis has been documented in recent years, with the use of IL-1β inhibitors shown to improve the course of disease in murine models (8, 12). In humans, IL-1β concentrations were found to correlate with lesion size, and previous research by our group has documented elevated expression of the NLRP3 inflammasome in monocytes obtained from the peripheral blood of CL patients, in addition to high levels of IL-1β in cultured peripheral blood mononuclear cells (PBMC) stimulated with SLA (8, 14). Moreover, NLRP3$^{-/-}$ BALB/c mice infected with *L. major* demonstrated a greater ability to control *Leishmania* infection when compared to wild-type mice (15).

Leishmania, and its soluble products, can trigger immune responses in innate immune cells prior to the onset of mononuclear cellular infection (13, 16, 17). For instance, *Leishmania* lipophosphoglycan (LPG) and DNA can induce the production of inflammatory mediators by mononuclear phagocytes through the activation of toll-like receptors (TLR) 2, 4 and 9 (18–20). Pathogen molecules are often secreted via extracellular vesicles (EV), also known as exosomes.

Exosomes, organelles ranging in size from 30-200nm, are secreted by various cell types. The invagination of regions of the endosomal membrane results in the formation of multivesicular bodies (MVB); the fusion of MVBs with the plasm membrane leads to exosome secretion (21, 22). These vesicles play a major role in molecular trafficking, e.g., proteins and nucleic acids, which once delivered may modulate host macrophage function (23–29). For example, glycoprotein (gp) 63-containing *Leishmania* exosomes was shown to induce TNF production by macrophages and exacerbate pathology in a CL mouse model (28, 30–32).

The present study aimed to assess the effects of *L. braziliensis* exosomes on human macrophagic responses, revealing that these vesicles induce both IL-1β and IL-6 production. Moreover, the pre-exposure of macrophages to *L. braziliensis* exosomes was found to prime these cells to enhance the production of pro-inflammatory mediators in response to *L. braziliensis* infection, potentially contributing to the pathogenesis of disease.

Methods

Parasite culture

An *L. braziliensis* isolate (MHOM/BR/LTCP11245) previously obtained from a CL patient's skin lesion was initially cultivated in biphasic medium (NNN). After isolation, parasites were identified by multilocus enzyme electrophoresis and cryopreserved in liquid nitrogen. Following selection, parasites were expanded and cultivated in Schneider's culture medium (SIGMA) supplemented with 20% inactive fetal bovine serum (FBS) (GIBCO), 1% L-glutamine and antibiotics.

L. braziliensis exosome isolation and characterization

L. braziliensis promastigotes were cultured at 37°C under 5% CO_2 for 4 hours to optimize protein and vesicle secretion (31). Supernatants collected from *in vitro* cultures were centrifuged (2500rpm) and filtered (0.22 μm), after which exosomes were isolated through sequential ultracentrifugation (10 x 10^{5}g). The EV particle-size distribution was determined by diffraction analysis using a NS300 particle-size tracker and Nanosight NTA 3.0 software using light scatter mode (Malvern Instruments Ltd., Technologies, Malvern, UK) (Figure 1) (33–35).

Isolation and culturing of peripheral blood mononuclear cells

Peripheral blood mononuclear cells (PBMC) were obtained from heparinized venous blood from healthy subjects by Ficoll-paque density gradient centrifugation (GE Healthcare). Cells were washed twice in saline, and monocytes were isolated from PBMCs using magnetic beads in accordance with the manufacturer's protocol (Dynabeads untouched human monocytes; Invitrogen Dynal AS, Oslo, Norway). This process was performed twice, after which cells were washed in phosphate-buffered saline (PBS), then adjusted to the desired concentration, and resuspended in RPMI 1640 (GIBCO BRL., Grand Island, NY USA) supplemented with 10% FBS (GIBCO BRL., Grand Island, NY USA) and antibiotics. Monocytes were then allowed to adhere to polystyrene culture plates and incubated for 6 days at 37°C under 5% CO_2 until differentiation into macrophages, as previously described (36).

Macrophage infection with L. braziliensis after stimulation with L. braziliensis soluble factors

Monocyte-derived macrophages (3 x 10^5) were stimulated, using a transwell membrane, with soluble factors from *L. braziliensis* for 24 hours at 37 °C, 5% CO_2 in RPMI (Figure 2A). Following stimulation, cells were washed twice in saline and
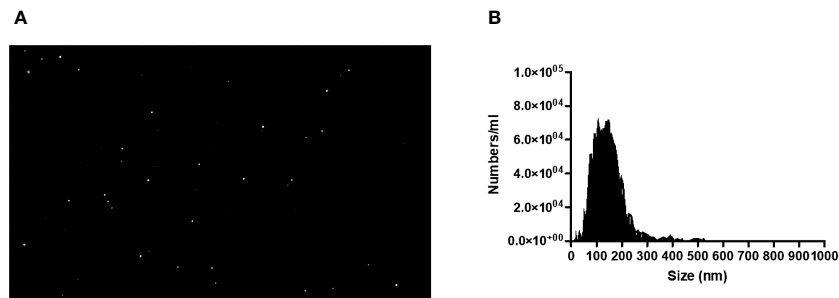
FIGURE 1
(A) Image of *L. Braziliensis* exosomes taken by a NS300 particle-sike tracker and Nanosight NTA 3.0 software using light scatter mode. **(B)** Quantification and Characterization of extracellular vesicles extracted from isolates of *L. braziliensis*.

infected or not with *L. braziliensis* (MOI 5:1) for 2 hours. Next, the remaining promastigotes were washed out, and cells were reincubated for another 24 hours at 37 °C, 5% CO_2 in RPMI. The slides were subsequently submitted to panoptic staining for posterior quantification of infected macrophages and amastigotes per 100 cells via optical microscopy.

Exosome stimulation and macrophage infection with L. braziliensis

Monocyte-derived macrophages ($3x10^5$) were stimulated with exosomes from *L. braziliensis* (300 vesicles/macrophage) for 24 hours at 37°C under 5% CO_2 in RPMI. After stimulation, cells were washed twice in saline and infected or not with *L. braziliensis* (MOI 5:1) for 2 hours. The remaining promastigotes were washed out,

then cells were incubated for another 24 hours (37 °C, 5% CO_2) in RPMI.

Parasite treatment with GW4869

For some experiments involving the inhibition of exosome/vesicle generation, $1x10^7$ *Leishmania*/mL were treated with GW4869 (20ng/ml), a vesicle generation inhibitor, (https://www.sigmaaldrich.com/BR/pt/product/sigma/d1692) for 30 minutes at room temperature, then washed three times to prevent contact between the inhibitor and human cells during stimulation/infection protocols. To assess GW4869 toxicity against *Leishmania* parasites, we evaluated *L. braziliensis* viability after treatment with GW4869 using propidium iodide as cell death marker, by flow cytometry.
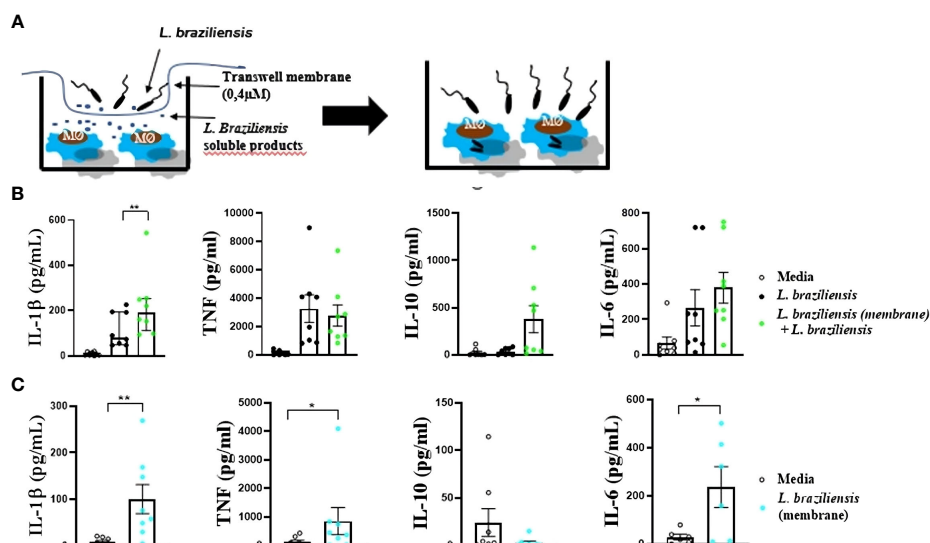
FIGURE 2
Macrophages from HS infected with *L. braziliensis* after sensitization with *L. braziliensis* through a transwell membrane (0,4μm). **(A)** Stimulation strategy. **(B)** Cytokine production by macrophages sensitized with soluble factors and infected with *L. braziliensis*. **(C)** Cytokine production by macrophages from HS sensitized with soluble factors from *L. braziliensis*. Levels of IL-1β, TNF, IL-10 and IL-6 were determined in culture supernatants by LUMINEX. Statistical analyses were performed using the Wilcoxon rank test *p<.05, **p<.01.

Macrophage treatment with glibenclamide

For the blockade of the NLRP3 inflammasome, monocyte-derived macrophages (3×10^5) were first treated with the NLRP3 inhibitor glibenclamide (100μM) for 2 hours, then stimulated with L. braziliensis exosomes (300:1) for 24 hours. Cells were then washed twice and infected or not with L. braziliensis (MOI 5:1) for 2 hours, washed again to remove any remaining promastigotes, and finally incubated for 24 hours at 37 °C under 5% CO_2in RPMI. Unstimulated macrophages and untreated stimulated cells were used as controls.

Infection rate assessment

To evaluate infection rate, 3×10^5 macrophages/well were plated on Nunc® Labtek® plates and stimulated with exosomes from *L. braziliensis* (300 vesicles/macrophage), then incubated for 24 hours at 37° C with 5% CO_2. Cells were then washed twice and infected or not with *L. braziliensis* (MOI 5:1) for 2 hours, washed again to remove any remaining promastigotes, and finally incubated for 24 hours at 37 °C under 5% CO_2 in RPMI. The slides were submitted to panoptic staining for the later quantification of infected macrophages and the number of amastigotes per 100 cells, performed via optical microscopy.

Cytokine quantification

Following stimulation and/or infection protocols, the supernatants from cultures were collected for cytokine (IL-1β, TNF, IL-6 and IL-10) quantification via Luminex (Bio-Plex Pro Human Cytokine 27-plex Assay) or ELISA.

Flow cytometry

Monocyte-derived macrophages from healthy subjects were stimulated with *L. braziliensis* exosomes for 24 hours and infected or not with *L. braziliensis* for another 24 hours, as described above. After the final incubation, cells were collected and placed in 5mL polystyrene FACS tubes (BD Biosciences Falcon™ 352052) for cell labeling with conjugated antibodies αCD14 (APC) and αHLA-DR (PerCP) to determine cell populations of interest, as well as αNLRP3 (PE). Events were acquired on a flow cytometer (BD LSRFortessa™ Cell analyzer) and data were analyzed using Flowjo® software.

Oxidative burst essay

To evaluate reactive oxygen species (ROS) production, macrophages were stimulated as described in "Exosome Stimulation and Macrophage infection with *L. braziliensis*" section, then treated with dihydrorhodamine-123 at 10ng/mL

(Cayman Chemical Company) for 10 minutes. Cells were subsequently labeled with αHLA-DR and αCD14 to evaluate fluorescence intensity by flow cytometry, with data analysis performed via FlowJo® software.

RNA extraction, NF-κB and TLR2 gene expression

Cells stimulated with exosomes and infected or not with *L. braziliensis*, followed by incubation at 37°C under 5% CO_2 for 2 hours, were harvested in TRIzol Reagent (Invitrogen). RNA extraction was performed using TRIzol RNA isolation, according to manufacturer's instructions. RNA concentration and integrity were determined by spectrophotometric optical density measurements (260 and 280 nm). Gene expression was analyzed performed as previously described (37).

Mouse macrophage cultures and infection

C57BL/6 mice, both wild-type and others genetically deficient for NLRP3$^{-/-}$, were obtained as previously described (38). All animals were maintained at the UFMG Animal Facility and used for experimentation at 6–8 weeks of age. Bone marrow-derived macrophages (BMDM) were prepared and infected as previously described (39, 40). Briefly, bone marrow cells were isolated from the femurs and tibias of the animals, cultured in RPMI 1640 supplemented with 30% L929 cell-conditioned medium and 20% FBS for 7 days. BMDM (0.5×10^6) were treated or not with lipopolysaccharide (LPS) for 6 hours (500 ng/ml) and stimulated or not with *L. braziliensis* exosomes (300:1), followed by infection with stationary phase *Leishmania braziliensis* (MOI 10:1) for 24 hours. After 48 hours, supernatants were harvested and IL-1β, TNF and IL-6 concentrations were detected by ELISA.

Statistical analysis

Statistical analysis was performed using the Wilcoxon test for paired variables and Mann-Whitney rank test for unpaired measurements (*$p<0.05$, **$p<0.01$, ***$p<0.001$, ****$p<0.0001$). All experimental data were analyzed using Prism GraphPad® 8.0.2, which was also used for graphical data representations.

Results

L. braziliensis soluble factors induce pro-inflammatory mediator production in human macrophages

Macrophages can be "trained" to enhance response to infection (41). For instance, macrophages exposed to *Saccharomyces cerevisiae* demonstrated an increased ability to produce TNF in

response to TLR ligands, such as LPS (42). To investigate whether soluble factors from *L. braziliensis* would interfere in cytokine production, human macrophages were cultured with *L. braziliensis* separated by a membrane, which allowed only soluble factors/small molecules to cross the barrier. Macrophages exposed to *L. braziliensis* products through the membrane produced more IL-1β upon infection than those that were not previously exposed to parasite factors (Figure 2B). Moreover, exposure to *L. braziliensis* soluble factors was also shown to induce the production of inflammatory mediators TNF, IL-6 and IL-1β by uninfected macrophages (Figure 2C). This data provides evidence that exposure to *L. braziliensis* modulates immune response prior to the establishment of cellular infection.

L. braziliensis exosomes induce pro-inflammatory mediator production by human macrophages

We first investigated whether *L. braziliensis* exosomes induced an inflammatory response in macrophages, and then assessed the effects of stimulating macrophages with these vesicles prior to infection with *L. braziliensis*. Compared to unstimulated cells, macrophages stimulation with EVs were found to induce IL-1β, TNF, IL-10 and IL-6 production (Figure 3). Pre-sensitization of macrophages with exosomes prior to infection was shown to increase IL-1β and IL-6 levels (Figure 3). Similarly, pre-sensitization with exosomes produced no influence on infection rate, nor the number of parasites internalized (data not shown).

Blockade of L. braziliensis exosome generation inhibits Leishmania-induced cytokine production by human macrophages

To further ascertain the role of exosomes in inducing inflammatory cytokine production, we infected human macrophages with *L. braziliensis* previously treated with GW4869, and then compared cytokine expression with other untreated *Leishmania*-infected cells. As in the experiments above, our data shows that cells infected with exosome-free *L. braziliensis* produced significantly less IL-1β, TNF, IL-10 and IL-6 upon infection

(Figure 4A). Although no differences were observed in parasite internalization by macrophages pre-sensitized with exosomes compared to unstimulated cells (data not shown), the cells infected with exosome-free *L. braziliensis* presented less infectivity, as evidenced by fewer numbers of infected macrophages and lower numbers of amastigotes within the cells (Figure 4B). As treatment with GW4869 could have interfered with *L. braziliensis* survival, we performed a dose-response curve with different GW4869 concentrations. Our experiments show no toxicity of GW4869 over *L. braziliensis* (Figure 4C).

L. braziliensis exosomes induce NLRP3 consumption/regulation

Most of the data presented in this study demonstrate the important association between *L. braziliensis* exosomes and IL-1β production. Consequently, the participation of NLRP3 in IL-1β production was investigated by evaluating both the expression of NLRP3 protein by cultured macrophages (Figure 5A) and the production of cytokines by cells stimulated with exosomes after the blockade of NLRP3 through glibenclamide treatment (Figure 5B). Our results indicate lower NLRP3 protein expression in cells stimulated with exosomes for 24 hours compared to basal level cells, while exosome stimulation in macrophages prior to infection induced more consumption, and probably further expression regulation, of this inflammasome than unsensitized cells (Figure 5A), which corroborates our previous results. Moreover, glibenclamide-treated cells were found to secrete less IL-1β, TNF, IL-6 and IL-10 than untreated cells, regardless of *L. braziliensis* infection or exosome stimulation. (Figure 5B), which suggests that cytokine expression induced by exosome stimulation is dependent on NLRP3.

BMDM from NLRP3⁻/⁻ C57BL/6 mice exhibit inhibited IL-1ß production following. braziliensis infection

The secretion of IL-1β may be dependent on inflammasome activation (8, 14, 39). NLRP3, the main inflammasome receptor responsible for inducing IL-1β production, forms a complex with ASC and Caspase-1 for the processing and secretion of IL-1β and
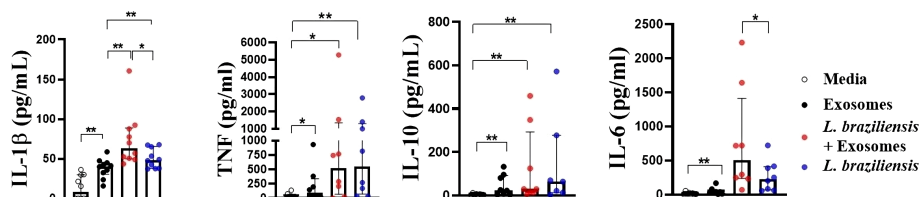
FIGURE 3
Cytokine production by macrophages from HS sensitized with *L. braziliensis* exosomes and infected with *L. braziliensis*. Macrophages from HS (n=8) were stimulated with exosomes isolated from *L. braziliensis* (300:1) for 24 hours and afterwards infected or not with *L. braziliensis* for another 24 hours. Levels of IL-1β, TNF, IL-10 and IL-6 were determined in culture supernatants by LUMNEX. Statistical analyses were performed using the Wilcoxon rank test *p<.05, **p<.01.
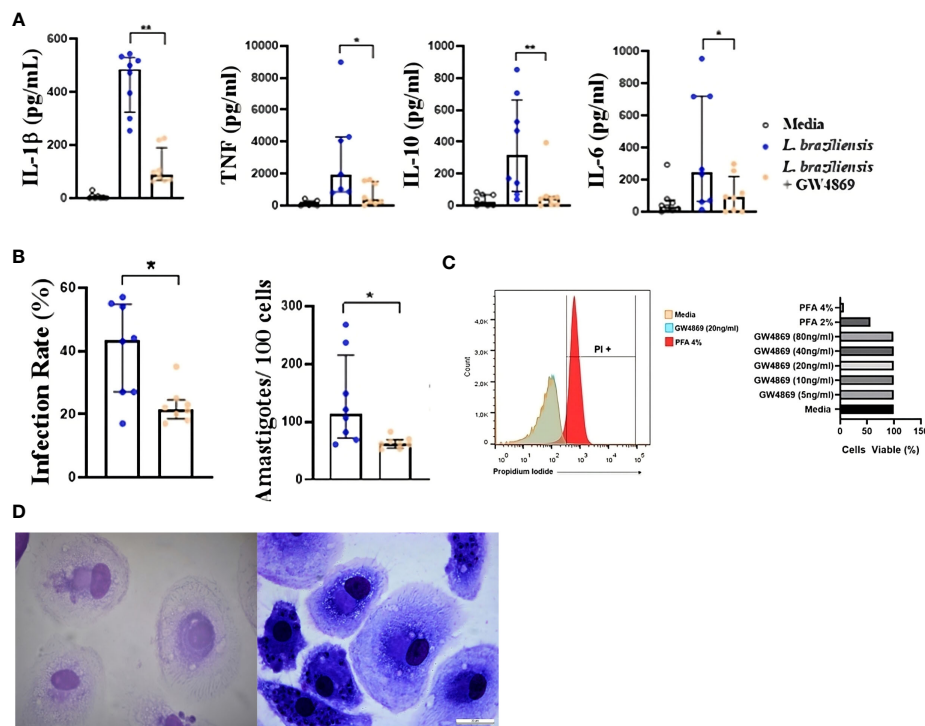
FIGURE 4

(A) Cytokine production and **(B)** Infection rate of macrophages from HS infected with *L. braziliensis* with exosome production inhibited. Axenic culture of *L. braziliensis* promastigotes was treated with GW4869 (20ng/ml), exosome production inhibitor, for 2 hours. Macrophages from HS (n=8) were infected with GW4869 treated *L. braziliensis* (5:1) for 24 hours. **(C)** *L. braziliensis* viability after GW4869 treatment was assessed using propidium iodide as cell death marker, by flow cytometry. **(D)** optical microscopy picture of panoptic stained macrophages infected with *L. braziliensis* treated (left) or not (right) with GW4869. Levels of IL-1β, TNF, IL-10 and IL-6 were determined in culture supernatants by LUMNEX. The percentage of infected cells as well as the number of intracellular parasites were determined by microscopic evaluation after panoptic staining. Statistical analyses were performed using the Wilcoxon rank test *p<.05, **p<.01.

IL-18 ([43](#), [44](#)). Since our results showed that *L. braziliensis* exosome stimulation followed by infection induced high levels of IL-1β secretion by human macrophages, we decided to investigate whether NLRP3 activation is required to drive IL-1β production upon *L. braziliensis* infection in a murine model.

Bone marrow-derived macrophages (BMDM) from C57BL/6 WT mice and mice deficient for NLRP3 were infected with *L. braziliensis* after previous stimulation with *L. braziliensis* exosomes. Levels of IL-1β, IL-6 and TNF were quantified by ELISA in cell supernatants. IL-1β production in mice was found to be dependent on the NLRP3 inflammasome, as IL-1β production was completely abrogated in cells from NLRP3$^{-/-}$ mice, regardless of stimulation. However, NLRP3 did not appear to be involved in the production of the other cytokines evaluated, as levels did not differ between WT and NLRP3$^{-/-}$ mouse cells (Figure 6).

L. braziliensis exosomes induce ROS production by macrophages

Our group previously showed that reactive oxygen species (ROS) constitute a major endogenous factor in *Leishmania* killing ([13](#), [45](#)). Furthermore, TNF production is directly associated with ROS production through the activation of the NF-κB signaling

pathway. Therefore, to investigate the role of *L. braziliensis* exosomes on ROS production, ROS expression (Figure 7) was evaluated in macrophages stimulated with exosomes further infected with *L. braziliensis*. Our data show that while *L. braziliensis* exosomes induced ROS production by uninfected macrophages, pre-sensitization did not interfere in ROS production following *in vitro* macrophage infection (Figure 7).

Macrophages stimulated with L. braziliensis exosomes express high levels of NF-κB and toll-like receptor 2

Herein *L. braziliensis* exosomes were found to induce TNF and ROS production by human macrophages. It has been shown that NF-kB activation induces TNF production through the activation of TLRs 2-4 upon *L. braziliensis* infection ([18](#)). To determine the role of *L. braziliensis* exosomes in TLR2 and NFkB expression, human macrophages were stimulated with EVs for 2 hours and infected or not with *L. braziliensis* for another 2 hours. Uninfected macrophages stimulated with exosomes were found to induce higher expression of NF-κB and TLR2 (Figure 8), yet infected cells previously stimulated with EVs demonstrated increased TLR2 expression, yet no effect on NF-κB expression (Figure 8). No
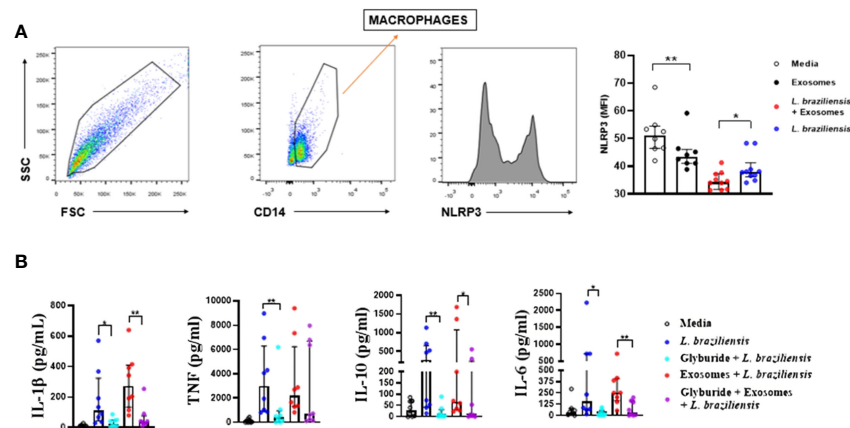
FIGURE 5

(A) Exosome stimulation enhance NLRP3 consumption by macrophages. Macrophages from healthy subjects (n=8) were sensitized with exosomes (300:1) for 24 hours and infected with *L. braziliensis* promastigotes for another 24 hours at a ratio of 5:1. Cells were stained with anti-CD14 and anti-NLRP3. Data were collected using flow cytometry and analyzed with FLOWJO® software. Representative gating strategy on CD14+ expression in macrophages from one healthy subject. NLRP3 MFI was taken from CD14+ population. The data represent the mean of fluorescence intensity (MFI) of NLRP3 expression by macrophages in the different stimulated groups. **(B)** Glyburide downmodulates exosome-induced cytokine production in macrophages from healthy subjects. Macrophages from 8 individuals were treated with glyburide (100µM) for 2 hours. Afterwards cells were stimulated for 24 hours with *L. braziliensis* exosomes and infected with the parasite for another 24 hours. Levels of IL-1β, TNF, IL-10, IL-10 and IL-6 were measured in culture supernatant by ELISA. Statistical analyses were performed using the Mann-Whitney test for unpaired groups and Wilcoxon rank test for paired measurements *p<.05 **p<.01.

differences were observed among the groups with regard to TLR4 expression. These data corroborate with our findings on exosome-induced TNF and ROS production, as these molecules are formed as a result of the NF-κB pathway.

Discussion

The initial events occurring upon *Leishmania* infection orchestrate immune response, constituting determinants in parasite proliferation and disease development. Among the factors contributing to disease expression, vector molecules, including salivary gland proteins, parasite-derived molecules and host immune response are of great importance (46, 47). On the

FIGURE 6

NLRP is key for *L. braziliensis* induced IL-1β production in mouse macrophages. BMDMs from wild-type C57BL/6 mices and deficient for NLRP3 were prepared, pulsed with LPS (500 ng/ml), stimulated with exosomes (300:1) and infected with *L. braziliensis* (MOI 10:1) or not. After 48 hours of culture ELISA for IL-1β was performed on supernatants. Statistical analyses were performed using the Mann-Whitney test and the Wilcoxon rank test. *p<0.05, **p<0.01.

parasite side, attention has been paid to the role of exosomes due to the close relationship between molecules present in the exosomes and their ability to modulate host immune response (28, 31, 32). The present study documented that *L. braziliensis* exosomes indeed modulate immune response by priming macrophages to produce more inflammatory molecules.

It has recently been suggested that macrophages could become "trained" to enhance infection response (41). For instance, macrophages exposed to *Saccharomyces cerevisiae* demonstrated an increased ability to produce TNF in response to TLR ligands, such as LPS. Moreover, monocytes "trained" with *S. cerevisiae* demonstrated heightened microbial activity (42). In the same vein, our results additionally indicate that *L. braziliensis* exosomes effectively "train" macrophages to produce higher cytokine concentrations in response to posterior *L. braziliensis* infection, suggesting that epigenetics in macrophages may play a role in subsequent exposure to *L. braziliensis* components.

Clearly, *Leishmania* vesicle contents vary across species, and thereby exert variable effects on host immune response. For instance, studies have shown that exosomes from *L. donovani* modulate monocyte response to IFN-γ and inhibit TNF while inducing IL-10 production. In this manner, mice stimulated with *L. donovani* exosomes prior to infection with the same species were found to exhibit higher macrophage infection rates within the spleen (26, 27). Also, stimulation with *L. major* exosomes prior to *L. major* parasite challenge produced a shift towards a Th2-type response in mice, as evidenced by a high frequency of CD4+ T cells producing IL-4, which led to disease exacerbation (27). Moreover, it was demonstrated that *L. major* exosomes contribute to CL pathology through the induction of an overproduction of inflammatory cytokines IL-23 and IL-17 in the lymph nodes of BALB/c mice (29).

FIGURE 7

Macrophagic stimulation with *L. braziliensis* exosomes enhance reactive oxygen species production. Macrophages from healthy subjects were evaluated after being stimulated with exosomes for 24 hours and infected with *L. braziliensis* for 24 hours (n=6) or not. The cells were treated with DHR (10ng/mL – 10 min) and stained with anti-CD14 and anti-HLA-DR. Data were collected using flow cytometry and analyzed by FLOWJO® software. **(A)** Representative gating strategy on CD14+ and HLA-DR+ expression in macrophages. DHR MFI were taken from CD14+ HLA-DR+ population. **(B)** The data represent the mean of fluorescence intensity (MFI) of oxidative burst production by macrophages stimulated with exosomes and infected with *L. braziliensis*. Statistical analyses were performed using the Wilcoxon rank test for paired measurements *p<.05.

The pathogenesis of *Leishmania* infection varies widely depending on the *Leishmania* species involved, and its specific effect on host immune response. In all cases, parasite control is associated with the expansion of CD4+ Th1 cells producing IFN-γ, which promotes the killing of parasites within infected cells (48). In some cases, the parasite evades the immune system silently, without inducing an immunological response, as is the case in infection by *L. donovani*. In *L. braziliensis* infection, however, an exaggerated Th1 response is observed, together with high levels of proinflammatory cytokines and a predominance of lymphocytes and mononuclear phagocytes at the lesion site. Herein we demonstrate that stimulation with *L. braziliensis* exosomes induces high levels of proinflammatory cytokines (TNF and IL-1β) as well as ROS, molecules known to be involved in CL due to *L. braziliensis* pathogenesis. In our experiments where we treated *L. braziliensis* with GW4869, a vesicle secretion inhibitor, we observed a decrease in cytokines production in infected macrophages. However, since GW4869 also decreased *L. braziliensis* internalization, further studies need to be performed to understand the mechanism by which *L. braziliensis* exosomes interfere in *Leishmania* uptake.

Some *Leishmania* species are known to inhibit several macrophage functions, such as macrophage activation, cytokine release and antigen presentation. For instance, down-regulation of class II MHC expression and the inability to produce IL-12 has been observed in several studies

(49–54). Also, TLR-induced up-regulation of co-stimulatory molecules, as well as TNF-alpha and IL-12 production, was notably impaired in *L. major*, *L. chagasi*, *L. donovani* and *L. mexicana*-infected macrophages, while in the case of *L. mexicana*, disruption of NF-κB signaling was observed (55, 56). In contrast, our results show that exosome sensitization increased the expression of NF-κB and TLR2, corroborating previously published data indicating that *L. braziliensis* infection promotes an inflammatory environment.

Inflammation is often associated with macrophage activation and intracellular parasite killing. Here we found that in spite of *L. braziliensis* exosomes enhancing IL-1b production by human macrophages, these vesicles have no effect on Leishmania parasite killing. These results are in accordance with our previous data showing no association between IL-1b production and L. brazileisns killing (8). Also, in our current results we found that exosomes do not increase the ability of macrophages to produce ROS in response to L. braziliensis infection, corroborating that these vesicles have no effect on L. braziliensis killing by macrophages. In the present study we found that the IL-1b production driven by *L. braziliensis* vesicles is NLPR3-dependent, corroborating our previous data involving *L. braziliensis*-infected macrophages (8). These findings favor the potential role of *L. braziliensis* EVs in the immunopathology observed in CL arising from *L. braziliensis*, in which ulcer development has been associated with an exaggerated inflammatory response that leads to tissue damage.
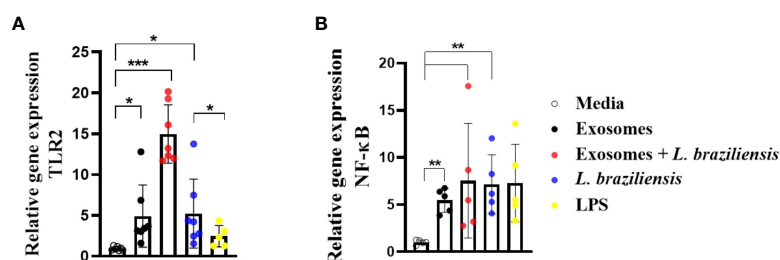
FIGURE 8

Macrophages stimulated with *L. braziliensis* exosomes express high levels of NF-κB and Toll-Like Receptor 2. **(A)** TLR2 and **(B)** NF-κ B gene expression, represented as $2^{-\Delta\Delta CT}$, following RT-PCR of RNA from macrophages-derived monocytes of HS (N=7) stimulated with exosomes for 24 hours and infected with *L. braziliensis* for 24 hours or not. Statistical analyses were performed using the Mann-Whitney test and the Wilcoxon rank test. *p<0.05, **p<0.01. ***p<0.001.

Previous results have shown that IL-1β concentrations in CL due to *L. braziliensis* correlate positively with lesion size and healing time (8, 12). It has been documented that *L. braziliensis* infection activates the NLRP3 inflammasome, thereby inducing ROS (8, 39). Therefore, the blockade of NLRP3 may constitute a sound therapeutic approach.

Considering the physiology and dynamics of vesicle secretion, studies involving *L. mexicana* demonstrated a substantial increase in vesicle secretion at a temperature of 37˚C (31). Herein we observed a similar phenomenon in *L. braziliensis*. The up-regulation in vesicle release induced at infection-like temperatures suggests that parasites release vesicles into the extracellular environment prior to invading host cells. Similarly, it has been suggested that *Leishmania* exosomes interact wi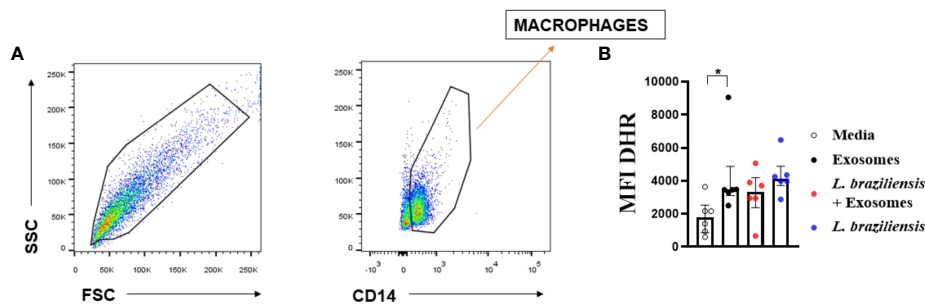th the host cell prior to the parasite itself, as evidenced by the presence of *Leishmania* molecules within uninfected macrophages (57). Moreover, as previous studies have shown that *Leishmania* secretes exosomes into the midgut of the sandfly vector, it has been hypothesized that these vesicles then become inoculated into the host alongside the parasite during sandfly blood-feeding, possibly enhancing the vesicle-induced effects of the parasite on immune response (29, 32). Although both *L. major* and *L. braziliensis* cause CL, the magnitude of inflammation caused by both parasite species is quite different, as infection with *L. braziliensis* induces higher inflammatory response in humans than *L. major*. Thus, further experiments need to be performed to determine differences in the contents of exosomes between both species.

In contrast to previously published data indicating the downregulatory effects of *L. donovoni* and *L. major* exosomes, *L. braziliensis* exosomes do not appear to contribute to a microenvironment favorable for parasite growth, but instead participate in an exacerbated pathologic inflammatory response, which may potentially exacerbate lesion development.

Data availability statement

The original contributions presented in the study are included in the article/supplementary materials. Further inquiries can be directed to the corresponding authors.

Ethics statement

The studies involving humans were approved by Institution Review Board of the Federal University of Bahia Medical School and the National Commission of Ethics in Research (CONEP) under the number 3.252.513. The studies were conducted in accordance with the local legislation and institutional requirements. The human samples used in this study were acquired from Peripheral blood was collected from healthy volunteers. Written informed consent for participation was not required from the participants or the participants' legal guardians/next of kin in accordance with the national legislation and institutional requirements. The animal study was approved by Institutional Animal Care and Use Committee of the Federal University of Minas Gerais (CEUA no. 165/2019). The study was conducted in accordance with the local legislation and institutional requirements.

Author contributions

FP: Conceptualization, Data curation, Formal Analysis, Investigation, Methodology, Writing – original draft, Writing – review & editing. DZ: Investigation, Methodology, Formal Analysis, Writing – review & editing. TC: Formal Analysis, Methodology, Writing – review & editing. MN: Investigation, Methodology, Writing – review & editing. RS: Methodology, Resources, Writing – review & editing. MA: Investigation, Writing – review & editing. PS: Funding acquisition, Resources, Visualization, Writing – review & editing. SO: Resources, Writing – review & editing. EC: Formal Analysis, Funding acquisition, Project administration, Resources, Supervision, Visualization, Writing – review & editing. LC: Conceptualization, Data curation, Formal Analysis, Funding acquisition, Investigation, Project administration, Resources, Supervision, Visualization, Writing – original draft, Writing – review & editing.

Conflict of interest

The authors declare that the research was conducted in the absence of any commercial or financial relationships that could be construed as a potential conflict of interest. The authors declared that they were an editorial board member of Frontiers, at the time of submission. This had no impact on the peer review process and the final decision.

Publisher's note

All claims expressed in this article are solely those of the authors and do not necessarily represent those of their affiliated organizations, or those of the publisher, the editors and the reviewers. Any product that may be evaluated in this article, or claim that may be made by its manufacturer, is not guaranteed or endorsed by the publisher.

References

1. Bittencourt AL, Barral A. Evaluation of the histopathological classifications of American cutaneous and mucocutaneous leishmaniasis. *Mem Inst Oswaldo Cruz* (1991) 86(1). doi: 10.1590/S0074-02761991000100009

2. Bacellar O, Lessa H, Schriefer A, MaChado P, De Jesus AR, Dutra WO, et al. Up-regulation of Th1-type responses in mucosal leishmaniasis patients. *Infect Immun* (2002) 70(12). doi: 10.1128/IAI.70.12.6734-6740.2002

3. Passos S, Carvalho LP, Costa RS, Campos TM, Novais FO, Magalhães A, et al. Intermediate monocytes contribute to pathologic immune response in leishmania Braziliensis infections. *J Infect Dis* (2015) 211(2). doi: 10.1093/infdis/jiu439

4. Amorim CF, Novais FO, Nguyen BT, Misic AM, Carvalho LP, Carvalho EM, et al. Variable gene expression and parasite load predict treatment outcome in cutaneous leishmaniasis. *Sci Transl Med* (2019) 11(519). doi: 10.1126/scitranslmed.aax4204

5. Saldanha MG, Pagliari C, Queiroz A, MaChado PRL, Carvalho L, Scott P, et al. Tissue damage in human cutaneous leishmaniasis: correlations between inflammatory cells and molecule expression. *Front Cell Infect Microbiol* (2020) 10. doi: 10.3389/fcimb.2020.00355

6. Campos TM, Passos ST, Novais FO, Beiting DP, Costa RS, Queiroz A, et al. Matrix metalloproteinase 9 production by monocytes is enhanced by TNF and participates in the pathology of human cutaneous leishmaniasis. *PloS Negl Trop Dis* (2014) 8(11). doi: 10.1371/journal.pntd.0003282

7. Campos TM, Novais FO, Saldanha M, Costa R, Lordelo M, Celestino D, et al. Granzyme B produced by natural killer cells enhances inflammatory response and contributes to the immunopathology of cutaneous leishmaniasis. *J Infect Dis* (2020) 221 (6). doi: 10.1093/infdis/jiz538

8. Santos D, Campos TM, Saldanha M, Oliveira SC, Nascimento M, Zamboni DS, et al. IL-1β Production by intermediate monocytes is associated with immunopathology in cutaneous leishmaniasis. *J Invest Dermatol* (2018) 138(5). doi: 10.1016/j.jid.2017.11.029

9. Novais FO, Carvalho LP, Graff JW, Beiting DP, Ruthel G, Roos DS, et al. Cytotoxic T cells mediate pathology and metastasis in cutaneous leishmaniasis. *PloS Pathog* (2013) 9(7). doi: 10.1371/journal.ppat.1003504

10. Novais FO, Scott P. CD8+ T cells in cutaneous leishmaniasis: the good, the bad, and the ugly. *Semin Immunopathology* (2015) 37. doi: 10.1007/s00281-015-0475-7

11. Santos CDS, Boaventura V, Ribeiro Cardoso C, Tavares N, Lordelo MJ, Noronha A, et al. CD8+ granzyme B+ -mediated tissue injury vs. CD4 + IFNγ+ -mediated parasite killing in human cutaneous leishmaniasis. *J Invest Dermatol* (2013) 133(6). doi: 10.1038/jid.2013.4

12. Novais FO, Carvalho AM, Clark ML, Carvalho LP, Beiting DP, Brodsky IE, et al. CD8+T cell cytotoxicity mediates pathology in the skin by inflammasome activation and IL-1β production. *PloS Pathog* (2017) 13(2). doi: 10.1371/journal.ppat.1006196

13. Carneiro PP, Conceição J, Macedo M, Magalhães V, Carvalho EM, Bacellar O. The role of nitric oxide and reactive oxygen species in the killing of Leishmania Braziliensis by monocytes from patients with cutaneous leishmaniasis. *PloS One* (2016) 11(2). doi: 10.1371/journal.pone.0148084

14. Carvalho AM, Novais FO, Paixão CS, de Oliveira CI, MaChado PRL, Carvalho LP, et al. Glyburide, a NLRP3 inhibitor, decreases inflammatory response and is a candidate to reduce pathology in leishmania Braziliensis infection. *J Invest Dermatol* (2020) 140(1). doi: 10.1016/j.jid.2019.05.025

15. Gurung P, Karki R, Vogel P, Watanabe M, Bix M, Lamkanfi M, et al. An NLRP3 inflammasome'triggered Th2-biased adaptive immune response promotes leishmaniasis. *J Clin Invest* (2015) 125(3):1329–38. doi: 10.1172/JCI79526

16. Carvalho LP, Pearce EJ, Scott P. Functional dichotomy of dendritic cells following interaction with leishmania braziliensis: Infected cells produce high levels of TNF-α, whereas bystander dendritic cells are activated to promote T cell responses. *J Immunol* (2008) 181(9). doi: 10.4049/jimmunol.181.9.6473

17. Becker I, Salaiza N, Aguirre M, Delgado J, Carrillo-Carrasco N, Kobeh LG, et al. Leishmania lipophosphoglycan (LPG) activates NK cells through toll-like receptor-2. *Mol Biochem Parasitol* (2003) 130(2). doi: 10.1016/S0166-6851(03)00160-9

18. Carneiro PP, Dórea AS, Oliveira WN, Guimarães LH, Brodskyn C, Carvalho EM, et al. Blockade of TLR2 and TLR4 attenuates inflammatory response and parasite load in cutaneous leishmaniasis. *Front Immunol* (2021) 12. doi: 10.3389/fimmu.2021.706510

19. Carvalho LP, Petritus PM, Trochtenberg AL, Zaph C, Hill DA, Artis D, et al. Lymph Node Hypertrophy following Leishmania major Infection Is Dependent on TLR9. *J Immunol* (2012) 188(3). doi: 10.4049/jimmunol.1101018

20. Sacramento LA, da Costa JL, de Lima MHF, Sampaio PA, Almeida RP, Cunha FQ, et al. Toll-like receptor 2 is required for inflammatory process development during Leishmania infantum infection. *Front Microbiol* (2017) 8(FEB). doi: 10.3389/fmicb.2017.00262

21. Bobrie A, Colombo M, Raposo G, Théry C. Exosome secretion: molecular mechanisms and roles in immune responses. *Traffic* (2011) 12. doi: 10.1111/j.1600-0854.2011.01225.x

22. Théry C, Zitvogel L, Amigorena S. Exosomes: Composition, biogenesis and function. *Nat Rev Immunol* (2002) 2. doi: 10.1038/nri855

23. Théry C, Ostrowski M, Segura E. Membrane vesicles as conveyors of immune responses. *Nat Rev Immunol* (2009) 9. doi: 10.1038/nri2567

24. Raposo G, Stoorvogel W. Extracellular vesicles: Exosomes, microvesicles, and friends. *J Cell Biol* (2013) 200. doi: 10.1083/jcb.201211138

25. Tkach M, Théry C. Communication by extracellular vesicles: where we are and where we need to go. (2016) *Cellpress* 164:Cell. doi: 10.1016/j.cell.2016.01.043

26. Silverman JM, Clos J, De'Oliveira CC, Shirvani O, Fang Y, Wang C, et al. An exosome-based secretion pathway is responsible for protein export from Leishmania and communication with macrophages. *J Cell Sci* (2010) 123(6). doi: 10.1242/jcs.056465

27. Silverman JM, Clos J, Horakova E, Wang AY, Wiesgigl M, Kelly I, et al. Leishmania exosomes modulate innate and adaptive immune responses through effects on monocytes and dendritic cells. *J Immunol* (2010) 185(9). doi: 10.4049/jimmunol.1000541

28. Hassani K, Shio MT, Martel C, Faubert D, Olivier M. Absence of metalloprotease GP63 alters the protein content of leishmania exosomes. *PloS One* (2014) 9(4). doi: 10.1371/journal.pone.0095007

29. Atayde VD, Aslan H, Townsend S, Hassani K, Kamhawi S, Olivier M. Exosome secretion by the parasitic protozoan leishmania within the sand fly midgut. *Cell Rep* (2015) 13(5). doi: 10.1016/j.celrep.2015.09.058

30. Alcolea PJ, Alonso A, Degayón MA, Moreno-Paz M, Jiménez M, Molina R, et al. *In vitro* infectivity and differential gene expression of Leishmania infantum metacyclic promastigotes: Negative selection with peanut agglutinin in culture versus isolation from the stomodeal valve of Phlebotomus perniciosus. *BMC Genomics* (2016) 17(1). doi: 10.1186/s12864-016-2672-8

31. Hassani K, Antoniak E, Jardim A, Olivier M. Temperature-induced protein secretion by leishmania mexicana modulates macrophage signalling and function. *PloS One* (2011) 6(5). doi: 10.1371/journal.pone.0018724

32. Silverman JM, Reiner NE. Leishmania exosomes deliver preemptive strikes to create an environment permissive for early infection. *Front Cell Infection Microbiol* (2011) 1. doi: 10.3389/fcimb.2011.00026

33. Dragovic RA, Gardiner C, Brooks AS, Tannetta DS, Ferguson DJP, Hole P, et al. Sizing and phenotyping of cellular vesicles using Nanoparticle Tracking Analysis. *Nanomedicine* (2011) 7(6):780–8. doi: 10.1016/j.nano.2011.04.003

34. Lötvall J, Hill AF, Hochberg F, Buzás EI, Di Vizio D, Gardiner C, et al. Minimal experimental requirements for definition of extracellular vesicles and their functions: a position statement from the International Society for Extracellular Vesicles. *J Extracell Vesicles* (2014) 3(1):26913. doi: 10.3402/jev.v3.26913

35. Cruz FF, Borg ZD, Goodwin M, Sokocevic D, Wagner DE, Coffey A, et al. Systemic administration of human bone marrow-derived mesenchymal stromal cell extracellular vesicles ameliorates *aspergillus* hyphal extract-induced allergic airway inflammation in immunocompetent mice. *Stem Cells Transl Med* (2015) 4(11):1302–16. doi: 10.5966/sctm.2014-0280

36. Giudice A, Vendrame C, Bezerra C, Carvalho LP, Delavechia T, Carvalho EM, et al. Macrophages participate in host protection and the disease pathology associated with Leishmania Braziliensis infection. *BMC Infect Dis* (2012) 12. doi: 10.1186/1471-2334-12-75

37. Almeida L, Silva JA, Andrade VM, MaChado P, Jamieson SE, Carvalho EM, et al. Analysis of expression of FLI1 and MMP1 in American cutaneous leishmaniasis caused by Leishmania Braziliensis infection. *Infection Genet Evol* (2017) 49. doi: 10.1016/j.meegid.2017.01.018

38. Vandanmagsar B, Youm YH, Ravussin A, Galgani JE, Stadler K, Mynatt RL, et al. The NLRP3 inflammasome instigates obesity-induced inflammation and insulin resistance. *Nat Med* (2011) 17(2). doi: 10.1038/nm.2279

39. Lima-Junior DS, Costa DL, Carregaro V, Cunha LD, Silva ALN, Mineo TWP, et al. Inflammasome-derived IL-1β production induces nitric oxide-mediated resistance to Leishmania. *Nat Med* (2013) 19(7). doi: 10.1038/nm.3221

40. Marim FM, Silveira TN, Lima DS, Zamboni DS. A method for generation of bone marrow-derived macrophages from cryopreserved mouse bone marrow cells. *PloS One* (2010) 5(12). doi: 10.1371/journal.pone.0015263

41. Netea MG, Latz E, Mills KHG, O'Neill LAJ. Innate immune memory: A paradigm shift in understanding host defense. *Nat Immunol* (2015) 16:675–9. doi: 10.1038/ni.3178

42. Rizzetto L, Ifrim DC, Moretti S, Tocci N, Cheng SC, Quintin J, et al. Fungal chitin induces trained immunity in human monocytes during cross-talk of the host with Saccharomyces cerevisiae. *J Biol Chem* (2016) 291(15). doi: 10.1074/jbc.M115.699645

43. Connolly DJ, Bowie AG. The emerging role of human PYHIN proteins in innate immunity: Implications for health and disease. *Biochem Pharmacol* (2014) 92. doi: 10.1016/j.bcp.2014.08.031

44. Man SM, Karki R, Kanneganti TD. AIM2 inflammasome in infection, cancer, and autoimmunity: Role in DNA sensing, inflammation, and innate immunity. *Eur J Immunol* (2016) 46. doi: 10.1002/eji.201545839

45. Novais FO, Carvalho LP, Passos S, Roos DS, Carvalho EM, Scott P, et al. Genomic profiling of human leishmania Braziliensis lesions identifies transcriptional modules associated with cutaneous immunopathology. *J Invest Dermatol* (2015) 135(1). doi: 10.1038/jid.2014.305

46. Carvalho AM, Viana SM, Andrade BB, Oliveira F, Valenzuela JG, Carvalho EM, et al. Immune response to linB13, a lutzomyia intermedia salivary protein correlates with disease severity in tegumentary leishmaniasis. *Clin Infect Dis* (2022) 75(10). doi: 10.1093/cid/ciac258

47. Carvalho AM, Fukutani KF, Sharma R, Curvelo RP, MIranda JC, Barral A, et al. Seroconversion to Lutzomyia intermedia LinB-13 as a biomarker for developing cutaneous leishmaniasis. *Sci Rep* (2017) 7(1). doi: 10.1038/s41598-017-03345-0

48. Carvalho LP, Passos S, Schriefer A, Carvalho EM. Protective and pathologic immune responses in human tegumentary leishmaniasis. *Front Immunol* (2012) 3. doi: 10.3389/fimmu.2012.00301

49. Carrera L, Gazzinelli RT, Badolato R, Hieny S, Müller W, Kühn R, et al. Leishmania promastigotes selectively inhibit interleukin 12 induction in bone marrow-derived macrophages from susceptible and resistant mice. *J Exp Med* (1996) 183(2). doi: 10.1084/jem.183.2.515

50. Kane MM, Mosser DM. Leishmania parasites and their ploys to disrupt macrophage activation. *Curr Opin Hematol* (2000) 7. doi: 10.1097/00062752-200001000-00006

51. Forget G, Gregory DJ, Whitcombe LA, Olivier M. Role of host protein tyrosine phosphatase SHP-1 in Leishmania donovani-induced inhibition of nitric oxide production. *Infect Immun* (2006) 74(11). doi: 10.1128/IAI.00853-05

52. Shweash M, Adrienne McGachy H, Schroeder J, Neamatallah T, Bryant CE, Millington O, et al. Leishmania mexicana promastigotes inhibit macrophage IL-12 production via TLR-4 dependent COX-2, iNOS and arginase-1 expression. *Mol Immunol* (2011) 48(15–16). doi: 10.1016/j.molimm.2011.05.013

53. Gupta P, Srivastav S, Saha S, Das PK, Ukil A. Leishmania donovani inhibits macrophage apoptosis and pro-inflammatory response through AKT-mediated regulation of β-catenin and FOXO-1. *Cell Death Differ* (2016) 23(11). doi: 10.1038/cdd.2016.101

54. Weinheber N, Wolfram M, Harbecke D, Aebischer T. Phagocytosis of Leishmania mexicana amastigotes by macrophages leads to a sustained suppression of IL-12 production. *Eur J Immunol* (1998) 28(8). doi: 10.1002/(SICI)1521-4141(199808)28:08<2467::AID-IMMU2467>3.0.CO;2-1

55. Parmar N, Chandrakar P, Vishwakarma P, Singh K, Mitra K, Kar S. Leishmania donovani exploits tollip, a multitasking protein, to impair TLR/IL-1R signaling for its survival in the host. *J Immunol* (2018) 201(3). doi: 10.4049/jimmunol.1800062

56. Cameron P, McGachy A, Anderson M, Paul A, Coombs GH, Mottram JC, et al. Inhibition of lipopolysaccharide-induced macrophage IL-12 production by leishmania mexicana amastigotes: the role of cysteine peptidases and the NF-κB signaling pathway. *J Immunol* (2004) 173(5). doi: 10.4049/jimmunol.173.5.3297

57. Gomez MA, Contreras I, Hallé M, Tremblay ML, McMaster RW, Olivier M. Leishmania GP63 alters host signaling through cleavage-activated protein tyrosine phosphatases. *Sci Signal* (2009) 2(90). doi: 10.1126/scisignal.2000213

Check for updates

NAIP/NLRC4 inflammasome participates in macrophage responses to *Trypanosoma cruzi* by a mechanism that relies on cathepsin-dependent caspase-1 cleavage

Marcelo Pires Amaral[1]*, Felipe Daniel Cardoso[1],
Ingrid Sancho de Farias[1], Rafael Queiroz de Souza[1],
Kely Catarine Matteucci[2], Ana Claudia Torrecilhas[3]
and Karina Ramalho Bortoluci[1]

[1]Departamento de Farmacologia, Escola Paulista de Medicina/Universidade Federal de São Paulo
(EPM/UNIFESP), São Paulo, SP, Brazil, [2]Plataforma de Medicina Translacional, Fundação Oswaldo Cruz
(FIOCRUZ), Faculdade de Medicina de Ribeirão Preto (FMRP), Ribeirão Preto, SP, Brazil,
[3]Departamento de Ciências Farmacêuticas, Instituto de Ciências Ambientais, Químicas e
Farmacêuticas, Universidade Federal de São Paulo (UNIFESP), Diadema, SP, Brazil

Inflammasomes are large protein complexes that, once activated, initiate inflammatory responses by activating the caspase-1 protease. They play pivotal roles in host defense against pathogens. The well-established role of NAIP/NLRC4 inflammasome in bacterial infections involves NAIP proteins functioning as sensors for their ligands. However, recent reports have indicated the involvement of NLRC4 in non-bacterial infections and sterile inflammation, even though the role of NAIP proteins and the exact molecular mechanisms underlying inflammasome activation in these contexts remain to be elucidated. In this study, we investigated the activation of the NAIP/NLRC4 inflammasome in response to *Trypanosoma cruzi*, the protozoan parasite responsible for causing Chagas disease. This parasite has been previously demonstrated to activate NLRP3 inflammasomes. Here we found that NAIP and NLRC4 proteins are also required for IL-1β and Nitric Oxide (NO) release in response to *T. cruzi* infection, with their absence rendering macrophages permissive to parasite replication. Moreover, $Nlrc4^{-/-}$ and $Nlrp3^{-/-}$ macrophages presented similar impaired responses to *T. cruzi*, underscoring the non-redundant roles played by these inflammasomes during infection. Notably, it was the live trypomastigotes rather than soluble antigens or extracellular vesicles (EVs) secreted by them, that activated inflammasomes in a cathepsins-dependent manner. The inhibition of cathepsins effectively abrogated caspase-1 cleavage, IL-1β and NO release, mirroring the phenotype observed in $Nlrc4^{-/-}/Nlrp3^{-/-}$ double knockout macrophages. Collectively, our findings shed light on the pivotal role of the NAIP/NLRC4 inflammasome in macrophage responses to *T. cruzi* infection, providing new insights into its broader functions that extend beyond bacterial infections.

KEYWORDS

NAIP/NLRC4, inflammasome, *Trypanosoma cruzi*, cathepsins, caspase-1

Introduction

Trypanosoma cruzi, the causative agent of Chagas disease, represents a significant global health burden, affecting millions of people primarily in Latin America (1). This intracellular parasite can evade host immune defenses, leading to chronic infection and the development of severe pathological consequences. Unraveling the intricate host-parasite interplay is crucial for the development of effective therapeutic strategies against *T. cruzi* (2, 3).

Inflammasomes, multiprotein complexes assembled in the cell cytosol in response to infections or cytosolic disturbances, act as key regulators of the innate immune response. They are responsible for the inflammatory caspase-1 activation, a cysteine protease that cleaves IL-1β, IL-18, and gasdermin-D (GSDM-D), culminating in cytokine secretion and pyroptosis (4, 5).

The role of the NLRP3 inflammasome during protozoan infections has been extensively demonstrated. NLRP3 is involved in host resistance against *Toxoplasma gondii* (6), *Plasmodium* spp. (7, 8), *Leishmania* spp. (9, 10), and *T. cruzi* (11, 12). On the other hand, it has been reported that NLRP3-deficient mice seem to be protected against cerebral (13) and placental malaria (14), as well as the severity of leishmaniasis caused by *L. braziliensis* (15) and *L. major* Seidman strain (16) infections. NLRP3 seems to be activated by common cytosolic disturbances induced by these parasites, such as cathepsins extravasation (7, 9, 11), reactive oxygen species (ROS) (17–19), potassium (K^+) efflux (9, 20), calcium (Ca^{2+}) influx (21, 22), and crystal accumulation (23).

NAIP/NLRC4 inflammasome activation occurs after recognition of bacterial components by the NLR family apoptosis inhibitory protein (NAIP) followed by NLRC4 recruitment (24, 25). However, several studies have reported the participation of NLRC4 in non-bacterial contexts, such as *Candida albicans* (26), *Neospora caninum* (27) and Human immunodeficiency virus (HIV) (28) infections, although the molecular mechanism involved in the inflammasome activation in these contexts remains to be elucidated.

In this study, we unveil a novel role for the NAIP/NLRC4 inflammasome in the context of a pathogenic protozoan parasite. Our research reveals that *T. cruzi* infection activates the NAIP/NLRC4 complex. Subsequently, this activation leads to the regulation of *iNOS* gene expression and secretion of nitric oxide (NO), a well-established trypanocidal molecule (29). Our findings suggest a coordinated action of both NLRP3 and NAIP/NLRC4 inflammasomes, with each playing a non-redundant role in controlling *T. cruzi* infection as evidenced by the strikingly similar responses of *Nlrc4*^{-/-} and *Nlrp3*^{-/-} macrophages to *T. cruzi*. Furthermore, our data establishes that the activation of inflammasomes in response to *T. cruzi* is primarily orchestrated by lysosomal cathepsins, without contribution of K^+ efflux or ROS generation. Lysosomal cathepsins modulate NAIP/NLRC4 and NLRP3 inflammasomes activation during *T. cruzi* infection by interfering with caspase-1 maturation. These findings shed light on the remarkable adaptability of these immune sensor platforms offering novel insights and potential therapeutic targets within the realm of the NAIP/NLRC4 inflammasome in the context of infections.

Materials and Methods

Animals and cells

C57BL/6, *Nlrp3*^{-/-} (30), *Nlrc4*^{-/-} (31), and *Nlrc4*^{-/-}/*Nlrp3*^{-/-} mice were purchased from the Center for the Development of Experimental Models for Medicine and Biology (CEDEME) – UNIFESP. *Naip1-7*^{-/-} and *Nlrc4*[S533D/S533D] mice were kindly provided by Dr. Vishva Dixit and Dr. Kim Newton (Genentech Inc). All mice (4-8 weeks old) were housed in a temperature-controlled, free access to water and food, light-cycled facility at UNIFESP.

Peritoneal macrophages (PMs) were obtained by peritoneal lavage 4 days after i.p. of 1% starch solution (Sigma Aldrich) in 2 mL of PBS (w/v). Cells were plated in R3% medium [RPMI 1640 (Gibco), 3% FBS (LGC), 0.16 mM Penicillin (Sigma Aldrich), 0.18 mM Streptomycin (Sigma Aldrich), 12.5 mM HEPES (Sigma Aldrich), 30 mM sodium bicarbonate (Sigma Aldrich), pH 7.2-7.4] and stimulated on the next day.

Bone marrow cells were obtained by femur and tibia flush with cold PBS. Cells were centrifuged, treated with Ammonium-Chloride-Potassium (150 mM NH_4Cl, 1 mM $KHCO_3$, 0.1 mM Na_2EDTA, pH 7.2-7.4) lysing buffer, washed, centrifuged, and 4.5×10^6 cells plated in non-adherent T75 flasks in R10% medium [RPMI 1640 (Gibco), 10% FBS (Gibco), 1% Penicillin-Streptomycin (Gibco), 1% GlutaMax (Gibco), 1% HEPES (Gibco), 1% Sodium Pyruvate (Gibco), 1% MEM Non-Essential Amino Acids (Gibco), 1% MEM Vitamin (Gibco), 20% L929 supernatant, and 55 µM β-mercaptoethanol (Sigma Aldrich), pH 7.2-7.4]. Cell medium was replaced on day 3 and 5. On day 7, cells were maintained for 15 minutes in cold PBS 2% EDTA and 2% FBS, collected, plated, and stimulated on the next day.

Cells were infected by *T. cruzi* in a ratio of 5:1 (parasites:cell) for 2 h, then replaced by fresh medium and maintained during all the infection time. When pertinent, cells were treated with cathepsins, K^+ efflux and ROS pharmacological inhibitors (25 µM CA-074Me, 30 mM KCl and 25 µM Apocynin, respectively) for 1.5 h before the stimuli and maintained during the entire experiment. Alternatively, the CA-074Me dose-response curve experiments were performed using concentrations ranging from 6 µM to 50 µM. For IL-1β secretion positive controls, cells were first primed with LPS (200 ng/mL) for 3 h and then the supernatant was replaced by 3 µg/mL of flagellin (Invivogen) inserted into lipid vesicles (DOTAP) (Sigma Aldrich) for 3 h or 10 µM of nigericin (Invivogen) for 1.5 h.

Parasites

The *T. cruzi* Y strain from the Dante Pazzanese Institute was cultured in LLC-MK2 cells and frozen in liquid nitrogen. For *in vitro* experiments, the parasites were thawed at 37°C, washed in R3% medium, centrifuged and resuspended in fresh R3% medium before use.

Parasite load

For the *in vitro* experiments parasite load was checked as previously described (32). Briefly, after each time point supernatant was collected and reserved. The plates were fixed with pure methanol (Merck) or 4% paraformaldehyde (Sigma Aldrich) diluted in PBS for at least 15 min at room temperature. Then the wells were gently washed with warm PBS and incubated with 5 µg/mL DAPI (blue) (Sigma Aldrich) diluted in PBS. At least 6 images of each well were acquired on the IN-Cell Analyzer 2200 equipment, counted, and the average per well was graphically plotted.

Extracellular vesicles and soluble *T. cruzi* antigens

EVs released from *T. cruzi* were obtained through the centrifugation of trypomastigotes (1000 x g for 15 min). The pellet washes with PBS and subsequently incubated in DMEM medium containing 2% glucose at 37°C with 5% CO_2 for a duration of 2 h. The parasites were then separated by centrifugation at 1000 x g for 10 min, leading to the collection of approximately 1 mL of supernatant. This supernatant was filtered and diluted 1:2 using 200 mM ammonium acetate (pH 6.5). The quantification of EVs was conducted using the NanoSight NS300 device produced by Malvern Panalytical Ltd, revealing that most particles (> 90%) ranged in size from approximately 138 nm to 230 nm.

For the nanoparticle tracking analysis (NTA), a 500 µL volume of the isolated EVs sample was meticulously introduced into the laser chamber of the NanoSight NS300 apparatus. This injection process was conducted with care to prevent the introduction of air bubbles or any loss of the sample. Readings were taken in triplicate for each sample, with each reading extending for 30 seconds at a frame rate of 25 frames per second. This approach facilitated the real-time tracking and measurement of EVs, capturing their Brownian motion. Subsequently, cells were exposed to a stimulation involving $1x10^8$ particles/well over a period of 48 hours.

In order to obtain soluble antigens, *T. cruzi* at a ratio of 5:1 (parasites:cell) per well were centrifuged at 3200 x g 10 min and resuspended in PBS. The parasites were lysed with 5 cycles of freezing in liquid nitrogen and thawing in a water bath at 37°C, followed by sonication for 30 s at 30%. The homogenate was again centrifuged at 3200 x g 10 min and the supernatant containing soluble *T. cruzi* antigens were diluted for *in vitro* stimulation for 48 h.

IL-1β, IL-6, LDH and NO measurement

The IL-1β and IL-6 cytokines quantification were performed by collecting the supernatant after each time point and a sandwich ELISA was executed according to the manufacturer's instructions (Invitrogen). The plates were read at 450 nm absorbance on SpectraMax equipment. The LDH measurement was performed according to the manufacturer's instructions (Invitrogen) by collecting the supernatant. The plate was read at 680 nm and subtracted by the 490 nm absorbance on SpectraMax equipment. The NO production was assessed indirectly by the measurement of nitrite concentration by *Griess* reaction immediately after the end of each time point. Briefly, 50 µL of Griess reagent (1% sulfanilamide, 0.1% naphthalene diamine dihydrochloride - NEED, 45% CH_3COOH) was added to 50 µL of supernatant samples and to 50 µL of a serial diluted standard curve. The samples were read at 540 nm absorbance on SpectraMax equipment.

RT-qPCR

To determine the relative gene expression, cells were infected with *T. cruzi* for 6 h for *iNOS* or 24 h for *Pro-IL-1β, Nlrp3* or *Nlrc4* expression. Briefly, the mRNAs were isolated using the TRIzol (Invitrogen) method. The concentration and purification of mRNAs were analyzed by reading in a NanoDrop 2000c spectrophotometer (ThermoFisher Scientific, Inc). The samples were evaluated in the ratio of 260/280 nm and 260/230 nm absorbance, where only ratios above 1.8 were used, indicating the absence of contaminants. The cDNA was generated from 500 ng of total RNA by M-MLV Reverse Transcriptase (Invitrogen) following the manufacturer's instructions. The cDNA (50 ng) was homogenized with TaqMan Universal PCR Master Mix (Applied Biosystems). All values were normalized using the expression level of the endogenous control *β-actin* (Mm02619580_g1). Gene expression levels were shown through relative expression analysis. The relative gene expression of *iNOS* in all genotypes was compared to uninfected C57BL/6 cells. Reactions were conducted in a 7500 Real Time PCR system (Applied Biosystems).

Immunofluorescence ASC specks

Cells were plated for 18 h in a 96-well black plate (Greiner) with a clear bottom for microscopy. On the next day cells were infected with *T. cruzi* as described above and after 4 h the supernatant was removed, and cells were fixed with 4% paraformaldehyde (Sigma Aldrich) diluted in PBS for at least 15 min. Then, wells were washed twice with warm PBS, followed by block/permeabilization buffer [10% BSA (Sigma Aldrich), 1% FBS (LGC), 0.5% Triton-X 100 (Sigma Aldrich), diluted in PBS] for 1 h at room temperature. Wells were carefully washed twice with warm PBS and incubated for 18 h at 4°C with 1:1000 anti-ASC (Millipore, clone 2EI-7). On the next day wells were washed again with warm PBS and incubated with secondary antibody Alexa-fluor 647 (red) (Invitrogen) 1:1000 for 1 h at room temperature. Wells were washed again, incubated with 5 µg/mL DAPI (blue) (Sigma Aldrich) and images were acquired on IN Cell Analyzer 2200 equipment.

Western blotting

For western blotting assays $1x10^6$ cells were plated, in duplicates, in a 24-well plate and maintained for 18 h at 37°C 5%

CO_2. On the next day cell media was replaced by OptiMem (Gibco) and treated with cathepsins inhibitor if necessary. Then, cells were infected with *T. cruzi* as described above for 24 h. The duplicate of supernatants were collected and combined, then precipitated with methanol and chloroform. While the duplicate cell samples were lysed, collected and combined. Samples were run on a 13.5% polyacrylamide SDS-PAGE, transferred to PVDF membrane (Merck), blocked with 5% BSA (Sigma Aldrich) diluted in TBStween 0.05% for 1 h at room temperature, washed 3x with TBStween 0.05% and incubated for 18 h with 1:500 anti-caspase-1 (Adipogen) at 4°C. The membrane was washed 3x with TBStween 0.05%, incubated with 1:1000 horseradish peroxidase-labeled goat anti-mouse IgG (Santa Cruz) for 1 h at room temperature, washed again, and developed by chemiluminescence using ECL (Santa Cruz) acquired in Alliance 4.7 software (Uvitec; Cambridge). Quantification of caspase-1 p20 bands was performed using ImageJ software.

Data analysis

Statistical significances (p-values) were calculated by One-way ANOVA followed by Tukey honestly significantly different (HSD) *post hoc* test or Student's t-test. Data were considered significant when p ≤ 0.0332 (∗), 0.0021 (∗∗), 0.0002 (∗∗∗), or 0.0001 (∗∗∗∗). Statistical analysis and graphical representation were performed using GraphPad Prism version 9.3.0 software.

Results

NAIP/NLRC4 inflammasome is required for macrophage trypanocidal activity

NLRC4 activation is well characterized in bacterial contexts (24, 25). Recent studies have reported the involvement of NLRC4 in non-bacterial infections such as *C. albicans*, *N. caninum* and HIV infection (26–28). Given that the involvement of NAIP in most of these studies remains to be elucidated, and the role of NAIP/NLRC4 in response to *T. cruzi* infection is largely unexplored, we decided to investigate *Naip1-7*^{−/−} and *Nlrc4*^{−/−} macrophage responses to *T. cruzi* infection. As previously demonstrated by our group (11), *T. cruzi* infection resulted in a time-dependent IL-1β secretion (Figure 1A). Notably, *T. cruzi*-infected *Naip1-7*^{−/−} and *Nlrc4*^{−/−} PMs exhibited diminished IL-1β response compared to the C57BL/6 wild-type (WT) PMs (Figure 1B).

To delve deeper into the potential contribution of the NAIP/NLRC4 inflammasome during *T. cruzi* infection on macrophages, we assessed intracellular parasites count at 2 h (parasite entry) and 96 h (parasite replication load) after infection. At 2 h post-infection the frequency of infected cells (Figure 1C) and the number of intracellular parasites (Figure 1D) observed in *Naip1-7*^{−/−} and *Nlrc4*^{−/−} PMs were similar to the C57BL/6 WT cells, demonstrating that cell invasion by *T. cruzi* was not affected by the absence of NAIP or NLRC4, similar as previously described for NLRP3 (11). However, at 96 h post-infection *Naip1-7*^{−/−} and *Nlrc4*^{−/−}

PMs were more permissive to *T. cruzi* replication than C57BL/6 WT cells, presenting higher frequency of infected cells (Figure 1C) and higher numbers of intracellular amastigotes (Figures 1D, E) in comparison to their littermate control cells. These observations underscore the involvement of NAIP/NLRC4 inflammasomes in the macrophages' ability to counteract the proliferation of *T. cruzi*.

NLRC4 phosphorylation on serine 533 (Ser 533) residue seems to optimize NAIP/NLRC4 inflammasome activation in response to their classical agonists (33). However, the constitutive phosphorylation of NLRC4 did not render macrophages more resistant to *T. cruzi*, since the frequency of infected cells were similar between phosphomimetic mutant *Nlrc4*[S533D/S533D] and C57BL/6 WT cells (Supplementary Figure 1A) and the amastigote numbers were even higher than those observed in C57BL/6 WT cells (Supplementary Figures 1B, C), thus reinforcing that NAIP/NLRC4, but not NLRC4 *phosphorylation*, is required for *T. cruzi* replication control by macrophages.

Both NLRP3 and NAIP/NLRC4 are required for macrophage responses to *T. cruzi* infection

We have previously demonstrated the involvement of NLRP3 inflammasome in controlling *T. cruzi* replication (11). To evaluate the relative roles of NLRP3 and NAIP/NLRC4 inflammasomes, we compared the responses of *Nlrp3*^{−/−}, *Naip1-7*^{−/−} and *Nlrc4*^{−/−} macrophages to *T. cruzi*. PMs presented reduced IL-1β secretion after *T. cruzi* infection when NLRP3, NAIP or NLRC4 proteins were absent (Figure 2A). Importantly, these macrophages responded as expected to nigericin and flagellin, the classical stimuli of NLRP3 and NAIP/NLRC4 inflammasomes, respectively (Supplementary Figure 2A). Similar results during *T. cruzi* infection were observed in bone marrow-derived macrophages (BMDM) (Supplementary Figure 2B).

Remarkably, *Nlrp3*^{−/−}, *Naip1-7*^{−/−} and *Nlrc4*^{−/−} macrophages were similarly permissive to *T. cruzi* replication with higher frequency of infected cells (Figure 2B) and intracellular amastigotes (Figures 2C, D) in comparison to C57BL/6 WT cells. Of note, *T. cruzi* infection resulted in a 40-times increase of *Nlrp3* expression in *Nlrc4*^{−/−} macrophages (Figure 2E), although a less robust increase of *Nlrc4* expression was observed in *Nlrp3*^{−/−} cells (Figure 2F). Thus, the elevated NLRP3 expression alone was insufficient to rescue the impairment of *Nlrc4*^{−/−} cells in controlling *T. cruzi* replication (Figures 2C, D), emphasizing once again the requirement of NLRC4 inflammasome for the macrophages' trypanocidal capacity.

We have previously demonstrated the role of NLRP3-mediated NO secretion, an important trypanocydal molecule (11, 29). Here our findings revealed that the permissiveness of *Naip1-7*^{−/−} and *Nlrc4*^{−/−} macrophages to *T. cruzi* replication was correlated to the impairment of NO secretion, similar as found for *Nlrp3*^{−/−} cells (Figure 2G). Furthermore, NLRP3, NAIP and NLRC4 seemed to control NO secretion through the transcriptional regulation of *iNOS* expression (Figure 2H). Altogether, these results demonstrate a non-compensatory role of NLRP3 and NAIP/NLRC4 inflammasomes in macrophage responses to *T. cruzi* infection.
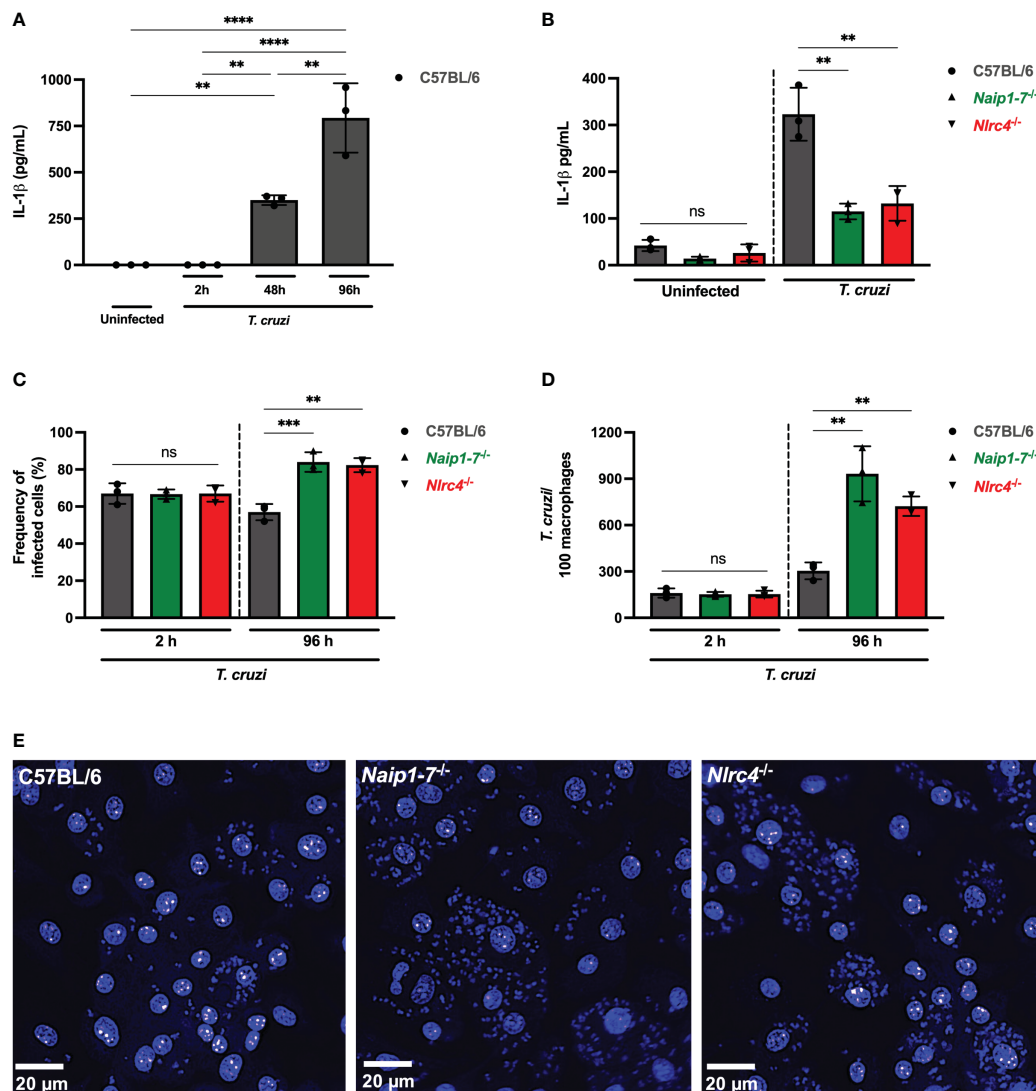
FIGURE 1

NAIP/NLRC4 inflammasome is activated during *T. cruzi* infection. Elicited PMs from C57BL/6, *Naip1-7*^{−/−} and *Nlrc4*^{−/−} mice were plated (5x10⁵/well) in triplicates and on the next day cells were infected by *T. cruzi* Y strain MOI 5:1 (parasites:cell) for 2 h, then supernatant was replaced by fresh R3% medium. After **(A)** 2 h, **(A, B)** 48 h and **(A)** 96 h the supernatant was collected to quantify IL-1β production. Then, the 96 h-infected cells were fixed with methanol for at least 15 min, replaced by DAPI (blue) staining and images were acquired immediately on IN Cell Analyzer 2200. **(C)** Frequency of infected cells. **(D)** Number of parasites/100 macrophages. **(E)** Representative images of *T. cruzi*-infected C57BL/6, *Naip1-7*^{−/−} and *Nlrc4*^{−/−} PMs. The experiments were performed at least twice. Statistical significance was calculated by One-way ANOVA followed by Tukey's *post hoc* test, **p < 0.0021, ***p < 0.0002, ****p < 0.0001, ns, not significant.

Inflammasome activation by *T. cruzi* requires live parasite and relies on lysosomal cathepsins

Since canonical activation of NLRC4 requires the recognition of bacterial ligands by NAIP, we next evaluated if molecules expressed or secreted by *T. cruzi* were able to activate NAIP/NLRC4 inflammasome. Soluble antigens or EVs secreted by *T. cruzi* did not induce IL-1β secretion by C57BL/6 WT PMs, unlike live trypomastigotes (Figure 3A). This data suggests that NAIP/NLRC4 inflammasome activation by *T. cruzi* could be a response to the cytosolic disturbances caused by the parasite infection, similar as observed for NLRP3.

While K⁺ efflux and ROS inhibition, known pathways associated with NLRP3 activation (5, 34), did not exert any discernible influence on IL-1β (Figure 3B) or NO (Figure 3C) release in *T. cruzi*-infected macrophages, a distinct outcome was observed upon cathepsins inhibition. The inhibition of lysosomal cathepsins, protease enzymes implicated in both NLRP3 (35) and NLRC4 (36, 37) activation, abrogated IL-1β and NO secretion in response to *T. cruzi* infection (Figures 3B, C). As expected, CA-074Me and KCl, but not NaCl or Apocynin, significantly reduced IL-1β secretion by nigericin-stimulated macrophages (Supplementary Figure 2C). Furthermore, cathepsins inhibition also reduced IL-1β secretion in macrophages stimulated with flagellin, classical activator of NAIP/NLRC4 inflammasomes
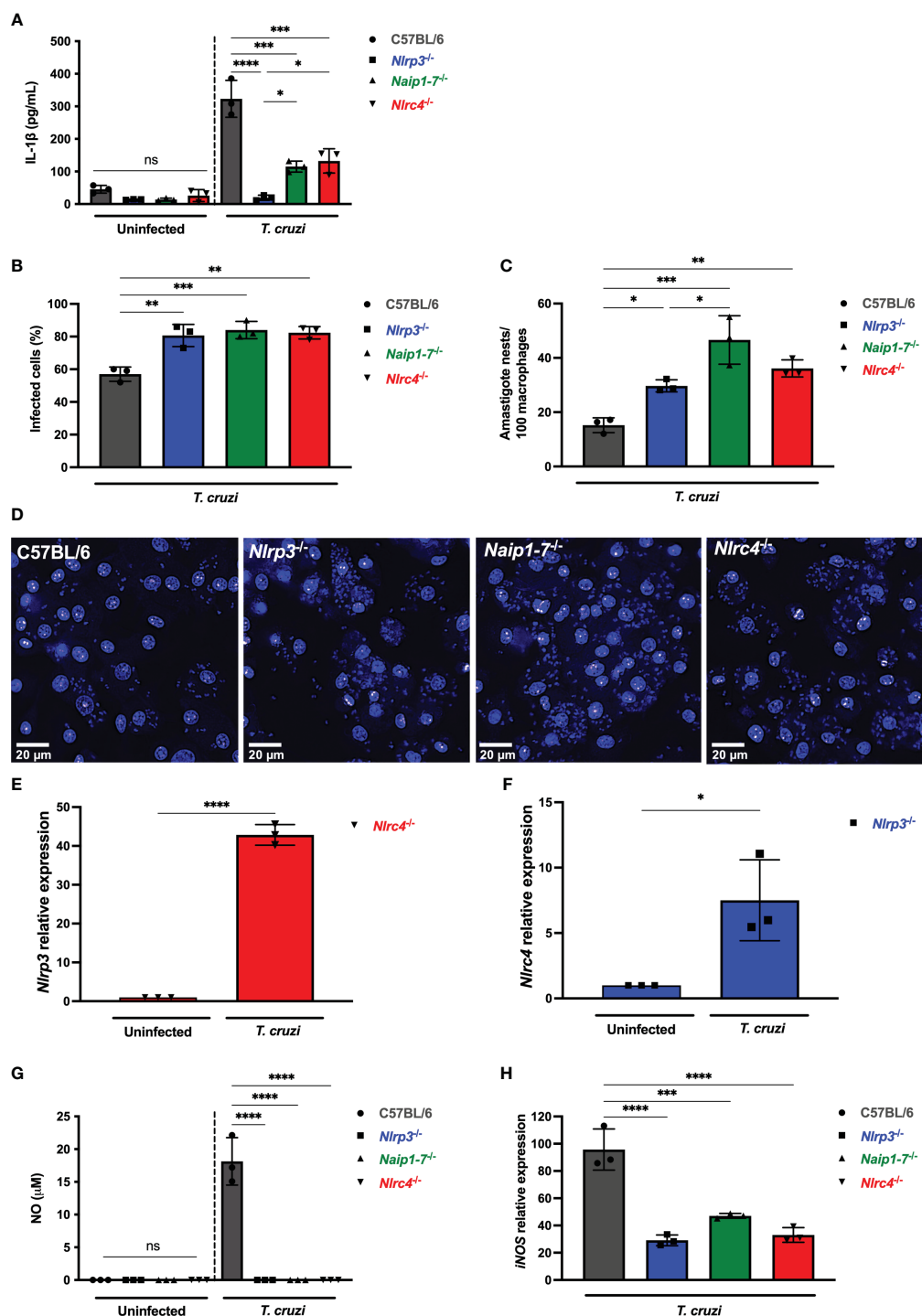
FIGURE 2

NLRP3 and NAIP/NLRC4 inflammasomes are required for effective macrophage responses to *T. cruzi* infection. **(A–D, G, H)** Elicited PMs from C57BL/6, *Nlrp3*^{-/-}, *Naip1-7*^{-/-} and *Nlrc4*^{-/-} mice were plated (5x10^5/well) in triplicates and on the next day cells were infected by *T. cruzi* Y strain MOI 5:1 (parasites:cell) for 2 h, then supernatant was replaced by fresh R3% medium. After **(A)** 48 h the supernatant was collected to quantify IL-1β production. **(B–D)** 96 h post-infection cells were fixed with methanol for at least 15 min, replaced by DAPI (blue) staining and images were acquired immediately on IN Cell Analyzer 2200. **(B)** Frequency of infected cells. **(C)** Parasite burden. Amastigote nests represent at least 15 parasites/nest. **(D)** Representative images of *T. cruzi*-infected C57BL/6, *Nlrp3*^{-/-}, *Naip1-7*^{-/-} and *Nlrc4*^{-/-} PMs. BMDM from *Nlrc4*^{-/-} and *Nlrp3*^{-/-} mice were plated (2x10^5/well), infected on the next day by *T. cruzi* Y strain MOI 5:1 (parasites:cell) for 2 h, then supernatant was replaced by fresh R3% medium and incubated for 24 h. The mRNA was extracted and the **(E)** *Nlrp3* and **(F)** *Nlrc4* relative gene expression to the paired uninfected cells were quantified by RT-qPCR. **(G)** The NO production and **(H)** *iNOS* expression (RT-qPCR) were quantified after 48 h and 6 h, respectively, after *T. cruzi* Y strain infection. The *iNOS* relative gene expression was compared to uninfected C57BL/6 cells. The experiments were performed at least twice. Statistical significance was calculated by **(A–C, G, H)** One-way ANOVA followed by Tukey's *post hoc* test or **(E, F)** Student's *t*-test, *p < 0.0332, **p < 0.0021, ***p < 0.0002, ****p < 0.0001, ns, not significant.
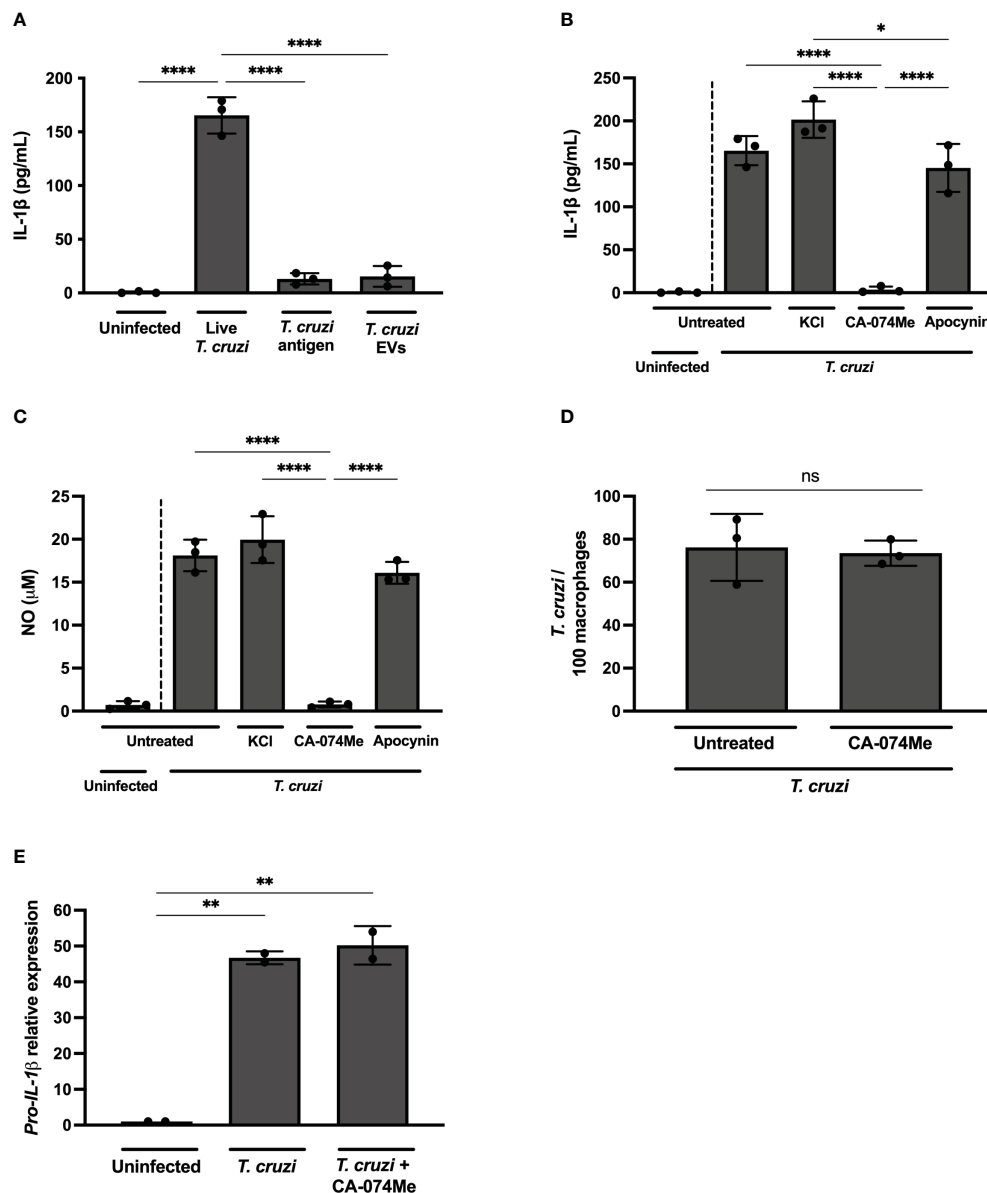
FIGURE 3

Live *T. cruzi* trypomastigotes activate inflammasomes in a cathepsin-dependent manner. Elicited PMs from C57BL/6 mice were plated (5×10^5/well) and on the next day cells were infected with *T. cruzi* Y strain MOI 5:1 (parasites:cell) for 2 h, then supernatant was replaced by fresh R3% medium for **(A–C)** 48 h, **(D)** 2 h or **(E)** 24 h. **(A)** Alternatively, cells were only incubated with *T. cruzi* soluble antigens or 1×10^8 EVs/well for 48 h. **(B–D)** Also, cells were pre-treated or not with KCl (30 mM), CA-074Me (25 µM) and Apocynin (25 µM) for 1.5 h prior to the infection and maintained during the entire experiment. The supernatant was collected and cells were fixed with methanol for at least 15 min when necessary. **(A, B)** IL-1β and **(C)** NO production. **(D)** Prevalence of *T. cruzi* infection. **(E)** The mRNA was extracted and the relative *Pro-IL-1β* gene expression was quantified by RT-qPCR and compared to the paired uninfected cells. The experiments were performed at least twice. Statistical significance was calculated by **(A–C, E)** One-way ANOVA followed by Tukey's *post hoc* test or **(D)** Student's *t*-test, *$p < 0.0332$, **$p < 0.0021$, ****$p < 0.0001$, ns, not significant.

(Supplementary Figure 2D). These results demonstrate the effect of cathepsins on both NLRP3 and NAIP/NLRC4-mediated responses.

CA-074Me inhibited NO (Supplementary Figure 3A) and IL-1β (Supplementary Figure 3B) but not IL-6 (Supplementary Figure 3C) in response to *T. cruzi* infection in a dose-dependent manner, ruling out off-target actions of this inhibitor. Furthermore, there was no cellular cytotoxicity observed in CA-074Me-treated cells, as evidenced by the absence of statistically significant differences in

LDH release, even at high concentrations of the chemical compound (Supplementary Figure 3D).

Of note, the number of intracellular parasites was similar at 2 h post infection in both CA-074Me-treated and untreated cells (Figure 3D), ruling out any impairment of *T. cruzi* invasion when cathepsins are inhibited. Moreover, the *Pro-IL-1β* expression was unaffected by CA-074Me, suggesting that cathepsins participate in the effector phase of inflammasome activation in response to *T. cruzi* infection, rather than during the priming phase (Figure 3E).

Cathepsins inhibition affects both NLRP3 and NLRC4 inflammasomes by interfering with caspase-1 cleavage in response to *T. cruzi* infection

Since cathepsins inhibition impaired IL-1β secretion, but not *Pro-IL-1β* expression in response to *T. cruzi* infection, we aimed to investigate how cathepsins regulated the inflammasome cascade in this context. First, we observed that inhibiting cathepsins with CA-074Me in *Nlrc4*^{−/−} or *Nlrp3*^{−/−} macrophages resulted in a minimal IL-1β response, mimicking the phenotype observed in treated and untreated *Nlrc4*^{−/−}/*Nlrp3*^{−/−} macrophages (Figure 4A).

In order to assess whether cathepsins interfere with inflammasomes assembly in response to *T. cruzi*, we analyzed the frequency of ASC speck formation in macrophages. The frequency of cells expressing ASC specks did not differ among C57BL/6 WT, *Nlrc4*^{−/−}, *Nlrp3*^{−/−} and *Nlrc4*^{−/−}/Nlrp3^{−/−} macrophages after *T. cruzi* infection (Figures 4B, C). Moreover, cells from all strains maintained similar numbers of ASC puncta when treated with CA-074Me (Figures 4B, C), suggesting that cathepsins act downstream inflammasomes assembly in response to *T. cruzi* infection.

Next, we investigated the role of cathepsins on caspase-1 maturation. As expected, cleaved caspase-1 (p20) in response to *T. cruzi* was reduced in the absence of NLRC4, and completely abrogated in cells lacking both NLRC4 and NLRP3 (Figure 4D). Furthermore, the inhibition of cathepsins abrogated caspase-1 activation in all genotypes, resembling the phenotype observed in *Nlrc4*^{−/−}/Nlrp3^{−/−} cells, thus demonstrating that cathepsins interfered with NLRP3- and NLRC4-dependent caspase-1 maturation during *T. cruzi* infection (Figure 4D). Notably, the *pro-caspase-1* expression was not affected by cathepsins inhibition (Figure 4D), reinforcing the role of cathepsins during the effector phase of NLRC4 and NLRP3 inflammasomes activation in response to *T. cruzi* infection, rather than during the priming phase.

Overall, our results support the concurrent activation of NAIP/NLRC4 and NLRP3 inflammasomes during *T. cruzi* infection. Importantly, cathepsins orchestrate these inflammasome responses by interfering with caspase-1 cleavage and the subsequent IL-1β maturation and NO secretion (Figure 5).

Discussion

Inflammasomes, pivotal components of the innate immune system, have garnered significant attention for their role in host defense against various pathogens. While much has been uncovered about inflammasome assembly, activation, and effector mechanisms, there are still many questions that remain unanswered (4, 5). Among the known inflammasomes, NLRP3 has been the most extensively studied due to its versatile activation by both sterile and non-sterile stimuli (34, 38). Whereas the mechanisms governing NAIP/NLRC4 inflammasome are better elucidated, primarily in the context of bacterial infections (24, 25, 39). However, recent findings have expanded the role of NLRC4 into non-bacterial (26–28) and sterile (40–50) conditions, although

the molecular regulation of NAIP/NLRC4 under these contexts remains to be elucidated. In this study, we demonstrated a previously unknown role of NAIP/NLRC4 inflammasome in response to the *T. cruzi* infection, a protozoan parasite responsible for causing Chagas disease. Interestingly, NAIP/NLRC4 activation by *T. cruzi* requires live parasites and relies on lysosomal cathepsins, similar as previously described for NLRP3 (11).

NAIP/NLRC4 inflammasome activation during bacterial infection occurs after recognition of their ligands by NAIP proteins (24, 25). Murine cells express seven NAIP proteins, while human cells have only one. Murine NAIP5 and NAIP6 bind to flagellins from distinct bacteria species, whereas NAIP1 and NAIP2 interact with the proteins from the bacterial type III secretion system (T3SS) (24, 25, 51, 52). NAIP3, NAIP4 and NAIP7 have no clear function so far. Human NAIP (hNAIP) covers all the murine NAIP functions (53). In addition to the direct interaction between NAIP and bacterial agonists, NLRC4 phosphorylation on serine 533 (Ser 533) residue seems to optimize NAIP/NLRC4 inflammasome activation (33). Here, we demonstrated that *Naip1-7*^{−/−} and *Nlrc4*^{−/−} macrophages were more permissive to *T. cruzi* replication than C57BL/6 WT cells. In contrast, macrophages from phosphomimetic mutant *Nlrc4*[S533D/S533D] mice, that harbors a constitutive phosphorylation on NLRC4 Ser 533, did not demonstrate any resistance to the infection. This highlights the pivotal role of NAIP, rather than NLRC4 phosphorylation, in mediating NLRC4-dependent control of *T. cruzi* by macrophages.

The participation of NAIP in non-bacterial infection was also demonstrated in HIV-1-infected human monocyte-derived macrophages, in which hNAIP was activated by HIV-1 glycoprotein 41 (gp41) leading to the NLRC4 recruitment and IL-18 secretion (28). Although the molecular mechanism of NAIP activation by *T. cruzi* remains to be elucidated, it seems not to involve the interaction with soluble ligands from parasites neither EV secreted by them, since the secretion of IL-1β was only observed in the presence of live trypomastigotes. Accordingly, a previous study demonstrated that irradiated- or heat-killed-*T. cruzi* lost the ability to induce IL-1β secretion in BMDM (12). Therefore, these findings support the hypothesis that inflammasome activation requires cytosolic disturbances induced by live trypomastigotes.

A proposed pathway for NAIP/NLRC4 activation under both infectious and sterile stimuli involves its interaction with other inflammasomes, particularly NLRP3 (27, 41, 42, 54–57). While the precise nature of this interaction is still a subject of debate (55), it has been suggested that the NAIP/NLRC4/ASC complex formed after *Salmonella* infection may recruit NLRP3, potentially amplifying caspase-1 cleavage and subsequent IL-1β cytokine release (42, 54, 57). Although the exact nature of the interaction between NAIP/NLRC4 and NLRP3 within the same inflammasome complex during *T. cruzi* infection requires further elucidation, our results demonstrated that macrophages lacking NLRP3, NAIP1-7, or NLRC4, all exhibited similar deficiencies in controlling parasite replication. This observation suggests a non-redundant role for both NLRP3 and NAIP/NLRC4 inflammasomes in enhancing the macrophage's trypanocidal capabilities, similar as previously described for macrophage responses to short noncoding retrotransposons (42).
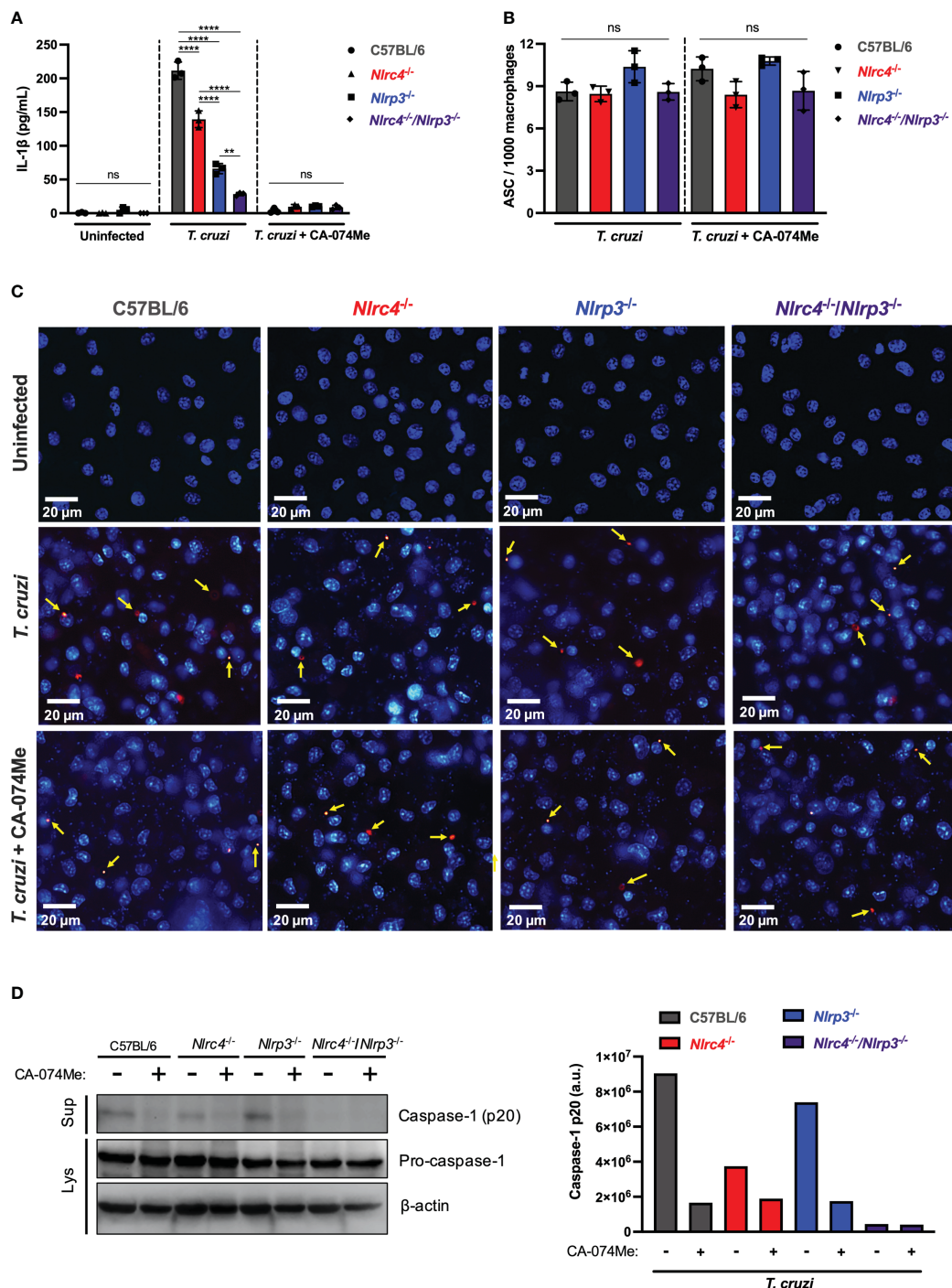
FIGURE 4

Cathepsins regulate inflammasomes activation during *T. cruzi* infection by modulating caspase-1 maturation. BMDM from C57BL/6, *Nlrc4*$^{-/-}$, *Nlrp3*$^{-/-}$ and *Nlrc4*$^{-/-}$/*Nlrp3*$^{-/-}$ mice were plated (2x10^5/well, or 1x10^6/well for western blotting assay) and on the next day cells were infected by *T. cruzi* Y strain MOI 5:1 (parasites:cell) for 2 h, then supernatant was replaced by fresh R3% medium for **(A)** 48 h and **(B, C)** 4 h, or OptiMem medium for **(D)** 24 h. When pertinent, cells were pre-treated with CA-074Me (25 μM) for 1.5 h prior to the infection and maintained during the entire experiment. **(A)** IL-1β quantification in culture supernatants. **(B)** Frequency of ASC specks. **(C)** Representative images obtained with IN Cell Analyzer 2200 of uninfected, *T. cruzi*- or *T. cruzi*+CA-074Me-infected C57BL/6, *Nlrc4*$^{-/-}$, *Nlrp3*$^{-/-}$ and *Nlrc4*$^{-/-}$/*Nlrp3*$^{-/-}$ macrophages. Yellow arrows indicate ASC speck. **(D)** Western blot assay for cleaved caspase-1 (p20) (culture supernatants: Sup), and *pro-caspase-1* and β-actin (cell lysates: Lys). Caspase-1 p20 bands quantification was performed using ImageJ software. The experiments were performed at least twice. Statistical significance was calculated by One-way ANOVA followed by Tukey's *post hoc* test, **p < 0.0021, ****p < 0.0001, ns, not significant.

FIGURE 5
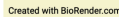
Cathepsins orchestrate the responses of both NAIP/NLRC4 and NLRP3 inflammasomes to *T. cruzi* by interfering with caspase-1 maturation. When *T. cruzi* trypomastigotes infect the host cell, they are initially confined within a parasitophorous vacuole (PV), which subsequently fuses with lysosomes. Following this, the protozoan parasites escape into the cytosol and differentiate into amastigotes for replication. The leakage of cathepsins after lysosomal membrane permeabilization (LMP) orchestrate NAIP/NLRC4 and NLRP3 inflammasome responses to live *T. cruzi* trypomastigotes, leading to caspase-1 cleavage and the consequent release of IL-1β and NO. Accordingly, the inhibition of cathepsins results in the abrogation of these effector responses, resembling the phenotype of double knockout macrophages (*Nlrc4^{-/-}/Nlrp3^{-/-}*), although the precise mechanisms by which cathepsins modulate caspase-1 maturation remain to be elucidated.

The susceptibility of $Nlrp3^{-/-}$, $Naip1\text{-}7^{-/-}$, and $Nlrc4^{-/-}$ macrophages to *T. cruzi* replication was associated with impaired NO secretion. NO is a well-established trypanocidal molecule (11, 29), and we have previously demonstrated the role of NLRP3-induced NO secretion in controlling *T. cruzi* replication in macrophages (11) and microglia (58). Interestingly, even in the presence of a 40-fold increase in $Nlrp3$ expression, $Nlrc4^{-/-}$ macrophages failed to release NO, highlighting the participation of the NLRC4 inflammasome in response to *T. cruzi*. NLRC4 has been shown to induce NO secretion in response to cytosolic flagellin by epigenetically regulating $Nos2$ through the cleavage of poly [ADP-ribose] polymerase1 (PARP1) by caspase-1 (59, 60). This is in line with our observations regarding the requirement of NLRP3, NAIP, and NLRC4 in regulating $Nos2$ expression at the transcriptional level in response to *T. cruzi*.

Interestingly, it appears that both NAIP/NLRC4 and NLRP3 inflammasomes are regulated by lysosomal cathepsins during *T. cruzi* infection. This is substantiated by the fact that pharmacological inhibition of these cysteine proteases effectively halted IL-1β secretion, NO release, and caspase-1 cleavage, whereas inhibition of K^+ efflux or ROS, had no such impact. These outcomes parallel the effects observed when both NLRP3 and NLRC4 proteins were genetically deleted. Lysosomal membrane permeabilization (LMP) and the consequent leakage of cathepsins into the cytosol are known pathways associated with NLRP3 activation in response to different stimuli (35, 61, 62), including protozoan infections (7, 9, 11). Recent studies have further highlighted the role of cathepsins in regulating NAIP/NLRC4-dependent IL-1β secretion by murine and human macrophages in response to cytosolic flagellin (37).

Several mechanisms have been proposed for cathepsin-mediated inflammasome activation. Cathepsins can influence ASC speck formation, caspase-1 maturation, $pro\text{-}IL\text{-}1\beta$ transcription, and IL-1β secretion in response to classical NLRP3 agonists like particulate material, ATP, or toxins (35, 63, 64). In response to flagellin, a well-known NLRC4 agonist, cathepsins seem to collaborate with gasdermin D (GSDMD) to enhance IL-1β secretion (37). This study, however, suggests that cathepsins likely do not play a role during the priming and assembly stages of NLRP3 and NAIP/NLRC4 inflammasomes in response to *T. cruzi*. This conclusion is further substantiated by the fact that CA-074Me treatment did not affect the transcription of $pro\text{-}IL\text{-}1\beta$ and $pro\text{-}caspase\text{-}1$ or the formation of ASC specks. Nonetheless, the presence of CA-074Me effectively inhibited caspase-1 cleavage, aligning with the observations noted in macrophages lacking both NLRC4 and NLRP3. These findings provide compelling evidence that cathepsins orchestrate the activation of both NAIP/NLRC4 and NLRP3 inflammasomes in response to *T. cruzi* infection.

Considering that *T. cruzi* actively recruits lysosomes during invasion, resulting in the formation of the parasitophorous vacuole (PV) (65, 66), it is reasonable to hypothesize that the leakage of lysosomal cathepsins, signaling the parasite's intrusion into host cells, might represent a pivotal event triggering inflammasome activation during *T. cruzi* infection in macrophages. This novel insight into the interplay between *T. cruzi* and inflammasomes highlights the dual involvement of both NAIP/NLRC4 and NLRP3 inflammasomes in generating effector molecules necessary for controlling *T. cruzi* infection. It

sheds light on the intricate functional mechanisms of inflammasomes in the context of infectious diseases, underscoring their significance as potential targets for therapeutic interventions and drug development.

Data availability statement

The original contributions presented in the study are included in the article/Supplementary Material. Further inquiries can be directed to the corresponding author.

Ethics statement

The animal study was approved by Comitê de Ética no Uso de Animais da UNIFESP (Institutional Animal Care and Use Committees from UNIFESP). The study was conducted in accordance with the local legislation and institutional requirements.

Author contributions

MA: Conceptualization, Data curation, Formal Analysis, Investigation, Methodology, Validation, Visualization, Writing – original draft, Writing – review & editing. FC: Data curation, Formal Analysis, Investigation, Methodology, Validation, Writing – review & editing. IF: Investigation, Methodology, Validation, Writing – review & editing. RS: Investigation, Writing – review & editing. KM: Methodology, Writing – review & editing. AT: Methodology, Resources, Writing – review & editing. KB: Conceptualization, Funding acquisition, Methodology, Project administration, Resources, Supervision, Validation, Writing – review & editing.

Funding

Acknowledgments

Conflict of interest

The authors declare that the research was conducted in the absence of any commercial or financial relationships that could be construed as a potential conflict of interest.

Publisher's note

All claims expressed in this article are solely those of the authors and do not necessarily represent those of their affiliated organizations, or those of the publisher, the editors and the reviewers. Any product that may be evaluated in this article, or claim that may be made by its manufacturer, is not guaranteed or endorsed by the publisher.

Supplementary material

The Supplementary Material for this article can be found online at: https://www.frontiersin.org/articles/10.3389/fimmu.2023.1282856/full#supplementary-material

SUPPLEMENTARY FIGURE 1
Constitutive NLRC4 phosphorylation does not improve *T. cruzi* replication restrain. Elicited PMs from C57BL/6 and *Nlrc4*$^{S533D/S533D}$ mice were plated ($5x10^5$/well) in triplicates and on the next day cells were infected by *T. cruzi* Y strain MOI 5:1 (parasites:cell) for 2 h, then supernatant was replaced by fresh R3% medium. After 96 h the supernatant was collected and cells were fixed with methanol for at least 15 min, replaced by DAPI (blue) staining and images were acquired immediately on IN Cell Analyzer 2200. **(A)** Frequency of infected cells. **(B)** Prevalence of *T. cruzi* infection. **(C)** Representative images of *T. cruzi*-infected C57BL/6 and *Nlrc4*$^{S533D/S533D}$ PMs. The experiments were performed at least twice. Statistical significance was calculated by Student's *t*-test, *p < 0.0332, ns, not significant.

SUPPLEMENTARY FIGURE 2
NLRP3 and NAIP/NLRC4 inflammasomes respond to *T. cruzi* infection and classical agonists. **(A, D)** Elicited PMs and **(B, C)** BMDM from C57BL/6, *Naip1-7*$^{-/-}$, *Nlrp3*$^{-/-}$ and *Nlrc4*$^{-/-}$ mice were plated in a density of **(A, D)** $5x10^5$/well and **(B, C)** $2x10^5$/well. **(A)** On the next day PMs were primed with LPS (200 ng/mL) for 3 h and then supernatant was replaced by 10 µM of nigericin for 1.5 h or 3 µg/mL of flagellin inserted into lipid vesicles (DOTAP) for 3 h. The supernatant was collected and IL-1β cytokine was quantified by ELISA. Alternatively, **(B)** BMDM were infected by *T. cruzi* Y strain MOI 5:1 (parasites:cell) for 2 h, then supernatant was replaced by fresh R3% medium. After 48 h the supernatant was collected to quantify IL-1β. The experiments were performed at least three times. **(C, D)** When pertinent, cells were pre-treated and maintained during the entire experiment with KCl (30 mM), CA-074Me (25 µM), Apocynin (25 µM) and NaCl (30 mM) for 1.5 h, primed with LPS (200 ng/mL) for 3 h, and then the supernatant was replaced by **(C)** 10 µM of nigericin for 1.5 h or **(D)** 3 µg/mL of flagellin inserted into lipid vesicles (DOTAP) for 3 h. The supernatant was collected and IL-1β cytokine was quantified by ELISA. The experiments were performed at least three times. Statistical significance was calculated by One-way ANOVA followed by Tukey's *post hoc* test, *p < 0.0332, **p < 0.0021, ***p < 0.0002, ****p < 0.0001.

SUPPLEMENTARY FIGURE 3
CA-074Me inhibits NO and IL-1β in dose-dependent manner without interfering on IL-6 production and cytotoxicity. BMDM from C57BL/6 mice were plated

(2x10^5/well) and on the next day cells were infected by *T. cruzi* Y strain MOI 5:1 (parasites:cell) for 2 h, then supernatant was replaced by fresh R3% medium for 48 h. When pertinent, cells were pre-treated with different doses of CA-074Me for 1.5 h prior to the infection and maintained during the entire experiment. The

supernatant was collected to quantify **(A)** NO, **(B)** IL-1β, **(C)** IL-6, and **(D)** LDH. The experiments were performed at least twice. Statistical significance was calculated by One-way ANOVA followed by Tukey's *post hoc* test, **p < 0.0021, ***p < 0.0002, ****p < 0.0001, ns, not significant.

References

1. Pérez-Molina JA, Molina I. Chagas disease. *Lancet (London England)* (2018) 391:82–94. doi: 10.1016/S0140-6736(17)31612-4

2. Flávia Nardy A, Freire-De-Lima CG, Morrot A. Immune evasion strategies of *trypanosoma cruzi*. *J Immunol Res* (2015) 2015. doi: 10.1155/2015/178947

3. Macaluso G, Grippi F, Di Bella S, Blanda V, Gucciardi F, Torina A, et al. A Review on the Immunological Response against *Trypanosoma cruzi*. *Pathogens* (2023) 12 (2):282. doi: 10.3390/pathogens12020282

4. Martinon F, Burns K, Tschopp J. The Inflammasome: A molecular platform triggering activation of inflammatory caspases and processing of proIL-β. *Mol Cell* (2002) 10(2):417–26. doi: 10.1016/S1097-2765(02)00599-3

5. Broz P, Dixit VM. Inflammasomes: mechanism of assembly, regulation and signalling. *Nat Rev Immunol* (2016) 16:407–20. doi: 10.1038/nri.2016.58

6. Gorfu G, Cirelli KM, Melo MB, Mayer-Barber K, Crown D, Koller BH, et al. Dual role for inflammasome sensors NLRP1 and NLRP3 in murine resistance to Toxoplasma gondii. *MBio* (2014) 5(1):10. doi: 10.1128/mBio.01117-13

7. Shio MT, Eisenbarth SC, Savaria M, Vinet AF, Bellemare MJ, Harder KW, et al. Malarial hemozoin activates the NLRP3 inflammasome through Lyn and Syk kinases. *PLoS Pathog* (2009) 5:e1000559. doi: 10.1371/annotation/abca067d-b82b-4de6-93c5-0fcc38e3df05

8. Dostert C, Guarda G, Romero JF, Menu P, Gross O, Tardivel A, et al. Malarial hemozoin is a Nalp3 inflammasome activating danger signal. *PLoS One* (2009) 4(8):e6510. doi: 10.1371/journal.pone.0006510

9. Lima-Junior DS, Costa DL, Carregaro V, Cunha LD, Silva AL, Mineo TW, et al. Inflammasome-derived IL-1beta production induces nitric oxide-mediated resistance to Leishmania. *Nat Med* (2013) 19:909–15. doi: 10.1038/nm.3221

10. de Sá KSG, Amaral LA, Rodrigues TS, Ishimoto AY, de Andrade WA, de Almeida L, et al. Gasdermin-D activation promotes NLRP3 activation and host resistance to Leishmania infection. *Nat Commun* (2023) 14(1):1049. doi: 10.1038/s41467-023-36626-6

11. Goncalves VM, Matteucci KC, Buzzo CL, Miollo BH, Ferrante D, Torrecilhas AC, et al. NLRP3 controls *Trypanosoma cruzi* infection through a caspase-1-dependent IL-1R-independent NO production. *PLoS Negl Trop Dis* (2013) 7:e2469. doi: 10.1371/journal.pntd.0002469

12. Silva GK, Costa RS, Silveira TN, Caetano BC, Horta CV, Gutierrez FRS, et al. Apoptosis-associated speck-like protein containing a caspase recruitment domain inflammasomes mediate IL-1beta response and host resistance to *Trypanosoma cruzi* infection. *J Immunol* (2013) 191:3373–83. doi: 10.4049/jimmunol.1203293

13. Reimer T, Shaw MH, Franchi L, Coban C, Ishii KJ, Akira S, et al. Experimental cerebral malaria progresses independently of the Nlrp3 inflammasome. *Eur J Immunol* (2010) 40:764–9. doi: 10.1002/eji.200939996

14. Reis AS, Barboza R, Murillo O, Barateiro A, Peixoto EP, Lima FA, et al. Inflammasome activation and IL-1 signaling during placental malaria induce poor pregnancy outcomes. *Sci Adv* (2020) 6(10):eaax6346. doi: 10.1126/sciadv.aax6346

15. Novais FO, Carvalho AM, Clark ML, Carvalho LP, Beiting DP, Brodsky IE, et al. CD8+ T cell cytotoxicity mediates pathology in the skin by inflammasome activation and IL-1β production. *PLoS Pathog* (2017) 13(2):e1006196. doi: 10.1371/journal.ppat.1006196

16. Charmoy M, Hurrell BP, Romano A, Lee SH, Ribeiro-Gomes F, Riteau N, et al. The Nlrp3 inflammasome, IL-1β, and neutrophil recruitment are required for susceptibility to a nonhealing strain of Leishmania major in C57BL/6 mice. *Eur J Immunol* (2016) 46:897–911. doi: 10.1002/eji.201546015

17. Lima-Junior DS, Mineo TWP, Calich VLG, Zamboni DS. Dectin-1 Activation during Leishmania amazonensis Phagocytosis Prompts Syk-Dependent Reactive Oxygen Species Production To Trigger Inflammasome Assembly and Restriction of Parasite Replication. *J Immunol* (2017) 199:2055–68. doi: 10.4049/jimmunol.1700258

18. Shio MT, Christian JG, Jung JY, Chang KP, Olivier M. PKC/ROS-mediated NLRP3 inflammasome activation is attenuated by leishmania zinc-metalloprotease during infection. *PLoS Negl Trop Dis* (2015) 9(6):e0003868. doi: 10.1371/journal.pntd.0003868

19. Dutra FF, Alves LS, Rodrigues D, Fernandez PL, De Oliveira RB, Golenbock DT, et al. Hemolysis-induced lethality involves inflammasome activation by heme. *Proc Natl Acad Sci U. S. A.* (2014) 111:E4110–8. doi: 10.1073/pnas.1405023111

20. Gov L, Schneider CA, Lima TS, Pandori W, Lodoen MB. NLRP3 and Potassium Efflux Drive Rapid IL-1beta Release from Primary Human Monocytes during Toxoplasma gondii Infection. *J Immunol* (2017) 199:2855–64. doi: 10.4049/jimmunol.1700245

21. Tanabe K, Mikkelsen RB, Wallach DFH. Calcium transport of Plasmodium chabaudi-infected erythrocytes. *J Cell Biol* (1982) 93:680–4. doi: 10.1083/jcb.93.3.680

22. Das R, Roy A, Dutta N, Majumder HK. Reactive oxygen species and imbalance of calcium homeostasis contributes to curcumin induced programmed cell death in *Leishmania donovani*. *Apoptosis* (2008) 13:867–82. doi: 10.1007/s10495-008-0224-7

23. Griffith JW, Sun T, McIntosh MT, Bucala R. Pure Hemozoin is inflammatory *in vivo* and activates the NALP3 inflammasome via release of uric acid. *J Immunol* (2009) 183:5208–20. doi: 10.4049/jimmunol.0713552

24. Kofoed EM, Vance RE. Innate immune recognition of bacterial ligands by NAIPs determines inflammasome specificity. *Nature* (2011) 477:592–5. doi: 10.1038/nature10394

25. Zhao Y, Yang J, Shi J, Gong YN, Lu Q, Xu H, et al. The NLRC4 inflammasome receptors for bacterial flagellin and type III secretion apparatus. *Nature* (2011) 477 (7366):596–600. doi: 10.1038/nature10510

26. Tomalka J, Ganesan S, Azodi E, Patel K, Majmudar P, Hall BA, et al. A novel role for the NLRC4 inflammasome in mucosal defenses against the fungal pathogen *Candida albicans*. *PLoS Pathog* (2011) 7:e1002379. doi: 10.1371/journal.ppat.1002379

27. Mota C, Lima-Junior DDS, Ferreira Franca FB, Aguillón Torres JD, Barros PDSC, Santiago FM, et al. Interplay between reactive oxygen species and the inflammasome are crucial for restriction of neospora caninum replication. *Front Cell Infect Microbiol* (2020) 10. doi: 10.3389/fcimb.2020.00243

28. Triantafilou K, Ward CJ, Czubala M, Ferris RG, Koppe E, Haffner C, et al. Differential recognition of HIV-stimulated IL-1β and IL-18 secretion through NLR and NAIP signalling in monocyte-derived macrophages. *PLoS Pathog* (2021) 17(4):e1009417. doi: 10.1371/journal.ppat.1006196

29. Vespa GN, Cunha FQ, Silva JS. Nitric oxide is involved in control of *Trypanosoma cruzi*-induced parasitemia and directly kills the parasite. *vitro. Infect Immun* (1994) 62:5177–82. doi: 10.1128/iai.62.11.5177-5182.1994

30. Mariathasan S, Weiss DS, Newton K, McBride J, O'Rourke K, Roose-Girma M, et al. Cryopyrin activates the inflammasome in response to toxins and ATP. *Nature* (2006) 440:228–32. doi: 10.1038/nature04515

31. Lara-Tejero M, Sutterwala FS, Ogura Y, Grant EP, Bertin J, Coyle AJ, et al. Role of the caspase-1 inflammasome in Salmonella typhimurium pathogenesis. *J Exp Med* (2006) 203:1407–12. doi: 10.1084/jem.20060206

32. Pacheco A, de OL, Amaral MP, de Farias IS, Bottino LZMF, Bortoluci KR. Concomitant isolation of primary astrocytes and microglia for protozoa parasite infection. *JoVE* (2020), e60680. doi: 10.3791/60680

33. Qu Y, Misaghi S, Izrael-Tomasevic A, Newton K, Gilmour LL, Lamkanfi M, et al. Phosphorylation of NLRC4 is critical for inflammasome activation. *Nature* (2012) 490:539e542. doi: 10.1038/nature11429

34. Swanson KV, Deng M, Ting JPY. The NLRP3 inflammasome: molecular activation and regulation to therapeutics. *Nat Rev Immunol* (2019) 19(8):477–489. doi: 10.1038/s41577-019-0165-0

35. Campden RI, Zhang Y. The role of lysosomal cysteine cathepsins in NLRP3 inflammasome activation. *Arch Biochem Biophys* (2019) 670:32–42. doi: 10.1016/j.abb.2019.02.015

36. Lage SL, Buzzo CL, Amaral EP, Matteucci KC, Massis LM, Icimoto MY, et al. Cytosolic flagellin-induced lysosomal pathway regulates inflammasome-dependent and -independent macrophage responses. *Proc Natl Acad Sci U. S. A.* (2013) 110:E3321–30. doi: 10.1073/pnas.1305316110

37. Branco LM, Amaral MP, Boekhoff H, de Lima ABF, Farias IS, Lage SL, et al. Lysosomal cathepsins act in concert with Gasdermin-D during NAIP/NLRC4-dependent IL-1β secretion. *Cell Death Dis 2022 1312* (2022) 13:1–10. doi: 10.1073/pnas.1305316110

38. Menu P, Vince JE. The NLRP3 inflammasome in health and disease: The good, the bad and the ugly. *Clin Exp Immunol* (2011) 166(1):1–15. doi: 10.1111/j.1365-2249.2011.04440.x

39. von Moltke J, Ayres JS, Kofoed EM, Chavarría-Smith J, Vance RE. Recognition of bacteria by inflammasomes. *Annu Rev Immunol* (2013) 31:73–106. doi: 10.1146/annurev-immunol-032712-095944

40. Lopes AH, Talbot J, Silva RL, Lima JB, França RO, Verri WA Jr, et al. Peripheral NLCR4 inflammasome participates in the genesis of acute inflammatory pain. *Pain* (2015) 156:451–9. doi: 10.1097/01.j.pain.0000460322.72396.53

41. Ip WKE, Medzhitov R. Macrophages monitor tissue osmolarity and induce inflammatory response through NLRP3 and NLRC4 inflammasome activation. *Nat Commun* (2015) 6:6931–42. doi: 10.1038/ncomms7931

42. Wang S, Narendran S, Hirahara S, Varshney A, Pereira F, Apicella I, et al. DDX17 is an essential mediator of sterile NLRC4 inflammasome activation by retrotransposon RNAs. *Sci Immunol* (2021) 6(66):eabi4493. doi: 10.1126/sciimmunol.abi4493

43. Liu L, Chan C. IPAF inflammasome is involved in interleukin-1beta production from astrocytes, induced by palmitate; implications for Alzheimer's Disease. *Neurobiol Aging* (2014) 35:309–21. doi: 10.1016/j.neurobiolaging.2013.08.016

44. Saadi M, Karkhah A, Pourabdolhossein F, Ataie A, Monif M, Nouri HR, et al. Involvement of NLRC4 inflammasome through caspase-1 and IL-1β augments neuroinflammation and contributes to memory impairment in an experimental model of Alzheimer's like disease. *Brain Res Bull* (2020) 154:81–90. doi: 10.1016/j.brainresbull.2019.10.010

45. Denes A, Coutts G, Lénárt N, Cruickshank SM, Pelegrin P, Skinner J, et al. AIM2 and NLRC4 inflammasomes contribute with ASC to acute brain injury independently of NLRP3. *Proc Natl Acad Sci U. S. A.* (2015) 112:4050–5. doi: 10.1016/j.brainresbull.2019.10.010

46. Poh L, Kang SW, Baik SH, Ng GYQ, She DT, Balaganapathy P, et al. Evidence that NLRC4 inflammasome mediates apoptotic and pyroptotic microglial death following ischemic stroke. *Brain. Behav Immun* (2019) 75:34–47. doi: 10.1016/j.bbi.2018.09.001

47. Yuan F, Kolb R, Pandey G, Li W, Sun L, Liu F, et al. Involvement of the NLRC4-inflammasome in diabetic nephropathy. *PloS One* (2016) 11:e0164135. doi: 10.1371/journal.pone.0164135

48. Hu B, Elinav E, Huber S, Booth CJ, Strowig T, Jin C, et al. Inflammation-induced tumorigenesis in the colon is regulated by caspase-1 and NLRC4. *Proc Natl Acad Sci U.S.A.* (2010) 107:21635–40. doi: 10.1371/journal.pone.0164135

49. Kolb R, Phan L, Borcherding N, Liu Y, Yuan F, Janowski AM, et al. Obesity-associated NLRC4 inflammasome activation drives breast cancer progression. *Nat Commun* (2016) 7:13007. doi: 10.1038/ncomms13007

50. Lim J, Kim MJ, Park Y, Ahn JW, Hwang SJ, Moon JS, et al. Upregulation of the NLRC4 inflammasome contributes to poor prognosis in glioma patients. *Sci Rep* (2019) 9(1):7895. doi: 10.1038/s41598-019-44261-9

51. Rayamajhi M, Zak DE, Chavarria-Smith J, Vance RE, Miao EA. Cutting edge: mouse NAIP1 detects the type III secretion system needle protein. *J Immunol* (2013) 191(8):3986–9. doi: 10.4049/jimmunol.1301549

52. Yang J, Zhao Y, Shi J, Shao F. Human NAIP and mouse NAIP1 recognize bacterial type III secretion needle protein for inflammasome activation. *Proc Natl Acad Sci U. S. A.* (2013) 110(35):14408–13. doi: 10.1073/pnas.1306376110

53. Reyes Ruiz VM, Ramirez J, Naseer N, Palacio NM, Siddarthan IJ, Yan BM, et al. Broad detection of bacterial type III secretion system and flagellin proteins by the human NAIP/NLRC4 inflammasome. *Proc Natl Acad Sci U.S.A.* (2017) 114:13242–7. doi: 10.1073/pnas.1306376110

54. Qu Y, Misaghi S, Newton K, Maltzman A, Izrael-Tomasevic A, Arnott D, et al. NLRP3 recruitment by NLRC4 during Salmonella infection. *J Exp Med* (2016) 213:877–85. doi: 10.1084/jem.20132234

55. McCoy AJ, Koizumi Y, Higa N, Suzuki T. Differential regulation of caspase-1 activation via NLRP3/NLRC4 inflammasomes mediated by aerolysin and type III secretion system during Aeromonas veronii infection. *J Immunol* (2010) 185:7077–84. doi: 10.4049/jimmunol.1002165

56. Broz P, Newton K, Lamkanfi M, Mariathasan S, Dixit VM, Monack DM. Redundant roles for inflammasome receptors NLRP3 and NLRC4 in host defense against Salmonella. *J Exp Med* (2010) 207:1745–55. doi: 10.1084/jem.20100257

57. Man SM, Hopkins LJ, Nugent E, Cox S, Glück IM, Tourlomousis P, et al. Inflammasome activation causes dual recruitment of NLRC4 and NLRP3 to the same macromolecular complex. *Proc Natl Acad Sci U. S. A.* (2014) 111:7403–8. doi: 10.1084/jem.20100257

58. Pacheco AL, Vicentini G, Matteucci KC, Ribeiro RR, Weinlich R, Bortoluci KR. The impairment in the NLRP3-induced NO secretion renders astrocytes highly permissive to *T. cruzi* replication. *J Leukoc. Biol* (2019) 106(1):201–7. doi: 10.1002/JLB.4AB1118-416RR

59. Buzzo CL, Campopiano JC, Massis LM, Lage SL, Cassado AA, Leme-Souza R, et al. A novel pathway for inducible nitric-oxide synthase activation through inflammasomes. *J Biol Chem* (2010) 285:32087–95. doi: 10.1074/jbc.M110.124297

60. Buzzo CDL, Medina T, Branco LM, Lage SL, Ferreira LCDS, Amarante-Mendes GP, et al. Epigenetic regulation of nitric oxide synthase 2, inducible (Nos2) by NLRC4 inflammasomes involves PARP1 cleavage. *Sci Rep* (2017) 7(1):41686. doi: 10.1038/srep41686

61. Hornung V, Bauernfeind F, Halle A, Samstad EO, Kono H, Rock KL, et al. Silica crystals and aluminum salts activate the NALP3 inflammasome through phagosomal destabilization. *Nat Immunol* (2008) 9:847–56. doi: 10.1038/ni.1631

62. Duewell P, Kono H, Rayner KJ, Sirois CM, Vladimer G, Bauernfeind FG, et al. NLRP3 inflammasomes are required for atherogenesis and activated by cholesterol crystals. *Nature* (2010) 464:1357–61. doi: 10.1038/nature08938

63. Orlowski GM, Sharma S, Colbert JD, Bogyo M, Robertson SA, Kataoka H, et al. Frontline Science: Multiple cathepsins promote inflammasome-independent, particle-induced cell death during NLRP3-dependent IL-1β activation. *J Leukoc. Biol* (2017) 102:7–17. doi: 10.1189/jlb.3HI0316-152R

64. Orlowski GM, Colbert JD, Sharma S, Bogyo M, Robertson SA, Rock KL. Multiple cathepsins promote pro-IL-1β Synthesis and NLRP3-Mediated IL-1β Activation. *J Immunol* (2015) 195:1685–97. doi: 10.4049/jimmunol.1500509

65. Mott GA, Burleigh BA. The role of host cell lysosomes in *Trypanosoma cruzi* invasion. *Subcell. Biochem* (2008) 47:165–73. doi: 10.1016/j.abb.2019.02.015

66. Caradonna KL, Burleigh BA. Mechanisms of host cell invasion by *Trypanosoma cruzi*. *Adv Parasitol* (2011) 76:33–61. doi: 10.1016/B978-0-12-385895-5.00002-5

Blockade of mGluR5 in astrocytes derived from human iPSCs modulates astrocytic function and increases phagocytosis

Izabella B. Q. de Lima[1†], Pablo L. Cardozo[1†], Julia S. Fahel[1], Juliana P. S. Lacerda[1], Aline S. Miranda[2], Antônio L. Teixeira[3] and Fabiola M. Ribeiro [ID][1*]

[1]Department of Biochemistry and Immunology, Institute of Biological Sciences (ICB), Universidade Federal de Minas Gerais, Belo Horizonte, Brazil, [2]Department of Morphology, Institute of Biological Sciences (ICB), Universidade Federal de Minas Gerais, Belo Horizonte, Brazil, [3]Neuropsychiatry Program, Department of Psychiatry and Behavioral Sciences, University of Texas Health Science Center at Houston, Houston, TX, United States

TNF-α is essential for induction and maintenance of inflammatory responses and its dysregulation is associated with susceptibility to various pathogens that infect the central nervous system. Activation of both microglia and astrocytes leads to TNF-α production, which in turn triggers further activation of these cells. Astrocytes have been implicated in the pathophysiology of a wide range of neurodegenerative diseases with either harmful or protective roles, as these cells are capable of secreting several inflammatory factors and also promote synapse elimination and remodeling. These responses are possible because they sense their surroundings via several receptors, including the metabotropic glutamate receptor 5 (mGluR5). Under neuroinflammatory conditions, mGluR5 activation in astrocytes can be neuroprotective or have the opposite effect. In the current study, we investigated the role of mGluR5 in hiPSC-derived astrocytes subjected to pro-inflammatory stimulation by recombinant TNF-α (rTNF-α). Our results show that mGluR5 blockade by CTEP decreases the secreted levels of pro-inflammatory cytokines (IL-6 and IL-8) following short rTNF-α stimulation, although this effect subsides with time. Additionally, CTEP enhances synaptoneurosome phagocytosis by astrocytes in both non-stimulated and rTNF-α-stimulated conditions, indicating that mGluR5 blockade alone is enough to drive synaptic material engulfment. Finally, mGluR5 antagonism as well as rTNF-α stimulation augment the expression of the reactivity marker SERPINA3 and reduces the expression of synaptogenic molecules. Altogether, these data suggest a complex role for mGluR5 in human astrocytes, since its blockade may have beneficial and detrimental effects under inflammatory conditions.

KEYWORDS

mGluR5, astrocyte, hiPSC, phagocytosis, TNFα

1 Introduction

Astrocytes are the most abundant glial cells of the mammalian central nervous system (CNS), playing important roles in CNS physiology and being implicated in the pathology of a diverse array of neurological diseases (1, 2). Astroglia is formed by a highly heterogeneous population of astrocytes (3). These cells may assume a reactive phenotype in pathological contexts, releasing inflammatory factors that might impact disease outcomes either in a detrimental or beneficial manner (4, 5). One important role played by glial cells is the phagocytosis of dead cells, synapses and myelin (6, 7). Although aberrant synapse pruning was shown to contribute to dementia (8), elimination of dystrophic synapses and dendrites, as well as phagocytosis of extracellular protein aggregates, such as amyloid-β (Aβ) (9, 10), is essential for proper brain function. Another important function of astrocytes is to promote synapse remodelling by secreting synaptogenic molecules, including brain derived neurotrophic factor (BDNF) (11), glypican-4 (GPC4) (12), hevin (13), and thrombospondins (TSPs) (13, 14).

The metabotropic glutamate receptor type 5 (mGluR5) is a G-protein-coupled receptor (GPCR) whose involvement in neurodegenerative disorders has been widely studied (15). As in neurons, mGluR5 stimulation in astrocytes activates the $G\alpha_{q/11}$/PLCβ/IP$_3$ pathway, increasing intracellular Ca^{2+}, which facilitates glutamate release (16–19). Moreover, stimulation of this receptor activates non-canonical cell signalling pathways, including mitogen-activated protein kinase (MAPK) and phospholipase D (PLD) (20, 21). Although mGluR5 expression in astrocytes declines postnatally (22, 23), previous works have shown an upregulation of this receptor in astrocytes in neurological diseases that most commonly affect adults or the elderly, such as amyotrophic lateral sclerosis (ALS) (24), multiple sclerosis (MS) (25), and Alzheimer's disease (AD) (26), suggesting a relevant role of mGluR5 in gliopathology. In microglia, the activation of mGluR5 has an anti-inflammatory effect, decreasing microglial expression of tumor necrosis factor-α (TNF-α) and production of reactive oxygen species (27, 28). However, the role of mGluR5 in astrocytes remains controversial, as some studies indicate that activation of astrocytic mGluR5 following injury is protective for neighbouring cells as it triggers the release of growth factors and synaptogenic molecules (29, 30), whereas others have shown that mGluR5 activation is harmful as it increases the production of inflammatory mediators (31, 32). For instance, the inhibition of mGluR5 by MPEP prevents methamphetamine-induced increase in IL-6 and IL-8 in a human astroglia cell line (32). Conversely, inhibition of mGluR5 in murine astrocytes can reduce the expression of IL-1β and MCP-1 (33). Furthermore, it has been shown that the activation of mGluR5 by DHPG has no effect on the IL-1β-induced expression of IL-6 in human astrocytes (34). Despite all these studies investigating the role of astrocytic mGluR5 in neurological disorders, it has been challenging to successfully replicate these findings in clinical trials. This discrepant results can be partially explained by the molecular differences between human and murine glial cells (35, 36). For instance, it has been pointed that these cells display species-specific gene expression profiles upon poly-I:C or TNF-α stimulation, with human astrocytes showing stronger immune response compared to their murine counterparts (35). Thus, more studies are needed to investigate how mGluR5 can impact the activation of human astrocytes and the production of inflammatory and synaptogenic mediators.

Astrocytes derived from human induced pluripotent stem cells (hiPSCs) are widely used to study cell physiology, as well as an *in vitro* model of neurological diseases (37–40). In this study we used cultured hiPSC-derived astrocytes to investigate the influence of mGluR5 on the astrocytic response to inflammatory stimulation with recombinant TNF-α (rTNF-α). TNF-α is essential for induction and maintenance of inflammatory responses and its dysregulation is associated with susceptibility to various CNS pathogens (41, 42). Moreover, reactive astrocytes lead to TNF-α production, which in turn triggers further activation of these cells. To modulate mGluR5 activity, we employed the mGluR5 negative allosteric modulator (NAM) CTEP, which is a potent and highly specific drug that acts as an inverse agonist of mGluR5, effectively blocking its constitutive activity (43). We show that, in the presence of rTNF-α, mGluR5 inhibition decreases the secreted levels of IL-6 and IL-8 and increases the expression of the reactive astrocyte marker *SERPINA3*. Since reactive astrogliosis can display different functional profiles (44) and given its role in synaptic turnover, a process altered in many neurological diseases (45), we also assessed the rate of phagocytosis of synaptoneurosomes by astrocytes and the expression of synaptogenic proteins. We show that CTEP enhanced phagocytosis regardless of rTNF-α, while both CTEP and rTNF-α downregulated the expression of synaptogenic molecules. Thereby, the current results reveal the multifaceted role of mGluR5 in astrocyte reactivity and function, highlighting its potential for both detrimental and beneficial effects depending on the specific context.

2 Materials and methods

2.1 Human-induced pluripotent stem cell line and cell culture maintenance

The 7889SA cell line was obtained from the New York Stem Cell Foundation (NYSCF ID CO0002-01-SV-003) and described previously (46). hiPSCs were maintained on 6-well plates coated with Geltrex (Gibco, cat no. A1413302) in StemFlex Medium (Gibco, cat no. A3349301). Upon reaching 80-90% confluence, cells were incubated for 3-4 min in 500 μM EDTA (Sigma, cat no. EDS) in PBS, dissociated in clumps and seeded into new 6-well Geltrex-coated plates for expansion. Media was changed every 48h.

2.2 Human astrocytes differentiation

Astrocytes were differentiated from hiPSCs as previously described (38). hiPSCs were dissociated into single cells using StemPro Accutase (Gibco, cat no. A1110501) and seeded into 6-

well Geltrex-coated plates at 3×10^4 cells/cm^2 in StemFlex Medium supplemented with 10 µM Rho-associated protein kinase (ROCK) inhibitor Thiazovivin (Sigma Aldrich, cat no. SML1045). In order to start differentiation (day 0), medium was changed to PSC Neural Induction Medium containing Neurobasal Medium (Gibco, cat no. 21103-049), Neural Induction Supplement (Gibco, cat no. A1647701) and 1% penicillin-streptomycin solution (Gibco, cat no. 15410-122). Media was changed every 48 h. On day 7, NSCs were dissociated with Accutase and plated at 1×10^5 cells/cm^2 in 60 mm Geltrex-coated dishes in NSC Expansion Medium containing 50% Advanced DMEM/F12 (Gibco, cat no. 12634010), 50% Neurobasal Medium, Neural Induction Supplement and 1% penicillin-streptomycin solution supplemented with 10 µM ROCK inhibitor Thiazovivin. Media changes were performed every 48h. When NSCs reached 90% confluence, cells were dissociated with Accutase and seeded at 5×10^4 cells/cm^2 in 25 cm^2 Geltrex-coated culture flasks in Astrocyte Induction Medium containing DMEM/F12 Medium (Gibco, cat no.12400024), N2 supplement (Gibco, cat no. 17502048), 1% fetal bovine serum (FBS) (Gibco, cat no. 12657-029) and 1% antibiotic-antimycotic solution (Gibco, cat no.15240112). Media was changed every 48 h for 21 days. During this period, upon reaching full confluence, cells were expanded at a ratio of 1:3 using Accutase to 75 cm^2 Geltrex-coated culture flasks. By the end of differentiation, media was switched to Astrocyte Maturation Medium (DMEM/F12, 10% FBS and 1% antibiotic-antimycotic solution) for an additional period of at least 5 weeks. During this period, media was changed twice a week and when reaching full confluence, cells were dissociated using Trypsin/EDTA 0,125% (Gibco, cat no. 25200072) and expanded to 175 cm^2 culture flasks at a ratio of 1:2 (without Geltrex coating). Cells were maintained under standard culture conditions (95% relative humidity and 5% CO2 at 37°C) and tested routinely for *Mycoplasma* contamination, as previously described (47).

2.3 Drug treatment

After nine weeks of maturation, upon reaching 100% confluence in 175 cm^2 culture flasks, hiPSC-derived astrocytes were dissociated with Trypsin/EDTA 0.125% (Gibco, cat no. 25200072) and seeded at 1×10^4 cells/cm^2 in 6-well plates. After 5 days in culture, cells were washed three times with PBS, DMEM/F12 media was replenished, and astrocytes were serum starved for 24 h. Then, cells were treated with either 10 µM CTEP (Axon Medchem, cat no. Axon 1972) or vehicle (DMSO; Sigma-Aldrich, cat no. 41639) and subsequently stimulated with 10 ng/mL rTNF-α (BioLegend, cat no. 717904) for either 4h or 24 h. In the case of lipopolysaccharide (LPS) treatment, astrocytes were treated with either 0.1 or 1 µg/mL LPS (Sigma, cat no. L6529) for 24 h. Drugs were kept in the media throughout the whole experiment. After treatment, the supernatant was flash frozen and stored at -80°C until further use, and cells were collected with 1 mL of TRIzol^{TM} reagent (Invitrogen, cat no. 15596018), transferred to 1.5 mL microcentrifuge tubes and frozen at -80°C.

2.4 Quantitative RT-PCR

Total RNA was isolated using TRIzol^{TM} reagent as per manufacturer's instructions and resuspended in 12 µL of nuclease-free water. RNA concentration and quality was analyzed by spectrophotometer (Multiskan$^®$ GO, Thermo Scientific). cDNAs were prepared from 800 ng of total RNA extracted in a 20 µL final reverse transcription reaction. Quantitative RT-PCR (RT-qPCR) was performed with 10x diluted cDNA using Power SYBR$^®$ Green PCR Master Mix in the QuantStudio^{TM} 7 Flex real-time PCR system platform (Applied Biosystems$^®$). RT-qPCR assays were performed to quantify the mRNA levels of the following genes: *C3* (NM_000064.3); *IPO8* (NM_006390.3); *RPLP0* (NM_001002.3); *MERTK* (NM_006343.2); *ITGAV* (NM_001144999.3); *SERPINA3* (NM_001085.5); *VCAM1* (NM_001078.5); *S100A10* (NM_002966.3); *BDNF* (NM_170735.6); *GPC4* (NM_001448.3); *TSP1* (NM_003246.4), *FKBP5* (NM_001145775.3), *SERPING1* (NM_000062.3), *GBP2* (NM_004120.5), *NFATC3* (NM_173163.3), *NFATC4* (NM_001198967.3), and *GRM5* (NM_001384268.1). Primers were designed using the Primer3Plus Program (48). Primer sequences are listed in Table 1.

Previous verification of undesired secondary formations or dimers between primers were performed using "OligoAnalyser 3.1" tool (Integrated DNA Technologies$^©$), available at https://www.idtdna.com/calc/analyzer. All primers used in this work were validated by serial dilution assay and the reaction efficiency was calculated, comprising 90-110% (data not shown). Changes in gene expression were calculated by the $2^{-\Delta Ct}$ method, using the average of the housekeeping genes *IPO8* and *RPLP0* for normalization.

2.5 Immunofluorescence staining

After 5 weeks of maturation, hiPSC-derived astrocytes were plated onto acid-etched clean glass coverslips coated with 50 µg/mL poly-D-lysine (Sigma, cat no. P6407) in 24-well plates at 1×10^3 cells/cm^2 in Astrocytes Maturation Media. After 5 days in culture, cells were fixed for 15 min in 4% paraformaldehyde (PFA) (Sigma, cat no. 158127) diluted in PBS. Samples were permeabilized with 0.3% Triton X-100 (Labsynth, cat no. T2502) diluted in PBS (PBST) for 10 min and blocked with 2% Bovine Serum Albumin (BSA) (Sigma, cat no. A7906) diluted in PBST (blocking solution) for 1 h at room temperature. Then, cells were washed three times with PBS and incubated overnight at 4°C with the following primary antibodies diluted in blocking solution: anti-mGluR5 (1:100, Millipore, cat no. AB5675), anti-S100β (1:200, Abcam, cat no. ab52642) and anti-GFAP (1:200, Cell Signaling, cat no. 12389). After incubation, cells were washed three times with PBS and incubated for 1 h at room temperature with the following secondary antibody and staining reagents diluted in blocking solution: anti-Rabbit IgG Alexa Fluor 488 (1:400, Invitrogen, cat no. A-11008), Hoechst (1:500, Invitrogen, cat no. H3570) and Alexa Fluor 633 Phalloidin (1:1000, Invitrogen, cat no. A22284). Coverslips were washed

TABLE 1 qPCR primer sequences.

Gene	Forward primer (5'-3')	Reverse primer (5'-3')
C3	CTGCCCAGTTTCGAGGTCAT	CGAGCCATCCTCAATCGGAA
IPO8	TCCGAACTATTATCGACAGGACC	GTTCAAAGAGCCGAGCTACAA
RPLP0	TTAAACCCTGCGTGGCAATC	ATCTGCTTGGAGCCCACATT
MERTK	TGGCGTAGAGCTATCACTG	CTGGCGTGAGGAAGGGATAA
ITGAV	AATCTTCCAATTGAGGATATCAC	AAAACAGCCAGTAGCAACAAT
SERPINA3	CCTGAGGCAGAGTTGAGAATGG	TCAAGTGGGCTGTTAGGGTG
VCAM1	CGAACCCAAACAAAGGCAGA	ACAGGATTTTCGGAGCAGGA
S100A10	AACAAAGGAGGACCTGAGAGTAC	CTTTGCCATCTCTACACTGGTCC
BDNF	AGTTGGGAGCCTGAAATAGTGG	AGGATGCTGGTCCAAGTGGT
GPC4	GTCAGCGAACAGTGCAATCAT	ACATTTCCCACCACGTAGTAAC
TSP1	GCCAACAAACAGGTGTGCAA	GCAGATGATGCCATTGCCAG
IL-6	AGAGGCACTGGCAGAAAAC	TGCAGGAACTGGATCAGGAC
IL-8	GAGAGTGATTGAGAGTGGAC	GAATTCTCAGCCCTCTTCAAA
GBP2	AATTAGGGGCCCAGTTGGAAG	AAGAGACGGTAACCTCCTGGT
NFATC3	GCGGCCTGCAGATCTTGAGC	TGATGTGGTAAGCAAAGTGGTGTGGT
NFATC4	CCCCGAGTACAGCAACAAGA	CCTCTTTGCAGATCACAGGC
GRM5	ATGCCGGGTGACATCATTATT	TGAATGCCATACTGTTCACGG

three times as mentioned above and mounted on clean glass slides with DAKO Mounting Medium (Agilent Technologies, cat no. S302380-2). Astrocytes were imaged using a Nikon A1 Laser Confocal Microscope (CGB, UFMG, Brazil).

2.6 Synaptoneurosomes isolation and staining

Housing and all methods and experimentations were carried out in compliance with the ARRIVE guidelines (49) and according to the guidelines of the Brazilian National Council of Control of Animal Experimentation (CONCEA) and approved by the Ethics Committee on Animal Use (CEUA) of Federal University of Minas Gerais, under the protocol number CEUA #120/2017. A 12-month-old male wild-type C57BL/6 mouse was obtained from UFMG Central Animal Facility. Mouse brain was dissected, weighed, and cut into sections of approximately 100 mg that were individually transferred to an ice-cold sterile Dounce homogenizer with 1 mL of synaptoneurosomes isolation buffer (SIB) (10 mM HEPES, 1 mM EDTA, 2 mM EGTA, 0.5 mM DTT and protease inhibitors, pH 7.0; sterile-filtered) (50). Tissue was broken with 10 slow strokes, homogenates were transferred to 1.5 mL microcentrifuge conical tubes and centrifuged at 1200 g for 10 min at 4°C. The supernatant was transferred to new 1.5 mL microcentrifuge tubes and centrifuged at 15000 g for 20 min at 4°C. The pelleted debris fraction and a small aliquot of the supernatant (synaptoneurosomal homogenate) were collected in SIB and stored at -80°C for later validation. The supernatant (cytosolic fraction) was collected into new 1.5 mL microcentrifuge tubes and frozen at -80°C and the pelleted synaptoneurosomes resuspended in SIB + 5% DMSO (Sigma, cat no. D8418), aliquoted and frozen at -80°C until later use.

On the day of synaptoneurosomal engulfment assay, synaptoneurosome aliquots were thawed and their protein concentration determined via the Bradford Protein Assay (Bio-rad, cat no. 5000205). Synaptoneuromes were spun down by centrifugation at 15000 g for 20 min at 4°C, supernatant was discarded, and the pellet resuspended in 2 µM Vybrant CM-Dil solution (Invitrogen, cat no. V22888) diluted in room temperature sterile PBS. Staining was performed according to manufacturer instructions. CM-Dil-labeled synaptoneurosomes were spun down as described above, washed twice with ice-cold PBS to remove fluorescent dye excess and resuspended in ice-cold PBS adjusting its concentration to 0.25 µg/µL. Synaptoneurosomes were kept on ice and protected from light until its use in the aforementioned assay. All procedures were carried out under sterile conditions.

2.7 Synaptoneurosome engulfment assay and analysis

hiPSC-derived astrocytes were plated onto acid-etched clean glass coverslips coated with 50 µg/mL poly-D-lysine in 24-well plates at 5.5×10^3 cells/cm^2 in Astrocytes Maturation Media. After 5 days in culture, cells were washed three times with PBS and stained with 10 µM CellTracker Blue CMF$_2$HC Dye (Invitrogen, cat no. C12881) diluted in warm DMEM/F12 without FBS and incubated for 45 min in the cell culture incubator. The staining solution was

removed, fresh DMEM/F12 media was replenished, and astrocytes serum starved for 22 h. On the following day, cells were pre-treated for 1 h with either 10 μM CTEP or vehicle (DMSO) and subsequently stimulated with 10 ng/mL rTNF-α for an extra hour. Then, 1.875 μg (7.5 μL) of CM-Dil-labeled synaptoneurosomes were added into each well and incubated for 24 h. After incubation, cells were washed twice with room temperature PBS to remove non-engulfed material and fixed for 15 min with 4% PFA solution diluted in PBS. Coverslips were washed three times as mentioned above and mounted on clean glass slides with DAKO Mounting Medium. Images were acquired using a Nikon A1 Laser Confocal Microscope. All assays were carried out in duplicates and twice independently.

Images were analyzed using FIJI (v. 1.53t) and CellProfiler (v. 4.2.5) software programs. Briefly, CellTracker-labeled astrocytes and CM-Dil-labeled synaptoneurosomes corresponding channels were split and images pre-processed using File S1 and File S2 macros in FIJI, respectively, saved and exported in .*tif* format. Pre-processed .*tif* files were imported to CellProfiler and analyzed using the File S3 pipeline. Phagocytic Index (PI) was calculated for each cell using the formula below:

$$PI = \frac{Engulfed \quad synaptoneurosomes \quad area \quad (\mu m^2)}{Total \quad cell \quad area \quad (\mu m^2)}$$

Orthogonal projections and 3D rendering (Supplementary Figure S5 and Movie S1) of z-stacks were generated using FIJI and FluoRender (v. 2.29.2), respectively.

2.8 Immunoblotting

Protein concentration of synaptoneurosomal preparation fractions (pelleted debris, synaptoneurosomal homogenate, cytosolic fraction and isolated synaptoneurosomes) was measured using the Bradford Protein Assay. Twenty-five μg of each fraction was diluted in Laemmli Sample Buffer, boiled at 95°C for 5 min and resolved in 10% SDS-PAGE. Proteins were transferred onto a 0.45 μm nitrocellulose membrane (Bio-Rad, cat no. 1620115), blocked with 5% BSA and 0.1% Tween-20 (Labsynth, cat no. T1028) diluted in TBS (TBST) for 1 h at room temperature, followed by overnight incubation at 4°C with the following primary antibodies in 3% BSA solution diluted in TBST: anti-syntaxin1 (1:200, Santa Cruz, cat no. sc-12736), anti-Homer (1:500, Santa Cruz, sc-8921) and anti-vinculin (1:10000, Abcam, ab129002). After incubation, primary antibodies were removed, membranes washed three times with TBST and incubated for 1 h at room temperature with secondary antibodies in 3% free-fat milk diluted in TBST: HRP-conjugated anti-mouse IgG (1:2500, Millipore, cat no. AP308P), HRP-conjugated anti-rabbit IgG (1:2500, Bio-Rad, cat no. 1706515) and HRP-conjugated anti-goat IgG (1:2500, Santa Cruz, sc-2354). Afterwards, membranes were washed three times as already described and incubated for 5 min with ECL Prime Western Blot Detection Reagent (Cytiva, cat no. RPN2232) for chemiluminescence detection using the ImageQuant LAS 4000 (GE Healthcare) platform.

2.9 Cytokine quantification

Cytokines were quantified in cell culture supernatants by flow cytometry using the BD Cytometric Bead Array Human Inflammatory Cytokines Kit (Becton, Dickinson and company - BD Biosciences, cat no. 551811), according to manufacturer's instructions. Briefly, equal amounts of each capture bead for human IL-1β, IL-6, IL-8, IL-10, TNF-α and IL12-p70 were mixed into a single tube. Fifty μL of the capture beads mix were added to assay tubes followed by addition of 50 μL of cell culture supernatants or cytokine standard dilutions. Then, 50 μL of PE detection reagent were added and assay tubes were incubated protected from light for 3 hours at room temperature. After incubation, samples were washed with 1 mL of wash buffer and tubes were centrifuged at 200 **g** for 5 minutes. Supernatants were aspirated and discarded and the bead pellets were resuspended in 300 μL of wash buffer. Sample acquisition was performed on the FACS Aria Fusion (BD Biosciences). The CBA Analysis Software (BD Biosciences) was used for data analysis based on standard concentration curves and the results were expressed as pg/mL.

2.10 Statistical analyses

Statistical analyses and data plots were performed using the GraphPad Prism (v. 8.0.1) software. Two-way ANOVA, followed by Tukey's multiple comparison tests with confidence level set to 0.95 ($\alpha = 0.05$) as the lowest accepted limit was carried out for all experiments, unless otherwise stated. For the synaptoneurosomes engulfment assay, the Kolmogorov-Smirnov test was executed, indicating the data followed a lognormal distribution. A generalized linear model fitted in the lognormal distribution, followed by Sidak's multiple comparison test with a confidence level set to 0.99 ($\alpha = 0.01$) as the lowest accepted limit was employed. This latter analysis was performed with the STATA (v. 14.0) software.

3 Results

3.1 mGluR5 blockade modulates rTNF-α-induced proinflammatory response in human astrocytes

Little is known about mGluR5 function in human cells. In order to investigate the role of mGluR5 in human astrocytes under proinflammatory conditions, astrocytes were differentiated from hiPSCs for four weeks and matured for an additional period of five weeks until they displayed strong expression of the canonical astrocytic markers GFAP (Figure 1A) and S100β (Figure 1B). In addition, these hiPSC-derived astrocytes also showed mGluR5 mRNA (Supplementary Figure S1) and protein (Figure 1C) expression. Stimulation of hiPSC-derived astrocytes with LPS 1 μg/mL led to only a marginal increase in IL-6 mRNA levels, whereas IL-8 expression remained unmodified (Supplementary Figure S2A
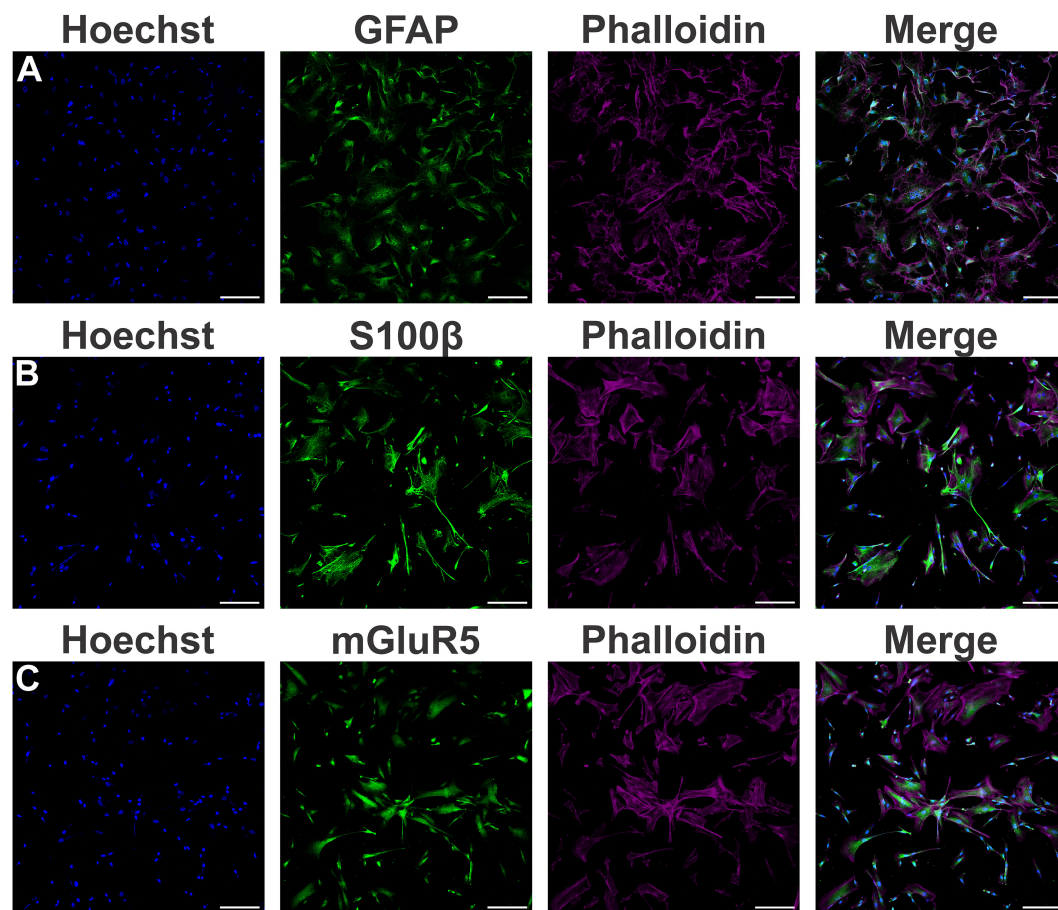
FIGURE 1
Characterization of astrocytes derived from human induced pluripotent stem cells (hiPSCs). **(A)** Shown are representative laser scanning confocal micrographs from hiPSC-derived astrocytes immunolabeled for phalloidin (magenta), GFAP (green), and Hoechst (blue). **(B)** Shown are representative laser scanning confocal micrographs from hiPSC-derived astrocytes immunolabeled for phalloidin (magenta), S100β (green), and Hoechst (blue). **(C)** Shown are representative laser scanning confocal micrographs from hiPSC-derived astrocytes immunolabeled for phalloidin (magenta), mGluR5 (green), and Hoechst (blue). Scale bar=200 μm.

and S2B). However, following stimulation with rTNF-α 10 ng/mL, astrocytes increased the mRNA levels of both IL-6 and IL-8 (Supplementary Figure S2C and S2D). Thus, we decided to employ rTNF-α in this study to induce an inflammatory response. To further evaluate cell activation, we stimulated astrocytes with rTNF-α 10 ng/mL and measured the production of inflammatory factors in the cell culture supernatant. Upon stimulation with rTNF-α, astrocytes quickly responded by up-regulating IL-6 and IL-8 levels (Figure 2), while IL-1β, IL-10 and IL-12p70 secretion was not detected. Both IL-6 and IL-8 secreted protein levels displayed a modest elevation at 4 h (Figures 2A, C), followed by a marked increase at 24 h post-stimulation (Figures 2B, D).

Blocking mGluR5 activity with CTEP (10 μM) led to a reduction in IL-6 and IL-8 secretion only at 4 h post-stimulation (Figures 2A, C), with this effect wearing off at 24h (Figures 2B, D). Moreover, treatment with either rTNF-α or CTEP did not alter mGluR5 expression in hiPSC-derived astrocytes (Supplementary Figure S1). These data indicate that mGluR5 antagonism can

prevent pro-inflammatory cytokine production by astrocytes during a short rTNF-α exposure.

3.2 mGluR5 modulates the expression of the reactive astrocyte marker SERPINA3 in human astrocytes

It has been proposed that astrocytes can be polarized to either an inflammatory and neurotoxic (A1 astrocytes) or a neuroprotective (A2 astrocytes) phenotype in response to external stimulation (51–53). Accordingly, we analyzed the expression of the general reactive astrocyte markers *SERPINA3*, *NFATC3*, and *NFATC4*; the A1-reactive markers *C3*, vascular cell adhesion molecule 1 (*VCAM-1*), *GBP2*, *FKBP5*, and *SERPING1*; and the A2-reactive marker *S100A10* (40, 51–53) in human astrocytes. rTNF-α stimulation promoted an augmentation in *SERPINA3*, *C3*, *VCAM-1*, and *GPB2* transcript levels at all tested timepoints (Figure 3), while the transcriptional levels of *NFATC3*, *NFATC4*,
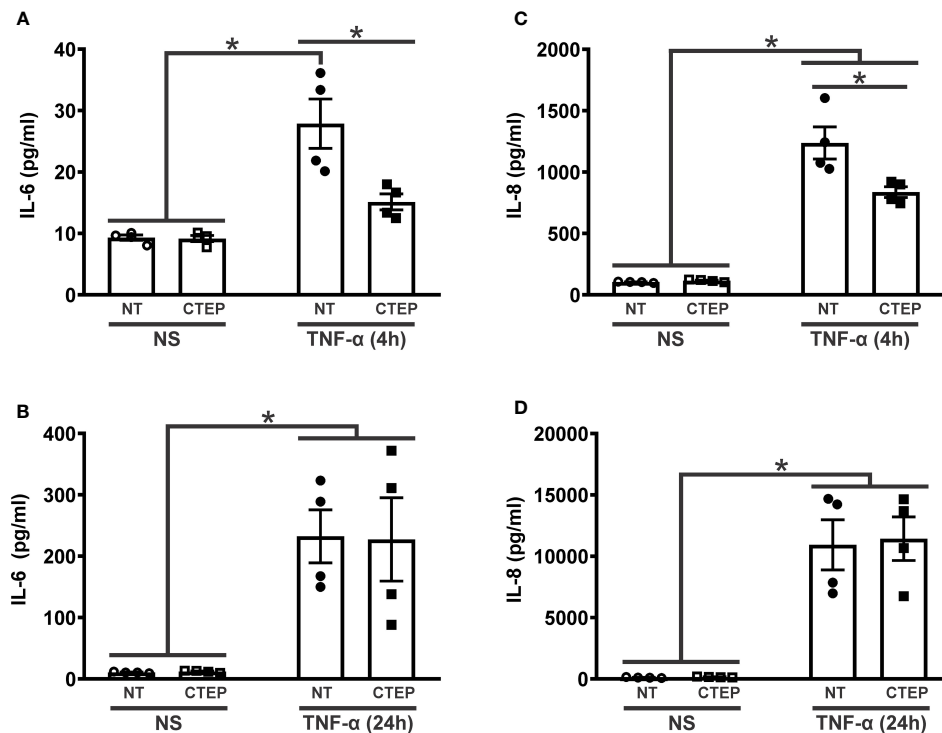
FIGURE 2

CTEP treatment reduces rTNF-α-induced expression of inflammatory factors. Graphs show protein quantification of IL-6 **(A)** and IL-8 **(C)** in the supernatant of hiPSC-derived astrocytes that were either unstimulated (NS) or stimulated with rTNF-α 10 ng/mL and treated with either vehicle (NT) or CTEP 10 μM for 4 h. Graphs show protein quantification of IL-6 **(B)** and IL-8 **(D)** in the supernatant of hiPSC-derived astrocytes that were either unstimulated (NS) or stimulated with rTNF-α 10 ng/mL and treated with either vehicle (NT) or CTEP 10 μM for 24 h. Protein levels were assessed by CBA, which was performed in duplicates. Data represents the means $\pm$ SEM, n=4-6. * (p<0.05) indicates significant differences.

FKBP5, *SERPING1*, and *S100A10* remained unchanged relative to non-stimulated astrocytes (Supplementary Figure S3). Notably, CTEP treatment led to an even greater up-regulation of *SERPINA3* gene expression in rTNF-α-stimulated astrocytes at all tested timepoints (Figures 3A, B). Additionally, CTEP treatment did not modify the expression of *FKBP5*, *SERPING1*, *NFATC3*, *NFATC4*, and *S100A10* (Supplementary Figure S3) or induce further alterations in the expression of the reactive astrocyte markers *C3*, *VCAM-1* and *GBP2*, either in the presence or in the absence of rTNF-α stimulation (Figures 3C–H). Therefore,
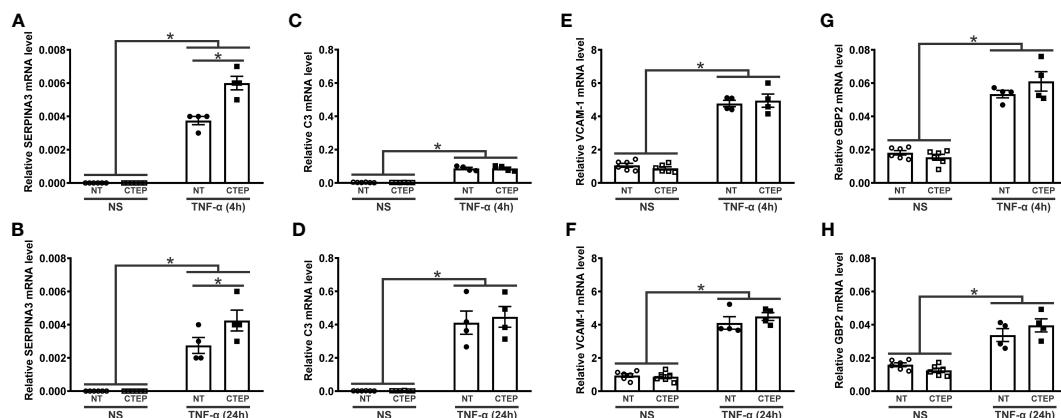
FIGURE 3

mGluR5 modulates the expression of the reactive astrocyte marker *SERPINA3* without modifying the expression of A1 and A2 markers. Graphs show mRNA levels of *SERPINA3* **(A)**, *C3* **(C)**, *VCAM-1* **(E)**, and *GBP2* **(G)** in hiPSC-derived astrocytes that were either unstimulated (NS) or stimulated with rTNF-α 10 ng/mL and treated with either vehicle (NT) or CTEP 10 μM for 4 h. Graphs show mRNA levels of *SERPINA3* **(B)**, *C3* **(D)**, *VCAM-1* **(F)**, and *GBP2* **(H)** in hiPSC-derived astrocytes that were either unstimulated (NS) or stimulated with rTNF-α 10 ng/mL and treated with either vehicle (NT) or CTEP 10 μM for 24 h. mRNA levels were assessed by quantitative RT-PCR, which was performed in triplicates and normalized to the average of *RPLP0* and *IPO8* mRNA levels. Data represents the means $\pm$ SEM, n=4-6. * (p<0.05) indicates significant differences.

mGluR5 blockade promotes a sustained upregulation of the reactive astrocyte marker *SERPINA3* under pro-inflammatory conditions, without changing the expression of A1- and A2-reactive markers.

3.3 CTEP treatment leads to enhanced synaptic material engulfment by human astrocytes

It has been shown that astrocyte reactivity affects its capacity to uptake synaptic material (52). Then, we decided to develop an assay to assess synaptic material phagocytosis by the hiPSC-derived astrocytes. First, we isolated synaptoneurosomes from mouse brain and evaluated if this procedure was effective in enriching both pre- and post-synaptic proteins. As seen in Supplementary Figure S4, both syntaxin-1 and Homer, respectively, pre- and postsynaptic markers, were enriched in the synaptoneurosomes fraction, while vinculin, a cytoskeleton protein, was mostly confined to the cytosolic compartment. Afterwards, we investigated whether the hiPSC-derived astrocytes could engulf

fluorescently-labeled synaptoneurosomes. Human astrocytes were capable to engulf synaptic material, as several red *puncta*, corresponding to fluorescently-labeled synaptoneurosomes, were observed inside the astrocyte cell bodies (Supplementary Figure S5 and Movie S1).

rTNF-α stimulation significantly increased astrocytic phagocytosis compared to non-stimulated cells (Figures 4A, C, E). As both rTNF-α and CTEP modified the expression of reactive astrocyte markers, next we analyzed whether mGluR5 blockade influences astrocytic phagocytosis. CTEP treatment led to enhanced synaptoneurosomal phagocytosis in human astrocytes in basal (no rTNF-α) conditions (Figures 4A, B, E). Interestingly, CTEP-treated astrocytes stimulated with rTNF-α showed even higher synaptic material engulfment (Figures 4C–E). In addition, both non-stimulated and rTNF-α-stimulated astrocytes that were pre-treated with 10 μM CTEP displayed similar synaptoneurosomal phagocytic level (Figures 4B, D, E). These data suggest that blocking mGluR5 activity is enough to enhance synaptic material engulfment by human astrocytes, even in the absence of proinflammatory stimulation.
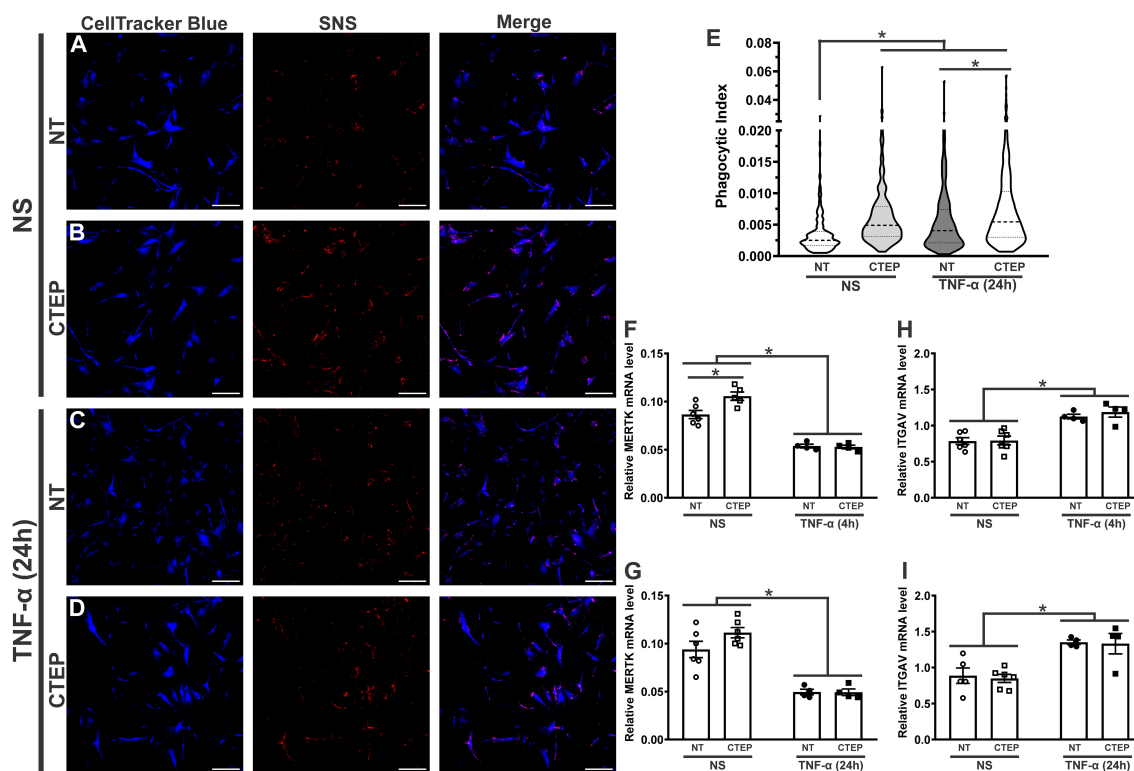
FIGURE 4
Both CTEP and rTNF-α increase astrocytic phagocytosis. Shown are representative laser scanning confocal micrographs from hiPSC-derived astrocytes labelled with CellTracker blue and synaptoneurosomes (SNS) labelled with Vybrant CM-Dil (red). hiPSC-derived astrocytes were either unstimulated (NS), and treated with either vehicle (NT) **(A)** or CTEP 10 μM **(B)**, or stimulated with rTNF-α 10 ng/mL, and treated with either vehicle (NT) **(C)** or CTEP 10 μM **(D)** for 24 h. Scale bar=200 μm. **(E)** Graph shows phagocytic index of hiPSC-derived astrocytes that were either unstimulated (NS) or stimulated with rTNF-α 10 ng/mL and treated with either vehicle (NT) or CTEP 10 μM for 24 h. Dashed line represents median and dotted lines represent interquartile interval, n=258-414. Graphs show mRNA levels of *MERTK* **(F)** or *ITGAV* **(H)** in hiPSC-derived astrocytes that were either unstimulated (NS) or stimulated with rTNF-α 10 ng/mL and treated with either vehicle (NT) or CTEP 10 μM for either 4 h. Graphs show mRNA levels of *MERTK* **(G)** or *ITGAV* **(I)** in hiPSC-derived astrocytes that were either unstimulated (NS) or stimulated with rTNF-α 10 ng/mL and treated with either vehicle (NT) or CTEP 10 μM for 24 h **(I)**. mRNA levels were assessed by quantitative RT-PCR, which was performed in triplicates and normalized to the average of *RPLP0* and *IPO8* mRNA levels. Data represents the means $\pm$ SEM, n=4-6. * (p<0.05) indicates significant differences.

Tyrosine-protein kinase mer (MERTK) and αvβ3/5 integrin, composed by the alpha chain V (ITGAV) and the beta 3/5 components, have been identified as important phagocytic receptors responsible for promoting synapse and myelin engulfment by astrocytes (10, 54, 55). Thus, we analyzed the expression of these receptors in human astrocytes upon rTNF-α stimulation and mGluR5 pharmacological inhibition. CTEP treatment increased *MERTK* gene expression in human astrocytes in basal conditions and this difference was statistically significant at the 4 h timepoint (Figures 4F, G). Conversely, rTNF-α stimulation reduced *MERTK* mRNA levels (Figures 4F, G), at the same time it enhanced *ITGAV* expression (Figures 4H, I) in all treatment groups at both 4 h and 24 h post-stimulation. CTEP treatment did not modify ITGAV expression (Figures 4H, I). Therefore, different phagocytic receptors might be involved in TNF-α- and mGluR5-induced phagocytosis by astrocytes.

3.4 rTNF-α stimulation and mGluR5 blockade decrease the expression of synaptogenic molecules in human astrocytes

The activation of mGluR5 can induce the expression of synaptogenic factors by astrocytes and promote synapse remodeling (30, 56, 57). To investigate whether mGluR5 could modulate the expression of synaptogenic molecules in an inflammatory context, hiPSC-derived astrocytes were subjected to rTNF-α stimulation for 4 h and 24 h followed by the analysis of gene expression of the synaptogenic factors *BDNF*, *GPC4* and *TSP1*. rTNF-α-stimulated astrocytes displayed reduced *BDNF* and *GPC4* mRNA levels at both timepoints (Figures 5A–D). *TSP1* expression,

on the other hand, was not affected by rTNF-α stimulation (Figures 5E, F). Furthermore, CTEP treatment had no impact in *BDNF* and *GPC4* expression when human astrocytes were subjected to rTNF-α stimulation (Figures 5A–D). However, CTEP treatment led to a reduction in *BDNF* expression under basal conditions (no rTNF-α) and this difference was significant in the case of the 4 h timepoint (Figures 5A, B). In addition, CTEP drove a reduction in *TSP1* gene expression, which was significantly different in the case of the 24 h timepoint (Figures 5E, F). Interestingly, this effect was observed regardless of rTNF-α-stimulation, indicating that mGluR5 antagonism alone is responsible for decreasing *TSP1* expression (Figure 5F). Altogether, these data indicate that both pro-inflammatory stimulation and mGluR5 negative allosteric modulation can dampen the production of synaptogenic molecules, which may contribute to the synaptic deficits often seen in neurodegenerative disorders (58, 59).

4 Discussion

It is well known that mGluR5 is involved in neuroinflammation and neurodegeneration processes and has hence been pointed as a potential pharmacological target for neuroprotection in a variety of neurodegenerative diseases (60). However, the literature has provided conflicting information concerning whether activation of neuronal mGluR5 is either neuroprotective or neurotoxic and whether mGluR5 stimulation in astrocytes would elicit protective or toxic effects on neighbouring cells. While some studies have reported positive effects of astrocytic mGluR5 activation following injury through the actions of growth factors and synaptogenic molecules (29, 30), others have shown that activation of this receptor may elicit harmful effects through the production of
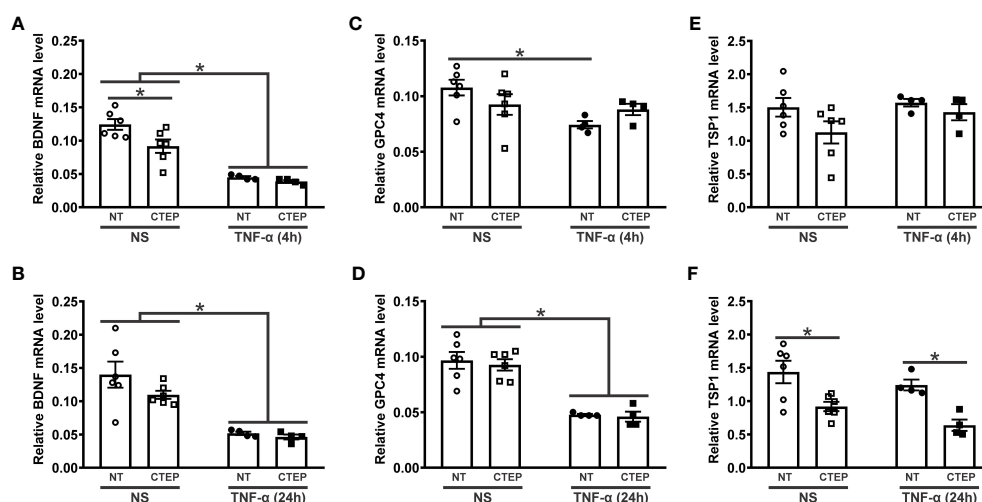
FIGURE 5
Both CTEP and rTNF-α decrease the expression of synaptogenic molecules. Graphs show mRNA levels of BDNF **(A)**, glypican-4 (GPC4) **(C)**, and trombospoindin-1 (TSP1) **(E)** in hiPSC-derived astrocytes that were either unstimulated (NS) or stimulated with rTNF-α 10 ng/mL and treated with either vehicle (NT) or CTEP 10 µM for 4 h. Graphs show mRNA levels of BDNF **(B)**, GPC4 **(D)**, and TSP1 **(F)** in hiPSC-derived astrocytes that were either unstimulated (NS) or stimulated with rTNF-α 10 ng/mL and treated with either vehicle (NT) or CTEP 10 µM for 24 h. mRNA levels were assessed by quantitative RT-PCR, which was performed in triplicates and normalized to the average of RPLP0 and IPO8 mRNA levels. Data represents the means ± SEM, n=4-6. * (p<0.05) indicates significant differences.

cytokines and inflammatory mediators (31, 32). Actually, it is possible that the utility of agonists or antagonists of the receptor may vary based on the underlying condition. For instance, stimulation of mGluR5 in astrocytes can lead to BDNF release, which supports myelin protein synthesis in the cuprizone-induced demyelination mouse model (30). On the other hand, in the case of AD, it was demonstrated that Aβ induces an increase in intracellular Ca^{2+} levels, which can be explained, at least in part, by an increase in mGluR5 expression in astrocytes (26, 61–65). Thus, in this case, mGluR5 antagonism is efficient to reverse Ca^{2+} rise, preventing Aβ-induced astrocytic Ca^{2+} signalling dysfunction (61, 63, 65). Moreover, mGluR5 blockade in cultured astrocytes derived from hSOD1^{G93A}, a transgenic mouse model of ALS, was shown to prevent cell death (31). Our results may shed some light on this dichotomy, as we showed that mGluR5 blockade by CTEP decreased the levels of inflammatory factors following short rTNF-α stimulation, with this effect wearing off at 24 h. This is in line with previous reports showing that mGluR5 antagonism prevents the secretion of IL-8 and IL-6 in an astrocytic cell line (32). However, it is surprising that CTEP augmented the gene expression of *SERPINA3*, which is a marker of reactive astrocytes. In addition, CTEP reduced the expression of trophic and synaptogenic molecules, such as *BDNF* and *TSP1*, and did not modify the expression of A1 and A2 reactive astrocyte markers.

Astrocytes play pivotal roles in neuronal survival and synapse remodelling by secreting trophic and synaptogenic factors, including *BDNF* (11), *GPC4* (12), hevin (13), and TSP (14). We showed that rTNF-α stimulation decreased the levels of *BDNF* and *GPC4*, without modifying *TSP1* mRNA levels. A previous study has shown that murine A1 astrocytes, under distinct inflammatory stimuli (IL-1α 3 ng/mL, TNF-α 30 ng/mL, and C1q 400 ng/mL), exhibit increased levels of GPC4 and TSP1/2 (52). While these contrasting results could be explained by differences in inflammatory stimuli, it is also possible that murine and human iPSC-derived astrocytes respond differently to inflammation, highlighting the importance of employing cell models relevant to humans. Interestingly, Although CTEP had an anti-inflammatory effect, mGluR5 blockade did not result in an increase in the expression of the aforementioned synaptogenic factors. In fact, CTEP decreased *BDNF* and *TSP-1* expression levels, which could contribute to further attenuation of synaptogenesis. These results were anticipated, as it has been shown that astrocytic mGluR5 is necessary for glypican-4, *BDNF* and *TSP1* secretion (30, 56, 57). In the case of BDNF, it has been shown that mGluR5 activation enhances the expression of this trophic factor by increasing the phosphorylation of CREB (66–69). In addition, previous data from our laboratory showed that mGluR5 genetic ablation leads to reduced dendritic spine numbers in a Huntington's disease mouse model (58), while mGluR5 positive allosteric modulation is capable of rescuing this phenotype (69), indicating that mGluR5 stimulation is synaptogenic. Thus, both rTNF-α and mGluR5 blockade may impair synaptogenesis and future studies will be important to determine whether either astrocyte conditioned media or co-culture of these astrocytes with neurons would lead to decreased number of synapses in human cells.

Phagocytosis is important to eliminate dead cells in both physiological and pathological conditions of the CNS. Synapses and myelin are also eliminated by phagocytosis to maintain or refine neural networks during development and adulthood (6, 7). However, aberrant synapse pruning by microglia is suggested to cause undesired synapse loss in AD (8). Although microglia play a major role in phagocytosis, astrocytes also prune synapses by phagocytosis in the developing brain and take up extracellular protein aggregates, such as Aβ (9, 10). In fact, recent findings indicate that hippocampal synapses are preferentially phagocytosed by astrocytes (70). In a mouse model of AD (APP/PS1 mice), dysfunctional synapses are engulfed by Aβ-associated astrocytes, but not microglia (71). However, this beneficial effect is limited, as progressive accumulation of Aβ impairs the phagocytosis of dystrophic synapses by astrocytes and decreases the expression of the phagocytic receptors MERTK and MEGF10 (72, 73). Even though healthy synapses should be preserved, accumulation of faulty synapses can result in an unhealthy synaptic environment, causing alterations in circuit connectivity consequent cognitive impairment and memory loss. The results shown here demonstrate that rTNF-α enhanced phagocytosis by astrocytes and increased the expression of the integrin alpha chain V, encoded by *ITGAV*, which is part of the phagocytic receptor αvβ3/5 integrin (54), whereas *MERTK* expression was decreased. In contrast, murine A1 astrocytes under inflammatory stimuli (IL-1α, TNF-α, and C1q) exhibit suppressed phagocytic activity for synapses and myelin, concomitantly with downregulation of the phagocytic receptors MERTK and MEGF10 (52). These data suggest that the combination of different inflammatory factors might produce contrasting results on the phagocytic activity of astrocytes, adding to the debate of whether this simplified dichotomic classification of astrocytes into A1 and A2 is enough to fully describe the myriad of phenotypes astrocytes can display (44).

Not many studies have addressed the role of mGluR5 on astrocytic phagocytosis. A recent study shows that a silent allosteric modulator (SAM) of mGluR5 prevents synaptic localization of the complement component C1q and synaptic engulfment by astrocytes in an AD mouse model (59). Here we show that CTEP treatment enhanced phagocytosis in the presence and in the absence of rTNF-α. However, although CTEP increased the expression of *MERTK* in the absence of rTNF-α, *MERTK* expression remained reduced in the presence of this inflammatory factor. This increase in *MERTK* expression by CTEP is in line with the enhanced phagocytosis observed in astrocytes treated with CTEP. Thus, CTEP seems to have a prominent effect to induce phagocytosis, regardless of the presence of rTNF-α. Considering that phagocytosis by microglia (74) and astrocytes (72) decline in certain diseases, including AD, CTEP could be an option to compensate impaired phagocytic clearance of Aβ and dystrophic synapses in AD and in other brain disorders caused by protein aggregates.

In conclusion, mGluR5 blockade by CTEP attenuates the rTNF-α-induced secretion of inflammatory factors, including IL-6 and IL-8 in the short-term, although this effect subsides with time. At the

same time, CTEP treatment did not modify either A1 or A2 astrocytic markers, while rTNF-α led to an increase in the A1 markers, *C3*, *VCAM-1* and *GBP2*. *SERPINA3* expression and astrocyte phagocytosis were enhanced by both CTEP and rTNF-α, whereas the expression of synaptogenic factors were decreased. Thus, CTEP treatment could be an option when augmented phagocytosis is desired, although it might lead to increased synaptic pruning and diminished synaptogenesis. These data illustrate the complexity of mGluR5 pharmacology and show that the simplified classification of reactive astrocytes into A1 and A2 falls short of capturing their phenotypic diversity.

Data availability statement

The original contributions presented in the study are included in the article/Supplementary Material. Further inquiries can be directed to the corresponding author.

Ethics statement

Ethical approval was not required for the studies on humans in accordance with the local legislation and institutional requirements because only commercially available established cell lines were used. The animal study was approved by Ethics Committee on Animal Use of the Federal University of Minas Gerais (CEUA #120/2017). The study was conducted in accordance with the local legislation and institutional requirements.

Author contributions

IL: Formal analysis, Writing – original draft, Writing – review & editing, Investigation, Methodology. PC: Formal analysis, Investigation, Methodology, Writing – original draft, Writing – review & editing. JF: Formal analysis, Investigation, Methodology, Writing – original draft, Writing – review & editing. JL: Investigation, Methodology, Writing – review & editing. AM: Writing – review & editing, Investigation, Data curation, Conceptualization, Resources, Supervision. AT: Writing – review & editing, Investigation, Data curation, Conceptualization, Supervision. FR: Writing – review & editing, Conceptualization, Data curation, Formal analysis, Funding acquisition, Project administration, Resources, Supervision, Validation, Visualization, Writing – original draft.

Conflict of interest

The authors declare that the research was conducted in the absence of any commercial or financial relationships that could be construed as a potential conflict of interest.

The author(s) declared that they were an editorial board member of Frontiers, at the time of submission. This had no impact on the peer review process and the final decision.

Publisher's note

All claims expressed in this article are solely those of the authors and do not necessarily represent those of their affiliated organizations, or those of the publisher, the editors and the reviewers. Any product that may be evaluated in this article, or claim that may be made by its manufacturer, is not guaranteed or endorsed by the publisher.

Supplementary material

The Supplementary Material for this article can be found online at: https://www.frontiersin.org/articles/10.3389/fimmu.2023.1283331/full#supplementary-material

References

1. Lee HG, Wheeler MA, Quintana FJ. Function and therapeutic value of astrocytes in neurological diseases. *Nat Rev Drug Discovery* (2022) 21:339–58. doi: 10.1038/s41573-022-00390-x

2. de Lima IBQ, Ribeiro FM. The implication of glial metabotropic glutamate receptors in alzheimer's disease. *Curr Neuropharmacol* (2023) 21:164–82. doi: 10.2174/1570159X20666211223140303

3. Verkhratsky A, Nedergaard M. Physiology of astroglia. *Physiol Rev* (2018) 98:239–389. doi: 10.1152/physrev.00042.2016

4. Moulson AJ, Squair JW, Franklin RJM, Tetzlaff W, Assinck P. Diversity of reactive astrogliosis in CNS pathology: heterogeneity or plasticity? *Front Cell Neurosci* (2021) 15:703810. doi: 10.3389/fncel.2021.703810

5. Verkhratsky A, Li B, Scuderi C, Parpura V. Principles of astrogliopathology. *Adv Neurobiol* (2021) 26:55–73. doi: 10.1007/978-3-030-77375-5_3

6. Trachtenberg JT, Chen BE, Knott GW, Feng G, Sanes JR, Welker E, et al. Long-term in *vivo* imaging of experience-dependent synaptic plasticity in adult cortex. *Nature* (2002) 420:788–94. doi: 10.1038/nature01273

7. Paolicelli RC, Bolasco G, Pagani F, Maggi L, Scianni M, Panzanelli P, et al. Synaptic pruning by microglia is necessary for normal brain development. *Science* (2011) 333:1456–8. doi: 10.1126/science.1202529

8. Hong S, Beja-Glasser VF, Nfonoyim BM, Frouin A, Li S, Ramakrishnan S, et al. Complement and microglia mediate early synapse loss in Alzheimer mouse models. *Science* (2016) 352:712–6. doi: 10.1126/science.aad8373

9. Koistinaho M, Lin S, Wu X, Esterman M, Koger D, Hanson J, et al. Apolipoprotein E promotes astrocyte colocalization and degradation of deposited amyloid-beta peptides. *Nat Med* (2004) 10:719–26. doi: 10.1038/nm1058

10. Chung WS, Clarke LE, Wang GX, Stafford BK, Sher A, Chakraborty C, et al. Astrocytes mediate synapse elimination through MEGF10 and MERTK pathways. *Nature* (2013) 504:394–400. doi: 10.1038/nature12776

11. Gomez-Casati ME, Murtie JC, Rio C, Stankovic K, Liberman MC, Corfas G. Nonneuronal cells regulate synapse formation in the vestibular sensory epithelium *via* erbB-dependent BDNF expression. *Proc Natl Acad Sci U.S.A.* (2010) 107:17005–10. doi: 10.1073/pnas.1008930107

12. Allen NJ, Bennett ML, Foo LC, Wang GX, Chakraborty C, Smith SJ, et al. Astrocyte glypicans 4 and 6 promote formation of excitatory synapses *via* GluA1 AMPA receptors. *Nature* (2012) 486:410–4. doi: 10.1038/nature11059

13. Kucukdereli H, Allen NJ, Lee AT, Feng A, Ozlu MI, Conatser LM, et al. Control of excitatory CNS synaptogenesis by astrocyte-secreted proteins Hevin and SPARC. *Proc Natl Acad Sci U.S.A.* (2011) 108:E440–449. doi: 10.1073/pnas.1104977108

14. Christopherson KS, Ullian EM, Stokes CC, Mullowney CE, Hell JW, Agah A, et al. Thrombospondins are astrocyte-secreted proteins that promote CNS synaptogenesis. *Cell* (2005) 120:421–33. doi: 10.1016/j.cell.2004.12.020

15. Ribeiro FM, Vieira LB, Pires RG, Olmo RP, Ferguson SS. Metabotropic glutamate receptors and neurodegenerative diseases. *Pharmacol Res* (2017) 115:179–91. doi: 10.1016/j.phrs.2016.11.013

16. Miller S, Romano C, Cotman CW. Growth factor upregulation of a phosphoinositide-coupled metabotropic glutamate receptor in cortical astrocytes. *J Neurosci* (1995) 15:6103–9. doi: 10.1523/JNEUROSCI.15-09-06103.1995

17. Pasti L, Volterra A, Pozzan T, Carmignoto G. Intracellular calcium oscillations in astrocytes: a highly plastic, bidirectional form of communication between neurons and astrocytes in situ. *J Neurosci* (1997) 17:7817–30. doi: 10.1523/JNEUROSCI.17-20-07817.1997

18. Biber K, Laurie DJ, Berthele A, Sommer B, Tolle TR, Gebicke-Harter PJ, et al. Expression and signaling of group I metabotropic glutamate receptors in astrocytes and microglia. *J Neurochem* (1999) 72:1671–80. doi: 10.1046/j.1471-4159.1999.721671.x

19. Paquet M, Ribeiro FM, Guadagno J, Esseltine JL, Ferguson SS, Cregan SP. Role of metabotropic glutamate receptor 5 signaling and homer in oxygen glucose deprivation-mediated astrocyte apoptosis. *Mol Brain* (2013) 6:9. doi: 10.1186/1756-6606-6-9

20. Peavy RD, Conn PJ. Phosphorylation of mitogen-activated protein kinase in cultured rat cortical glia by stimulation of metabotropic glutamate receptors. *J Neurochem* (1998) 71:603–12. doi: 10.1046/j.1471-4159.1998.71020603.x

21. Servitja JM, Masgrau R, Sarri E, Picatoste F. Group I metabotropic glutamate receptors mediate phospholipase D stimulation in rat cultured astrocytes. *J Neurochem* (1999) 72:1441–7. doi: 10.1046/j.1471-4159.1999.721441.x

22. Cai Z, Schools GP, Kimelberg HK. Metabotropic glutamate receptors in acutely isolated hippocampal astrocytes: developmental changes of mGluR5 mRNA and functional expression. *Glia* (2000) 29:70–80. doi: 10.1002/(SICI)1098-1136(20000101)29:1<70::AID-GLIA7>3.0.CO;2-V

23. Sun W, McConnell E, Pare JF, Xu Q, Chen M, Peng W, et al. Glutamate-dependent neuroglial calcium signaling differs between young and adult brain. *Science* (2013) 339:197–200. doi: 10.1126/science.1226740

24. Aronica E, Catania MV, Geurts J, Yankaya B, Troost D. Immunohistochemical localization of group I and II metabotropic glutamate receptors in control and amyotrophic lateral sclerosis human spinal cord: upregulation in reactive astrocytes. *Neuroscience* (2001) 105:509–20. doi: 10.1016/S0306-4522(01)00181-6

25. Geurts JJ, Wolswijk G, Bo L, van der Valk P, Polman CH, Troost D, et al. Altered expression patterns of group I and II metabotropic glutamate receptors in multiple sclerosis. *Brain* (2003) 126:1755–66. doi: 10.1093/brain/awg179

26. Shrivastava AN, Kowalewski JM, Renner M, Bousset L, Koulakoff A, Melki R, et al. beta-amyloid and ATP-induced diffusional trapping of astrocyte and neuronal metabotropic glutamate type-5 receptors. *Glia* (2013) 61:1673–86. doi: 10.1002/glia.22548

27. Byrnes KR, Stoica B, Loane DJ, Riccio A, Davis MI, Faden AI. Metabotropic glutamate receptor 5 activation inhibits microglial associated inflammation and neurotoxicity. *Glia* (2009) 57:550–60. doi: 10.1002/glia.20783

28. Loane DJ, Stoica BA, Pajoohesh-Ganji A, Byrnes KR, Faden AI. Activation of metabotropic glutamate receptor 5 modulates microglial reactivity and neurotoxicity by inhibiting NADPH oxidase. *J Biol Chem* (2009) 284:15629–39. doi: 10.1074/jbc.M806139200

29. Fulmer CG, VonDran MW, Stillman AA, Huang Y, Hempstead BL, Dreyfus CF. Astrocyte-derived BDNF supports myelin protein synthesis after cuprizone-induced demyelination. *J Neurosci* (2014) 34:8186–96. doi: 10.1523/JNEUROSCI.4267-13.2014

30. Saitta KS, Lercher LD, Sainato DM, Patel A, Huang Y, McAuliffe G, et al. CHPG enhances BDNF and myelination in cuprizone-treated mice through astrocytic metabotropic glutamate receptor 5. *Glia* (2021) 69:1950–65. doi: 10.1002/glia.24003

31. Rossi D, Brambilla L, Valori CF, Roncoroni C, Crugnola A, Yokota T, et al. Focal degeneration of astrocytes in amyotrophic lateral sclerosis. *Cell Death Differ* (2008) 15:1691–700. doi: 10.1038/cdd.2008.99

32. Shah A, Silverstein PS, Singh DP, Kumar A. Involvement of metabotropic glutamate receptor 5, AKT/PI3K signaling and NF-kappaB pathway in methamphetamine-mediated increase in IL-6 and IL-8 expression in astrocytes. *J Neuroinflamm* (2012) 9:52. doi: 10.1186/1742-2094-9-52

33. Kim H, Woo JH, Lee JH, Joe EH, Jou I. 22(R)-hydroxycholesterol induces HuR-dependent MAP kinase phosphatase-1 expression *via* mGluR5-mediated Ca(2+)/PKCalpha signaling. *Biochim Biophys Acta* (2016) 1859:1056–70. doi: 10.1016/j.bbagrm.2016.05.008

34. Aronica E, Gorter JA, Rozemuller AJ, Yankaya B, Troost D. Activation of metabotropic glutamate receptor 3 enhances interleukin (IL)-1beta-stimulated release of IL-6 in cultured human astrocytes. *Neuroscience* (2005) 130:927–33. doi: 10.1016/j.neuroscience.2004.10.024

35. Li J, Pan L, Pembroke WG, Rexach JE, Godoy MI, Condro MC, et al. Conservation and divergence of vulnerability and responses to stressors between human and mouse astrocytes. *Nat Commun* (2021) 12:3958. doi: 10.1038/s41467-021-24232-3

36. Degl'Innocenti E, Dell'Anno MT. Human and mouse cortical astrocytes: a comparative view from development to morphological and functional characterization. *Front Neuroanat* (2023) 17:1130729. doi: 10.3389/fnana.2023.1130729

37. Kondo T, Asai M, Tsukita K, Kutoku Y, Ohsawa Y, Sunada Y, et al. Modeling Alzheimer's disease with iPSCs reveals stress phenotypes associated with intracellular Abeta and differential drug responsiveness. *Cell Stem Cell* (2013) 12:487–96. doi: 10.1016/j.stem.2013.01.009

38. Trindade P, Loiola EC, Gasparotto J, Ribeiro CT, Cardozo PL, Devalle S, et al. Short and long TNF-alpha exposure recapitulates canonical astrogliosis events in human-induced pluripotent stem cells-derived astrocytes. *Glia* (2020) 68:1396–409. doi: 10.1002/glia.23786

39. Zhao J, Fu Y, Yamazaki Y, Ren Y, Davis MD, Liu CC, et al. APOE4 exacerbates synapse loss and neurodegeneration in Alzheimer's disease patient iPSC-derived cerebral organoids. *Nat Commun* (2020) 11:5540. doi: 10.1038/s41467-020-19264-0

40. Leng K, Rose IVL, Kim H, Xia W, Romero-Fernandez W, Rooney B, et al. CRISPRi screens in human iPSC-derived astrocytes elucidate regulators of distinct inflammatory reactive states. *Nat Neurosci* (2022) 25:1528–42. doi: 10.1038/s41593-022-01180-9

41. Tsenova L, Bergtold A, Freedman VH, Young RA, Kaplan G. Tumor necrosis factor alpha is a determinant of pathogenesis and disease progression in mycobacterial infection in the central nervous system. *Proc Natl Acad Sci U.S.A.* (1999) 96:5657–62. doi: 10.1073/pnas.96.10.5657

42. Klein RS, Garber C, Howard N. Infectious immunity in the central nervous system and brain function. *Nat Immunol* (2017) 18:132–41. doi: 10.1038/ni.3656

43. Lindemann L, Jaeschke G, Michalon A, Vieira E, Honer M, Spooren W, et al. CTEP: a novel, potent, long-acting, and orally bioavailable metabotropic glutamate receptor 5 inhibitor. *J Pharmacol Exp Ther* (2011) 339:474–86. doi: 10.1124/jpet.111.185660

44. Escartin C, Galea E, Lakatos A, O'Callaghan JP, Petzold GC, Serrano-Pozo A, et al. Reactive astrocyte nomenclature, definitions, and future directions. *Nat Neurosci* (2021) 24:312–25. doi: 10.1038/s41593-020-00783-4

45. Cardozo PL, de Lima IBQ, Maciel EMA, Silva NC, Dobransky T, Ribeiro FM. Synaptic elimination in neurological disorders. *Curr Neuropharmacol* (2019) 17:1071–95. doi: 10.2174/1570159X17666190603170511

46. Kwart D, Gregg A, Scheckel C, Murphy EA, Paquet D, Duffield M, et al. A Large Panel of Isogenic APP and PSEN1 Mutant Human iPSC Neurons Reveals Shared Endosomal Abnormalities Mediated by APP beta-CTFs, Not Abeta. *Neuron* (2019) 104:256–270.e255. doi: 10.1016/j.neuron.2019.07.010

47. Molla Kazemiha V, Shokrgozar MA, Arabestani MR, Shojaei Moghadam M, Azari S, Maleki S, et al. PCR-based detection and eradication of mycoplasmal infections from various mammalian cell lines: a local experience. *Cytotechnology* (2009) 61:117–24. doi: 10.1007/s10616-010-9252-6

48. Untergasser A, Nijveen H, Rao X, Bisseling T, Geurts R, Leunissen JA. Primer3Plus, an enhanced web interface to Primer3. *Nucleic Acids Res* (2007) 35:71–4. doi: 10.1093/nar/gkm306

49. Kilkenny C, Browne WJ, Cuthill IC, Emerson M, Altman DG. Improving bioscience research reporting: the ARRIVE guidelines for reporting animal research. *PloS Biol* (2010) 8:e1000412. doi: 10.1371/journal.pbio.1000412

50. Villasana LE, Klann E, Tejada-Simon MV. Rapid isolation of synaptoneurosomes and postsynaptic densities from adult mouse hippocampus. *J Neurosci Methods* (2006) 158:30–6. doi: 10.1016/j.jneumeth.2006.05.008

51. Zamanian JL, Xu L, Foo LC, Nouri N, Zhou L, Giffard RG, et al. Genomic analysis of reactive astrogliosis. *J Neurosci* (2012) 32:6391–410. doi: 10.1523/JNEUROSCI.6221-11.2012

52. Liddelow SA, Guttenplan KA, Clarke LE, Bennett FC, Bohlen CJ, Schirmer L, et al. Neurotoxic reactive astrocytes are induced by activated microglia. *Nature* (2017) 541:481–7. doi: 10.1038/nature21029

53. Fan YY, Huo J. A1/A2 astrocytes in central nervous system injuries and diseases: Angels or devils? *Neurochem Int* (2021) 148:105080. doi: 10.1016/j.neuint.2021.105080

54. Mills EA, Davis CH, Bushong EA, Boassa D, Kim KY, Ellisman MH, et al. Astrocytes phagocytose focal dystrophies from shortening myelin segments in the optic nerve of Xenopus laevis at metamorphosis. *Proc Natl Acad Sci U.S.A.* (2015) 112:10509–14. doi: 10.1073/pnas.1506486112

55. Konishi H, Koizumi S, Kiyama H. Phagocytic astrocytes: Emerging from the shadows of microglia. *Glia* (2022) 70:1009–26. doi: 10.1002/glia.24145

56. Kim SK, Hayashi H, Ishikawa T, Shibata K, Shigetomi E, Shinozaki Y, et al. Cortical astrocytes rewire somatosensory cortical circuits for peripheral neuropathic pain. *J Clin Invest* (2016) 126:1983–97. doi: 10.1172/JCI82859

57. Danjo Y, Shigetomi E, Hirayama YJ, Kobayashi K, Ishikawa T, Fukazawa Y, et al. Transient astrocytic mGluR5 expression drives synaptic plasticity and subsequent chronic pain in mice. *J Exp Med* (2022) 219. doi: 10.1084/jem.20210989

58. de Souza JM, Ferreira-Vieira TH, Maciel EMA, Silva NC, Lima IBQ, Doria JG, et al. mGluR5 ablation leads to age-related synaptic plasticity impairments and does not improve Huntington's disease phenotype. *Sci Rep* (2022) 12:8982. doi: 10.1038/s41598-022-13029-z

59. Spurrier J, Nicholson L, Fang XT, Stoner AJ, Toyonaga T, Holden D, et al. Reversal of synapse loss in Alzheimer mouse models by targeting mGluR5 to prevent synaptic tagging by C1Q. *Sci Transl Med* (2022) 14:eabi8593. doi: 10.1126/scitranslmed.abi8593

60. Spampinato SF, Copani A, Nicoletti F, Sortino MA, Caraci F. Metabotropic glutamate receptors in glial cells: A new potential target for neuroprotection? *Front Mol Neurosci* (2018) 11:414. doi: 10.3389/fnmol.2018.00414

61. Casley CS, Lakics V, Lee HG, Broad LM, Day TA, Cluett T, et al. Up-regulation of astrocyte metabotropic glutamate receptor 5 by amyloid-beta peptide. *Brain Res* (2009) 1260:65–75. doi: 10.1016/j.brainres.2008.12.082

62. Lim D, Iyer A, Ronco V, Grolla AA, Canonico PL, Aronica E, et al. Amyloid beta deregulates astroglial mGluR5-mediated calcium signaling *via* calcineurin and Nf-kB. *Glia* (2013) 61:1134–45. doi: 10.1002/glia.22502

63. Grolla AA, Fakhfouri G, Balzaretti G, Marcello E, Gardoni F, Canonico PL, et al. Abeta leads to Ca(2)(+) signaling alterations and transcriptional changes in glial cells. *Neurobiol Aging* (2013) 34:511–22. doi: 10.1016/j.neurobiolaging.2012.05.005

64. Grolla AA, Sim JA, Lim D, Rodriguez JJ, Genazzani AA, Verkhratsky A. Amyloid-beta and Alzheimer's disease type pathology differentially affects the calcium signalling toolkit in astrocytes from different brain regions. *Cell Death Dis* (2013) 4:e623. doi: 10.1038/cddis.2013.145

65. Ronco V, Grolla AA, Glasnov TN, Canonico PL, Verkhratsky A, Genazzani AA, et al. Differential deregulation of astrocytic calcium signalling by amyloid-beta, TNFalpha, IL-1beta and LPS. *Cell Calcium* (2014) 55:219–29. doi: 10.1016/j.ceca.2014.02.016

66. Mao L, Wang JQ. Phosphorylation of cAMP response element-binding protein in cultured striatal neurons by metabotropic glutamate receptor subtype 5. *J Neurochem* (2003) 84:233–43. doi: 10.1046/j.1471-4159.2003.01256.x

67. Wang H, Zhuo M. Group I metabotropic glutamate receptor-mediated gene transcription and implications for synaptic plasticity and diseases. *Front Pharmacol* (2012) 3:189. doi: 10.3389/fphar.2012.00189

68. Doria JG, de Souza JM, Andrade JN, Rodrigues HA, Guimaraes IM, Carvalho TG, et al. The mGluR5 positive allosteric modulator, CDPPB, ameliorates pathology and phenotypic signs of a mouse model of Huntington's disease. *Neurobiol Dis* (2015) 73:163–73. doi: 10.1016/j.nbd.2014.08.021

69. Doria JG, de Souza JM, Silva FR, Olmo IG, Carvalho TG, Alves-Silva J, et al. The mGluR5 positive allosteric modulator VU0409551 improves synaptic plasticity and memory of a mouse model of Huntington's disease. *J Neurochem* (2018) 147:222–39. doi: 10.1111/jnc.14555

70. Lee JH, Kim JY, Noh S, Lee H, Lee SY, Mun JY, et al. Astrocytes phagocytose adult hippocampal synapses for circuit homeostasis. *Nature* (2021) 590:612–7. doi: 10.1038/s41586-020-03060-3

71. Gomez-Arboledas A, Davila JC, Sanchez-Mejias E, Navarro V, Nunez-Diaz C, Sanchez-Varo R, et al. Phagocytic clearance of presynaptic dystrophies by reactive astrocytes in Alzheimer's disease. *Glia* (2018) 66:637–53. doi: 10.1002/glia.23270

72. Iram T, Trudler D, Kain D, Kanner S, Galron R, Vassar R, et al. Astrocytes from old Alzheimer's disease mice are impaired in Abeta uptake and in neuroprotection. *Neurobiol Dis* (2016) 96:84–94. doi: 10.1016/j.nbd.2016.08.001

73. Sanchez-Mico MV, Jimenez S, Gomez-Arboledas A, Munoz-Castro C, Romero-Molina C, Navarro V, et al. Amyloid-beta impairs the phagocytosis of dystrophic synapses by astrocytes in Alzheimer's disease. *Glia* (2021) 69:997–1011. doi: 10.1002/glia.23943

74. Krabbe G, Halle A, Matyash V, Rinnenthal JL, Eom GD, Bernhardt U, et al. Functional impairment of microglia coincides with Beta-amyloid deposition in mice with Alzheimer-like pathology. *PloS One* (2013) 8:e60921. doi: 10.1371/journal.pone.0060921

frontiers | Frontiers in Immunology

Bystander activation of microglia by *Brucella abortus*-infected astrocytes induces neuronal death via IL-6 trans-signaling

Julia Rodríguez[1], Julia De Santis Arévalo[1], Vida A. Dennis[2],
Ana M. Rodríguez[1†] and Guillermo H. Giambartolomei [ID][1*†]

[1]Instituto de Inmunología, Genética y Metabolismo (INIGEM), Consejo Nacional de Investigaciones
Científicas y Técnicas (CONICET), Facultad de Farmacia y Bioquímica, Universidad de Buenos Aires, Buenos
Aires, Argentina, [2]Center for NanoBiotechnology Research and Department of Biological Sciences, Alabama
State University, Montgomery, AL, United States

Inflammation plays a key role in the pathogenesis of neurobrucellosis where glial
cell interactions are at the root of this pathological condition. In this study, we
present evidence indicating that soluble factors secreted by *Brucella abortus*-
infected astrocytes activate microglia to induce neuronal death. Culture
supernatants (SN) from *B. abortus*-infected astrocytes induce the release of
pro-inflammatory mediators and the increase of the microglial phagocytic
capacity, which are two key features in the execution of live neurons by
primary phagocytosis, a recently described mechanism whereby *B. abortus*-
activated microglia kills neurons by phagocytosing them. IL-6 neutralization
completely abrogates neuronal loss. IL-6 is solely involved in increasing the
phagocytic capacity of activated microglia as induced by SN from *B. abortus*-
infected astrocytes and does not participate in their inflammatory activation.
Both autocrine microglia-derived and paracrine astrocyte-secreted IL-6 endow
microglial cells with up-regulated phagocytic capacity that allows them to
phagocytose neurons. Blocking of IL-6 signaling by soluble gp130 abrogates
microglial phagocytosis and concomitant neuronal death, indicating that IL-6
activates microglia via trans-signaling. Altogether, these results demonstrate that
soluble factors secreted by *B. abortus*-infected astrocytes activate microglia to
induce, via IL-6 trans-signaling, the death of neurons. IL-6 signaling inhibition
may thus be considered a strategy to control inflammation and CNS damage
in neurobrucellosis.

Introduction

Neurobrucellosis is an inflammatory disorder generated by the invasion of *Brucella* to the nervous system. It mostly affects the central nervous system (CNS) and has an ominous prognosis (1). Once *Brucella* spp. invades the CNS, it induces meningoencephalitis, central and peripheral demyelination, and neuritis together with neurocognitive abnormalities (2–6). *Brucella*-induced pathology in the CNS is a very complex process and it has yet many aspects to be untangled, being the reactive inflammation one of the main contributors to neuronal dysfunction (7, 8).

Astrocytes, microglia, oligodendrocytes, pericytes, and endothelial cells are part of a highly controlled microenvironment that is vital for proper neuronal function within the CNS (9). Initially, glial cells were thought to simply provide trophic support for neurons. Nowadays, it is clear that a closely intermingled neuron-glia network is a crucial requisite for adequate CNS function (10–13). Interactions between astrocytes and microglia control CNS physiology in health and disease (12–17). This molecular dialogue between microglia and astrocytes initiates early during colonization of the CNS parenchyma and plays an essential role in neuronal function (18). Yet, this reciprocal crosstalk between astrocytes and microglia may also induce CNS inflammation through the secretion of multiple cytokines and inflammatory mediators (19).

In recent years, we have demonstrated that CNS infection by *B. abortus* causes the development of a powerful inflammatory response. This response generates reactive microgliosis, astrogliosis, and cellular infiltrates (20, 21). We have also shown that after infection, glial cells secrete pro-inflammatory cytokines, chemokines, metalloproteases, and nitric oxide (NO) (8, 20, 21). Moreover, we have hypothesized that the neurocognitive symptoms associated with neurobrucellosis may be the result of neuronal damage due to the inflammatory response to infection (20, 22–24). Indeed, we have demonstrated that *B. abortus*-activated microglia induce neuronal death through primary phagocytosis (8). Nitric oxide secreted by *B. abortus*-infected microglia induced neuronal exposure of the "eat-me" signal phosphatidylserine (PS), which was sufficient to trigger the microglial milk fat globule epidermal growth factor-8 (MFG-E8)/vitronectin receptor pathway which leads to subsequent neuronal engulfment and death (8).

The role of activated microglia either as positive (16, 25) or negative regulators (26) of astrocytic pathogenic responses is well established. However, since it is becoming more apparent that inflammatory astrocytes are also able to regulate microglial activity (17, 27–29), we sought to investigate the putative role of *B. abortus*-infected astrocytes on microglial activation and the effect that this interaction might have on neuronal wellbeing. Here, we present the result of our study.

Materials and methods

Animals

Mice were used to obtain primary cultures of neurons, astrocytes, and microglia. BALB/c mice were provided by the School of Pharmacy and Biochemistry, University of Buenos Aires, Argentina. Interleukin-6 (IL-6) knock-out (KO) mice and C57BL/6 wild-type (WT) mice were provided by the National University of San Martín, Argentina. Mice were housed under specific pathogen-free conditions in positive-pressure cabinets and provided with sterile food and water *ad libitum*, under controlled temperature (22 ± 2°C) and artificial light (12 h cycle period). All animal procedures were performed according to the National Institute of Health (USA) rules and standards. Animal experiments were approved by the Ethics Committee of Care and Use of Laboratory Animals of the School of Medicine, University of Buenos Aires (Protocol #181/2020).

Primary cell cultures

Cultures of cortical neurons (>95%) were generated from E16-E18 mouse forebrain fetuses, as described before (8). Briefly, meninges were removed from the brain, and cortices were dissected and treated with 0.25% trypsin-EDTA (Gibco). Cells were dissociated mechanically and plated onto glass coverslips pre-treated with poly-L-lysine (1 mg/mL) (Sigma Aldrich) at a density of 2×10^5 cells/well in 24-well plates. Cultures were initially maintained with Dulbecco's modified Eagle's medium-F12 (DMEM-F12, Gibco) plus 10% fetal bovine serum (FBS, Gibco) for 3 h. Then, the medium was changed by a Neurobasal medium supplemented with B27 and N2 (all from Gibco). All media contained glucose, GlutaMAX (Gibco), streptomycin, and penicillin (Gibco). Astrocytes and microglia cultures (>95%) were obtained from the P1-P3 mouse forebrain following previously described procedures (20). In short, brain tissue was subjected to mechanical and enzymatic digestion with 0.25% trypsin-1mM EDTA (Gibco) along with magnetic agitation for 20 min at room temperature. The cell suspension was seeded in culture flasks previously treated with 2% w/v gelatin (Sigma Aldrich) and was grown at 37°C, 5% CO_2 humidified incubator in DMEM with high glucose, supplemented with L-glutamine, sodium pyruvate, penicillin, streptomycin, fungizone, and 10% FBS (all from Gibco). After 2-3 weeks of culture, microglia were harvested by orbital shaking (2 h at 37°C, 180 rpm) and astrocytes were harvested by orbital shaking and subsequent trypsinization. Co-cultures of neurons/microglia were established by adding 1×10^5 microglial cells on top of neuron cultures and were allowed to adhere for 18 h before treatment. Astrocytes were cultured at a density of 3.5×10^5 astrocytes/well in 24-well plates.

Bacteria

B. abortus S2308 was grown for 3 to 5 days in tryptic soy agar (TSA, Merck) at 37°C. An inoculum of the bacteria was suspended in sterile phosphate-buffered saline (PBS) and their number was estimated by measuring the OD600 in a spectrophotometer (Amersham Biosciences). All manipulations with viable bacteria were performed in biosafety level 3 facilities located at the INBIRS (School of Medicine, University of Buenos Aires). When indicated,

B. abortus organisms were washed in PBS, heat-killed at 70°C for 20 min (HKBA), aliquoted, and stored at -70°C until their use to stimulate cultures. The absence of *B. abortus* viability after heat-killing was verified by the lack of bacterial growth on TSA.

Production of astrocyte culture supernatants

Astrocyte cultures were infected with *B. abortus* at multiplicity of infection (MOI) 100 for 24 h in 0.5 mL of DMEM, supplemented with 2 mM of L-glutamine, 1 mM of sodium pyruvate, and 10% FBS (complete medium) without antibiotics. Non-infected astrocytes were cultured in the same conditions. Then, culture supernatants were collected and sterilized using a 0.22 µm filter (JetBiofil) to eliminate non-internalized bacteria, which were ultracentrifuged when mentioned (at 100,000 x g for 5 h at 4°C), aliquoted, and stored at -70°C until their use to stimulate cultures.

Culture treatment

Neurons/microglia co-cultures or microglia cultures were stimulated for 48 h with SN from non-infected or *B. abortus*-infected astrocytes diluted in complete medium (1/2, unless otherwise stated). Untreated wells were used as a negative control. When indicated, co-cultures were treated with astrocytes SN in the presence of recombinant annexin V (200 nM; eBioscience), cyclic RGD peptide (cRGD, Cyclo(-Arg-Gly-Asp-D-Phe-Val)), cRAD (Cyclo(-Arg-Ala-Asp-D-Phe-Val)) peptides (100 µM; Bachem), or recombinant mouse IL-6 (5, 10 or 15 ng/mL; Peprotech). Also, co-cultures were pre-treated for 1 h with aminoguanidine (AG) (200 µM; Sigma Aldrich) or recombinant mouse gp130Fc chimera protein (100 ng/mL; R&D Systems), then they were treated with astrocytes SN for 48 h in the presence of the inhibitor. Neutralization experiments were performed using anti-mouse TNF-α (10 µg/mL; clone MP6-XT3; BD Pharmingen), anti-mouse IL-1β (10 µg/mL; clone B122; eBioscience), anti-mouse IL-6 (5 µg/mL; clone MP5-20F3; BD Pharmingen) monoclonal antibodies, or an isotype control (10 µg/mL; BioLegend). Culture supernatants from *B. abortus*-infected astrocytes were pre-incubated with the respective neutralizing antibodies for 1 h at 37°C before stimulating neurons/microglia co-cultures.

Immunofluorescence and quantification of neuronal density

Neurons/microglia co-cultures were fixed with 4% paraformaldehyde (PFA) for 20 min at RT 48 h after treatment. Cells were permeabilized with 0.125% v/v Triton X-100 (Promega) and blocked with PBS 5% FBS. Neurons were labeled with anti-β-Tubulin III monoclonal antibody (1:750 dilution; clone 2G10; Sigma Aldrich) followed by Alexa Fluor 546-labeled anti-mouse IgG2a (1:200 dilution; Life Technologies Inc.). Microglia were labeled with biotinylated *Griffonia simplicifolia* isolectin-B4 (1:500

dilution; Vector Laboratories) followed by Alexa Fluor 488-labeled streptavidin (1:200 dilution; BioLegend). To dye nuclear structures, 4',6-diamidino-2-phenylindole (DAPI, Molecular Probes) were used and nuclear morphology was analyzed to identify viable *vs.* apoptotic neurons. Images were acquired by a Nikon Eclipse Ti-E PFS microscope and analyzed using ImageJ software. Five microscopic fields per duplicate coverslip (100-150 neurons) were counted. Neuronal viability was calculated with respect to untreated controls (expressed as a percentage).

Determination of gene expression by RT-qPCR

The total RNA of microglia cells was extracted using Quick-RNA MiniPrep Kit (Zymo Research) following the manufacturer's instructions. cDNA was synthesized from 1 µg of total RNA using the reverse transcriptase Improm-II enzyme (Promega). Real-time quantitative PCR (RT-qPCR) was performed with the master mix FastStart Universal SYBR Green Master (ROX, Roche) in a StepOne Real-Time PCR System (Applied Biosystems). Primers used were as follows: TNF-α forward: 5'-ATGGCCTCCCTCTCATCAGT-3', reverse: 5'-TTTGCTACGACGTGGGCTAC-3'; IL-1β forward: 5'-GCCACCTTTTGACAGTGATGAG-3', reverse: 5'-GACAGCCCAGGTCAAAGGTT-3'; IL-6 forward: 5'-AGACAAAGCCAGAGTCCTTCAG-3', reverse: 5'-GAGCATTGGAAATTGGGGTAGG-3'; iNOS forward: 5'-CAGCTGGGCTGTACAAACCTT-3', reverse: 5'-CATTGGAAGTGAAGCGTTTCG-3'; β-actin forward: 5'-AACAGTCCGCCTAGAAGCAC-3', reverse: 5'-CGTTGACATCCGTAAAGACC-3'. The amplification cycle was the following: 10 min at 95°C, 40 cycles at 95°C for 15 s, 60°C for 30 s, and 72°C for 60 s. All primer sets (Invitrogen) yielded a single amplification product by melting curve analysis. The fold change (relative expression) in gene expression was calculated using the relative quantitation method ($2^{-\Delta\Delta Ct}$). Relative expression levels were normalized to the expression of β-actin and plotted in a $\log_2$ scale.

Measurement of cytokines and nitric oxide

Mouse IL-6, IL-1β, and TNF-α were measured in culture supernatants by ELISA according to the manufacturer's instructions (BD Pharmingen). The preexisting levels of cytokines in astrocytes SN were subtracted in order to show the specific secretion by microglia. Levels of nitric oxide (NO) in culture supernatants were evaluated by measurement of nitrite concentration using the colorimetric Griess reaction.

Phagocytosis assays

The phagocytic capacity of microglia was evaluated by the uptake of *Escherichia coli* or negatively charged fluorescent beads. For phagocytosis assay with *E. coli*, microglial cells were washed after 24 h of culture stimulation, and *E. coli* DH5α (Invitrogen) was added for 30 min at 37°C and 5% CO_2. Unphagocytosed bacteria

were removed by washing and gentamicin treatment (100 µg/mL) for 30 min. Microglia were lysed with 0.1% v/v Triton X-100 in distilled water, and the lysates were plated on TSA and incubated overnight at 37°C. Phagocytosed bacteria were assessed by counting colony-forming units (CFU). For phagocytosis assay with fluorescent beads, after 48 h of culture stimulation, microglial cells were incubated with 0.003% w/v of 5-5.9 µm carboxyl fluorescent Nile red particles (Spherotech) for 2 h at 37°C and 5% CO_2. Then, cells were thoroughly washed with ice-cold PBS to arrest bead internalization and fixed with 4% PFA.

Statistical analysis

Experiments were executed at least three times using different primary cultures. Statistical analysis was performed with two-way ANOVA followed by the *post hoc* Tukey test in experiments of neuronal viability, one-way ANOVA followed by the *post hoc* Bonferroni test in experiments comparing more than two groups, or two-tailed Student's t-test in experiments comparing two groups, using GraphPad Prism 6.0 software. Data are represented as mean ± SEM.

Results

Culture supernatants from *B. abortus*-infected astrocytes induce neuronal death in co-cultures of neurons/microglia

We examined whether activation of microglia by astrocytes within the inflammatory milieu generated by *B. abortus* in the CNS promoted neuronal death. To model this scenario, *in vitro* co-cultures of neurons/microglia were stimulated with SN from *B. abortus*-infected astrocytes, and neuronal viability was determined by microscopy after 24 and 48 h of culture. In parallel, co-cultures were stimulated with SN from non-infected astrocytes or left untreated (control). The addition of SN from *B. abortus*-infected astrocytes to co-cultures of neurons/microglia induced a significant dose- and time-dependent reduction ($p < 0.05$) in the number of healthy neurons when compared with untreated controls. In all cases, the number of apoptotic neurons was low and not different from co-cultures stimulated with SN from uninfected astrocytes or unstimulated co-cultures (Figures 1A–C). This result did not depend on a particular co-culture or SN preparation since it was corroborated in five independent experiments using neurons, microglia, and astrocytes SN from different animals (Figure 1D). *Brucella* spp. releases outer-membrane vesicles (OMVs) containing lipopolysaccharide (LPS), outer membrane proteins, and other bacterial components (30). To rule out the possibility that the remaining OMVs present in SN after astrocyte infection were implicated in microglia activation, we performed ultracentrifugation of SN, as previously described (30, 31). Co-cultures were then incubated with OMV-free SN for 48 h and neuronal death was evaluated. The percentage of neuronal death was not significantly different ($p > 0.05$) between non-depleted and

OMV-free SN (Figure 1E). Importantly, *B. abortus*-infected astrocytes SN had no direct effect on neuronal viability if microglia were not present in the culture (Figure 1F), indicating that SN are activating microglia to induce neuronal demise. These results indicate that secreted factors from *B. abortus*-infected astrocytes are responsible for microglia activation and concomitant neuronal death.

SN from *B. abortus*-infected astrocytes induce microglial activation

To investigate the effects that SN from *B. abortus*-infected astrocytes have on microglia, we evaluated several parameters of microglia activation. Treatment with SN from *B. abortus*-infected astrocytes induced a significant ($p < 0.05$) inflammatory activation of microglia measured as an increased gene transcription and secretion of TNF-α, IL-1β, and IL-6 (Figure 2A); increased gene transcription of the inducible nitric oxide (NO) synthase (iNOS) expression with concomitant NO release (Figure 2B); and increased microglial proliferation (Figure 2C). Treatment also increased the phagocytic capacity of microglia. Microglia treated with SN from *B. abortus*-infected astrocytes significantly ($p < 0.0005$) increased the phagocytosis of *E. coli* when compared with unstimulated control microglia or microglia stimulated with SN from uninfected astrocytes (Figure 3A). Activation of microglia caused by treatment with SN from *B. abortus*-infected astrocytes also significantly ($p < 0.05$) improved phagocytic uptake of beads, increasing both the number of phagocytic microglia and the number of beads taken per microglia (Figures 3B, C), when compared with microglia incubated with SN from uninfected astrocytes or unstimulated control microglia. Overall, these results indicate that SN from *B. abortus*-infected astrocytes induce an inflammatory activation of microglia with the release of pro-inflammatory mediators and the increase in their proliferation and phagocytic capacity which results in the death of neurons.

Microglia activated by SN from *B. abortus*-infected astrocytes induce neuronal death by primary phagocytosis

In a previous report, we have demonstrated that *B. abortus*-infected microglia induce neuronal loss by primary phagocytosis (also named phagoptosis) of live neurons (8). The elimination of neurons relies on two simultaneous events: inflammatory signaling–specifically NO secretion–and the increased phagocytic capacity of microglia. NO secreted by *B. abortus*-activated microglia induced neuronal exposure of the "eat-me" signal PS which allows the microglial engulfment of live neurons through the vitronectin receptor, using MFG-E8 as a bridging molecule. Blocking either of the two mechanisms (NO secretion or phagocytosis) abrogates neuronal death without inhibiting microglial overall activation (8). Thus, to investigate if phagoptosis was involved in the neuronal death induced by microglia activated by SN from *B. abortus*-infected astrocytes, we first inhibited the PS/MGF-E8/
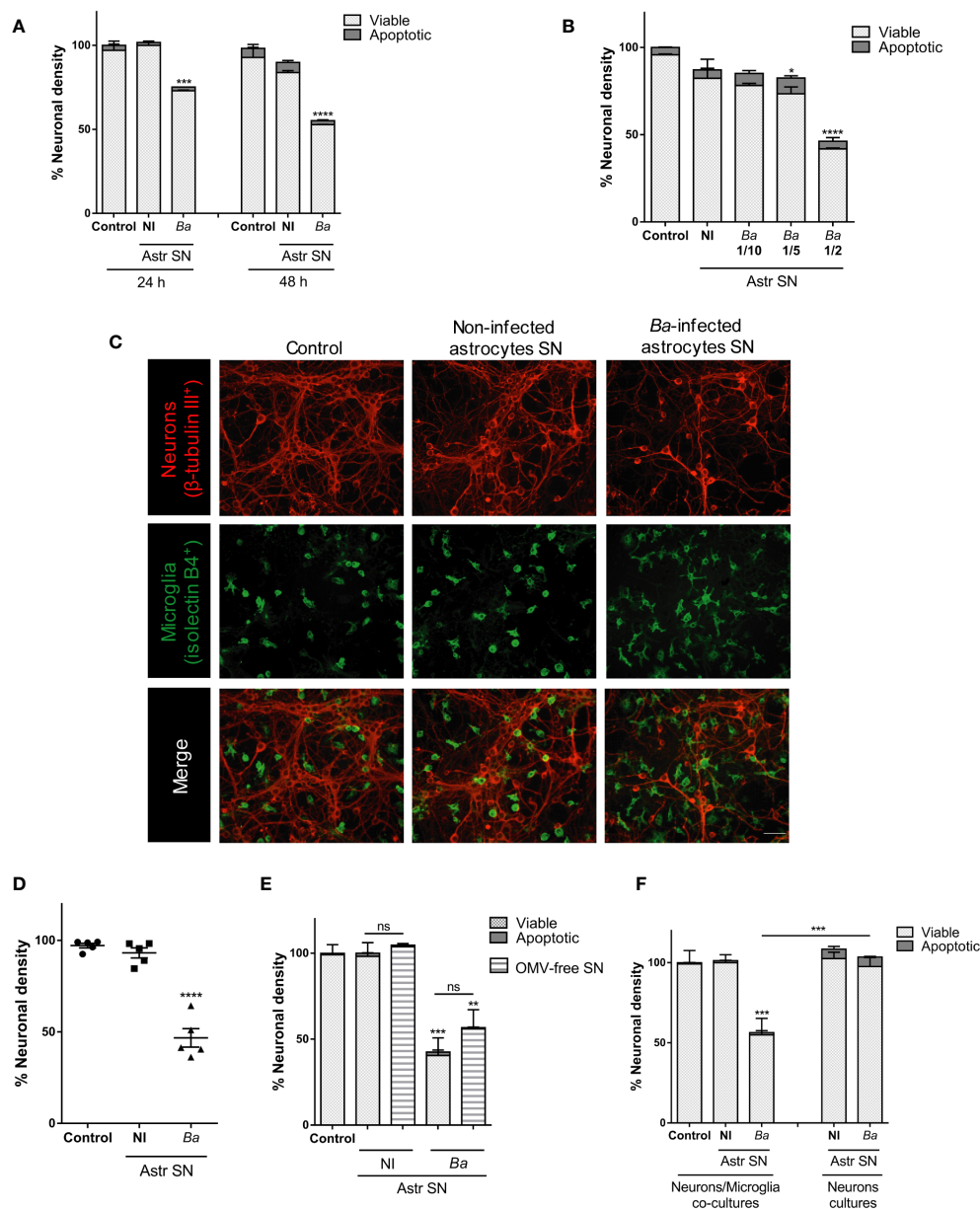
FIGURE 1

SN from *B. abortus*-infected astrocytes induce neuronal death in co-cultures of neurons/microglia. Neurons/microglia co-cultures were stimulated with SN from non-infected (NI) or *B. abortus*-infected (*Ba*) astrocytes (Astr SN) diluted in complete medium (1/2) or left untreated (control) for 24 h or 48 h **(A)**, or with different dilutions of SN from infected astrocytes for 48 h **(B)**. Representative images from neurons/microglia co-cultures showing neurons labeled with anti-β-Tubulin III antibody (red) and microglia labeled with isolectin-B4 (green). Scale bar: 50 μm **(C)**. The percentage (%) of neuronal density was evaluated in five independent experiments using neurons, microglia, and astrocytes SN from different animals **(D)**. Astrocytes SN were ultracentrifuged (OMVs-free SN) or not and used to stimulate neurons/microglia co-cultures for 48 h **(E)**. Cultures of neurons with microglia or neurons alone were treated with SN from non-infected or *B. abortus*-infected astrocytes for 48 h and neuronal density was evaluated **(F)**. The density of neurons was evaluated by fluorescence microscopy. The percentage (%) of viable and apoptotic neurons was calculated vs. control condition. Data are shown as mean ± SEM from a representative experiment of three performed, except where indicated. *p < 0.05; **p < 0.005; ***p < 0.0005; ****p < 0.0001 vs. control condition, except where indicated. Non-significant (ns).

vitronectin receptor pathway. Blocking the MFG-E8–neuron's PS interaction (using recombinant annexin V) or the interaction between MFG-E8 and the microglia's vitronectin receptor (using cRGD) completely inhibited the neuronal loss induced by microglia activated by SN from *B. abortus*-infected astrocytes (Figures 4A, B). As expected, the control peptide cRAD did not prevent neuronal death. Of note, in both cases (annexin V and cRGD), the number of

apoptotic neurons was not higher than controls (Figures 4A, B), indicating that microglial phagocytosis of neurons was the cause of death rather than its consequence. Certainly, if neurons had been killed first by microglia and afterward phagocytosed by them, when inhibition of phagocytosis was performed, apoptotic neurons should have been visualized in the culture. Instead, we have found only live neurons in the cultures. Likewise, the addition of
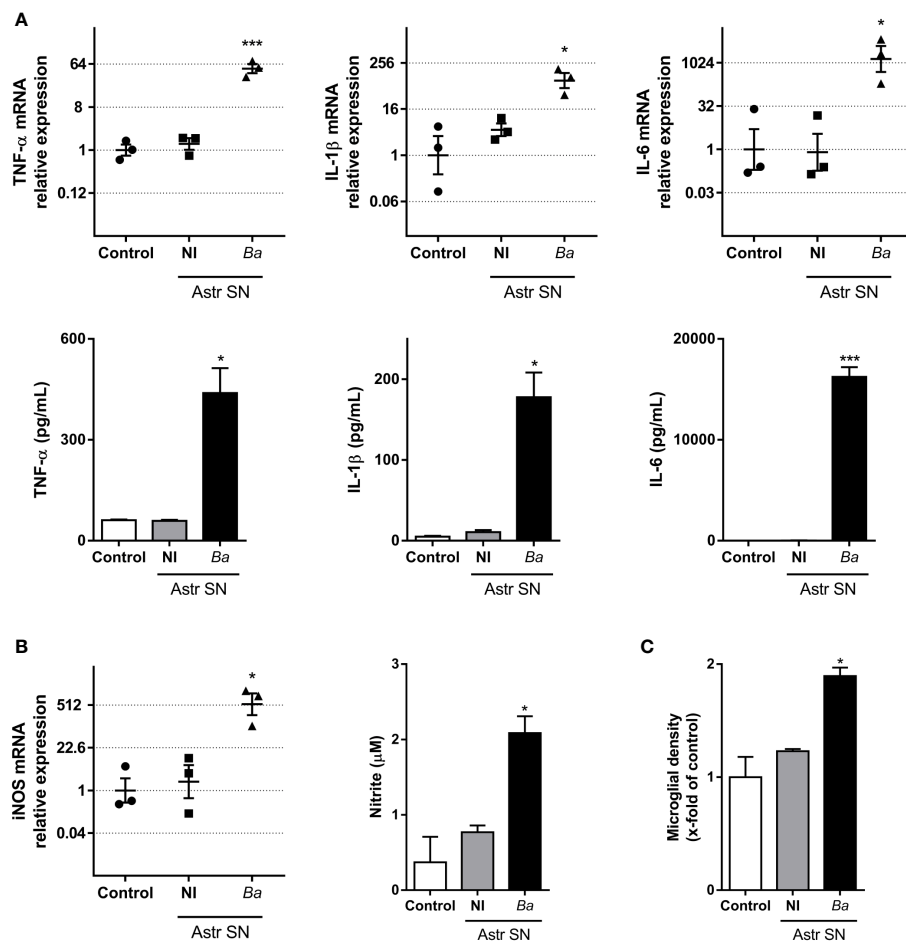
FIGURE 2

SN from *B. abortus*-infected astrocytes induce an inflammatory phenotype on microglia. Microglia were treated with SN from non-infected (NI) or *B. abortus*-infected (Ba) astrocytes (Astr SN) or left untreated (control) for 48 h. Gene expression of TNF-α, IL-1β, and IL-6 was analyzed by RT-qPCR in three independent experiments (plotted in a log2 scale) and cytokine secretion was measured by ELISA **(A)**. Gene expression of iNOS was determined by RT-qPCR in three independent experiments and the level of NO was evaluated by Griess reaction **(B)**. Proliferation was assessed by fluorescence microscopy **(C)**. Data are shown as mean ± SEM from a representative experiment of three performed, except where indicated. *p < 0.05; ***p < 0.0005 vs. control condition.

aminoguanidine, an inhibitor of both constitutive and iNOS and therefore the release of NO (8), significantly reduced (*p* < 0.005) the neuronal death induced by microglia activated by SN from *B. abortus*-infected astrocytes (Figure 4C). These results indicate that microglia stimulated by SN from *B. abortus*-infected astrocytes kill live neurons by primary phagocytosis.

Neutralization of IL-6 prevents neuronal death induced by SN-activated microglia

Our results indicate that soluble factors secreted by *Brucella*-infected astrocytes are involved in the activation of microglia which leads to neuronal death by primary phagocytosis. TNF-α, IL-1β, and IL-6 have been shown to be key inducers of microglial activation and regulators of microglia effector functions (32–35). Because these cytokines are secreted upon infection of astrocytes with *B. abortus* (20), we sought to investigate their role in the activation of microglia by SN from *B. abortus*-infected astrocytes.

To investigate the role of IL-6, IL-1β, and TNF-α in neuronal phagoptosis induced by microglia activated by SN from *B. abortus*-infected astrocytes, we pre-incubated SN with IL-6, IL-1β, or TNF-α neutralizing antibodies before adding them to microglia/neurons co-cultures. Neutralization of IL-6 but not TNF-α or IL-1β resulted in complete abrogation of neuronal death induced by activated microglia. Isotype control antibody had no effect on primary phagocytosis of neurons induced by activated microglia (Figure 5). This result indicates that IL-6 is a key factor in activating microglia to induce neuronal death.

IL-6 secreted by both astrocytes and microglia contributes to neuronal death induced by *B. abortus*-activated microglia

Our results (Figure 2A and (20)) indicate that *Brucella*-activated microglia are capable of secreting IL-6. This, together with the experimental design of the neutralization assay performed above
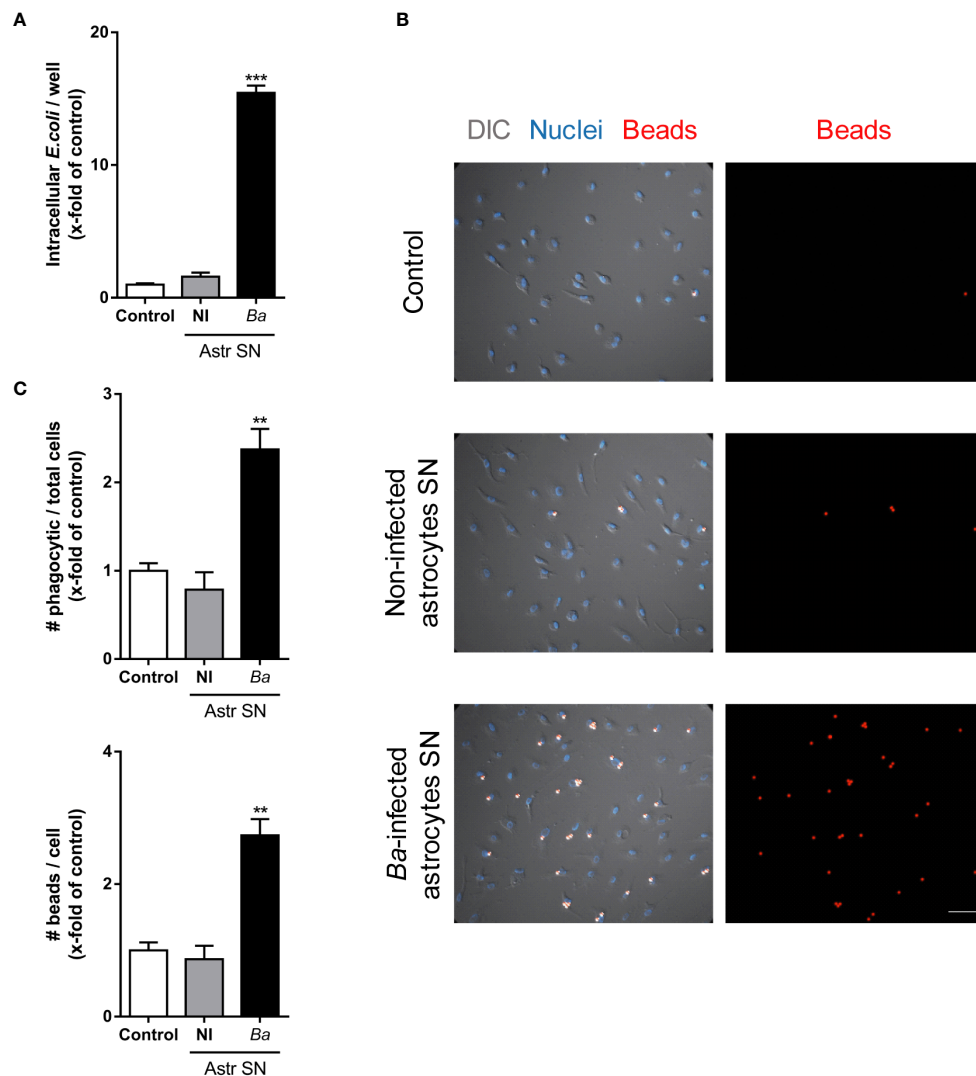
FIGURE 3

SN from *B. abortus*-infected astrocytes increase the phagocytic activity of microglia. Microglia cultures were treated with SN from non-infected (NI) or *B. abortus*-infected (*Ba*) astrocytes (Astr SN), or left untreated (control). The phagocytic activity of microglia was evaluated by two different phagocytosis assays using *E. coli* **(A)** or negatively charged fluorescent 5 μm beads **(B, C)**. Phagocytized bacteria were evaluated by intracellular CFU counting, and phagocytized beads were evaluated by fluorescence microscopy. Scale bar: 50 μm. Data are shown as mean ± SEM from a representative experiment of three performed. **p < 0.005; ***p < 0.0005 vs. control condition.

cannot rule out a putative contribution of microglial-secreted IL-6 in the phagoptosis induced by microglia activated by SN from *B. abortus*-infected astrocytes. To decipher the source of IL-6 (microglia or astrocyte SN, or both) that drives activated microglia to kill neurons, we performed co-cultures with microglia and astrocyte SN from mice deficient in the IL-6 gene (IL-6 knock-out, KO). At first, we treated wild-type (WT) co-cultures of neurons/microglia with SN from *B. abortus*-infected WT or IL-6 KO astrocytes (Figure 6A). As was shown before, when SN from *B. abortus*-infected WT astrocytes were employed to activate WT microglia (▲), a significant (*p* < 0.0001) neuronal death was achieved when compared to control cultures (●). Stimulation of WT microglia with SN from *B. abortus*-infected IL-6 KO astrocytes (◆) caused a significant neuronal death compared with the control condition (●, *p* < 0.005) even though

the percentage of neuronal death was significantly less (*p* < 0.05) than the one obtained with SN from WT-infected astrocytes (▲). Conversely, we performed co-cultures of neurons with WT or IL-6 KO microglia and treated them with SN from *B. abortus*-infected WT astrocytes (Figure 6B). Likewise, if IL-6 KO microglia were activated with SN from *B. abortus*-infected WT astrocytes (◆), the percentage of neuronal death was significantly less than the one obtained in co-cultures with WT microglia (▲, *p* < 0.005) although still significant from the untreated control co-cultures with IL-6 KO microglia (○, *p* < 0.05). Finally, in co-cultures where both microglia and SN from *B. abortus*-infected astrocytes were obtained from IL-6 KO mice, no neuronal death was achieved (Figure 6C) indicating the key role of this cytokine in mediating microglia-induced neuronal death. Indeed, the importance of IL-6 in the overall phagoptotic phenomenon was corroborated by stimulating
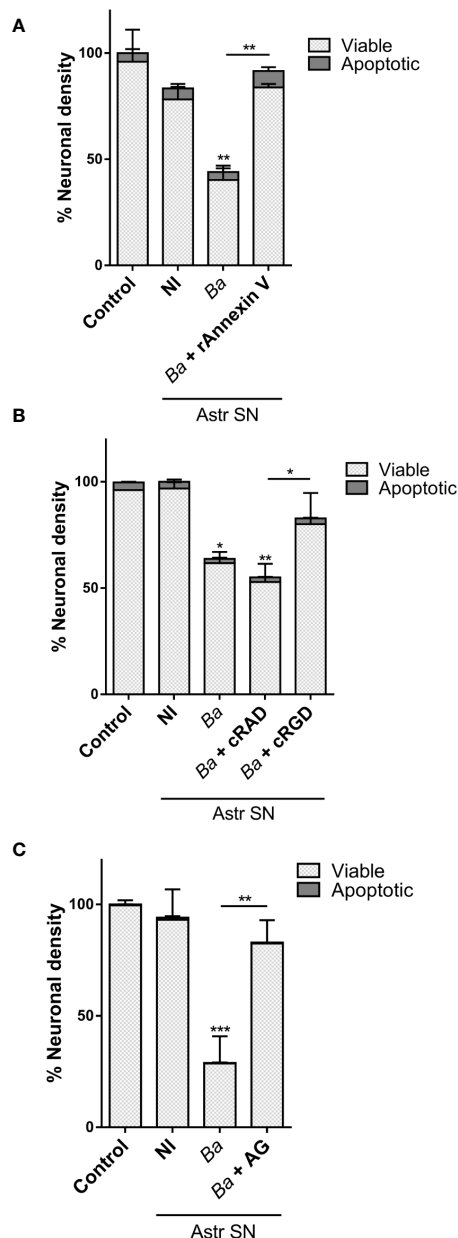
FIGURE 4

Microglia activated by *B. abortus*-infected astrocytes induce neuronal death by primary phagocytosis. Neurons/microglia co-cultures were stimulated with culture supernatants (Astr SN) from non-infected (NI) or *B. abortus*-infected (*Ba*) astrocytes for 48 h in the absence or the presence of recombinant Annexin V (rAnnexin V; 200 nM) **(A)**, the cyclic (c) peptides cRAD or cRGD (100 μM) **(B)**, or aminoguanidine (AG; 200 μM) **(C)**. Untreated co-cultures were used as control conditions (control). The density of neurons was evaluated by fluorescence microscopy. The percentage (%) of viable and apoptotic neurons was calculated vs. control. Data are shown as mean ± SEM from a representative experiment of three performed. *p < 0.05; **p < 0.005; ***p < 0.0005 vs. control condition, except where indicated.
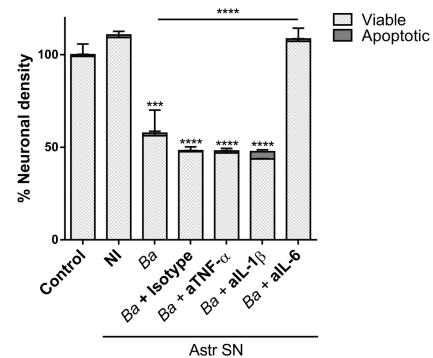

FIGURE 5

Neutralization of IL-6 prevents neuronal death induced by bystander-activated microglia. SN from non-infected (NI) or *B. abortus*-infected (*Ba*) astrocytes (Astr SN) were pre-incubated or not with anti-TNF-α (aTNF-α; 10 μg/mL), anti-IL-1β (aIL-1β; 10 μg/mL), anti-IL-6 (aIL-6; 5 μg/mL) monoclonal antibodies, or isotype control (10 μg/mL) and used to stimulate neurons/microglia co-cultures for 48 h. Untreated co-cultures were used as control conditions (control). The percentage (%) of viable and apoptotic neurons was calculated vs. control. Data are shown as mean ± SEM from a representative experiment of three performed. ***p < 0.0005; ****p < 0.0001 vs. control condition, except where indicated.

neuronal death (Figure 6E). These results indicate that IL-6 from both astrocytes and microglia contributes to neuronal death and demonstrate the critical of this cytokine in the phagoptosis of neurons induced by *B. abortus* regardless of its cellular source.

IL-6 neutralization inhibits the phagocytic activity of microglia, but not its inflammatory activation

As we have mentioned before, the elimination of neurons by primary phagocytosis relies on two simultaneous events: NO secretion (which induces the exposure of the "eat-me" signal PS on neurons) and the increased phagocytic capacity of microglia (8). To investigate in which of these two phenomena (if not in both) IL-6 is involved, we performed neutralization experiments using IL-6 neutralizing antibodies and evaluated microglia functions. Neutralization of IL-6 resulted in complete abrogation of the phagocytic ability of microglia as induced by SN from *B. abortus*-infected astrocytes, as compared to microglia treated with SN from uninfected astrocytes or untreated control ones, when the phagocytic capacity was evaluated as uptake of negatively charged microbeads (both the number of phagocytic microglia and the number of beads taken per microglia) (Figure 7A). Conversely, the inflammatory activation of microglia measured as TNF-α secretion; and more importantly, NO release, was not modified when SN were treated with neutralizing IL-6 antibodies (Figures 7B, C). Isotype control antibody has no effect in none of these phenomena. These results indicate that IL-6 increases the phagocytic activity of microglia, but it does not modify its inflammatory activation. Indeed, although recombinant IL-6 increased the microglial phagocytosis of beads (Figure 7D), without inducing an inflammatory response (as TNF-α and NO

microglia with heat-killed *B. abortus* (HKBA), a surrogate of infection (8). At variance with WT microglia, IL-6 KO microglia were unable to induce neuronal phagoptosis upon activation by *B. abortus* directly (Figure 6D). Also, infection of WT microglia in the presence of IL-6 neutralizing antibody completely abrogated
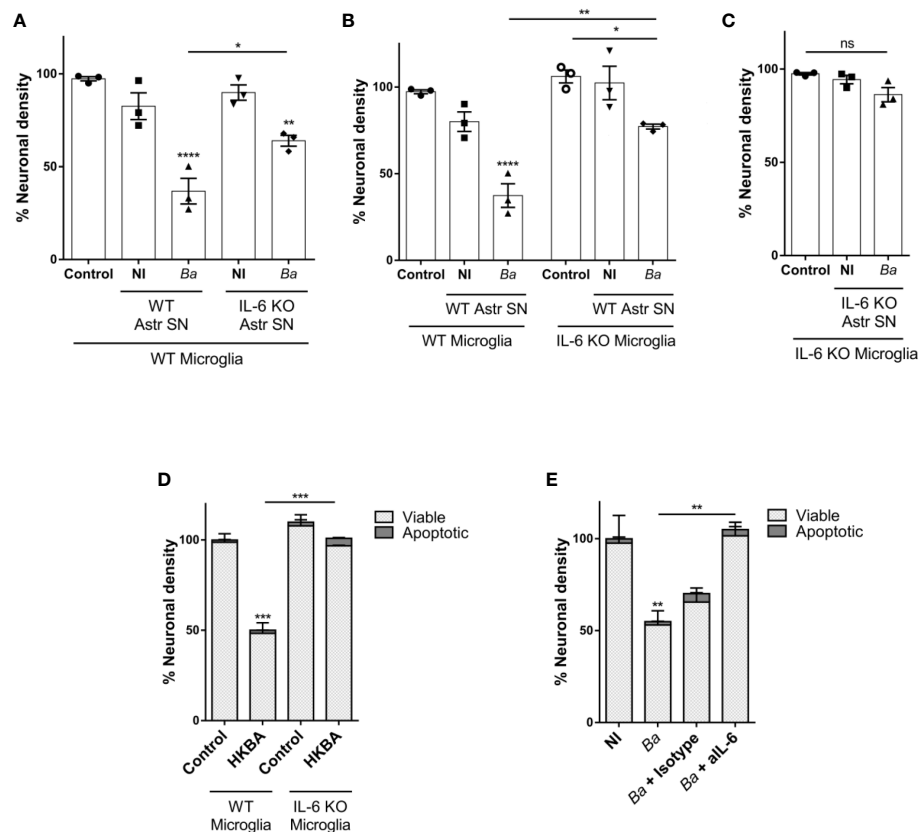
FIGURE 6

IL-6 secreted by both astrocytes and microglia contributes to neuronal death by primary phagocytosis. Neurons/microglia wild-type (WT) co-cultures were stimulated with SN from non-infected (NI) or *B. abortus*-infected (*Ba*) WT and IL-6 knock out (KO) astrocytes (Astr SN) for 48 h **(A)**. Co-cultures of neurons and WT or IL-6 KO microglia were treated with SN from non-infected (NI) or (*B*) *abortus*-infected (*Ba*) WT astrocytes for 48 h **(B)**. Co-cultures of WT neurons and IL-6 KO microglia were treated with SN from non-infected (NI) or (*B*) *abortus*-infected (*Ba*) IL-6 KO astrocytes for 48 h **(C)**. Co-cultures of neurons and WT or IL-6 KO microglia were stimulated with heat-killed (*B*) *abortus* (HKBA; 1x10⁸ bacteria/mL) for 48 h **(D)**. Neurons/microglia co-cultures were infected with *B. abortus* (MOI 100) in the presence of anti-IL-6 monoclonal antibody (aIL-6; 5 µg/mL) or its isotype control (5 µg/mL) for 48 h **(E)**. The percentage (%) of neuronal density is shown as mean ± SEM from three independent experiments using neurons, microglia, and astrocytes SN from different animals **(A-C)**. The percentage (%) of viable and apoptotic neurons was calculated vs. WT control (untreated) condition. Data are shown as mean ± SEM from a representative experiment of three performed **(D, E)**. *p < 0.05; **p < 0.005; ***p < 0.0005; ****p < 0.0001 vs. WT control condition, except where indicated. Non-significant (ns).

secretion) (Figures 7E, F), it did not induce neuronal loss (Figure 7G). Overall, these results indicate that IL-6 is necessary, but not sufficient to induce neuronal death by primary phagocytosis since it is only involved in the increased phagocytic capacity of microglial cells.

IL-6 activates microglia via trans-signaling

IL-6 may stimulate responses in a target cell in two different manners. Classical signaling involves the binding of IL-6 to the membrane-bound IL-6 receptor (IL-6R). As the IL-6R lacks intrinsic signal transduction capacity, subsequent downstream signaling takes place upon engagement of its β-receptor gp130 on the cell membrane (36, 37). IL-6R also exists as a soluble protein (sIL-6R), which forms a complex with IL-6 and stimulates cells that express gp130 with or without endogenous IL-6R expression in a mechanism known as trans-signaling (38). To complicate things

further, a soluble form of gp130 (sgp130) is also formed. sgp130 acts as a decoy receptor and can inhibit trans-signaling but does not affect classical signaling (39). As neutralizing IL-6 antibodies block both classical and trans-signaling, we used a recombinant gp130-Fc chimerical protein to investigate which signaling pathway is involved in the activation of microglia. For this, neurons/microglia co-cultures were treated with SN from *B. abortus*-infected astrocytes in the presence of gp130-Fc and its effect vis-à-vis the effect of IL-6 neutralizing antibodies was compared. The presence of gp130-Fc completely inhibited neuronal death induced by activated microglia. Again, neutralization of IL-6 also resulted in complete abrogation of neuronal death induced by activated microglia. Isotype control antibody had no effect on primary phagocytosis of neurons induced by activated microglia (Figure 8A). Moreover, the presence of gp130-Fc resulted in complete abrogation of microglia´s phagocytic capacity induced by SN from *B. abortus*-infected astrocytes (Figure 8B). Thus, trans-signaling was involved in mediating the phagocytic activity of
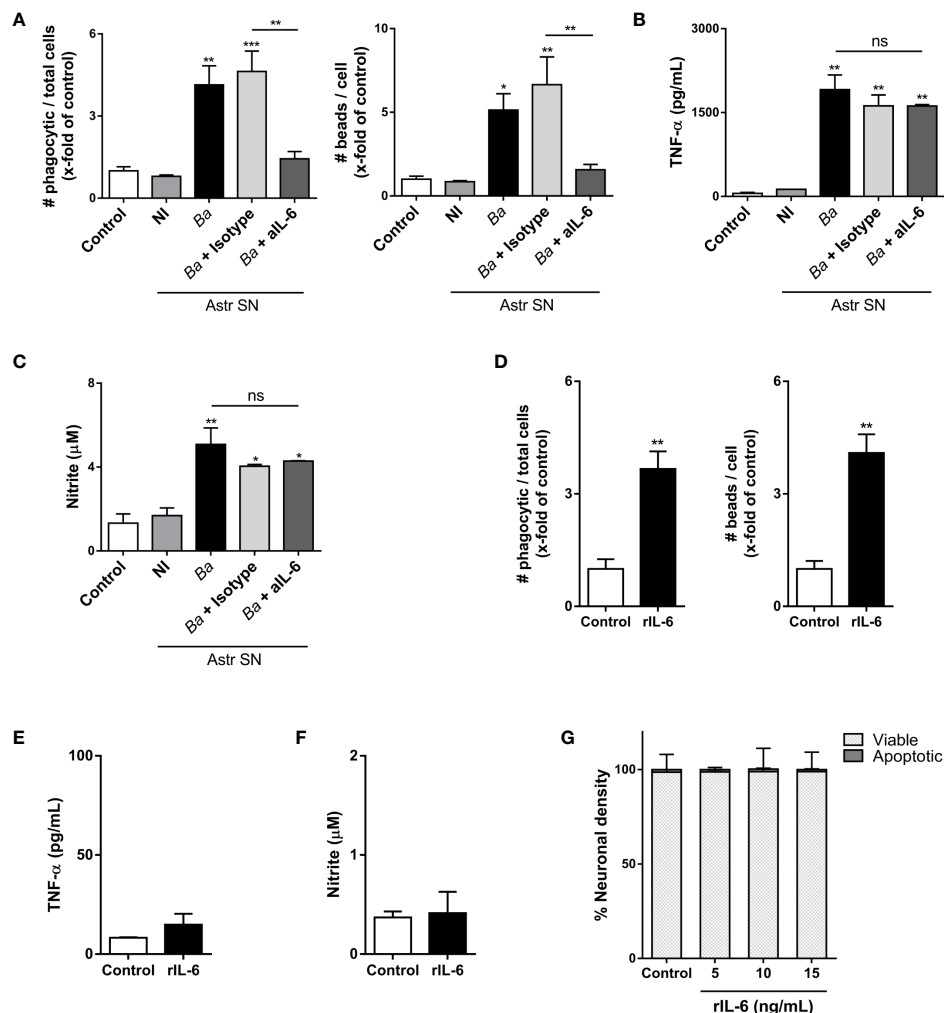
FIGURE 7

IL-6 neutralization inhibits the phagocytic activity of microglia, but not its inflammatory activation. Microglia cultures were stimulated with SN from non-infected (NI) or *B. abortus*- infected (*Ba*) astrocytes (Astr SN) in the presence of anti-IL-6 monoclonal antibody (aIL-6; 5 µg/mL) or its isotype control (5 µg/mL) for 48 (h) Untreated co-culture was used as a control condition (control). Phagocytic activity was evaluated by a phagocytosis assay with fluorescent 5 µm beads that were visualized by fluorescence microscopy **(A)**. Secretion of TNF-α **(B)** and NO **(C)** were also measured in cultured supernatants. Microglia cultures were treated with recombinant IL-6 (rIL-6; 15 ng/mL) for 48 h and phagocytic activity **(D)**, secretion of TNF-α **(E)**, and release of NO **(F)** were measured. Neurons/microglia co-cultures were treated with different concentrations of rIL-6 for 48 h, and neuronal density was evaluated. Untreated co-culture was used as a control condition (control). The percentage (%) of viable and apoptotic neurons was calculated vs. control **(G)**. Data are shown as mean $\pm$ SEM from a representative experiment of three performed. *$p < 0.05$; **$p < 0.005$; ***$p < 0.0005$ vs. control condition, except where indicated. Non-significant (ns).

microglia treated with SN from *B. abortus*-infected astrocytes. These results indicate that IL-6 trans-signaling increases microglia phagocytosis, leading to neuronal death.

Discussion

The entry of *B. abortus* to the brain parenchyma takes place within infected monocytes as a Trojan horse after peripheral inflammation of the blood-brain barrier induced by the bacterium (31, 40). In turn, these infected monocytes served as bacterial sources for *de novo* infection for astrocytes and microglia (40). Infection of glial cells has a profound impact on neurobrucellosis physiopathology, provoking deleterious consequences on astrocytes

(20), the blood-brain barrier (41), and neurons (8). Although it is well recognized that when *B. abortus* infects a cell population, *Brucella*-infected cells constitute only 5-10% of all cells (42, 43); the activation of astrocytes and microglia during neurobrucellosis is widespread (20), potentially indicating that a bystander activation of non-infected glial cells could be taking place in the inflammatory milieu generated by infection. Thus, we sought to investigate the role of *B. abortus*-infected astrocytes on microglial activation and how this interaction might affect neuronal health.

Our results demonstrate that SN from *B. abortus*-infected astrocytes induce the inflammatory activation of microglia, which, in turn, execute the death of neurons. It has been well documented that in the context of infection, there exists a bystander activation of uninfected cells by inflammatory mediators released by adjacent
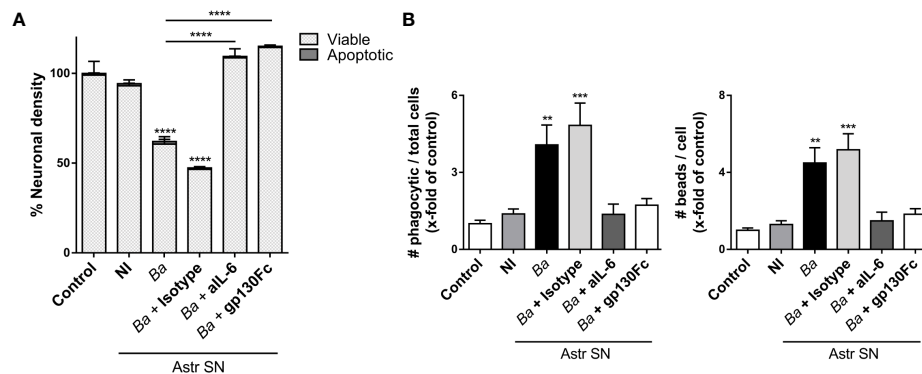
FIGURE 8
IL-6 activates microglia via trans-signaling. SN from non-infected (NI) or *B. abortus*-infected (*Ba*) astrocytes (Astr SN) were pre-incubated or not with recombinant gp130Fc (100 ng/mL), anti-IL-6 (aIL-6; 5 µg/mL) monoclonal antibody, or its isotype control (5 µg/mL) and used to stimulate neurons/microglia co-cultures **(A)** or microglia cultures **(B)** for 48 (h) Untreated cultures were used as control conditions (control). Percentage (%) of viable and apoptotic neurons was calculated vs. control **(A)**. The phagocytic activity of microglia was evaluated **(B)**. Data are shown as mean ± SEM from a representative experiment of three performed. **p < 0.005; ***p < 0.0005,****p < 0.0001 vs. control condition, except where indicated.

infected cells that allow the amplification and propagation of deleterious innate immune responses in most tissues (44–46). In this context, the relevance of infection of astrocytes relies on the fact that these cells are the most abundant cellular type of the CNS, in comparison with microglia which comprise approximately 5-10% of the brain parenchyma (47). Thus, astrocytic inflammatory activation would have a profound impact on the overall innate immune activation of CNS during neurobrucellosis by activating neighboring glial cells such as microglia (48), which in turn become lethal to neurons.

SN from *B. abortus*-infected astrocytes could not directly induce neuronal death, which is similar to our previous observations using conditioned media from *B. abortus*-infected microglia (8). In both cases, we have demonstrated the requirement of the presence of and close contact between microglia and neurons for neuronal demise to occur, a condition that enables phagocytosis of live neurons by activated microglia. SN from *B. abortus*-infected astrocytes induce the overall activation of microglia with the release of pro-inflammatory mediators and the increase of their phagocytic capacity. These two features were key in the execution of live neurons by phagoptosis, a recently described mechanism whereby microglia activated by *B. abortus* kill neurons by phagocytosing them (8). Thus, the phagoptosis of neurons by *B. abortus*-activated microglia might be triggered at least in two ways: by direct *B. abortus* infection of microglia or by a bystander microglial activation through inflammatory mediators secreted by *Brucella*-infected astrocytes, vindicating primary phagocytosis of neurons as a major contributor of CNS pathology in brucellosis.

It has been described that a transgenic mouse model with astrocytes overexpressing IL-6 (GFAP-IL6) in the CNS exhibits neurodegeneration associated with learning (49) and motor impairment (50, 51). Interestingly, brain sections of these mice exhibit activation of microglia (microgliosis), which correlates with the loss of different neuronal subpopulations. However, the molecular mechanisms underlying neuronal death in these models have not been reported. Our findings describe a mechanism in which IL-6 is implicated in the neuronal death

induced by microglia activated by SN from *B. abortus*-infected astrocytes. Moreover, our results demonstrate that IL-6 is a key cytokine necessary for primary phagocytosis of neurons to occur since neutralization of this cytokine completely abrogates neuronal loss. The mechanism of action, the cellular source, and the signaling pathway of IL-6 in our model merit discussion.

IL-6 is solely involved in increasing the phagocytic capacity of activated microglia as induced by SN from *B. abortus*-infected astrocytes and does not participate in their inflammatory activation, ascribing to IL-6 a direct action on the microglial phagocytic function. This is true in our neurobrucellosis model and also in other models in which IL-6 elicited transcriptomic and molecular changes that increase the phagocytic capacity of phagocytes (52, 53). Moreover, in some of these models, the IL-6-mediated increment of the phagocytic capacity of microglia also correlates with neurodegeneration (54, 55). Interestingly, IL-6 was also shown to increase the expression and the adhesion capacity of the α_v subunit of the vitronectin receptor (56), the receptor involved in the neuronal loss induced by *B. abortus*-activated microglia ((8) and Figure 4). Our results also indicate that although necessary, IL-6 is not sufficient to induce microglia-mediated neuronal death since the concomitant release of NO by activated microglia must take place for neuronal loss to occur.

IL-6 is a major cytokine in the CNS produced by glial cells, neurons, and endothelial cells under physiological and pathological conditions (57), including neurobrucellosis (20, 41, 58). Particularly, in neurobrucelosis, infiltrating CD8+ T-cells (59) could also be a source of IL-6, as it has been described in multiple sclerosis (60). Despite its autocrine action on many of these IL-6-producing cells (61–63), the functions exerted by IL-6 in CNS are induced in most cases in a paracrine way on neighboring cells (27, 54, 55, 64). In this complex scenario, astrocyte-derived IL-6 seems to have a major role in microglia functions (29, 51, 55). Our results show that both autocrine microglia-derived and paracrine astrocyte-secreted IL-6 add up to endow microglial cells with up-regulated phagocytic capacity that allows them to phagocytose neurons and go along with the contention of a multicellular

source of production for IL-6 in CNS to undertake both physiological and pathological functions (34, 57).

The pleiotropic functions of IL-6 are clearly depicted in CNS where it promotes anti- and pro-inflammatory outcomes (65). IL-6 also plays a critical role in the normal homeostasis of neuronal tissue stimulating neurogenesis, neuronal differentiation, and neuroprotection against tissue injury (65, 66). Under homeostatic conditions, low levels of IL-6 are detectable in the brain (66). Yet, its production increases during many pathological conditions, including neurobrucellosis (58). This IL-6 overproduction in the brain usually leads to neurodegeneration (49, 50). In fact, several authors suggest that IL-6 might be a relevant biomarker for poor prognosis in several mental pathologies such as depressive disorders (67) and schizophrenia (68), or in the use of drugs such as cannabis and ketamine (69, 70), which are conditions related to neuronal dysfunction and with similar symptoms to the ones of neurobrucellosis (3–5). In any case, classification of anti- or pro-inflammatory profiles by IL-6 on CNS is sensitive not only to its levels (low levels under healthy steady state conditions vs. high levels during pathological conditions), cellular source (neurons, astrocytes, oligodendrocytes, microglia, and endothelial cells), and targets of IL-6 itself but more important to the IL-6 signaling pathway.

Our results demonstrate that neuronal death induced by microglia activated by SN from *B. abortus*-infected astrocytes proceeds via trans-signaling and agree with the contention that neuronal damage depends on trans-signaling in the CNS, whereas classical signaling has a regenerative role in neural tissue (71). Of note, although IL-6 by itself has been reported to elicit gp130-mediated signaling in IL-6R-bearing microglial cells, these cells are also responsive to hyper-IL-6 (a recombinant chimera that mimics trans-signaling) (34, 72). Notably, in pathological states, it seems that classical signaling is not involved in the activation of microglial cells as microglia become pro-inflammatory when exposed to hyper-IL-6 *versus* IL-6 alone (73), emphasizing the different pathological consequences between classical and trans-signaling on microglia.

In fact, classical IL-6 signaling has been hypothesized to have a neuroprotective role within the CNS (74–76). Although still under debate in the field, currently available data have confirmed a context-dependent and mutual modulation of classical or trans-signaling IL-6 pathways that lead to anti- and pro-inflammatory responses (65).

Finally, it is our contention that neuronal death caused by primary phagocytosis induced by *B. abortus*-activated microglia is at the basis of neurocognitive symptoms observed in neurobrucellosis (8, 24). In the present study, we have evidence that, besides infection, the bystander activation of microglia through inflammatory mediators secreted by *Brucella*-infected astrocytes can also induce such a phenomenon and that IL-6 is essential for the phagocytosis of neurons to take place. Since the use of humanized anti-interleukin-6 receptor antibody (tocilizumab) has been identified as a putative treatment for inflammatory encephalopathies involving neurological symptoms (77–79), the data presented in this paper suggest that the use of such a therapeutic approach might represent a medical strategy to restrict IL-6 signaling, possibly reducing the symptoms associated

with neurobrucellosis or other neurological diseases in which the phagocytic activation of microglia is involved.

Data availability statement

The raw data supporting the conclusions of this article will be made available by the authors, without undue reservation.

Ethics statement

The animal study was approved by Ethics Committee of Care and Use of Laboratory animals of the School of Medicine, Universidad de Buenos Aires. The study was conducted in accordance with the local legislation and institutional requirements.

Conflict of interest

The authors declare that the research was conducted in the absence of any commercial or financial relationships that could be construed as a potential conflict of interest.

Publisher's note

All claims expressed in this article are solely those of the authors and do not necessarily represent those of their affiliated organizations, or those of the publisher, the editors and the reviewers. Any product that may be evaluated in this article, or claim that may be made by its manufacturer, is not guaranteed or endorsed by the publisher.

References

1. Pappas G, Akritidis N, Bosilkovski M, Tsianos E. Brucellosis. *N Engl J Med* (2005) 352(22):2325–36. doi: 10.1056/NEJMra050570

2. Bouza E, Garcia de la Torre M, Parras F, Guerrero A, Rodriguez-Creixems M, Gobernado J. Brucellar meningitis. *Rev Infect Dis* (1987) 9(4):810–22. doi: 10.1093/clinids/9.4.810

3. McLean DR, Russell N, Khan MY. Neurobrucellosis: clinical and therapeutic features. *Clin Infect diseases: an Off Publ Infect Dis Soc America.* (1992) 15(4):582–90. doi: 10.1093/clind/15.4.582

4. Nalini A, Nagarathna S, Rajeshwari S, Rose D, Veena Kumari HB, Nagalingam M. Dementia, peripheral neuropathy, and chronic meningitis in Neurobrucellosis. *Indian J Pathol Microbiol* (2012) 55(1):128–30. doi: 10.4103/0377-4929.94896

5. Shehata GA, Abdel-Baky L, Rashed H, Elamin H. Neuropsychiatric evaluation of patients with brucellosis. *J neurovirology.* (2010) 16(1):48–55. doi: 10.3109/13550280903586386

6. Wallach JC, Baldi PC, Fossati CA. Clinical and diagnostic aspects of relapsing meningoencephalitis due to Brucella suis. *Eur J Clin Microbiol Infect diseases: Off Publ Eur Soc Clin Microbiol* (2002) 21(10):760–2. doi: 10.1007/s10096-002-0817-y

7. Giambartolomei GH, Wallach JC, Baldi PC. Neurobrucellosis. In: *Encephalitis: Diagnosis and Treatment*, vol. 14. . USA: The Egerton Group New York (2008). p. 255–72.

8. Rodriguez AM, Delpino MV, Miraglia MC, Costa Franco MM, Barrionuevo P, Dennis VA, et al. Brucella abortus-activated microglia induce neuronal death through primary phagocytosis. *Glia.* (2017) 65(7):1137–51. doi: 10.1002/glia.23149

9. Allen NJ, Lyons DA. Glia as architects of central nervous system formation and function. *Science.* (2018) 362(6411):181–5. doi: 10.1126/science.aat0473

10. Chung WS, Allen NJ, Eroglu C. Astrocytes control synapse formation, function, and elimination. *Cold Spring Harbor Perspect Biol* (2015) 7(9):a020370. doi: 10.1101/cshperspect.a020370

11. Fields RD, Stevens-Graham B. New insights into neuron-glia communication. *Science.* (2002) 298(5593):556–62. doi: 10.1126/science.298.5593.556

12. Liddelow SA, Barres BA. Reactive astrocytes: production, function, and therapeutic potential. *Immunity.* (2017) 46(6):957–67. doi: 10.1016/j.immuni.2017.06.006

13. Wheeler MA, Clark IC, Tjon EC, Li Z, Zandee SEJ, Couturier CP, et al. MAFG-driven astrocytes promote CNS inflammation. *Nature.* (2020) 578(7796):593–9. doi: 10.1038/s41586-020-1999-0

14. Colombo E, Farina C. Astrocytes: key regulators of neuroinflammation. *Trends Immunol* (2016) 37(9):608–20. doi: 10.1016/j.it.2016.06.006

15. Prinz M, Jung S, Priller J. Microglia biology: one century of evolving concepts. *Cell.* (2019) 179(2):292–311. doi: 10.1016/j.cell.2019.08.053

16. Rothhammer V, Borucki DM, Tjon EC, Takenaka MC, Chao CC, Ardura-Fabregat A, et al. Microglial control of astrocytes in response to microbial metabolites. *Nature.* (2018) 557(7707):724–8. doi: 10.1038/s41586-018-0119-x

17. Vainchtein ID, Chin G, Cho FS, Kelley KW, Miller JG, Chien EC, et al. Astrocyte-derived interleukin-33 promotes microglial synapse engulfment and neural circuit development. *Science.* (2018) 359(6381):1269–73. doi: 10.1126/science.aal3589

18. Pfrieger FW, Barres BA. Synaptic efficacy enhanced by glial cells in vitro. *Science* (1997) 277(5332):1684–7. doi: 10.1126/science.277.5332.1684

19. Matejuk A, Ransohoff RM. Crosstalk between astrocytes and microglia: an overview. *Front Immunol* (2020) 11:1416. doi: 10.3389/fimmu.2020.01416

20. Garcia Samartino C, Delpino MV, Pott Godoy C, Di Genaro MS, Pasquevich KA, Zwerdling A, et al. Brucella abortus induces the secretion of proinflammatory mediators from glial cells leading to astrocyte apoptosis. *Am J pathology.* (2010) 176(3):1323–38. doi: 10.2353/ajpath.2010.090503

21. Miraglia MC, Scian R, Samartino CG, Barrionuevo P, Rodriguez AM, Ibanez AE, et al. Brucella abortus induces TNF-alpha-dependent astroglial MMP-9 secretion through mitogen-activated protein kinases. *J neuroinflammation.* (2013) 10:47. doi: 10.1186/1742-2094-10-47

22. Baldi PC, Giambartolomei GH. Immunopathology of brucella infection. *Recent patents anti-infective Drug discovery.* (2013) 8(1):18–26. doi: 10.2174/1574891X11308010005

23. Baldi PC, Giambartolomei GH. Pathogenesis and pathobiology of zoonotic brucellosis in humans. *Rev scientifique technique.* (2013) 32(1):117–25. doi: 10.20506/rst.32.1.2192

24. Rodriguez AM, Delpino MV, Miraglia MC, Giambartolomei GH. Immune mediators of pathology in neurobrucellosis: from blood to central nervous system. *Neuroscience.* (2019) 410:264–73. doi: 10.1016/j.neuroscience.2019.05.018

25. Liddelow SA, Guttenplan KA, Clarke LE, Bennett FC, Bohlen CJ, Schirmer L, et al. Neurotoxic reactive astrocytes are induced by activated microglia. *Nature.* (2017) 541(7638):481–7. doi: 10.1038/nature21029

26. White RE, Yin FQ, Jakeman LB. TGF-alpha increases astrocyte invasion and promotes axonal growth into the lesion following spinal cord injury in mice. *Exp neurology.* (2008) 214(1):10–24. doi: 10.1016/j.expneurol.2008.06.012

27. Sanchis P, Fernandez-Gayol O, Comes G, Escrig A, Giralt M, Palmiter RD, et al. Interleukin-6 derived from the central nervous system may influence the pathogenesis of experimental autoimmune encephalomyelitis in a cell-dependent manner. *Cells* (2020) 9(2):330. doi: 10.3390/cells9020330

28. Wheeler MA, Jaronen M, Covacu R, Zandee SEJ, Scalisi G, Rothhammer V, et al. Environmental control of astrocyte pathogenic activities in CNS inflammation. *Cell.* (2019) 176(3):581–96.e18. doi: 10.1016/j.cell.2018.12.012

29. Savarin C, Hinton DR, Valentin-Torres A, Chen Z, Trapp BD, Bergmann CC, et al. Astrocyte response to IFN-gamma limits IL-6-mediated microglia activation and progressive autoimmune encephalomyelitis. *J neuroinflammation.* (2015) 12:79. doi: 10.1186/s12974-015-0293-9

30. Pollak CN, Delpino MV, Fossati CA, Baldi PC. Outer membrane vesicles from Brucella abortus promote bacterial internalization by human monocytes and modulate their innate immune response. *PloS One* (2012) 7(11):e50214. doi: 10.1371/journal.pone.0050214

31. Rodriguez AM, Trotta A, Melnyczajko AP, Miraglia MC, Kim KS, Delpino MV, et al. Brucella abortus-Stimulated Platelets Activate Brain Microvascular Endothelial Cells Increasing Cell Transmigration through the Erk1/2 Pathway. *Pathogens* (2020) 9(9):708. doi: 10.3390/pathogens9090708

32. Harms AS, Lee JK, Nguyen TA, Chang J, Ruhn KM, Trevino I, et al. Regulation of microglia effector functions by tumor necrosis factor signaling. *Glia* (2012) 60(2):189–202. doi: 10.1002/glia.21254

33. West PK, Viengkhou B, Campbell IL, Hofer MJ. Microglia responses to interleukin-6 and type I interferons in neuroinflammatory disease. *Glia* (2019) 67(10):1821–41. doi: 10.1002/glia.23634

34. Rothaug M, Becker-Pauly C, Rose-John S. The role of interleukin-6 signaling in nervous tissue. *Biochim Biophys Acta* (2016) 1863(6 Pt A):1218–27. doi: 10.1016/j.bbamcr.2016.03.018

35. Monif M, Reid CA, Powell KL, Drummond KJ, O'Brien TJ, Williams DA. Interleukin-1beta has trophic effects in microglia and its release is mediated by P2X7R pore. *J neuroinflammation.* (2016) 13(1):173. doi: 10.1186/s12974-016-0621-8

36. Taga T, Hibi M, Hirata Y, Yamasaki K, Yasukawa K, Matsuda T, et al. Interleukin-6 triggers the association of its receptor with a possible signal transducer, gp130. *Cell.* (1989) 58(3):573–81. doi: 10.1016/0092-8674(89)90438-8

37. Hibi M, Murakami M, Saito M, Hirano T, Taga T, Kishimoto T. Molecular cloning and expression of an IL-6 signal transducer, gp130. *Cell.* (1990) 63(6):1149–57. doi: 10.1016/0092-8674(90)90411-7

38. Rose-John S, Heinrich PC. Soluble receptors for cytokines and growth factors: generation and biological function. *Biochem J* (1994) 300(Pt 2):281–90. doi: 10.1042/bj3000281

39. Jostock T, Mullberg J, Ozbek S, Atreya R, Blinn G, Voltz N, et al. Soluble gp130 is the natural inhibitor of soluble interleukin-6 receptor transsignaling responses. *Eur J Biochem* (2001) 268(1):160–7. doi: 10.1046/j.1432-1327.2001.01867.x

40. Miraglia MC, Rodriguez AM, Barrionuevo P, Rodriguez J, Kim KS, Dennis VA, et al. Brucella abortus traverses brain microvascular endothelial cells using infected monocytes as a trojan horse. *Front Cell infection Microbiol* (2018) 8:200. doi: 10.3389/fcimb.2018.00200

41. Miraglia MC, Costa Franco MM, Rodriguez AM, Bellozi PM, Ferrari CC, Farias MI, et al. Glial cell-elicited activation of brain microvasculature in response to brucella abortus infection requires ASC inflammasome-dependent IL-1beta production. *J Immunol* (2016) 196(9):3794–805. doi: 10.4049/jimmunol.1500908

42. Celli J, de Chastellier C, Franchini DM, Pizarro-Cerda J, Moreno E, Gorvel JP. Brucella evades macrophage killing via VirB-dependent sustained interactions with the endoplasmic reticulum. *J Exp Med* (2003) 198(4):545–56. doi: 10.1084/jem.20030088

43. Barrionuevo P, Delpino MV, Pozner RG, Velasquez LN, Cassataro J, Giambartolomei GH. Brucella abortus induces intracellular retention of MHC-I

molecules in human macrophages down-modulating cytotoxic CD8(+) T cell responses. *Cell Microbiol* (2013) 15(4):487–502. doi: 10.1111/cmi.12058

44. Dolowschiak T, Chassin C, Ben Mkaddem S, Fuchs TM, Weiss S, Vandewalle A, et al. Potentiation of epithelial innate host responses by intercellular communication. *PloS Pathog* (2010) 6(11):e1001194. doi: 10.1371/journal.ppat.1001194

45. Copenhaver AM, Casson CN, Nguyen HT, Duda MM, Shin S. IL-1R signaling enables bystander cells to overcome bacterial blockade of host protein synthesis. *Proc Natl Acad Sci United States America.* (2015) 112(24):7557–62. doi: 10.1073/pnas.1501289112

46. Woodward JJ, Iavarone AT, Portnoy DA. c-di-AMP secreted by intracellular Listeria monocytogenes activates a host type I interferon response. *Science.* (2010) 328 (5986):1703–5. doi: 10.1126/science.1189801

47. Salter MW, Stevens B. Microglia emerge as central players in brain disease. *Nat Med* (2017) 23(9):1018–27. doi: 10.1038/nm.4397

48. Farina C, Aloisi F, Meinl E. Astrocytes are active players in cerebral innate immunity. *Trends Immunol* (2007) 28(3):138–45. doi: 10.1016/j.it.2007.01.005

49. Heyser CJ, Masliah E, Samimi A, Campbell IL, Gold LH. Progressive decline in avoidance learning paralleled by inflammatory neurodegeneration in transgenic mice expressing interleukin 6 in the brain. *Proc Natl Acad Sci United States America.* (1997) 94(4):1500–5. doi: 10.1073/pnas.94.4.1500

50. Campbell IL, Abraham CR, Masliah E, Kemper P, Inglis JD, Oldstone MB, et al. Neurologic disease induced in transgenic mice by cerebral overexpression of interleukin 6. *Proc Natl Acad Sci United States America.* (1993) 90(21):10061–5. doi: 10.1073/pnas.90.21.10061

51. Gyengesi E, Rangel A, Ullah F, Liang H, Niedermayer G, Asgarov R, et al. Chronic microglial activation in the GFAP-IL6 mouse contributes to age-dependent cerebellar volume loss and impairment in motor function. *Front Neurosci* (2019) 13:303. doi: 10.3389/fnins.2019.00303

52. Gou X, Yuan J, Wang H, Wang X, Xiao J, Chen J, et al. IL-6 during influenza-streptococcus pneumoniae co-infected pneumonia-A protector. *Front Immunol* (2019) 10:3102. doi: 10.3389/fimmu.2019.03102

53. Frisdal E, Lesnik P, Olivier M, Robillard P, Chapman MJ, Huby T, et al. Interleukin-6 protects human macrophages from cellular cholesterol accumulation and attenuates the proinflammatory response. *J Biol Chem* (2011) 286(35):30926–36. doi: 10.1074/jbc.M111.264325

54. Chakrabarty P, Jansen-West K, Beccard A, Ceballos-Diaz C, Levites Y, Verbeeck C, et al. Massive gliosis induced by interleukin-6 suppresses Abeta deposition in *vivo*: evidence against inflammation as a driving force for amyloid deposition. *FASEB journal: Off Publ Fed Am Societies Exp Biol* (2010) 24(2):548–59. doi: 10.1096/fj.09-141754

55. West PK, McCorkindale AN, Guennewig B, Ashhurst TM, Viengkhou B, Hayashida E, et al. The cytokines interleukin-6 and interferon-alpha induce distinct microglia phenotypes. *J neuroinflammation.* (2022) 19(1):96. doi: 10.1186/s12974-022-02441-x

56. Schoeler D, Grutzkau A, Henz BM, Kuchler J, Kruger-Krasagakis S. Interleukin-6 enhances whereas tumor necrosis factor alpha and interferons inhibit integrin expression and adhesion of human mast cells to extracellular matrix proteins. *J Invest Dermatol* (2003) 120(5):795–801. doi: 10.1046/j.1523-1747.2003.12126.x

57. Erta M, Quintana A, Hidalgo J. Interleukin-6, a major cytokine in the central nervous system. *Int J Biol Sci* (2012) 8(9):1254–66. doi: 10.7150/ijbs.4679

58. Krishnan C, Kaplin AI, Graber JS, Darman JS, Kerr DA. Recurrent transverse myelitis following neurobrucellosis: immunologic features and beneficial response to immunosuppression. *J neurovirology.* (2005) 11(2):225–31. doi: 10.1080/13550280590922801

59. Seidel G, Pardo CA, Newman-Toker D, Olivi A, Eberhart CG. Neurobrucellosis presenting as leukoencephalopathy: the role of cytotoxic T lymphocytes. *Arch Pathol Lab Med* (2003) 127(9):e374–7. doi: 10.5858/2003-127-e374-NPALTR

60. Trinschek B, Lüssi F, Haas J, Wildemann B, Zipp F, Wiendl H, et al. Kinetics of IL-6 production defines T effector cell responsiveness to regulatory T cells in multiple sclerosis. *PloS One* (2013) 8(10):e77634. doi: 10.1371/journal.pone.0077634

61. Ramesh G, Alvarez AL, Roberts ED, Dennis VA, Lasater BL, Alvarez X, et al. Pathogenesis of Lyme neuroborreliosis: Borrelia burgdorferi lipoproteins induce both proliferation and apoptosis in rhesus monkey astrocytes. *Eur J Immunol* (2003) 33 (9):2539–50. doi: 10.1002/eji.200323872

62. Van Wagoner NJ, Benveniste EN. Interleukin-6 expression and regulation in astrocytes. *J neuroimmunology* (1999) 100(1-2):124–39. doi: 10.1016/S0165-5728(99) 00187-3

63. Marz P, Cheng JG, Gadient RA, Patterson PH, Stoyan T, Otten U, et al. Sympathetic neurons can produce and respond to interleukin 6. *Proc Natl Acad Sci United States America.* (1998) 95(6):3251–6. doi: 10.1073/pnas.95.6.3251

64. Kummer KK, Zeidler M, Kalpachidou T, Kress M. Role of IL-6 in the regulation of neuronal development, survival and function. *Cytokine.* (2021) 144:155582. doi: 10.1016/j.cyto.2021.155582

65. Garcia-Juarez M, Camacho-Morales A. Defining the role of anti- and pro-inflammatory outcomes of interleukin-6 in mental health. *Neuroscience.* (2022) 492:32–46. doi: 10.1016/j.neuroscience.2022.03.020

66. Baune BT, Konrad C, Grotegerd D, Suslow T, Birosova E, Ohrmann P, et al. Interleukin-6 gene (IL-6): a possible role in brain morphology in the healthy adult brain. *J neuroinflammation.* (2012) 9:125. doi: 10.1186/1742-2094-9-125

67. Ting EY, Yang AC, Tsai SJ. Role of interleukin-6 in depressive disorder. *Int J Mol Sci* (2020) 21(6):2194. doi: 10.3390/ijms21062194

68. Chase KA, Cone JJ, Rosen C, Sharma RP. The value of interleukin 6 as a peripheral diagnostic marker in schizophrenia. *BMC Psychiatry* (2016) 16:152. doi: 10.1186/s12888-016-0866-x

69. Abdel-Salam OME. The neurotoxic effects of cannabis on brain: review of clinical and experimental data. *Mol Sci Applications.* (2022) 2:11–23. doi: 10.37394/232023.2022.2.3

70. Abdel-Salam OME, Youness ER, Omara AASEA.Oxidative stress and neuronal injury after cannabis and ketamine administration*WSEAS Trans Biol Biomedicine* (2021) 18:126–35 doi: 10.37394/23208.2021.18.15

71. Campbell IL, Erta M, Lim SL, Frausto R, May U, Rose-John S, et al. Trans-signaling is a dominant mechanism for the pathogenic actions of interleukin-6 in the brain. *J neuroscience: Off J Soc Neurosci* (2014) 34(7):2503–13. doi: 10.1523/JNEUROSCI.2830-13.2014

72. Hsu MP, Frausto R, Rose-John S, Campbell IL. Analysis of IL-6/gp130 family receptor expression reveals that in contrast to astroglia, microglia lack the oncostatin M receptor and functional responses to oncostatin M. *Glia.* (2015) 63(1):132–41. doi: 10.1002/glia.22739

73. Lin HW, Levison SW. Context-dependent IL-6 potentiation of interferon-gamma-induced IL-12 secretion and CD40 expression in murine microglia. *J neurochemistry.* (2009) 111(3):808–18. doi: 10.1111/j.1471-4159.2009.06366.x

74. Hirota H, Kiyama H, Kishimoto T, Taga T. Accelerated Nerve Regeneration in Mice by upregulated expression of interleukin (IL) 6 and IL-6 receptor after trauma. *J Exp Med* (1996) 183(6):2627–34. doi: 10.1084/jem.183.6.2627

75. Chucair-Elliott AJ, Conrady C, Zheng M, Kroll CM, Lane TE, Carr DJ. Microglia-induced IL-6 protects against neuronal loss following HSV-1 infection of neural progenitor cells. *Glia.* (2014) 62(9):1418–34. doi: 10.1002/glia.22689

76. Yang P, Wen H, Ou S, Cui J, Fan D. IL-6 promotes regeneration and functional recovery after cortical spinal tract injury by reactivating intrinsic growth program of neurons and enhancing synapse formation. *Exp neurology.* (2012) 236(1):19–27. doi: 10.1016/j.expneurol.2012.03.019

77. Muccioli L, Pensato U, Cani I, Guerra L, Provini F, Bordin G, et al. COVID-19-related encephalopathy presenting with aphasia resolving following tocilizumab treatment. *J neuroimmunology.* (2020) 349:577400. doi: 10.1016/j.jneuroim.2020.577400

78. Borah P, Deb PK, Chandrasekaran B, Goyal M, Bansal M, Hussain S, et al. Neurological consequences of SARS-CoV-2 infection and concurrence of treatment-induced neuropsychiatric adverse events in COVID-19 patients: navigating the uncharted. *Front Mol biosciences.* (2021) 8:627723. doi: 10.3389/fmolb.2021.627723

79. Liu L, Liu S, Guan W, Zhang L. Efficacy of tocilizumab for psychiatric symptoms associated with relapsing polychondritis: the first case report and review of the literature. *Rheumatol Int* (2016) 36(8):1185–9. doi: 10.1007/s00296-016-3509-0

Guanylate-binding protein-5 is involved in inflammasome activation by bacterial DNA but only the cooperation of multiple GBPs accounts for control of *Brucella abortus* infection

Fabio V. Marinho[1†], Camila Brito[1†],
Ana Carolina V. S. C. de Araujo[2,3] and Sergio C. Oliveira[1,3*]

[1]Instituto de Ciências Biológicas, Departamento de Bioquímica e Imunologia, Universidade Federal de Minas Gerais, Belo Horizonte, Brazil, [2]Instituto de Ciências Biológicas, Departamento de Genética, Ecologia e Evolução, Universidade Federal de Minas Gerais, Belo Horizonte, Brazil, [3]Instituto de Ciências Biomédicas, Departamento de Imunologia, Universidade de São Paulo, São Paulo, Brazil

Introduction: Guanylate-binding proteins (GBPs) are produced in response to pro-inflammatory signals, mainly interferons. The most studied cluster of GBPs in mice is on chromosome 3. It comprises the genes for GBP1-to-3, GBP5 and GBP7. In humans, all GBPs are present in a single cluster on chromosome 1. Brucella abortus is a Gram-negative bacterium known to cause brucellosis, a debilitating disease that affects both humans and animals. Our group demonstrated previously that GBPs present on murine chromosome 3 (GBPchr3) is important to disrupt Brucella-containing vacuole and GBP5 itself is important to Brucella intracellular LPS recognition. In this work, we investigated further the role of GBPs during B. abortus infection.

Methods and results: We observed that all GBPs from murine chromosome 3 are significantly upregulated in response to B. abortus infection in mouse bone marrow-derived macrophages. Of note, GBP5 presents the highest expression level in all time points evaluated. However, only GBPchr3-/- cells presented increased bacterial burden compared to wild-type macrophages. Brucella DNA is an important Pathogen-Associated Molecular Pattern that could be available for inflammasome activation after BCV disruption mediated by GBPs. In this regard, we observed reduced IL-1β production in the absence of GBP2 or GBP5, as well as in GBPchr3-/- murine macrophages. Similar result was showed by THP-1 macrophages with downregulation of GBP2 and GBP5 mediated by siRNA. Furthermore, significant reduction on caspase-1 p20 levels, LDH release and Gasdermin-D conversion into its mature form (p30 N-terminal subunit) was observed only in GBPchr3-/- macrophages. In an *in vivo* perspective, we found that GBPchr3-/- mice had increased B. abortus burden and higher number of granulomas per area of liver tissue, indicating increased disease severity.

Discussion/conclusion: Altogether, these results demonstrate that although GBP5 presents a high expression pattern and is involved in inflammasome activation by bacterial DNA in macrophages, the cooperation of multiple GBPs from murine chromosome 3 is necessary for full control of Brucella abortus infection.

1 Introduction

Interferons (IFNs) are crucial cytokines of the host's defense against microorganisms. IFNs signaling leads to the induction of genes called IFN-stimulated genes (ISGs) that will act as potent inducers of antimicrobial effector response against intracellular bacteria. Among the most important ISGs are GTPases. Currently, four families of IFN-induced GTPases are described, namely Immunity-Related GTPases (IRGs), Myxoma resistance proteins (MX), Very Large Inducible GTPases (VLIGs/GVINs), and Guanylate-Binding Proteins (GBPs) (1, 2). GBPs range from 65 to 73 kDa and are among the most abundantly IFN-gamma induced genes (3). These proteins are included in the dynamin GTPase protein superfamily, alike the other IFN-induced GTPases (2). GBP genes are clustered on two chromosomes in mice. One cluster on chromosome 3 contains GBP1, GBP2, GBP3, GBP5 and GBP7 genes, while another cluster on chromosome 5 includes GBP4, GBP6, GBP8, GBP9, GBP10, GBP11 genes. Conversely, humans have 7 GBPs (numbered 1-to-7) and all of them are in a single cluster on chromosome 1 (4, 5). A new classification of GBPs has been proposed recently, which is based on phylogenetic analysis. According to that, only GBP2, GBP5 (both in chromosome 3), and GBP6 (chromosome 5) are orthologs from primates' GBPs. The other GBPs genes were incorrectly annotated and the nomenclature should change (6). As this is still a matter of debate, herein we will use the former nomenclature, with murine GBPs numbered from 1-to-11. GBPs are relevant for protection against intracellular bacteria, including *Listeria monocytogenes*, *Mycobacterium bovis*, *Francisella novicida*, and *Chlamydia sp* (7–11). Moreover, these proteins also have roles in the immune responses against viruses and parasites, e.g. being related to resistant phenotype against Ectromelia virus infection and cerebral toxoplasmosis (12, 13). In cancer as well, GBPs are involved in improved response against tumor growth (14). Among GBPs antimicrobial functions, we can include induction of inflammasome activation, direct killing of the pathogen, changes in the autophagy pathway, and release of Pathogen-Associated Molecular Patterns (PAMPs) that can activate the cell (11, 15). These functions can take place concurrently, as found in *F. novicida* infection (10), or unlinked, as happens during *Chlamydia* infection, where GBPs-mediated inflammasome activation is uncoupled from vacuole rupture or direct killing (8).

Brucella abortus is Gram-negative bacterium classified as facultative intracellular. It infects mainly macrophages and dendritic cells, which will function as replicative niches for this pathogen. To survive and replicate inside host cells, *B. abortus* induces the formation of a membranous compartment known as *Brucella*-containing vacuole (BCV) (16). This compartment interacts with Endoplasmic Reticulum (ER) and is an important step of the *Brucella* intracellular cycle (16). Several virulence factors help this bacterium to replicate while remaining stealthy. For instance, the VirB Type IV secretion system is necessary to deliver virulence factors that will control BCV-ER interactions. Also, *Brucella* LPS is non-classical, being less toxic and less active in Toll-Like Receptor 4 (TLR4) stimulation than other Gram-negative bacteria (17). Thus, comprehension of the mechanisms that permeate this host-pathogen interaction can help to deal better with stealthy infections.

Overall, the cluster of GBPs from murine chromosome 3 (from here on referred to as GBPchr3) are the most studied, notably GBP1, GBP2 and GBP5 (18). Our group has demonstrated that GBPchr3 is important to induce BCV disruption and inflammasome activation, increasing bacterial burden upon *B. abortus* infection (19). Furthermore, GBP5 has been shown to participate in *B. abortus* LPS intracellular recognition in macrophages and non-canonical inflammasome activation (20). Another important PAMP that may gain access to host cytosol after BCV disruption is bacterial DNA. Once in the cytoplasm, it can activate STING or AIM2 inflammasome pathways (19, 21). It was shown that activation of AIM2 by *B. abortus* DNA is essential for IL-1β production and control of *B. abortus* infection (21). However, it is still unclear if GBP5 also influences on *Brucella* DNA inflammasome activation and protection against brucellosis. In this study, we show that GBP5 participates in bacterial DNA-inflammasome activation, although cooperation of multiple GBPs from murine chromosome 3 is necessary for defense against *B. abortus* infection.

Abbreviations: BMDM, bone marrow-derived macrophages; BCV, *Brucella*-containing vacuole; GBP, Guanylate-binding protein; GBPchr3, the cluster of GBPs from murine chromosome 3 (GBP1-to-3, GBP5 and GBP7).

2 Materials and methods

2.1 Animals

C57BL/6 wild-type mice were obtained from the Federal University of Minas Gerais (UFMG) animal facility. Dr. Thirumala-Devi Kanneganti from St. Jude Children's Research Hospital, Memphis, USA, provided GBP5^{-/-} mice. Dr. Petr Broz from the University of Lausanne, Lausanne, Switzerland, provided GBPchr3^{-/-} and GBP2^{-/-} mice. All mice were kept in a laboratory facility free of pathogens. Male and female mice were used at 8-12 weeks of age. All experimental protocols were reviewed and approved by the Animal Studies Committee (protocol CEUA/ UFMG 69/2020).

2.2 Bacteria, growth conditions and DNA extraction

Brucella abortus virulent strain S2308 from our bacteria library was grown in *Brucella* broth (BB; BD Biosciences, Franklin Lakes, NJ) for 3 days under constant agitation (180 RPM, 37°C). Bacterial suspension was pelleted (4000 RPM, 4°C), suspended in glycerol 10% and frozen at -80°C until use. Prior to *in vitro* infection or DNA extraction, freshly unfrozen *B. abortus* was grown in BB under constant agitation at 37°C. *B. abortus* DNA was obtained using Illustra bacteria genomicPrep Spin Kit (GE HealthCare, Chicago, IL) accordingly to manufacturer instructions.

2.3 Generation of bone marrow-derived macrophages and *in vitro* stimulation

Macrophages were obtained from the bone marrow of mice (bone marrow-derived macrophages; BMDMs), as described in (11). Briefly, bone marrow cells were removed from femurs and tibias and cultured in DMEM (Gibco/Thermo Fisher Scientific, Waltham, MA) containing 10% heat-inactivated FBS (Gibco/Thermo Fisher Scientific), 1% HEPES, penicillin G sodium (100 U/mL), streptomycin sulfate (100 µg/mL) and 20% L929 cell-conditioned medium (LCCM) in petri dishes (approximately 1×10^7 cells/petri dish). Cells were incubated at 37°C with 5% CO_2 for a total of 7 days. On the fourth day of culture, 10 mL of fresh medium was added. At seventh day, macrophages were detached and seeded in 24-well plates

$(5 \times 10^5$ cells/well) and used for *in vitro* studies. To stimulate BMDMs, *B. abortus* (MOI 100:1) suspended in supplemented DMEM (1% FBS, 1% HEPES) was added. To evaluate inflammasome activation mediated by *B. abortus* DNA, cells were first primed with Pam3CSK4 (Pam, 1 µg/mL; InvivoGen, San Diego, CA) for 4 hours. Following, medium was changed and cells were transfected with bacterial DNA (1 µg/mL) using FuGENE HD (Promega, Madison, WI), accordingly to manufacturer instructions. Unless otherwise specified, stimulation was performed for 17 hours. As a positive control for inflammasome activation, cells were primed with Pam (1 µg/mL) for 4 hours following addition of 20 µM nigericin sodium salt (Sigma-Aldrich) in the last 45 minutes of incubation. Stimulation with Pam (1 µg/mL) for 17h was used as internal control. Culture supernatants were collected and subsequently used for cytokine analysis, western blot, or LDH release evaluation. IL-1β, TNF-α, IL-6 and IL-12p40 production was measured in the supernatants of cells by ELISA using a DuoSet kit (R&D Systems, Minneapolis, MN), according to the manufacturer's guidelines.

2.4 Knockdown of GBP genes in THP-1 cells and BMDMs via small interfering RNA

THP-1 cells culture was performed as described in (22). THP-1 macrophages were then transfected with siRNA from siGENOME SMARTpools (Dharmacon, Lafayette, CO) using the GenMute siRNA transfection reagent according to the manufacturer's instructions (SignaGen, Rockville, MD). siGENOME SMARTpool siRNAs specific for human GBP1 (M-005153-02-0005), GBP2 (M-011867-00-0005), GBP3 (M-031864-01-0005), GBP5 (M-018178-00-0005), and GBP7 (M-032072-01-0005) were used in this study. A control siRNA pool was used (D-001206-14-05). After 42 hours of siRNA transfection, cells were stimulated as described for BMDMs. Culture supernatants were collected and subsequently used for cytokine analysis and LDH release evaluation. Human IL-1β production was measured in the supernatants of cells by ELISA using a DuoSet kit (R&D Systems). Alternatively, BMDMs from C57BL/6 wild-type mice were transfected with siGENOME SMARTpool siRNAs specific for mouse GBP2 (M-040199-00-0005), GBP5 (M-054703-01-0005), or submitted to an integrated co-transfection using a pre-mixture of both siRNAs to achieve double knockdown of GBP2 and GBP5. A control siRNA pool was used. Forty-two hours later, cells were stimulated as described above for evaluation of IL-1β production and LDH release.

TABLE 1 Primers for quantitative real-time PCR.

Primers	Forward 5'-3'	Reverse 5'-3'
mGBP1	GAGTACTCTCTGGAAATGGCCTCAGAAA	TAGATGAAGGTGCTGCTGAGGAGGACTG
mGBP2	CTGCACTATGTGACGGAGCTA	CGGAATCGTCTACCCCACTC
mGBP3	CTGACAGTAAATCTGGAAGCCAT	CCGTCCTGCAAGACGATTCA
mGBP5	CTGAACTCAGATTTTGTGCAGGA	CATCGACATAAGTCAGCACCAG
mGBP7	TCCTGTGTGCCTAGTGGAAAA	CAAGCGGTTCATCAAGTAGGAT
mβ-actin	GGCTGTATTCCCCTCCATCG	CCAGTTGGTAACAATGCCATGT

2.5 Quantitative real-time PCR

BMDMs were stimulated in 24-well plates and homogenized in TRIzol reagent (Invitrogen, Carlsbad, CA, USA) to obtain total RNA accordingly to manufacturer guidelines. Quantitative Real-Time PCR was performed as described in (11). Briefly, cDNA was synthesized by reverse transcription of 2 µg of total RNA. The Quantitative Real-Time PCR reaction used SYBR Green PCR Master Mix (Thermo Fischer Scientific) and was performed in a QuantStudio 3 Real-Time PCR System (Thermo Fischer Scientific). Primers used to amplify a specific fragment corresponding to the gene target are shown in Table 1. Data analysis was performed using the threshold cycle ($\Delta\Delta C_t$) method and results were presented as relative expression units after normalization to the housekeeping gene. PCR measurements were conducted in duplicates.

2.6 Western blot

Western blot for evaluating inflammasome activation was performed as described previously (23). Briefly, cell lysate from BMDM cultures was harvested after *in vitro* stimulation. Cell lysis was performed with Mammalian Protein Extraction Reagent (M-PER) (Thermo Fisher Scientific) supplemented with 1 mM Na_3VO_4, 10 mM NaF and 1:100 of protease inhibitor cocktail (Sigma-Aldrich). Equal protein amounts (25 µg of cell lysate) or equal supernatant volumes (20 µL) were subjected to electrophoresis on 15% polyacrylamide gel, followed by western blotting according to standard techniques. Anti-mouse primary antibodies were used in this study: Mouse monoclonal caspase-1 (p20) (clone Casper 1; AdipoGen Life Sciences, San Diego, CA, USA), Rabbit monoclonal GSDMD (clone EPR19828; Abcam, Cambridge, UK) and Rabbit monoclonal β-actin (clone 12E5; Cell Signaling Technology, Danvers, MA, USA). Loading control (β-actin) was performed using primary antibodies at a 1:5000 dilution. For detection of the other targets, the primary antibodies were used at 1:1000 dilution. Immunoreactive bands were visualized using Luminol chemiluminescent HRP substrate (Millipore, Billerica, MA, USA) in an Amersham Imager 600 (GE HealthCare). Intensity of bands was quantified and normalized using ImageJ software (National Institutes of Health, Bethesda, MD, USA; available at http://imagej.nih.gov/ij/). Unless otherwise specified, numbers below each band represent its intensity relative to the respective β-actin.

2.7 Quantification of lactate dehydrogenase release

The activity of lactate dehydrogenase enzyme was evaluated using a CytoTox96 LDH release kit (Promega) according to the manufacturer's instructions.

2.8 *In vitro* infection and measurement of bacterial intracellular growth

BMDMs (5×10^5 cells; 24-well plates) were plated with DMEM supplemented with 1% FBS and 1% HEPES. Cells were infected with *B. abortus* (MOI 100:1) in 300 µL/well of medium and were incubated for 2 hours at 37°C in a 5% CO_2 atmosphere. Next, to remove noninternalized bacteria, the cells were washed with warm saline and incubated in DMEM supplemented with 10% FBS and 1% HEPES for 24 hours (37°C; 5% CO_2). To obtain the number of intracellular bacteria, macrophages were lysed 2 h (T0) and 24 hours post-infection with sterile and ice-cold H_2O. Serial dilutions were plated in BB agar medium, and the colony-forming units (CFUs) were counted after 3 days of incubation at 37°C.

2.9 *In vivo* infection and immune evaluation

Mice were challenged intraperitoneally with 1 x 10^6 CFU *B. abortus*. Two weeks post-infection, mice were euthanized and both spleen and liver were harvested aseptically from each animal. Spleens were homogenized in saline (NaCl 0.9%), serially diluted, and plated on BB agar for measurement of bacterial burden. The plates were incubated at 37°C for 3 days for CFU determination. The results are shown as Log_{10} CFU mean per gram of organ. Alternatively, spleen cells (1×10^6 cells; 96-well plates) were plated with RPMI supplemented with 10% FBS and penicillin G sodium (100 U/mL)/streptomycin sulfate (100 µg/mL). Cells were infected with *B. abortus* (MOI 100:1). Stimulation with *E. coli* LPS (1 µg/mL) or Concanavalin A (ConA; 5 µg/mL) were used as internal controls. Cells were incubated for 48 hours or 72 hours at 37°C in a 5% CO_2 atmosphere for measurement of TNF-α and IFN-γ levels, respectively, in the supernatants by ELISA using a DuoSet kit (R&D Systems).

2.10 Histopathology

The liver histopathology was performed as described before (11). Briefly, the liver of infected mice was collected and immediately fixed in a 10% buffered formaldehyde solution. Next, tissue was dehydrated, diaphanized, and embedded in paraffin. Tissue sections (2–3 ?m) were stained with Hematoxylin and Eosin (H&E). Digital images of the slides were obtained with an Olympus SC30 camera (Olympus, Tokyo, Japan) using 10× objective lens. Granulomas were identified and quantified by observing the presence of round-shaped cellular infiltrates in the tissue parenchyma. Using ImageJ software, the total area of each section was quantified by converting pixels to square millimeters. Results are expressed as number of granulomas per square centimeter of tissue.

2.11 Statistics

Results are shown as the mean ± SD. Statistically significant differences between the groups were evaluated by two-way ANOVA followed by the Bonferroni *post hoc* test ($p < 0.05$) or one-way ANOVA followed by the Tukey *post hoc* test ($p < 0.05$). GraphPad Prism 9.0 (GraphPad Software, San Diego, CA, USA) was used for the analyses.

3 Results

3.1 GBP5 is upregulated in response to *B. abortus* but cooperation of multiple GBPs is required for control of bacterial growth in macrophages

The GBPs are strongly responsive to IFN-γ but are also induced in response to type-I IFN, TNF-α, IL1-β, IL-1α and TLR agonists (5). However, *Brucella* has different mechanisms to promote a stealthy infection (17). First, we determined the kinetics of GBPs expression in *B. abortus* infected wild-type BMDMs. As early as 2 hours post-infection, we observed significantly increased GBP2, GBP5 and GBP7 mRNA levels compared to non-infected cells (Figure 1A). However, only after 4 hours of infection all GBPs evaluated reached significantly higher expression compared to non-infected cells. These higher expression levels of GBPs remained up to 17 hours, the last time point investigated. Interestingly, GBP5 showed the highest expression level in all time points studied among the GBPs evaluated. Therefore, for the following experiments we selected GBP5 to investigate its role during *B. abortus* infection. Besides GBP5, we also studied GBP2, due to its high expression profile and its aggregation near BCVs during infection (19). Next, we investigated whether higher expression of GBP2 and GBP5 would influence bacterial burden in macrophages. BMDMs from GBP2^{-/-} or

GBP5^{-/-} single deficient mice, from GBPchr3^{-/-} (deficient in all GBPs from murine chromosome 3) and from wild-type mice, were compared concerning *B. abortus* intracellular growth control. Despite the absence of GBP2 or GBP5 did not increase bacterial burden in macrophages (p=0.22 GBP2^{-/-} versus wild-type; p=0.47 GBP5^{-/-} versus wild-type), GBPchr3^{-/-} cells presented significant replication of intracellular *B. abortus* compared to wild-type cells (Figure 1B). Noteworthy, bacterial burden in GBP2^{-/-} and GBP5^{-/-} macrophages are not statistically different from GBPchr3^{-/-} cells, despite being smaller (p=0.77 GBP2^{-/-} versus GBPchr3^{-/-}; p=0.52 GBP5^{-/-} versus GBPchr3^{-/-}). This finding indicates that deficiency on GBP2 or GBP5 alone slightly hampers the control of *B. abortus* growth, but not to a level where bacterial burden becomes significantly higher than wild-type macrophages, like in GBPchr3^{-/-} cells. Together, these data suggest although GBP2 and GBP5 showed high and fast expression pattern, remarkably GBP5, the cooperation of GBPs is necessary for control of *B. abortus* growth intracellularly.

3.2 GBP2 and GBP5 are important for inflammasome activation mediated by *B. abortus* DNA

During the *B. abortus* intracellular cycle, bacterial DNA may become available in cytosol to activate inflammasome pathway after
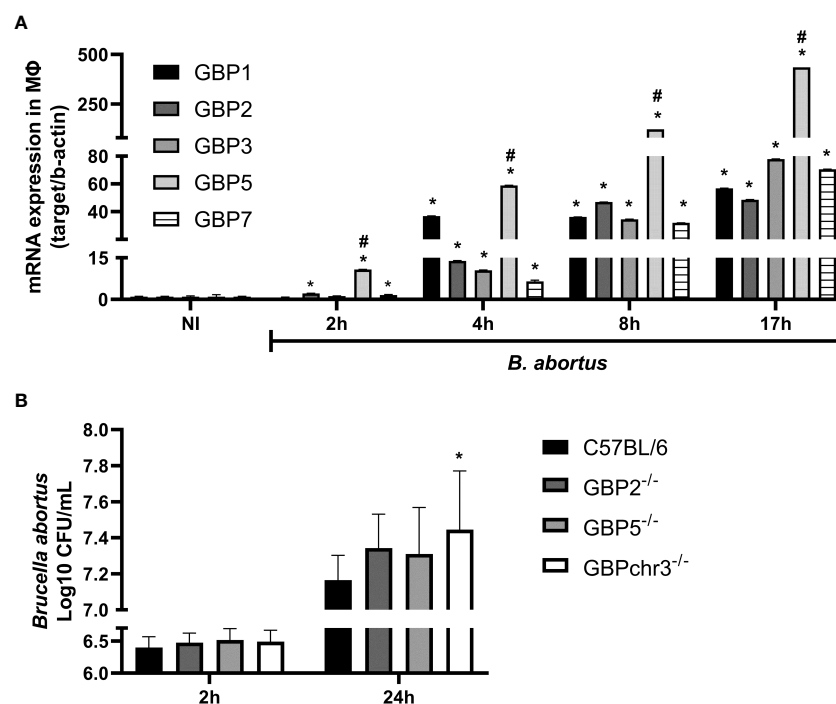
FIGURE 1
GBP5 presents fast expression profile but the participation of multiple GBPs is required to control *B. abortus* intracellular growth in macrophages. **(A)** BMDMs were obtained from C57BL/6 mice and infected with *B. abortus* (MOI 100:1). The expression kinetics of GBPs from murine chromosome 3 was assessed up to 17 hours post-infection. *Significant compared to NI; #Significant compared to GBP1, GBP2, GBP3 and GBP7. Data shown are representative of three independent experiments performed. **(B)** BMDMs from wild-type, GBP2^{-/-}, GBP5^{-/-} or GBPchr3^{-/-} C57BL/6 mice were infected with *B. abortus* (MOI 100:1). After 2 hours cells were washed to remove noninternalized bacteria. The number of intracellular *B. abortus* was obtained by lysis of macrophages at 2 hours and 24 hours post-infection. *Significant compared to C57BL/6. Data shown are pooled from three independent experiments performed.

BCV disruption ([19]). That said, we investigated if GBP2 or GBP5 plays a role in *B. abortus* DNA recognition in macrophages. To mimic this scenario, cells were primed with Pam3CSK4 (Pam) for 4 hours followed by transfection of *B. abortus* DNA to evaluate inflammasome activation. In our experimental design, Pam (TLR2 ligand) was used as first signal replacing LPS (TLR4 ligand) to avoid type-I IFN production, which could cause induction on GBPs expression and mask the results. As shown in Figure 2, we found GBP2$^{-/-}$ and GBP5$^{-/-}$ BMDMs presented reduced IL-1β production and caspase-1 cleavage into its mature form (p20 subunit). Interestingly, GBPchr3$^{-/-}$ BMDMs showed further

reduction in IL-1β and caspase-1 p20 levels, and diminished LDH release and Gasdermin-D (GSDMD) conversion into its mature form (p30 N-terminal subunit). These data suggest GBP2 and GBP5 are important for mature IL-1β secretion but all GBPs from murine chromosome 3 act synergically for full inflammasome activation mediated by bacterial DNA. In a different manner, deficiency in GBP2 or GBP5 alone does not compromise inflammasome activation induced by *B. abortus* infection. In this context, only GBPchr3$^{-/-}$ BMDMs presented diminished IL-1β, caspase-1 p20 and GSDMD p30 levels, and reduced LDH release (Figures 2A–C). To evaluate whether these findings could be extended to human

FIGURE 2
GBP2 and GBP5 contribute to *B. abortus* DNA-triggering of inflammasome response, but full activation requires GBPchr3 in macrophages. BMDMs from wild-type, GBP2$^{-/-}$, GBP5$^{-/-}$ or GBPchr3$^{-/-}$ C57BL/6 mice were infected with *B. abortus* (MOI 100:1) for 17 hours. Alternatively, BMDMs were primed with Pam3CSK4 (Pam; 1 μg/mL) for 4 hours. Following, the medium was changed and cells were transfected with *B. abortus* DNA (1 μg/mL) to evaluate inflammasome activation (17 hours of DNA stimulation). The levels of **(A)** IL-1β production and **(B)** LDH release were assessed in supernatants. *Significant compared to wild-type C57BL/6 BMDMs; #Significant compared to GBP2$^{-/-}$ and GBP5$^{-/-}$ BMDMs. **(C)** p20 subunit of caspase-1 was measured in supernatants while GSDMD was evaluated in cell's lysate. For caspase-1 p20, the quantification of densitometry is expressed as target relative to the housekeeping protein β-actin. For GSDMD, the conversion of Full Length (FL) protein into p30 N-terminal fragment (NT; mature form) was quantified by densitometry. Data shown are representative of three independent experiments performed.
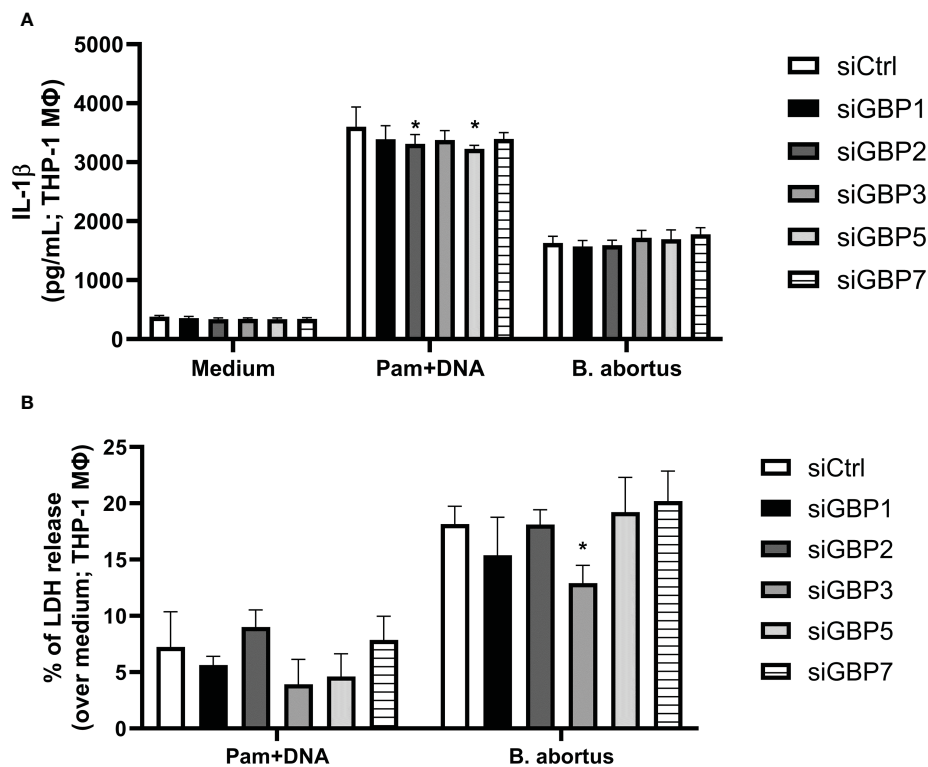
FIGURE 3

GBP2 and GBP5 contribute to IL-1β production in *B. abortus* DNA-stimulated THP-1 cells. THP-1 cells were differentiated into macrophages in the presence of PMA (100 nM; 48 hours). THP-1 macrophages were then transfected with siRNA for knocking down human GBPs (siGBPs) or control siRNA pool (siCTL). Forty-two hours after siRNA transfection, cells were infected with *B. abortus* (MOI 100:1) for 17 hours. Alternatively, macrophages were primed with Pam3CSK4 (Pam; 1 µg/mL) for 4 hours. Following, the medium was changed and cells were transfected with *B. abortus* DNA (1 µg/mL) to evaluate inflammasome activation (17 hours of DNA stimulation). The levels of **(A)** IL-1β production and **(B)** LDH release were assessed in supernatants. *Significant compared to siCTL. Data shown are representative of three independent experiments performed.

macrophages, THP-1 monocyte lineage was used. We knocked down with siRNA all orthologs of murine GBPchr3 and reproduced the conditions of infection or *B. abortus* DNA inflammasome activation as in murine macrophages. The silencing of single human GBPs (hGBPs) expression was not sufficient to alter IL-1β production upon *B. abortus* infection (Figure 3A). However, downregulation of hGBP2 and hGBP5 expression resulted in small but significant reduction in IL-1β levels in response to bacterial DNA, like what was found with BMDMs (Figure 3A). Additionally, knockdown of hGBP2 or hGBP5 did not change significantly LDH release (Figure 3B). These data corroborate the findings in mouse macrophages. Moreover, deficiency in GBPs in BMDMs or knockdown of hGBPs in THP-1 cells did not change inflammasome activation upon Pam + Nigericin stimulation, a NLRP3 inflammasome inducer, indicating that downregulation of GBPs does not influence inflammasome induction by this agonist (Supplementary Figure 1). To further address the interplay of GBPs, we knocked down simultaneously GBP2 and GBP5 in BMDMs. Interestingly, double knockdown of GBP2 and GBP5 results in additional reduction on Pam+DNA-induced IL-1β production compared to single knockdown of either GBP2 or GBP5 (Supplementary Figure 2). Moreover, reduced LDH release was also found in GBP2/5 double silenced BMDMs, although it did

not reach statistical significance (p=0.06 comparing siGBP2/5 versus siCTL; Supplementary Figure 2). These data suggest that GBP2 and GBP5 may cooperate to mediate DNA-induced inflammasome activation. It is important to mention that production of other proinflammatory cytokines, namely TNF-α, IL-6 and IL-12, by BMDMs in response to *B. abortus* infection was not influenced by deficiency of GBPs (Supplementary Figure 3). These results indicate that GBP2 and GBP5 have a role in inflammasome activation mediated by intracellular bacterial DNA in both murine and human macrophages, but multiple GBPs are required for full inflammasome activation upon infection.

3.3 Cooperation of multiple GBPs is necessary to control *B. abortus* infection *in vivo*

Brucellosis is a debilitating infection that tends to become chronic (24). The innate immune responses triggered in early phase of the disease can influence its progression. Since GBP5 is highly induced in macrophages upon *B. abortus* infection, affecting bacterial DNA inflammasome activation, we wonder if this GBP would influence *in vivo* protection. In this regard, C57BL/6 wild-type, GBP2$^{-/-}$, GBP5$^{-/-}$ and GBPchr3$^{-/-}$ mice were infected with *B. abortus* and monitored for
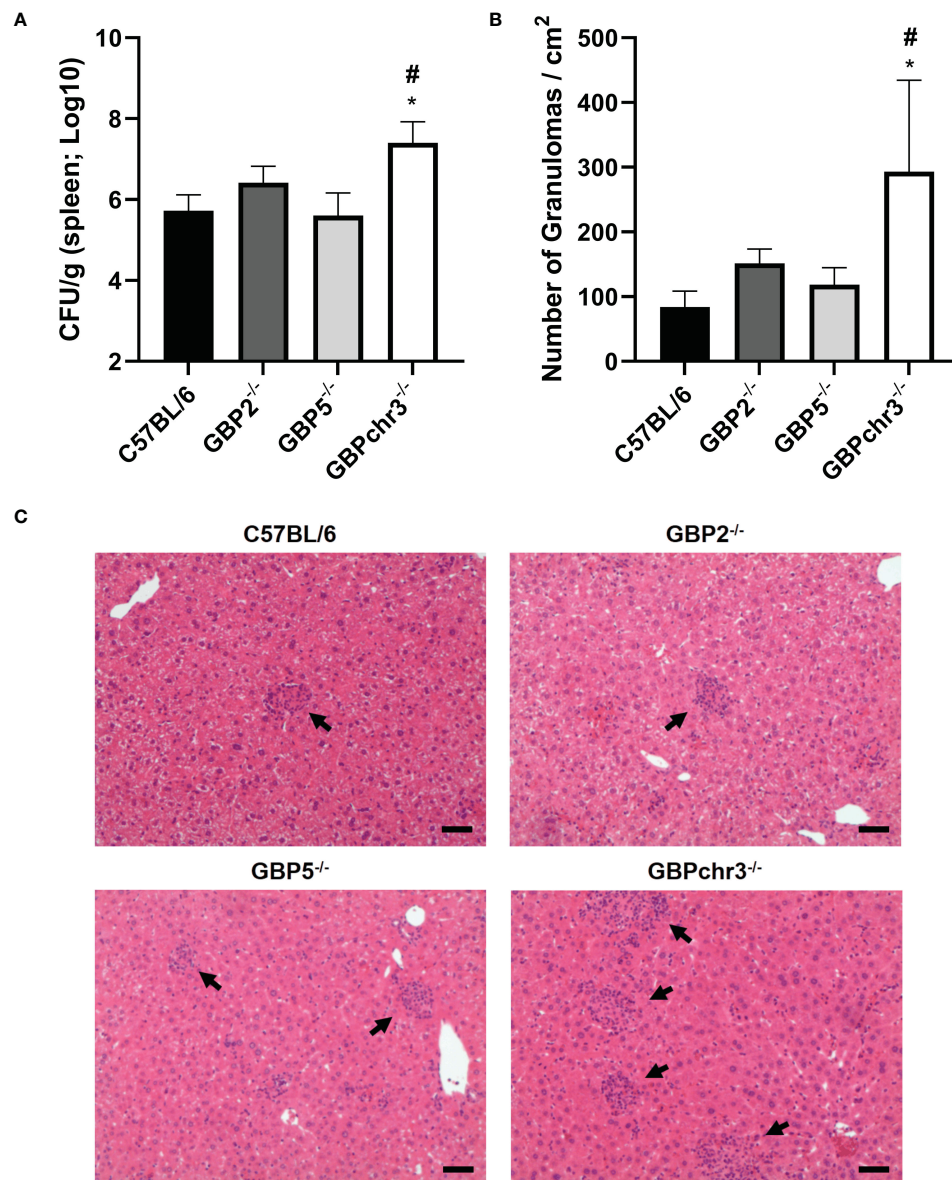
FIGURE 4

Multiple GBPs from murine chromosome 3 are required for *in vivo* control of *B. abortus* infection. Wild-type, GBP2^{-/-}, GBP5^{-/-} and GBPchr3^{-/-} C57BL/6 mice were infected i.p. with 1x10^6 *B. abortus* and monitored for two weeks post-infection. **(A)** The spleen of infected mice was individually macerated, serially diluted, and plated for colony-forming units (CFU) counting. Bacterial burden is shown as Log_{10} CFU mean per gram of organ. *Significant compared to wild-type C57BL/6 mice; #Significant compared to GBP2^{-/-} and GBP5^{-/-} mice. **(B)** The liver of infected mice was collected, embedded in paraffin, and stained with H&E. Slides were evaluated for the number of granulomas and normalized by the covered area (in square centimeters). *Significant compared to wild-type C57BL/6 mice. **(C)** Representative images of each group are shown. The arrows indicate examples of granulomas. Scale bars: 50μm. Data shown are representative of three independent experiments performed.

two weeks post-infection (Figure 4). The single deficiency in GBP5 or GBP2 did not change either the bacterial burden assessed in spleen or the number of granulomas per area found in liver, compared to wild-type mice. Conversely, deficiency in the cluster of GBPs from murine chromosome 3 resulted in increased susceptibility to infection, with enhanced *B. abortus* burden and number of granulomas in mouse livers. Noteworthy, the production of TNF-α and IFN-γ by spleen cells recall response against re-stimulation with *B. abortus* was not influenced by deficiency of GBPs (Supplementary Figure 3). These data suggest multiple GBPs cooperation is necessary for *in vivo* control of bacterial growth and correlated granuloma formation. Altogether,

these results indicate GBP5 has the fastest and highest expression profile among the GBPs present in mouse chromosome 3 upon *B. abortus* infection, influencing bacterial DNA inflammasome activation. However, the cooperation of these GBPs is required for host protection.

4 Discussion

Brucellosis is a widespread zoonosis that affects a great diversity of hosts. The investigation of immune mechanisms that could influence this disease progression is relevant since low antibiotic

treatment success due to high relapse rate of infection is very common in humans (25). In addition, there is no vaccine available to be used on human beings (25). In this study, we found that all GBPs contained in the murine chromosome 3 (GBP1-3, 5 and 7) are significantly upregulated during *B. abortus* infection in BMDMs. Of note, GBP5 presents the fastest and highest expression level. Additionally, both GBP5 and GBP2 influence inflammasome activation mediated by *Brucella* DNA, once deficiency in either GBPs leads to reduced caspase-1 p20 cleavage and IL-1β production. Likewise, the knockdown of GBP5 and GBP2 by siRNA in THP-1 macrophages resulted in decreased IL-1β secretion levels. Nevertheless, severe impairment of *B. abortus*-elicited immune response in macrophages was observed only due to the knockout of all GBPs from murine chromosome 3. This condition rendered cells with decreased ability to control bacterial intracellular growth, hampered inflammasome activation, represented by diminished IL-1β, caspase-1 p20 and GSDMD p30 levels, and reduced LDH release. Additionally, a similar response was observed when GBPch3$^{-/-}$ macrophages were stimulated with *Brucella* DNA delivery in cytosol. These findings correlated with the *in vivo* investigation, where we found that only GBPchr3$^{-/-}$ mice had increased disease severity. Thus, GBP5 and GBP2 contribute to inflammasome activation mediated by intracellular bacterial DNA, but multiple GBPs cooperation is necessary for host protection against *B. abortus* infection.

IFN-induced GTPases are important for an adequate antimicrobial response, particularly against vacuolar pathogens (2). GBPs are conserved between mouse and human and can be triggered by a diverse set of inflammatory signals. They participate in cell-autonomous immune response against various intracellular pathogens. GBPs main functions involve the disruption of parasite-containing vacuoles or microbial membranes, and the supporting for assemble inflammasome complexes and/or recruitment of antimicrobial effectors (26). We found GBPs 1-3, 5 and 7 reach significantly increased expression after 4 hours following *B. abortus* infection. Remarkably, GBP5 presents increased induction 2 hours post-infection and it remains with the highest expression level in all time points evaluated (up to 17 hours). Indeed, as early as 6 hours post-infection with *B. abortus*, it is possible to observe BCV rupture in macrophages, a process that is significantly reduced in GBPchr3$^{-/-}$ cells (19). Moreover, correlating with our data, GBP5 is found among the most expressed genes, presenting several orders of magnitude over non-stimulated cells in *F. novicida* infected BMDMs and LPS + IFN-γ induced M1 human macrophages (10, 27).

The release of bacterial products by GBP-mediated lysis of pathogen's vacuoles or cells activates cytosolic immune pathways, including inflammasomes (26). Here in, we show that GBPchr3$^{-/-}$ macrophages present impaired inflammasome activation and GSDMD cleavage upon *B. abortus* infection. This observation supports previous findings by our group where GBPchr3 deficient BMDMs were unable to trigger pore formation in response to infection, a process that was shown to be dependent on GSDMD and caspase-11 (20). *Brucella* LPS and GBP5 were identified as important players in this context (20). Another PAMP that becomes available after GBPs-mediated disruption of membranes (of

vacuoles or the pathogen itself) is bacterial DNA. It was shown that during *F. novicida* infection, GBPs and AIM2 act ensemble to provide a DNA-based inflammasome activation (9, 10). In this regard, we showed both GBP5 and GBP2 working in *B. abortus* DNA-dependent inflammasome activation. THP-1 macrophages presented similar phenotype, expanding this observation to human cells. It is worth mentioning that GBP5 and GBP2 participated in IL-1β production and caspase-1 activation, but did not influence GSDMD conversion or LDH release. Thus, other GBPs may collaborate in resolving downstream steps of inflammasome activation and pyroptotic fate decision. In accordance, diminished DNA-mediated inflammasome activation was observed in GBPchr3$^{-/-}$ BMDMs, being significantly lower than levels found in GBP5$^{-/-}$ or GBP2$^{-/-}$ cells. Overall, this scenario suggests that several GBPs cooperate in the DNA-mediated inflammasome activation, which was not observed for LPS triggering of the noncanonical inflammasome, where GBP5 alone played a prominent role in the process (20). Interestingly, GBPs relevance on proinflammatory cytokines production in response to *B. abortus* infection seems to be mainly concerning IL-1β production, as TNF-α, IL-6, IL-12 and IFN-γ levels remained similar among wild-type and knockout cells.

Most of the research into the mechanism of GBPs role in infections is carried out in myeloid cells, which are the main niche for *B. abortus* growth. They act as vectors for systemic dissemination to other organs, including spleen and liver, where the bacteria persist within granulomatous inflammatory lesions (24, 25). The single deficiency in GBP5 or GBP2 did not alter significantly the capacity of macrophages to control *B. abortus* replication. However, the absence of the entire cluster of GBPs on mouse chromosome 3 resulted in reduced ability of cells in limiting bacterial growth. This phenotype was translated into increased bacterial burden and elevated number of granulomas per liver tissue area in infected mice, characterizing higher severity of the disease in GBPchr3$^{-/-}$ animals. The augmented *in vivo* susceptibility may result of a deficient recruitment and function of phagocytes, such as macrophages and neutrophils. *Brucella abortus* load often correlates with granuloma formation, which might function as reservoir of bacteria and result in chronic disease (24, 28–30). Similar results were obtained concerning other bacteria such as *M. bovis* BCG and *F. novicida*, where macrophage bacterial burden correlated with host severity of infection (7, 9–11). Indeed, in most scenarios where GBPs influence inflammasome activation, it results in increased susceptibility *in vivo*. Notwithstanding, GBPs also impact other pathways, such as autophagy induction, NADPH oxidase recruitment, or cell activation (7, 11, 31). However, while individual GBPs were identified as crucial for protection against other pathogens (7, 9, 15, 32), this was not observed in *B. abortus* infection. So far, it is the cooperation of multiple GBPs that protects the host.

The manipulation of endosomes to become vacuoles permissive to replication or the escape to the cell cytosol are strategies employed by pathogens to limit immune stimulation. GBPs function as hubs to several intracellular pathways by disrupting parasitic niches, by assessing directly the infectious agent, and/or by acting as platforms that bridge the foreign insult and effector

molecules (7, 10, 19, 33). Both murine and human GBPs form homo- and hetero-polymers to accomplish their antimicrobial function (2). In this regard, GBPs can accumulate in the pathogen's vacuole as densely packed multimers (34). Of note, GBP1, GBP2 and GBP5 can be isoprenylated on their C-terminal domain, which confers affinity to membranes (35). It is suggested that mobilization of GBPs occurs in a hierarchical manner, with GBPs 1, 2 and 5 being the first to be recruited, followed by engagement of other GBPs and/or additional host factors (2). These characteristics place them of central importance to control intracellular infections. Nevertheless, there is emerging evidence that highly virulent pathogens can overcome GBPs activation. For example, although GBPs are important to control *M. bovis* BCG infection, this is not the case for *M. tuberculosis*. The resistance to GBPs mechanisms is, at least partially, dependent on ESX-1 secretion system that is present in *M. tuberculosis* (36). Moreover, the strain *F. tularensis* SCHU S4 (highly virulent), is not susceptible to GBP-mediated control of infection, contrasting the low virulent *F. novicida*. The findings suggest that the virulent bacterium avoids activation of this mechanism (37). In this regard, it remains to be

shown if the *Brucella* VirB secretion system has any role in limiting GBPs activation or if more virulent species, such as *B. melitensis*, can subvert GBPs activation (21, 38). In summary, *B. abortus* induces a fast expression of the cluster of GBPs present on murine chromosome 3, especially GBP5. All these GBPs are important for inflammasome activation, with GBP5 or GBP2 individually playing an important role concerning the intracellular DNA-mediated induction. However, the cooperation of multiple GBPs is indispensable for limiting *Brucella* growth in macrophages and *in vivo*, contributing to less severe disease. Together with former data obtained by our group, we can set an overview of GBPs role during *B. abortus* infection. At the earliest interaction between macrophage and pathogen, there is induction of an immune response dependent on microRNAs (specifically mmu-miR-21a-5p) that will result in increased expression of GBP5 (39). This initial GBPs availability may be sufficient for incipient BCV rupture (40). Following, STING activation mediated by bacterial cyclic dinucleotides will be responsible for further augmentation in GBPs expression, leading to increased BCV disruption and release of PAMPs, including LPS and DNA (19).
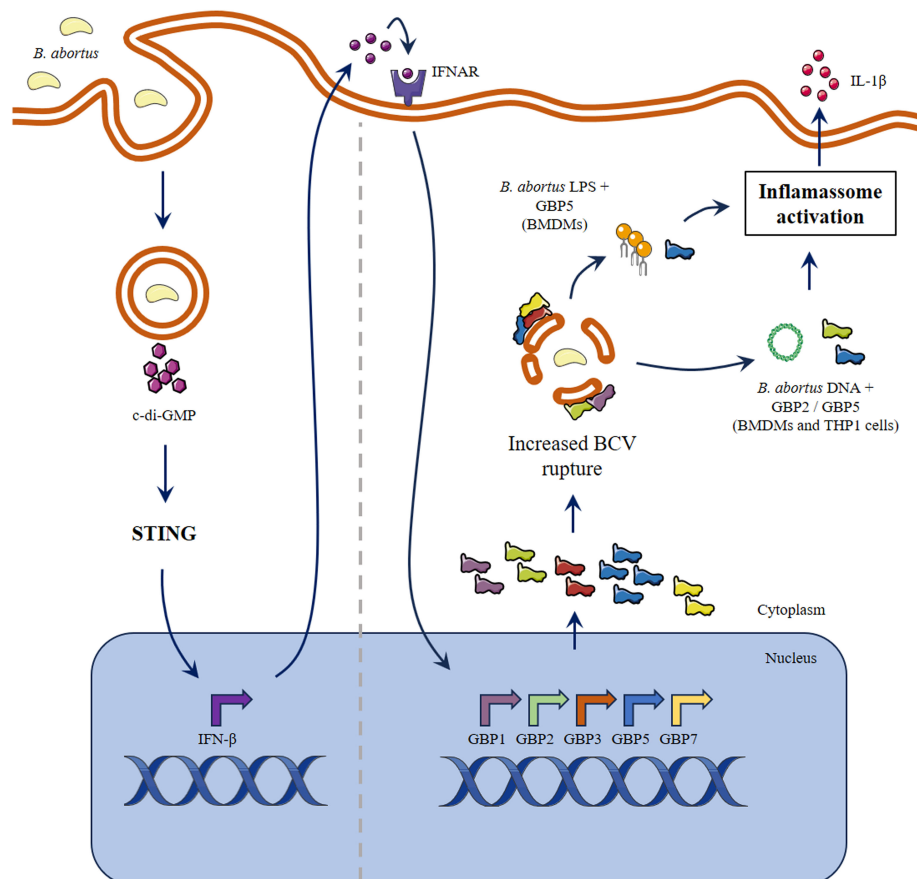

FIGURE 5

Schematic model proposed for the role of GBPs in inflammasome activation during *B. abortus* infection. The early interaction between macrophage and *B. abortus* results in STING activation mediated by bacterial cyclic dinucleotides. In response to type-I IFN and/or other pro-inflammatory stimuli, there is augmentation in expression of the cluster of GBPs on murine chromosome 3. Next, GBPs will be responsible for increased BCV disruption and PAMPs release. The induction of non-canonical inflammasome activation by LPS is dependent on GBP5. On the other hand, *B. abortus* DNA can activate inflammasome in a process where GBP5 and GBP2 participate. Parts of the figure were drawn by using pictures from Servier Medical Art. Servier Medical Art by Servier is licensed under a Creative Commons Attribution 3.0 Unported License (https://creativecommons.org/licenses/by/3.0/).

In this regard, GBP5 will act on LPS-induced noncanonical inflammasome activation [20]. *Brucella* DNA will be free to activate AIM2 inflammasome, in a process where GBP5 and GBP2 participate, or it can also further stimulate STING in a cGAS-dependent manner (Figure 5) [19, 41]. This infection also induces other immune responses that indirectly upregulate GBPs expression, such as Unfolded Protein Response and Galectin-3 immune activation [42, 43]. The immune environment provided is responsible for limiting bacterial growth, which will reflect in fewer granulomas in affected tissues and less severe disease. Altogether, this work extends the knowledge of the relevance of GBPs on *B. abortus* infection.

Data availability statement

The raw data supporting the conclusions of this article will be made available by the authors, without undue reservation.

Ethics statement

Ethical approval was not required for the studies on humans in accordance with the local legislation and institutional requirements because only commercially available established cell lines were used. The animal study was approved by Animal Studies Committee (protocol CEUA/UFMG 69/2020). The study was conducted in accordance with the local legislation and institutional requirements.

Author contributions

FM: Conceptualization, Data curation, Formal Analysis, Investigation, Writing – original draft, Writing – review & editing. CB: Conceptualization, Data curation, Formal Analysis, Investigation, Writing – review & editing. AA: Data curation, Formal Analysis, Investigation, Writing – review & editing. SO: Conceptualization, Funding acquisition, Supervision, Writing – review & editing.

Funding

Conflict of interest

The authors declare that the research was conducted in the absence of any commercial or financial relationships that could be construed as a potential conflict of interest.

The author(s) declared that they were an editorial board member of Frontiers, at the time of submission. This had no impact on the peer review process and the final decision.

Publisher's note

Supplementary material

The Supplementary Material for this article can be found online at: https://www.frontiersin.org/articles/10.3389/fimmu.2024.1341464/full#supplementary-material

References

1. Meunier E, Broz P. Interferon-inducible GTPases in cell autonomous and innate immunity. *Cell Microbiol* (2016) 18:168–80. doi: 10.1111/cmi.12546

2. Rafeld HL, Kolanus W, Van Driel IR, Hartland EL. Interferon-induced GTPases orchestrate host cell-autonomous defence against bacterial pathogens. *Biochem Soc Trans* (2021) 49:1287–97. doi: 10.1042/BST20200900

3. Boehm U, Guethlein L, Klamp T, Ozbek K, Schaub A, Futterer A, et al. Two families of GTPases dominate the complex cellular response to IFN-gamma. *J Immunol* (1998) 161:6715–23. doi: 10.4049/jimmunol.161.12.6715

4. Olszewski MA, Gray J, Vestal DJ. In silico genomic analysis of the human and murine guanylate-binding protein (GBP) gene clusters. *J Interferon Cytokine Res* (2006) 26:328–52. doi: 10.1089/jir.2006.26.328

5. Kresse A, Konermann C, Degrandi D, Beuter-Gunia C, Wuerthner J, Pfeffer K, et al. Analyses of murine GBP homology clusters based on in silico, in *vitro* and in *vivo* studies. *BMC Genomics* (2008) 9:158. doi: 10.1186/1471-2164-9-158

6. Corte-Real JV, Baldauf HM, Melo-Ferreira J, Abrantes J, Esteves PJ. Evolution of guanylate binding protein (GBP) genes in muroid rodents (Muridae and cricetidae) reveals an outstanding pattern of gain and loss. *Front Immunol* (2022) 13:752186. doi: 10.3389/fimmu.2022.752186

7. Kim BH, Shenoy AR, Kumar P, Das R, Tiwari S, Macmicking JD. A family of IFN-gamma-inducible 65-kD GTPases protects against bacterial infection. *Science* (2011) 332:717–21. doi: 10.1126/science.1201711

8. Finethy R, Jorgensen I, Haldar AK, De Zoete MR, Strowig T, Flavell RA, et al. Guanylate binding proteins enable rapid activation of canonical and noncanonical inflammasomes in Chlamydia-infected macrophages. *Infect Immun* (2015) 83:4740–9. doi: 10.1128/IAI.00856-15

9. Man SM, Karki R, Malireddi RK, Neale G, Vogel P, Yamamoto M, et al. The transcription factor IRF1 and guanylate-binding proteins target activation of the AIM2 inflammasome by Francisella infection. *Nat Immunol* (2015) 16:467–75. doi: 10.1038/ni.3118

10. Meunier E, Wallet P, Dreier RF, Costanzo S, Anton L, Ruhl S, et al. Guanylate-binding proteins promote activation of the AIM2 inflammasome during infection with Francisella novicida. *Nat Immunol* (2015) 16:476–84. doi: 10.1038/ni.3119

11. Marinho FV, Fahel JS, De Araujo A, Diniz LTS, Gomes MTR, Resende DP, et al. Guanylate binding proteins contained in the murine chromosome 3 are important to control mycobacterial infection. *J Leukoc Biol* (2020) 108:1279–91. doi: 10.1002/JLB.4MA0620-526RR

12. Anand N, Lutshumba J, Whitlow M, Abdelaziz MH, Mani R, Suzuki Y. Deficiency in indoleamine-2, 3-dioxygenase induces upregulation of guanylate binding protein 1 and inducible nitric oxide synthase expression in the brain during cerebral infection with Toxoplasma gondii in genetically resistant BALB/c mice but not in genetically susceptible C57BL/6 mice. *Microbes Infect* (2022) 24:104908. doi: 10.1016/j.micinf.2021.104908

13. Gao Z, Meng Z, He X, Chen G, Fang Y, Tian H, et al. Guanylate-binding protein 2 exerts GTPase-dependent anti-ectromelia virus effect. *Microorganisms* (2023) 11:1–13. doi: 10.3390/microorganisms11092258

14. Britzen-Laurent N, Lipnik K, Ocker M, Naschberger E, Schellerer VS, Croner RS, et al. GBP-1 acts as a tumor suppressor in colorectal cancer cells. *Carcinogenesis* (2013) 34:153–62. doi: 10.1093/carcin/bgs310

15. Feng S, Enosi Tuipulotu D, Pandey A, Jing W, Shen C, Ngo C, et al. Pathogen-selective killing by guanylate-binding proteins as a molecular mechanism leading to inflammasome signaling. *Nat Commun* (2022) 13:4395. doi: 10.1038/s41467-022-32127-0

16. Celli J. The changing nature of the Brucella-containing vacuole. *Cell Microbiol* (2015) 17:951–8. doi: 10.1111/cmi.12452

17. Glowacka P, Zakowska D, Naylor K, Niemcewicz M, Bielawska-Drozd A. Brucella - virulence factors, pathogenesis and treatment. *Pol J Microbiol* (2018) 67:151–61. doi: 10.21307/pjm-2018-029

18. Schelle L, Corte-Real JV, Esteves PJ, Abrantes J, Baldauf HM. Functional cross-species conservation of guanylate-binding proteins in innate immunity. *Med Microbiol Immunol* (2023) 212:141–52. doi: 10.1007/s00430-022-00736-7

19. Costa Franco MM, Marim F, Guimaraes ES, Assis NRG, Cerqueira DM, Alves-Silva J, et al. Brucella abortus Triggers a cGAS-Independent STING Pathway To Induce Host Protection That Involves Guanylate-Binding Proteins and Inflammasome Activation. *J Immunol* (2018) 200:607–22. doi: 10.4049/jimmunol.1700725

20. Cerqueira DM, Gomes MTR, Silva ALN, Rungue M, Assis NRG, Guimaraes ES, et al. Guanylate-binding protein 5 licenses caspase-11 for Gasdermin-D mediated host resistance to Brucella abortus infection. *PloS Pathog* (2018) 14:e1007519. doi: 10.1371/journal.ppat.1007519

21. Gomes MT, Campos PC, Oliveira FS, Corsetti PP, Bortoluci KR, Cunha LD, et al. Critical role of ASC inflammasomes and bacterial type IV secretion system in caspase-1 activation and host innate resistance to Brucella abortus infection. *J Immunol* (2013) 190:3629–38. doi: 10.4049/jimmunol.1202817

22. Marinho FV, Fahel JS, Scanga CA, Gomes MT, Guimaraes G, Carvalho GR, et al. Lack of IL-1 receptor-associated kinase-4 leads to defective th1 cell responses and renders mice susceptible to mycobacterial infection. *J Immunol* (2016) 197:1852–63. doi: 10.4049/jimmunol.1502157

23. De Araujo A, De Queiroz N, Marinho FV, Oliveira SC. Bacillus Calmette-Guerin-Trained Macrophages Elicit a Protective Inflammatory Response against the Pathogenic Bacteria Brucella abortus. *J Immunol* (2023) 211(5):791–803. doi: 10.4049/jimmunol.2200642

24. Grillo MJ, Blasco JM, Gorvel JP, Moriyon I, Moreno E. What have we learned from brucellosis in the mouse model? *Vet Res* (2012) 43:29. doi: 10.1186/1297-9716-43-29

25. Khurana SK, Sehrawat A, Tiwari R, Prasad M, Gulati B, Shabbir MZ, et al. Bovine brucellosis - a comprehensive review. *Vet Q* (2021) 41:61–88. doi: 10.1080/01652176.2020.1868616

26. Huang S, Meng Q, Maminska A, Macmicking JD. Cell-autonomous immunity by IFN-induced GBPs in animals and plants. *Curr Opin Immunol* (2019) 60:71–80. doi: 10.1016/j.coi.2019.04.017

27. Fujiwara Y, Hizukuri Y, Yamashiro K, Makita N, Ohnishi K, Takeya M, et al. Guanylate-binding protein 5 is a marker of interferon-gamma-induced classically activated macrophages. *Clin Transl Immunol* (2016) 5:e111. doi: 10.1038/cti.2016.59

28. Enright FM, Araya LN, Elzer PH, Rowe GE, Winter AJ. Comparative histopathology in BALB/c mice infected with virulent and attenuated strains of Brucella abortus. *Vet Immunol Immunopathol* (1990) 26:171–82. doi: 10.1016/0165-2427(90)90065-Z

29. Fahel JS, De Souza MB, Gomes MT, Corsetti PP, Carvalho NB, Marinho FA, et al. 5-Lipoxygenase negatively regulates Th1 response during Brucella abortus infection in mice. *Infect Immun* (2015) 83:1210–6. doi: 10.1128/IAI.02592-14

30. Giambartolomei GH, Delpino MV. Immunopathogenesis of hepatic brucellosis. *Front Cell Infect Microbiol* (2019) 9:423. doi: 10.3389/fcimb.2019.00423

31. Yu Y, Pan J, Liu M, Jiang H, Xiong J, Tao L, et al. Guanylate-Binding protein 2b regulates the AMPK/mTOR/ULK1 signalling pathway to induce autophagy during Mycobacterium bovis infection. *Virulence* (2022) 13:875–89. doi: 10.1080/21505594.2022.2073024

32. Selleck EM, Fentress SJ, Beatty WL, Degrandi D, Pfeffer K, Virgin HWT, et al. Guanylate-binding protein 1 (Gbp1) contributes to cell-autonomous immunity against Toxoplasma gondii. *PloS Pathog* (2013) 9:e1003320. doi: 10.1371/journal.ppat.1003320

33. Praefcke GJK. Regulation of innate immune functions by guanylate-binding proteins. *Int J Med Microbiol* (2018) 308:237–45. doi: 10.1016/j.ijmm.2017.10.013

34. Kravets E, Degrandi D, Ma Q, Peulen TO, Klumpers V, Felekyan S, et al. Guanylate binding proteins directly attack Toxoplasma gondii via supramolecular complexes. *Elife* (2016) 5:1–30. doi: 10.7554/eLife.11479

35. Britzen-Laurent N, Bauer M, Berton V, Fischer N, Syguda A, Reipschlager S, et al. Intracellular trafficking of guanylate-binding proteins is regulated by heterodimerization in a hierarchical manner. *PloS One* (2010) 5:e14246. doi: 10.1371/journal.pone.0014246

36. Olive AJ, Smith CM, Baer CE, Coers J, Sassetti CM. Mycobacterium tuberculosis evasion of guanylate binding protein-mediated host defense in mice requires the ESX1 secretion system. *Int J Mol Sci* (2023) 24:1–13. doi: 10.3390/ijms24032861

37. Mohammadi N, Lindgren H, Yamamoto M, Martin A, Henry T, Sjostedt A. Macrophages demonstrate guanylate-binding protein-dependent and bacterial strain-dependent responses to francisella tularensis. *Front Cell Infect Microbiol* (2021) 11:784101. doi: 10.3389/fcimb.2021.784101

38. Hayoun MA, Muco E, Shorman M. "Brucellosis,". In: *StatPearls*. Treasure Island (FL): StatPearls Publishing LLC (2023).

39. Corsetti PP, De Almeida LA, Goncalves ANA, Gomes MTR, Guimaraes ES, Marques JT, et al. miR-181a-5p Regulates TNF-alpha and miR-21a-5p Influences Gualynate-Binding Protein 5 and IL-10 Expression in Macrophages Affecting Host Control of Brucella abortus Infection. *Front Immunol* (2018) 9:1331. doi: 10.3389/fimmu.2018.01331

40. Liu BC, Sarhan J, Panda A, Muendlein HI, Ilyukha V, Coers J, et al. Constitutive interferon maintains GBP expression required for release of bacterial components upstream of pyroptosis and anti-DNA responses. *Cell Rep* (2018) 24:155–168e155. doi: 10.1016/j.celrep.2018.06.012

41. Costa Franco MMS, Marim FM, Alves-Silva J, Cerqueira D, Rungue M, Tavares IP, et al. AIM2 senses Brucella abortus DNA in dendritic cells to induce IL-1beta secretion, pyroptosis and resistance to bacterial infection in mice. *Microbes Infect* (2019) 21:85–93. doi: 10.1016/j.micinf.2018.09.001

42. Guimaraes ES, Gomes MTR, Campos PC, Mansur DS, Dos Santos AA, Harms J, et al. Brucella abortus cyclic dinucleotides trigger STING-dependent unfolded protein response that favors bacterial replication. *J Immunol* (2019) 202:2671–81. doi: 10.4049/jimmunol.1801233

43. Tana FL, Guimaraes ES, Cerqueira DM, Campos PC, Gomes MTR, Marinho FV, et al. Galectin-3 regulates proinflammatory cytokine function and favours Brucella abortus chronic replication in macrophages and mice. *Cell Microbiol* (2021) 23:e13375. doi: 10.1111/cmi.13375

Impact of glucocorticoids and rapamycin on autophagy in Candida glabrata-infected macrophages from BALB/c mice

Zhenghui Yang, Xinyi Wang, Tianxiang Dong, Wei-Jia Zhao and Hongbin Li*

Department of Dermatology and Venereology, First Affiliated Hospital of Kunming Medical University, Kunming, Yunnan, China

Objective: In the defense against microorganisms like Candida albicans, macrophages recruit LC3(Microtubule-associated protein 1A/1B-light chain 3) to the periplasm, engaging in the elimination process through the formation of a single-membrane phagosome known as LC3-associated phagocytosis (LAP). Building on this, we propose the hypothesis that glucocorticoids may hinder macrophage phagocytosis of Candida glabrata by suppressing LAP, and rapamycin could potentially reverse this inhibitory effect.

Methods: RAW264.7 cells were employed for investigating the immune response to Candida glabrata infection. Various reagents, including dexamethasone, rapamycin, and specific antibodies, were utilized in experimental setups. Assays, such as fluorescence microscopy, flow cytometry, ELISA (Enzyme-Linked Immunosorbent Assay), Western blot, and confocal microscopy, were conducted to assess phagocytosis, cytokine levels, protein expression, viability, and autophagy dynamics.

Results: Glucocorticoids significantly inhibited macrophage autophagy, impairing the cells' ability to combat Candida glabrata. Conversely, rapamycin exhibited a dual role, initially inhibiting and subsequently promoting phagocytosis of Candida glabrata by macrophages. Glucocorticoids hinder macrophage autophagy in Candida glabrata infection by suppressing the MTOR pathway (mammalian target of rapamycin pathway), while the activation of MTOR pathway by Candida glabrata diminishes over time.

Conclusion: Our study elucidates the intricate interplay between glucocorticoids, rapamycin, and macrophage autophagy during Candida glabrata infection. Understanding the implications of these interactions not only sheds light on the host immune response dynamics but also unveils potential therapeutic avenues for managing fungal infections.

Introduction

Long-term use of glucocorticoids significantly increases the risk of invasive candidiasis (1). Despite this known association, the impact of glucocorticoids on macrophage-mediated Candida phagocytosis remains unclear. In our study, we discovered that glucocorticoids inhibit macrophage secretion of inflammatory cytokines and impede autophagy. Notably, glucocorticoid treatment initially inhibits the MTOR pathway in macrophages, followed by time-dependent attenuation and eventual activation. Furthermore, alternative pathways beyond MTOR may be involved in glucocorticoid-mediated impairment of macrophage autophagy.

The impaired macrophage phagocytosis of Candida glabrata under glucocorticoid influence was evident. Interestingly, the autophagy agonist rapamycin progressively enhanced macrophage autophagy against Candida glabrata in the presence of glucocorticoids. This leads us to hypothesize that glucocorticoids hinder macrophage phagocytosis by suppressing autophagy, introducing a potential novel mechanism underlying glucocorticoid-mediated immunosuppression and the development of invasive candidiasis.

Invasive candidiasis, predominantly involving Candida albicans, presents a global health concern with a mortality rate of 50-71% (2). Long-term glucocorticoid use is a prevalent risk factor, affecting 41.24% of invasive candidiasis patients (1). Despite being crucial for various treatments, glucocorticoids exhibit associations beyond fungal infections, exacerbating conditions like fungal keratitis and contributing to Pneumocystis carinii pneumonia (3, 4).

Macrophages, essential innate immune cells, play a pivotal role in recognizing and responding to various pathogens (5). Autophagy, a dynamic cellular process, is crucial for immune system maintenance (6). Our investigation focuses on the impact of glucocorticoids on macrophage phagocytosis of Candida glabrata, revealing a temporal inhibition of the MTOR pathway and subsequent hindrance of autophagy, ultimately attenuating macrophage phagocytosis. This sheds light on a potential mechanism underlying glucocorticoid-mediated immunosuppression against invasive candidiasis.

Cryptococcus neoformans, a fungus capable of establishing a latent infection within macrophages, highlights the intricate interplay between macrophages and fungal pathogens (7). Recognition of the fungus involves Dectin-1, a surface pattern recognition receptor, and the subsequent activation of the macrophage respiratory burst function, triggering the elimination of the phagocytosed fungus (8, 9). This interplay emphasizes the multifaceted role of macrophages in orchestrating host defense mechanisms against fungal pathogens (10).

Autophagy, an intrinsic and dynamic cellular process, involves the lysosomal degradation of damaged, aged, or surplus biomolecules and organelles, releasing small molecules for cellular recycling (11). This crucial mechanism plays a pivotal role in safeguarding the body's immune system against microbial invasions (12). In mammals, deficiencies or disorders in autophagy mechanisms may contribute to inflammation, autoimmunity, or broader immune dysregulation (11).

Autophagy, an intrinsic cellular process, is vital for degrading damaged biomolecules and organelles, contributing to immune system defense (6). Deficiencies in autophagy mechanisms can lead to inflammation, autoimmunity, and immune dysregulation (12). Our study underscores the pivotal role of autophagy in enhancing the Candida-killing capacity of macrophages.

In conclusion, our investigation delves into the impact of glucocorticoids on macrophage phagocytosis of Candida glabrata, revealing a complex interplay involving the MTOR pathway, autophagy, and the subsequent attenuation of macrophage phagocytosis. This sheds light on a potential novel mechanism underlying glucocorticoid-mediated immunosuppression and the development of invasive candidiasis. Our findings contribute to understanding the intricate relationship between glucocorticoids, macrophages, and fungal infections, offering insights for future therapeutic strategies.

Our study holds particular relevance in the context of glucocorticoids' widespread therapeutic use for conditions such as autoimmune diseases and severe illnesses. Despite their therapeutic benefits, the observed association between glucocorticoid usage and increased susceptibility to invasive candidiasis raises critical questions about balancing therapeutic advantages with potential immunosuppressive effects.

Furthermore, understanding the intricate molecular mechanisms involved in glucocorticoid-mediated immunosuppression can guide the development of targeted therapeutic strategies. For instance, our observation that the autophagy agonist rapamycin enhances macrophage autophagy in the presence of glucocorticoids suggests a potential avenue for therapeutic intervention. Investigating the modulation of autophagy pathways may provide novel insights into mitigating the immunosuppressive effects associated with glucocorticoid therapy.

In summary, our study elucidates the impact of glucocorticoids on macrophage-mediated immune responses against Candida glabrata. The revealed inhibition of the MTOR pathway and autophagy, along with impaired phagocytosis, establishes a foundation for further exploration of the complex interplay between glucocorticoids and immune defense mechanisms. By unraveling these mechanisms, we aim to contribute valuable knowledge that may inform future therapeutic strategies to minimize the risk of invasive candidiasis in individuals undergoing glucocorticoid treatment.

Materials and methods

Cell line

The murine monocyte-macrophage cell line RAW264.7 (obtained from Guangzhou Ye Shan Biotechnology Co.) was utilized in this study. The RAW264.7 cell line used in this study was derived from BALB/c mice, specifically isolated from peritoneal macrophages. Cells were cultured in DMEM supplemented with penicillin-streptomycin and maintained at 37°C in a 5% CO_2 atmosphere.

Reagents

Fetal bovine serum (Hyclone, SH30087.01), DMEM-High Glucose Culture Medium (Hyclone, SH30022.01B), Penicillin-Streptomycin (Hyclone, SH30010), PBS Phosphate Buffered Solution (Hyclone, SH30256.01B). Sabouraud Dextrose Agar Plates (Guangdong Huan Kai Microbial Technology Co, CP0170). DHR123 (Sigma, D1054). Calcofluor White (Sigma, 18909-F). Dexamethasone (Source Leaf Biotech, S17003). Rapamycin (Cell Signaling, 9904S). Bafilomycin A1 (Selleck, S1413). Mouse IL-6 (Interleukin-6) ELISA Kit (Solarbio, SEKM-0007). Mouse TNF-α (Tumor Necrosis Factor-alpha) ELISA Kit (Solarbio, SEKM-0034). Anti-LC3B Antibody - Autophagosome Marker (Abcam, ab48394). Anti-mTOR (phospho S2448) Antibody [EPR426(2)] (Abcam, ab109268). p-mTOR Antibody (296.Ser 2481) (Santa Cruz, sc-293132). Phospho-p70 S6 Kinase (Thr389) (108D2) Rabbit mAb (Cell Signaling Technology, 9234P). Phospho-p70 S6 Kinase (Ser371) Antibody (Cell Signaling Technology, 9208T). Phospho-Raptor (Ser792) (E4V6C) Rabbit mAb (Cell Signaling Technology, 89146). Phospho-S6 Ribosomal Protein (Ser240/244) (D68F8) XP$^{®}$ Rabbit mAb (Cell Signaling Technology, 5364). Phospho-S6 Ribosomal Protein (Ser235/236) (D57.2.2E) XP$^{®}$ (Cell Signaling Technology, 4858). Phospho-4E-BP1 (Thr37/46) (236B4) Rabbit mAb (Cell Signaling Technology, 2855T). AO-EB Dual Staining Kit (Solarbio, CA1140). Gelatin (Sigma, G1393). Premo^{TM} Autophagy Sensor (Thermo Fisher Scientific, P36235).

Candida culture and infection

Candida glabrata was cultured in SDA (Sabouraud Dextrose Agar) medium and incubated at 37°C for 24 hours. Petri dishes were subsequently rinsed with sterile saline, and the liquid containing Candida glabrata was collected into centrifuge tubes. After centrifugation, the cells were ground, quantified using a haematocrit technical plate, and finally prepared into a suspension with a concentration of 10^8 CFU (Colony-Forming Unit)/ml. The Candida glabrata suspensions were subjected to heat inactivation by incubating in a water bath at 56°C for 30 minutes. The inactivated Candida glabrata suspensions were stained with 0.1 mg/mL CFW (Calcofluor White) for 30 minutes at room temperature, washed twice with PBS, and utilized for fluorescence microscopy. For Candida glabrata spore preparation, spores were incubated with 30 μmol/L DHR123 (Dihydrorhodamine 123) at 37°C for 30 minutes, followed by centrifugation, washing with PBS, heat inactivation, and subsequent preparation for phagocytosis detection using flow cytometry.

Fluorescence microscopy

Mouse monocyte-macrophage leukemia cells Raw264.7 (10^5/ml) were co-cultured with Candida glabrata stained with CFW (10^6CFU/ml) for 30 minutes, 1 hour, 2 hours, and 4 hours. At each time point, three randomly selected fields of view were captured, and the phagocytosis rate of Candida glabrata by macrophages was assessed. The percentage of cells phagocytosing more than three fungi was quantified under a 40x microscope. The phagocytosis rate was calculated as the number of macrophages phagocytosing Candida glabrata divided by the total number of macrophages, multiplied by 100%. The percentage of Candida glabrata with more than three fungi was determined as the number of macrophages phagocytosing three or more Candida glabrata divided by the total number of macrophages, multiplied by 100%.

Flow cytometry

Mouse monocyte-macrophage leukemia cells Raw264.7 (10^5/ml) were co-cultured with DHR123-labeled Candida glabrata (10^6 CFU/ml) for various time points (30 min, 1 h, 2 h, and 4 h). Gating based on FSC (Forward Scatter) and SSC (Side Scatter), phagocytosis was assessed, and 10,000 cells were collected per sample. The acquired data were analyzed using FlowJo to determine the proportion of cells positive for fluorescence and the Mean Fluorescence Intensity (MFI) for statistical evaluation.

Experimental group

Mouse monocyte macrophage leukemia cells Raw264.7 (10^5/ml) were co-cultured with inactivated Candida glabrata (10^6 CFU/ml) to generate the Candida suspension. Dexamethasone was introduced to the Candida suspension at a concentration of 200 ng/μl, followed by the addition of 100 μM rapamycin. To establish a baseline, Raw264.7 cells infected without Candida glabrata were designated as the control group ("C"). The experimental groups included Raw264.7 cells infected with Candida glabrata, labeled as the "Cg" group. Measurements were conducted at 6, 12, and 24 hours of co-cultivation. Another group, designated as "DEX+Cg", consisted of Raw264.7 cells infected with Candida glabrata and pre-treated with dexamethasone, with measurements taken at the same time intervals. The third group, "DEX+Rapa+Cg", involved Raw264.7 cells infected with Candida glabrata and pre-treated with dexamethasone and rapamycin, with measurements at 6, 12, and 24 hours of co-cultivation.

In our study, Raw264.7 cells were co-cultured with DHR123-labeled Candida glabrata at a ratio of 1:10. The untreated cell group served as the control, denoted as "1:10Cg". Raw264.7 cells were seeded at a density of 1.5×10^5/dish and pretreated for 24 hours under different conditions: the control group ("1:10Cg"), and experimental groups: "10DEX1d+1:10Cg", "100DEX1d+1:10Cg", and "200DEX1d+1:10Cg", with dexamethasone concentrations of 10ng/μl, 100ng/μl, and 200ng/μl, respectively. Additionally, Raw264.7 cells were pretreated with 100 μmol/L rapamycin for 12 hours and then co-cultured with Candida glabrata. This group of cells was labeled as "Rapa 12h+1:10Cg". Macrophage phagocytosis of Candida glabrata was investigated at different time points (0.5h, 1h, 2h, and 4h) during co-culture.

ELISA

Levels of IL-6 and TNF-α in the supernatant from Raw264.7 macrophage cell cultures and Candida suspension were assessed using ELISA (Solarbio, SEKM-0034) and ELISA (Solarbio, SEKM-0007). The Candida suspension was co-treated for 6h, 12h, and 24h, respectively. Direct supernatant (100 µL) and diluted samples (20-50 times) were subjected to analysis on ELISA plates. Cytokine concentrations were determined in accordance with the manufacturer's instructions.

Western blot analysis

Protein extraction from the Candida suspension was performed using Radio-Immunoprecipitation Assay (RIPA) lysate. The protein concentration was determined, and the collected protein samples were supplemented with an appropriate amount of concentrated Sodium Dodecyl Sulfate Polyacrylamide Gel Electrophoresis (SDS-PAGE) Protein Sampling Buffer. The mixture was heat-treated in a boiling water bath for 3-5 minutes to achieve complete protein denaturation. After cooling to room temperature, the protein samples were directly loaded into the SDS-PAGE wells. Separated proteins from the gel were transferred onto a membrane (Polyvinylidene difluoride - PVDF) via electroblotting. Non-specific binding sites on the membrane were blocked by incubating it with a blocking solution. The membrane was then incubated with a primary antibody specific to the target protein. Following this, the membrane was washed to remove unbound primary antibodies. Subsequently, the membrane was incubated with a secondary antibody conjugated to an enzyme, and unbound secondary antibodies were washed away. Protein detection was achieved using BeyoECL Plus reagents. The resulting film was scanned or photographed and analyzed by Quantity One for determining the molecular weight and net optical density values of the target bands.

AO/EB staining

A working solution of Acridine Orange (AO) and Ethidium Bromide (EB) was prepared by mixing the two dyes in a ratio of 1:1. After treatment, Raw264.7 cells were harvested and washed with PBS. The AO/EB working solution was then added to the cell pellet, and the cells were incubated for 2-5 minutes at room temperature in the dark. Stained cells were visualized under a fluorescence microscope using appropriate filter sets for AO (green fluorescence) and EB (red fluorescence). Digital images of the stained cells were captured using a fluorescence microscope equipped with a camera. The percentage of viable cells was quantified based on the intensity and morphology of the fluorescence signals.

Autophagy monitoring assay

Add 2 µL of Premo™ LC3B-GFP Kit Autophagy Sensor (Component A) medium per 10,000 Raw264.7 cells and incubate the cells at 37°C for 16 hours. The different stages of autophagy were monitored using the Premo™ Autophagy Sensor GFP-LC3B Kit (Thermo, P36235) following the manufacturer's instructions.

Confocal microscopy

Utilizing laser confocal microscopy, we conducted a comprehensive examination of macrophage fluorescence, emphasizing both quantification and spatial distribution subsequent to transfection with GFP-LC3B baculovirus. Moreover, the visualization of macrophage viability was achieved through the observation of live and dead cells stained with Acridine Orange and Ethidium Bromide (AO/EB) using laser confocal microscopy.

Statistical analysis

Statistical analysis was conducted using GraphPad Prism 5.0 software (GraphPad Software, San Diego, CA). ELISA, AO/EB staining, Western blot, and macrophage phagocytosis of Candida glabrata were assessed, with data presented as the mean ± standard error of the mean (SEM). One-way analysis of variance (ANOVA) was employed to compare data among three or more groups. Differences were considered statistically significant when the p-value was less than 0.05.

Results

Dexamethasone and rapamycin exhibit inhibitory effects on macrophage secretion of proinflammatory cytokines, while dexamethasone additionally enhances macrophage survival

Under Candida glabrata stimulation, the secretion of TNF-α and IL-6 by macrophages exhibited a time-dependent increase, demonstrating statistical significance (P<0.05, Figures 1A, B). This indicates that Candida glabrata induces the secretion of pro-inflammatory factors TNF-α and IL-6 by macrophages. To explore the impact of glucocorticoids on intrinsic immunity during Candida glabrata phagocytosis by macrophages, cells were pre-treated with the glucocorticoid dexamethasone. The co-culture of macrophages with Candida glabrata for 24 hours revealed a significant inhibition of TNF-α and IL-6 expression levels by glucocorticoids (P<0.05, Figures 1A, B). This suggests that
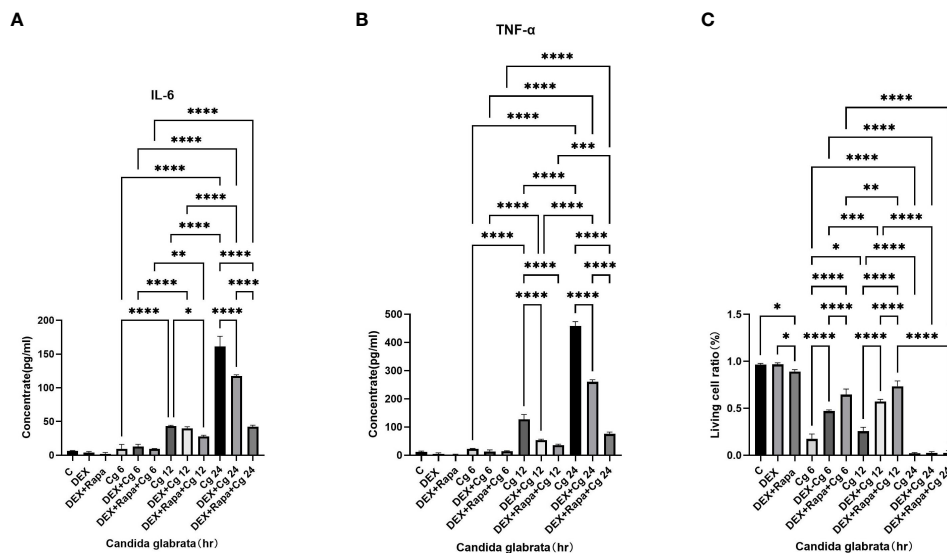
FIGURE 1
TNF-α **(A)** and IL-6 **(B)** levels in cell supernatants were assessed through ELISA. The proportion of viable cells **(C)** was determined using the AO/EB staining method. Data are shown as the mean $\pm$ SEM of three independent experiments. *$p < 0.05$; **$p < 0.01$; ***$p < 0.001$; ****$p < 0.0001$.

glucocorticoids suppress intrinsic immunity during Candida glabrata infection. To investigate whether glucocorticoids inhibit intrinsic immunity by influencing macrophage autophagy, macrophages were pre-treated with the autophagy inducer rapamycin. Under the influence of glucocorticoids, rapamycin further decreased the expression levels of IL-6 and TNF-α when macrophages were co-cultured with Candida glabrata for 24 hours ($P<0.05$, Figures 1A, B).

The viability of macrophages significantly decreased ($P<0.01$, Figures 1C, 2) after 24 hours of co-culture with Candida glabrata. This observation aligns with previous findings, indicating a notable surge in IL-6 and TNFα secretion by macrophages at the 24-hour co-culture mark compared to earlier time points (Figures 1A, B). In contrast, when macrophages were co-cultured with Candida glabrata for 6 and 12 hours, treatment with glucocorticoids resulted in a remarkable increase in macrophage viability ($P<0.01$, Figures 1C, 2). Furthermore, under the influence of glucocorticoids, rapamycin treatment significantly enhanced the macrophage viability ($P<0.01$, Figures 1C, 2).

Excessive production of proinflammatory factors has been associated with macrophage apoptosis. Both rapamycin and glucocorticoids are known for their robust immunosuppressive properties. Therefore, it is postulated that glucocorticoids and rapamycin function to inhibit macrophage apoptosis during the phagocytosis of Candida glabrata.

Dexamethasone hinders the phagocytosis of Candida glabrata by macrophages

In the context of glucocorticosteroid influence on macrophages, the phagocytosis rate of Candida glabrata by macrophages and the proportion of macrophages engulfing more than three yeast cells significantly increased at 4h compared to 0.5h, 1h, and 2h ($P<0.05$, Figure 3B). The number of Candida glabrata phagocytosed by macrophages demonstrated a time-dependent escalation (Figure 3). Dexamethasone treatment hindered the phagocytosis of Candida glabrata by macrophages ($P<0.05$, Figures 3–5), but the phagocytosis rate was not distinct under varying glucocorticosteroid concentrations (Figure 3A). The autophagy inducer rapamycin had no substantial impact on the phagocytosis of Candida glabrata by macrophages (Figure 3). For co-culture durations of 0.5h and 1h, rapamycin marginally inhibited the phagocytosis, with no discernible difference (Figure 3). However, for 2h and 4h co-culture, rapamycin enhanced the phagocytosis, yet without significant differentiation (Figure 3).

Dexamethasone exerts inhibitory effects on macrophage autophagy, and this inhibition is effectively reversed by the administration of rapamycin

Dexamethasone exhibited a significant inhibitory effect on the phagocytosis of Candida glabrata by macrophages. Interestingly, the impact of the autophagy inducer rapamycin on phagocytosis displayed a dual nature, showing both inhibitory and promotional effects on Candida glabrata phagocytosis by macrophages (Figure 3). Consequently, further investigation is warranted to elucidate the specific interactions between dexamethasone and autophagy in this context.

During cellular autophagy, the transition of the LC3BI (LC3 cytoplasmic phenotype) to a LC3BII (LC3 membrane phenotype)
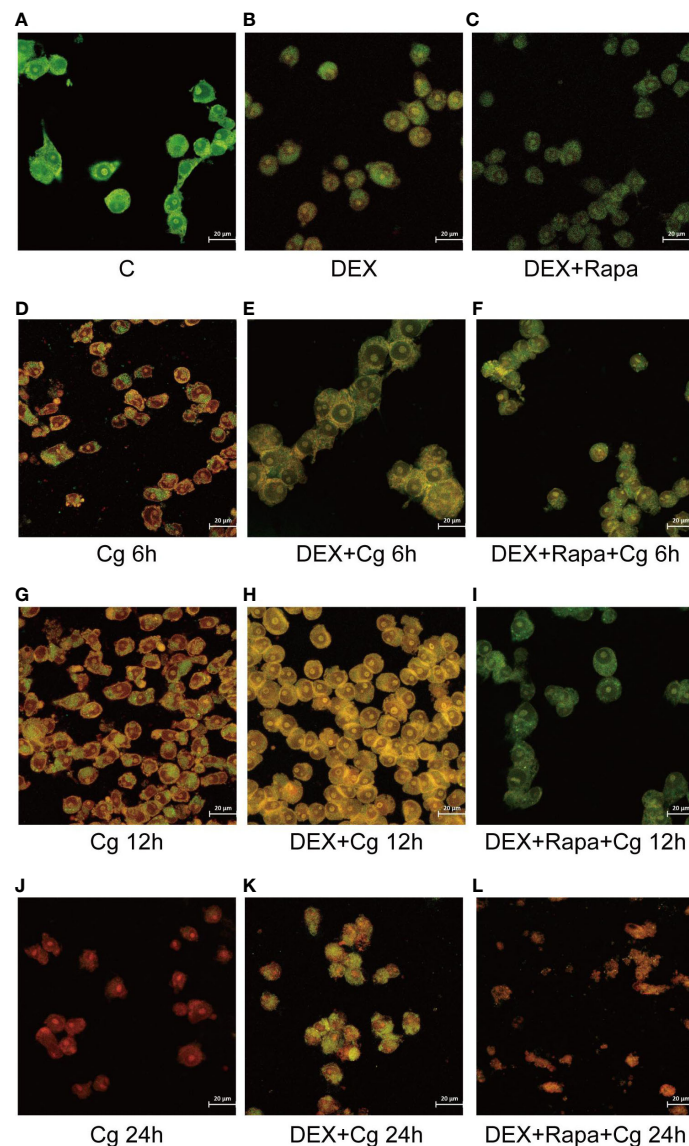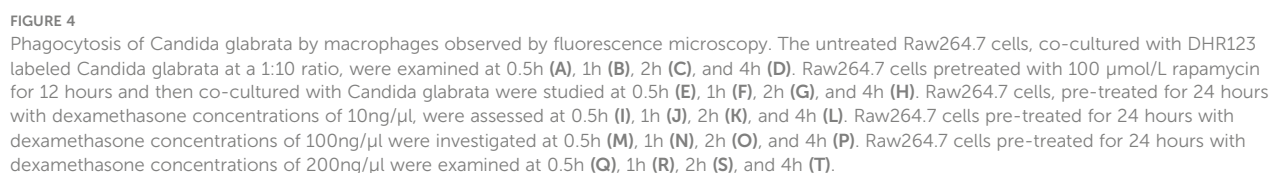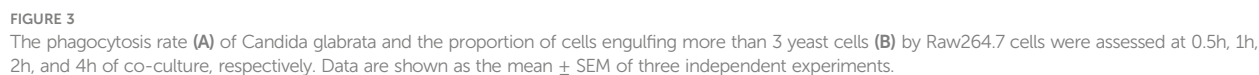
FIGURE 2
Laser confocal microscopy was employed to observe AO/EB staining in both dead and living cells. AO led to the emission of green light in chimeric DNA double strands, while others emitted red light. EB emitted red light uniformly without base-specificity. Raw264.7 cells not infected with Candida glabrata as control group **(A)**. Raw264.7 cells pre-treated with dexamethasone **(B)**. Raw264.7 cells pre-treated with dexamethasone and rapamicin **(C)**. Raw264.7 cells infected with Candida glabrata, co-cultured for 6 hours **(D)**. Raw264.7 cells pre-treated with dexamethasone and infected with Candida glabrata, co-cultured for 6 hours **(E)**. Raw264.7 cells infected with Candida glabrata and pre-treated with dexamethasone and rapamycin, co-cultured for 6 hours **(F)**. Raw264.7 cells infected with Candida glabrata, co-cultured for 12 hours **(G)**. Raw264.7 cells pre-treated with dexamethasone and infected with Candida glabrata, co-cultured for 12 hours **(H)**. Raw264.7 cells infected with Candida glabrata and pre-treated with dexamethasone and rapamycin, co-cultured for 12 hours **(I)**. Raw264.7 cells infected with Candida glabrata, co-cultured for 24 hours **(J)**. Raw264.7 cells pre-treated with dexamethasone and infected with Candida glabrata, co-cultured for 24 hours **(K)**. Raw264.7 cells infected with Candida glabrata and pre-treated with dexamethasone and rapamycin, co-cultured for 24 hours **(L)**.

occurs. This process, impeded by the BAF-A1 (lysosomal inhibitor bafilomycin-A1) at the final step of autophagy, leads to the LC3BII/LC3BI or LC3BII/GAPDH(Glyceraldehyde 3-phosphate dehydrogenase) ratio, serving as an indicator of autophagy levels. The ratio positively correlates with the extent of autophagy. LC3B predominantly localizes to the cell membrane of macrophages (Figure 6A). Under Candida glabrata stimulation, dexamethasone significantly reduced the accumulation of LC3BII in macrophages, indicating the inhibition of macrophage autophagy($P<0.01$, Figures 6, 7). These differences were statistically significant after co-cultivation of Candida glabrata with macrophages for 6h, 12h, and 24h ($P<0.01$, Figures 6, 7). Additionally, the autophagy inducer

FIGURE 3
The phagocytosis rate **(A)** of Candida glabrata and the proportion of cells engulfing more than 3 yeast cells **(B)** by Raw264.7 cells were assessed at 0.5h, 1h, 2h, and 4h of co-culture, respectively. Data are shown as the mean ± SEM of three independent experiments.

FIGURE 4
Phagocytosis of Candida glabrata by macrophages observed by fluorescence microscopy. The untreated Raw264.7 cells, co-cultured with DHR123 labeled Candida glabrata at a 1:10 ratio, were examined at 0.5h **(A)**, 1h **(B)**, 2h **(C)**, and 4h **(D)**. Raw264.7 cells pretreated with 100 μmol/L rapamycin for 12 hours and then co-cultured with Candida glabrata were studied at 0.5h **(E)**, 1h **(F)**, 2h **(G)**, and 4h **(H)**. Raw264.7 cells, pre-treated for 24 hours with dexamethasone concentrations of 10ng/μl, were assessed at 0.5h **(I)**, 1h **(J)**, 2h **(K)**, and 4h **(L)**. Raw264.7 cells pre-treated for 24 hours with dexamethasone concentrations of 100ng/μl were investigated at 0.5h **(M)**, 1h **(N)**, 2h **(O)**, and 4h **(P)**. Raw264.7 cells pre-treated for 24 hours with dexamethasone concentrations of 200ng/μl were examined at 0.5h **(Q)**, 1h **(R)**, 2h **(S)**, and 4h **(T)**.
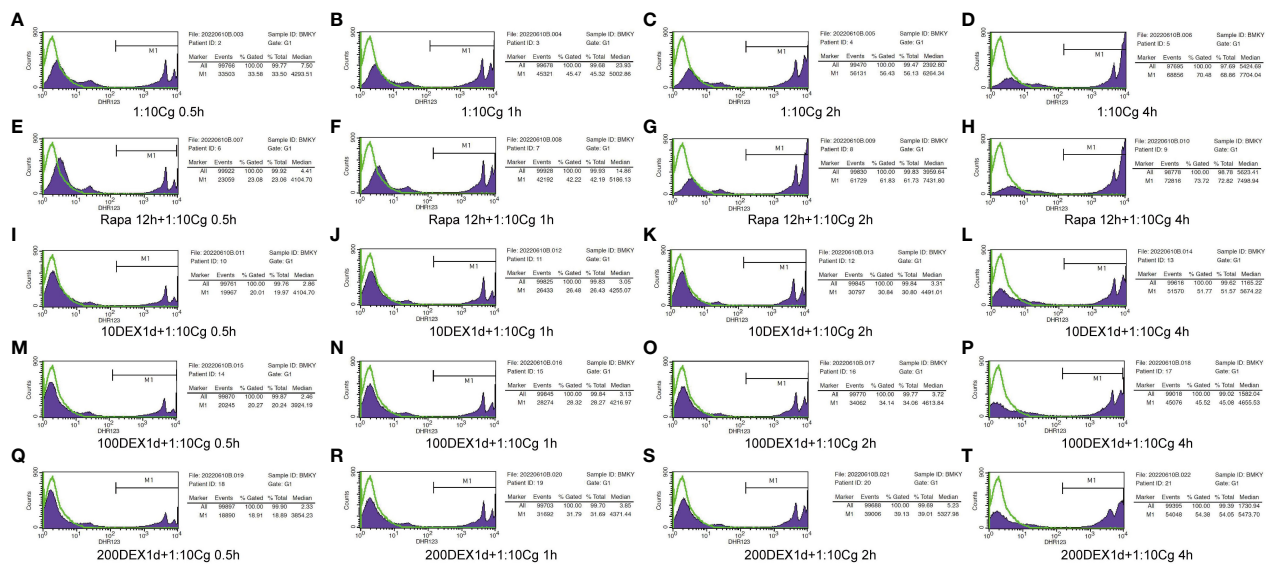
FIGURE 5

Phagocytosis of Candida glabrata by macrophages detected by flow cytometry. Add behind: The untreated Raw264.7 cells, co-cultured with DHR123 labeled Candida glabrata at a 1:10 ratio, were examined at 0.5h **(A)**, 1h **(B)**, 2h **(C)**, and 4h **(D)**. Raw264.7 cells pretreated with 100 μmol/L rapamycin for 12 hours and then co-cultured with Candida glabrata were studied at 0.5h **(E)**, 1h **(F)**, 2h **(G)**, and 4h **(H)**. Raw264.7 cells, pre-treated for 24 hours with dexamethasone concentrations of 10ng/μl, were assessed at 0.5h **(I)**, 1h **(J)**, 2h **(K)**, and 4h **(L)**. Raw264.7 cells pre-treated for 24 hours with dexamethasone concentrations of 100ng/μl were investigated at 0.5h **(M)**, 1h **(N)**, 2h **(O)**, and 4h **(P)**. Raw264.7 cells pre-treated for 24 hours with dexamethasone concentrations of 200ng/μl were examined at 0.5h **(Q)**, 1h **(R)**, 2h **(S)**, and 4h **(T)**.

rapamycin enhanced the accumulation level of LC3BII in macrophages (P<0.05, Figures 6, 7), highlighting its potential to promote macrophage autophagy.

Candida glabrata activation induces the MTOR pathway in macrophages, whereas dexamethasone treatment is observed to inhibit the MTOR pathway in macrophages

In our preceding experiments, we established that glucocorticoids hinder macrophage phagocytosis of Candida glabrata by suppressing macrophage autophagy. To delve deeper into the mechanistic link between glucocorticoids and cellular autophagy regulation through the MTOR pathway, we investigated alterations in the MTOR pathway within each macrophage group. As pivotal serine/threonine kinases, the MTOR pathway serves as a principal regulator of cellular metabolism, and its inhibition is known to induce autophagy.

Upon co-culturing Candida glabrata with macrophages, we observed that Candida glabrata triggered the activation of the MTOR pathway (Figure 8). However, this activation diminished over time. Conversely, when Candida glabrata and macrophages were co-cultured and subjected to glucocorticoid stimulation, the inhibitory impact of glucocorticoids on the MTOR pathway showed a time-dependent reduction, and by 24 hours, glucocorticoids exhibited an activating effect on the MTOR pathway (Figure 8). Furthermore, under glucocorticoid stimulation, co-culturing Candida glabrata with macrophages and applying rapamycin resulted in the inhibition of the MTOR pathway (Figure 8).

Discussion

Glucocorticoids find extensive use in the treatment of immune disorders and endocrine system diseases. However, it is noteworthy that glucocorticoid therapy presents a substantial risk factor for candidaemia (13). Glucocorticoids have been observed to stimulate the proliferation of Candida in the cornea, concurrently diminishing neutrophil infiltration. Moreover, glucocorticoids impede the formation of neutrophil extracellular traps, culminating in an exacerbation of fungal keratitis (3).

Candida glabrata, a conditionally pathogenic organism prevalent in mucous membranes, poses a significant risk for systemic fungal infections, particularly in immunocompromised individuals, those undergoing glucocorticoid therapy, or utilizing catheters (14). Notably, systemic fungal infections attributable to Candida glabrata represent the second most frequent among Candida genera in both the United States and Europe (15). In contrast to Candida albicans, Candida glabrata exhibits heightened resistance to the antifungal effects of reactive oxygen species (ROS) secreted by macrophages (16). This increased resistance may contribute to the elevated mortality observed in patients with Candida glabrata candidemia (17).

In the immune defense against fungal infections, macrophages play a pivotal role as primary effectors in eliminating Candida. Recognition of fungal-pathogen-associated molecular patterns (PAMPs) by pattern recognition receptors (PRRs) on the macrophage cell membrane initiates the phagocytic process. Subsequently, nascent phagosomes undergo fusion with lysosomes, maturing into phagolysosomes within macrophages. These phagolysosomes create a hostile environment lethal to
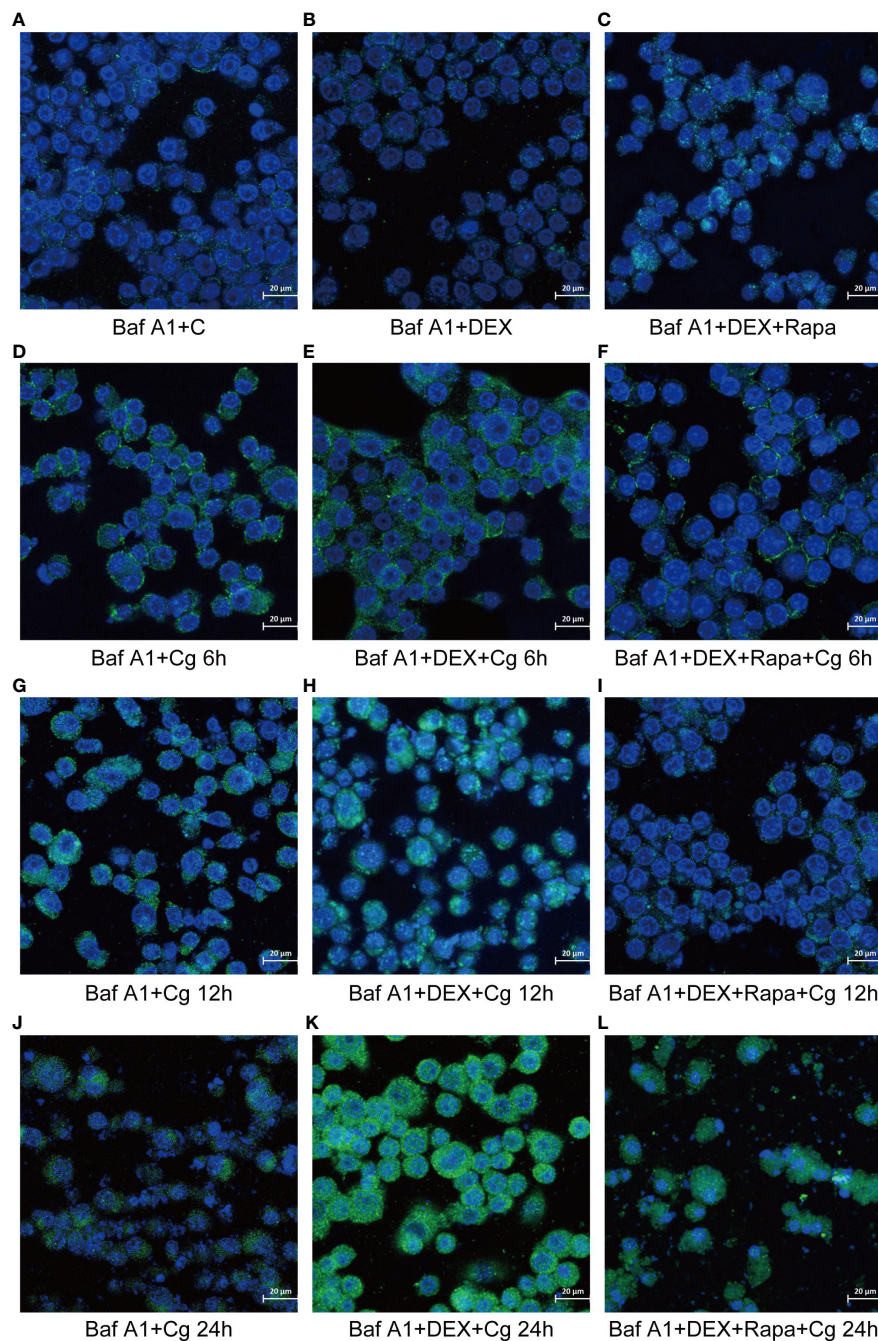
FIGURE 6

Laser confocal microscopy was employed to observe the distribution of GFP-LC3B, a fusion protein of Green Fluorescent Protein (GFP) and LC3B, in macrophages. In the images, LC3B was represented in green fluorescence, and the cell nuclei were stained in blue with DAPI. This approach allowed for a detailed examination of the subcellular localization and distribution of GFP-LC3B within the macrophages, providing valuable insights into the dynamics of autophagy in the studied cellular context. Raw264.7 cells not infected with Candida glabrata as control group **(A)**. Raw264.7 cells pre-treated with dexamethasone **(B)**. Raw264.7 cells pre-treated with dexamethasone and rapamicin **(C)**. Raw264.7 cells infected with Candida glabrata, co-cultured for 6 hours **(D)**. Raw264.7 cells pre-treated with dexamethasone and infected with Candida glabrata, co-cultured for 6 hours **(E)**. Raw264.7 cells infected with Candida glabrata and pre-treated with dexamethasone and rapamycin, co-cultured for 6 hours **(F)**. Raw264.7 cells infected with Candida glabrata, co-cultured for 12 hours **(G)**. Raw264.7 cells pre-treated with dexamethasone and infected with Candida glabrata, co-cultured for 12 hours **(H)**. Raw264.7 cells infected with Candida glabrata and pre-treated with dexamethasone and rapamycin, co-cultured for 12 hours **(I)**. Raw264.7 cells infected with Candida glabrata, co-cultured for 24 hours **(J)**. Raw264.7 cells pre-treated with dexamethasone and infected with Candida glabrata, co-cultured for 24 hours **(K)**. Raw264.7 cells infected with Candida glabrata and pre-treated with dexamethasone and rapamycin, co-cultured for 24 hours **(L)**.

Candida, contributing to fungal clearance. Moreover, macrophages engage in LC3-associated phagocytosis (LAP), a mechanism that aids in combating fungi (18). Additionally, monocytes and macrophages play a crucial role in recruiting neutrophils, further enhancing the clearance of Candida. This collaborative immune response underscores the complexity and effectiveness of the host
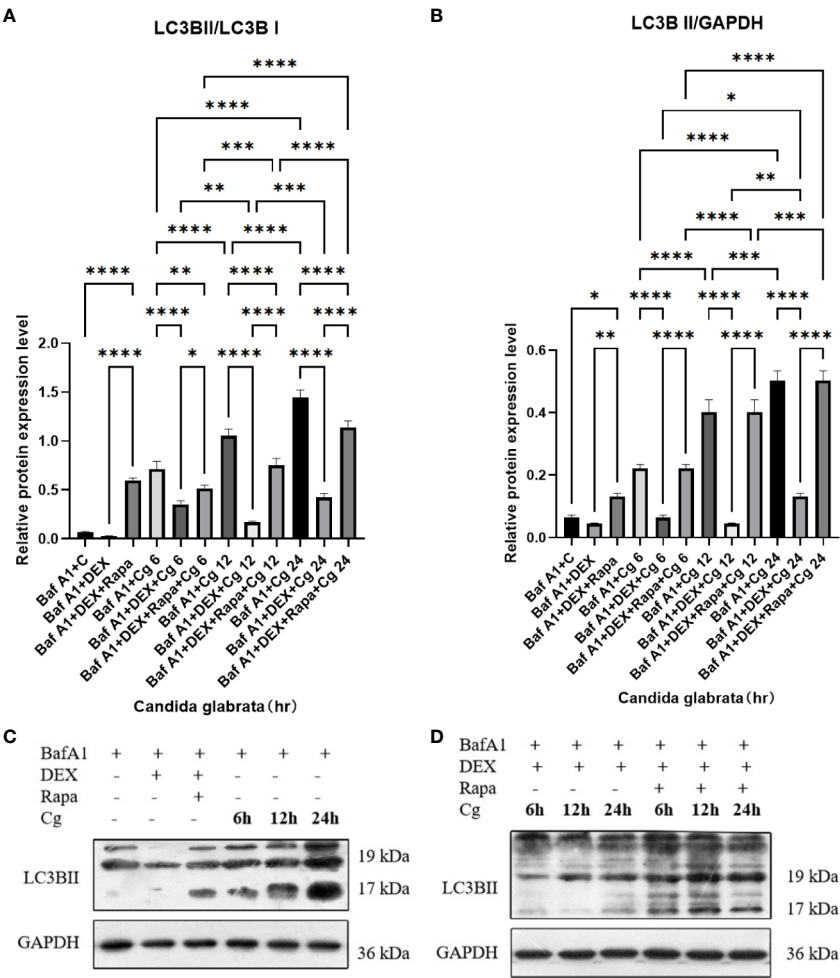
FIGURE 7
The evaluation of macrophage autophagy, represented by LC3BII/LC3BI **(A)** and LC3BII/GAPDH **(B)**, was conducted through Western blot analysis. Western blot analysis was performed to detect the expression of LC3BII protein in Raw264.7 cells for groups "C", "DEX", "DEX+Rapa", "Cg 6h", "Cg 12h" and "Cg 24h" **(C)**. Western blot analysis was conducted to assess the expression of LC3BII protein in Raw264.7 cells for groups "DEX+Cg 6h", "DEX+Cg 12h", "DEX+Cg 24h", "DEX+Rapa+Cg 6h", "DEX+Rapa+Cg 12h" and "DEX+Rapa+Cg 24h" **(D)**. Data are shown as the mean $\pm$ SEM of three independent experiments. *p < 0.05; **p < 0.01; ***p < 0.001; ****p < 0.0001.

defense against fungal pathogens. Understanding these intricate interactions provides insights into potential therapeutic strategies for managing fungal infections in clinical settings (19). Despite the phagocytosis by macrophages, Candida glabrata exhibits resilience and the ability to survive and replicate within these immune cells. This survival is attributed to various mechanisms, including the modulation of phagolysosomes, regulation of phagolysosomal pH, adaptation to the antimicrobial activities of macrophages, and the ability to adjust to the challenging nutrient environment within macrophages through autophagy (20, 21). The intricate strategies employed by Candida glabrata to evade the antimicrobial defenses of macrophages highlight the sophistication of the fungal pathogen's immune evasion mechanisms. Further elucidating these mechanisms is crucial for developing targeted therapeutic interventions to enhance the effectiveness of macrophage-mediated clearance of Candida glabrata (20). The survival of Candida glabrata within macrophages is a key evasion strategy against immune clearance. This highlights the pathogen's adaptability and resilience. Unraveling this interaction is vital for developing

targeted therapies to counteract these evasion tactics and boost host defenses (20). Administering the MTOR pathway inhibitor rapamycin to mice with candidaemia demonstrates a noteworthy reduction in macrophage apoptosis, leading to improved overall survival (22). This observation underscores the direct protective impact of rapamycin on macrophages, suggesting its potential as a therapeutic intervention in candidaemia management (22).

Following the phagocytosis of Candida glabrata, the activation of the MTOR pathway in macrophages suggests a potential mechanism through which Candida glabrata may inhibit cellular autophagy. It is noteworthy that autophagy serves as a crucial self-protection mechanism in organisms and plays a pivotal immunomodulatory role in countering environmental stressors, particularly in chronic inflammation and infection models. Further investigations are imperative to elucidate the intricate interplay between Candida glabrata and the autophagic response, shedding light on potential therapeutic avenues for manipulating this pathway in immune regulation (23). The suppression of macrophage autophagy by Candida glabrata may serve as a
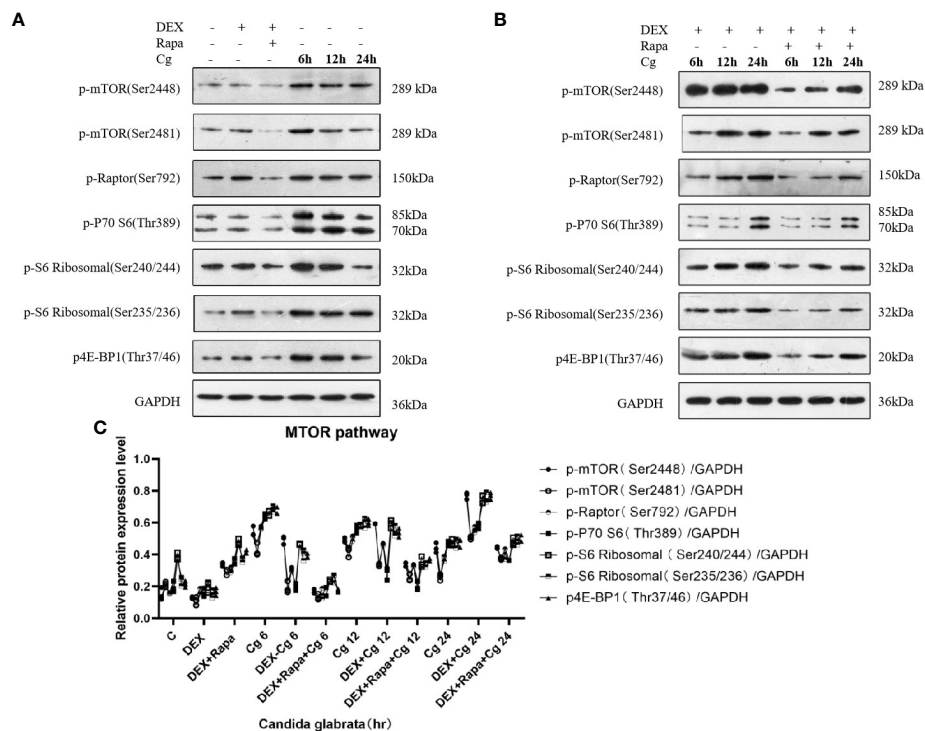
FIGURE 8

Western blot analysis was conducted to examine the expression of MTOR pathway-related proteins in Raw264.7 cells for groups "C", "DEX", "DEX+Rapa", "Cg 6h", "Cg 12h", and "Cg 24h" **(A)**. Western blot analysis was performed to assess the expression of MTOR pathway-related proteins in Raw264.7 cells for groups "DEX+Cg 6h", "DEX+Cg 12h", "DEX+Cg 24h", "DEX+Rapa+Cg 6h", "DEX+Rapa+Cg 12h", and "DEX+Rapa+Cg 24h" **(B)**. The relative protein expression levels of MTOR pathway-related proteins were compared among different cell groups **(C)**.

mechanism enabling the continuous survival and replication of Candida glabrata within macrophages. Post-phagocytosis, there was a notable elevation in the secretion of IL-6 and TNFα by macrophages (P<0.05), accompanied by a significant reduction in the ratio of viable cells (P<0.05). These findings suggest that Candida glabrata stimulates the secretion of inflammatory factors by macrophages, contributing to macrophage death.

The inhibition of the Src/Syk pathway and the consequent reduction in reactive oxygen species production in macrophages, induced by glucocorticoids, disrupt the recruitment of LC3BII to the phagosomes of phagocytes that have internalized Aspergillus spp. This disruption, specifically the inhibition of LC3-associated phagocytosis (LAP), could be a contributing factor to the pathogenesis of invasive Aspergillus under glucocorticoid induction (24). Consistent with these findings, glucocorticoids were observed to inhibit LAP in macrophages engulfing Candida glabrata (P<0.05). Intriguingly, glucocorticoids inhibited the MTOR pathway in macrophages that had engulfed Candida glabrata, and this inhibition decreased with time, displaying activation of the MTOR pathway at 24h. Rapamycin partially mitigated the inhibition of LAP by glucocorticoids in macrophages engulfing Candida glabrata. The intricate interplay of various intracellular signaling pathways, including MTOR, AMPK (AMP-activated Protein Kinase), and JNK (c-Jun N-terminal Kinase), in autophagy suggests that glucocorticoids may exert their effects on macrophage autophagy through multiple pathways beyond MTOR. Further investigation is

warranted to unravel the comprehensive regulatory network governing macrophage autophagy in response to glucocorticoids.

In the current investigation, glucocorticoids were identified to impede the phagocytosis of Candida glabrata by macrophages. Conversely, rapamycin exhibited the potential to induce phagocytosis of Candida glabrata by macrophages over time. When macrophages engulfed Candida glabrata, both glucocorticoids and rapamycin demonstrated inhibitory effects on the secretion of pro-inflammatory factors, namely IL-6 and TNFα, subsequently leading to an increased macrophage viable cell ratio. Notably, glucocorticoids suppressed macrophage autophagy, whereas rapamycin induced autophagy in macrophages. In murine experiments, glucocorticoids were observed to induce and worsen candidaemia, while rapamycin contributed to the improved survival of mice afflicted with candidaemia (22). Hence, macrophage autophagy emerges as a crucial determinant for the effective elimination of Candida glabrata subsequent to its phagocytosis. In summary, glucocorticoids impede macrophage autophagy by inhibiting the phagocytosis of Candida glabrata. This inhibition may potentially contribute to the dissemination of Candida glabrata *in vivo*, thereby fostering the development of systemic Candida infections.

The attenuation of macrophage autophagy by glucocorticoids appears to intensify with prolonged exposure, underscoring the importance of early intervention in patients with candidaemia undergoing long-term glucocorticoid treatment—a high-risk

factor. Furthermore, the potential therapeutic application of rapamycin in the treatment of candidaemia emerges as a promising avenue worth exploring.

Data availability statement

The datasets presented in this study can be found in online repositories. The names of the repository/repositories and accession number(s) can be found in the article/supplementary material.

Ethics statement

Ethical approval was not required for the studies on animals in accordance with the local legislation and institutional requirements because only commercially available established cell lines were used.

Author contributions

ZY: Conceptualization, Data curation, Investigation, Software, Writing – review & editing. XW: Methodology, Supervision, Writing – original draft, Writing – review & editing. TD: Funding acquisition, Validation, Writing – review & editing. W-JZ: Formal analysis, Writing – original draft, Supervision, Writing – review & editing. HL: Formal analysis, Funding acquisition, Project administration, Resources, Validation, Visualization, Writing – original draft.

Conflict of interest

The authors declare that the research was conducted in the absence of any commercial or financial relationships that could be construed as a potential conflict of interest.

Publisher's note

All claims expressed in this article are solely those of the authors and do not necessarily represent those of their affiliated organizations, or those of the publisher, the editors and the reviewers. Any product that may be evaluated in this article, or claim that may be made by its manufacturer, is not guaranteed or endorsed by the publisher.

References

1. Wen SR, Yang ZH, Dong TX, Li YY, Cao YK, Kuang YQ, et al. Deep fungal infections among general hospital inpatients in Southwestern China: A 5-year retrospective study. *Front Public Health*. (2022) 10:842434. doi: 10.3389/fpubh.2022.842434

2. Yang SP, Chen YY, Hsu HS, Wang FD, Chen LY, Fung CP. A risk factor analysis of healthcare-associated fungal infections in an intensive care unit: a retrospective cohort study. *BMC Infect Dis*. (2013) 13:10. doi: 10.1186/1471-2334-13-10

3. Fan F, Huang X, Yuan K, Zhu B, Zhao Y, Hu R, et al. Glucocorticoids may exacerbate fungal keratitis by increasing fungal aggressivity and inhibiting the formation of neutrophil extracellular traps. *Curr Eye Res*. (2020) 45:124–33. doi: 10.1080/02713683.2019.1657464

4. Wang Y, Li K, Zhao W, Liu Y, Li T, Yang H-Q, et al. Integrated multi-omics analyses reveal the altered transcriptomic characteristics of pulmonary macrophages in immunocompromised hosts with Pneumocystis pneumonia. *Front Immunol*. (2023) 14:1179094. doi: 10.3389/fimmu.2023.1179094

5. Zhang L, Wang CC. Inflammatory response of macrophages in infection. *Hepatobil Pancreat Dis Int*. (2014) 13:138–52. doi: 10.1016/S1499-3872(14)60024-2

6. Kinsella RL, Nehls EM, Stallings CL. Roles for autophagy proteins in immunity and host defense. *Vet Pathol*. (2018) 55:366–73. doi: 10.1177/0300985818754967

7. Alanio A, Vernel-Pauillac F, Sturny-Leclère A, Dromer F. Cryptococcus neoformans host adaptation: toward biological evidence of dormancy. *mBio*. (2015) 6. doi: 10.1128/mBio.02580-14

8. Kimura Y, Chihara K, Honjoh C, Takeuchi K, Yamauchi S, Yoshiki H, et al. Dectin-1-mediated signaling leads to characteristic gene expressions and cytokine secretion via spleen tyrosine kinase (Syk) in rat mast cells. *J Biol Chem*. (2014) 289:31565–75. doi: 10.1074/jbc.M114.581322

9. Bose N, Wurst LR, Chan AS, Dudney CM, LeRoux ML, Danielson ME, et al. Differential regulation of oxidative burst by distinct β-glucan-binding receptors and signaling pathways in human peripheral blood mononuclear cells. *Glycobiology*. (2014) 24:379–91. doi: 10.1093/glycob/cwu005

10. Cheng SC, van de Veerdonk FL, Lenardon M, Stoffels M, Plantinga T, Smeekens S, et al. The dectin-1/inflammasome pathway is responsible for the induction of protective T-helper 17 responses that discriminate between yeasts and hyphae of Candida albicans. *J Leukoc Biol*. (2011) 90:357–66. doi: 10.1189/jlb.1210702

11. Perrotta C, Cattaneo MG, Molteni R, De Palma C. Autophagy in the regulation of tissue differentiation and homeostasis. *Front Cell Dev Biol*. (2020) 8:602901. doi: 10.3389/fcell.2020.602901

12. Harris J, Lang T, Thomas JPW, Sukkar MB, Nabar NR, Kehrl JH. Autophagy and inflammasomes. *Mol Immunol*. (2017) 86:10–5. doi: 10.1016/j.molimm.2017.02.013

13. Xiao JL, Xu GC, de Hoog S, Qiao JJ, Fang H, Li YL. Oral prevalence of candida species in patients undergoing systemic glucocorticoid therapy and the antifungal sensitivity of the isolates. *Infect Drug Resist*. (2020) 13:2601–7. doi: 10.2147/IDR.S262311

14. Eliaš D, Gbelská Y. Candida glabrata - basic characteristics, virulence, treatment, and resistance. *Epidemiol Mikrobiol Imunol*. (2022) 71:118–34.

15. Perlroth J, Choi B, Spellberg B. Nosocomial fungal infections: epidemiology, diagnosis, and treatment. *Med Mycol*. (2007) 45:321–46. doi: 10.1080/13693780701218689

16. Briones-Martin-Del-Campo M, Orta-Zavalza E, Juarez-Cepeda J, Gutierrez-Escobedo G, Cañas-Villamar I, Castaño I, et al. The oxidative stress response of the opportunistic fungal pathogen Candida glabrata. *Rev Iberoam Micol*. (2014) 31:67–71. doi: 10.1016/j.riam.2013.09.012

17. Silva S, Negri M, Henriques M, Oliveira R, Williams DW, Azeredo J. Candida glabrata, Candida parapsilosis and Candida tropicalis: biology, epidemiology, pathogenicity and antifungal resistance. *FEMS Microbiol Rev*. (2012) 36:288–305. doi: 10.1111/j.1574-6976.2011.00278.x

18. Duan Z, Chen Q, Du L, Tong J, Xu S, Zeng R, et al. Phagocytosis of candida albicans inhibits autophagic flux in macrophages. *Oxid Med Cell Longev*. (2018) 2018:4938649. doi: 10.1155/2018/4938649

19. Drummond RA, Swamydas M, Oikonomou V, Zhai B, Dambuza IM, Schaefer BC, et al. CARD9(+) microglia promote antifungal immunity via IL-1β- and CXCL1-mediated neutrophil recruitment. *Nat Immunol*. (2019) 20:559–70. doi: 10.1038/s41590-019-0377-2

20. Kasper L, Seider K, Hube B. Intracellular survival of Candida glabrata in macrophages: immune evasion and persistence. *FEMS Yeast Res*. (2015) 15:fov042. doi: 10.1093/femsyr/fov042

21. Seider K, Gerwien F, Kasper L, Allert S, Brunke S, Jablonowski N, et al. Immune evasion, stress resistance, and efficient nutrient acquisition are crucial for intracellular survival of Candida glabrata within macrophages. *Eukaryot Cell*. (2014) 13:170–83. doi: 10.1128/EC.00262-13

22. Desai JV, Kumar D, Freiwald T, Chauss D, Johnson MD, Abers MS, et al. C5a-licensed phagocytes drive sterilizing immunity during systemic fungal infection. *Cell*. (2023) 186:2802–2822.e22. doi: 10.1016/j.cell.2023.04.031

23. Das LM, Binko AM, Traylor ZP, Peng H, Lu KQ. Vitamin D improves sunburns by increasing autophagy in M2 macrophages. *Autophagy*. (2019) 15:813–26. doi: 10.1080/15548627.2019.1569298

24. Kyrmizi I, Gresnigt MS, Akoumianaki T, Samonis G, Sidiropoulos P, Boumpas D, et al. Corticosteroids block autophagy protein recruitment in Aspergillus fumigatus phagosomes via targeting dectin-1/Syk kinase signaling. *J Immunol*. (2013) 191:1287–99. doi: 10.4049/jimmunol.1300132

Frontiers in Immunology

Explores novel approaches and diagnoses to treat immune disorders.

The official journal of the International Union of Immunological Societies (IUIS) and the most cited in its field, leading the way for research across basic, translational and clinical immunology.

Discover the latest Research Topics

See more →

Frontiers

Avenue du Tribunal-Fédéral 34
1005 Lausanne, Switzerland
frontiersin.org

Contact us

+41 (0)21 510 17 00
frontiersin.org/about/contact

Frontiers in
Immunology

frontiers | Research Topics